Distribution and characteristics of gas hydrates in shallow sediments of pockmarks and seepage sites

Dissertation

Zur Erlangung des
Doktorgrades der Naturwissenschaften
(Dr. rer. nat.)

Im Fachbereich der Geowissenschaften
der Universität Bremen

vorgelegt von
Jiangong Wei

Bremen, Dezember 2014

Gutachter:

1. Prof. Dr. Gerhard Bohrmann
2. Prof. Dr. Achim J. Kopf

Contents

Abstract

Cold seeps are regions where fluid migrates from deep subsurface and escapes to the water column through the sea floor. Such fluids are usually rich in low molecular weight hydrocarbons, mainly methane, with small amount of other gases, such as carbon dioxide and hydrogen sulfide. In areas of water depth greater than 300-600m, gas hydrate could form depending on the bottom water temperature and geothermal gradients. Formation and decomposition of gas hydrate potentially change the properties of marine sediment. Therefore, in order to understand the evolution and morphological changes of marine cold seeps, it is important to know the distribution of gas hydrate in shallow sediment. Gas enclathrated in hydrate also contains important information and is helpful to understand the source of the gas.

One aim of the thesis is to understand the distribution of gas hydrate within the sediment of a pockmark field at the Nigerian continental margin by using infrared thermal scanning and pore water chloride concentration. Both methods show similar hydrate distribution with different resolutions. By using coring information, the seismic profiles obtained in 2008 were calibrated to show the overview of free gas accumulation and hydrate distribution in the whole pockmark field. Elevated geothermal gradients were observed in the center of a pockmark where gas flares in the water column were imaged by hydroacoustic method, indicating the pockmark was active. The interaction among the fluid flow, hydrate formation and dissolution, and the thermal regime governs the formation and evolution of the pockmarks in this area.

Knowledge of gas composition and crystal structure of natural gas hydrates is important for determining the stability of hydrate, which is a key factor to understand the fate of methane gas bubbles and hydrate bulks in the water column and the size of the hydrate reservoir in marine sediment. Methane is the dominant gas of hydrate samples recovered from pockmarks at the Nigerian continental margin, indicating that the gas is mainly biogenic. Besides methane, hydrogen sulfide and carbon dioxide were also detected using both Raman spectroscopy and gas chromatography. The thickness of gas hydrate stability zone (GHSZ) increases significantly due to the existence of hydrogen sulfide and carbon dioxide although their contents are relatively low.

Hydrogen sulfide containing hydrate has only been discovered at Hydrate Ridge and Niger delta. It is a big surprise to observe hydrogen sulfide within the samples from Nigerian continental margin. In order to know whether such type of hydrate is restricted only in specific areas, we did additional Raman spectroscopy analysis on the hydrate samples recovered at cold seeps from different areas, including the Black Sea and the Makran continental margin. Results show that both samples contain hydrogen sulfide. Therefore,

we infer that hydrogen sulfide containing hydrate is not restricted to certain area, but widely occurs within seepage sites where intensive upward methane flux exists and sustains high activity of anaerobic methane oxidation that produces hydrogen sulfide. Sudden release of hydrogen sulfide from hydrate due to changes of the ambient condition might dramatically affect the distribution of chemosynthetic community.

Chapter 1 Introduction

1.1 Introduction on gas hydrate

Gas hydrates are solid, non-stoichiometric compounds, which crystallize from water and guests, often gas molecules. The gas molecules (guests) are trapped within cavities (host) which are composed of hydrogen-bonded water molecules. The formation of gas hydrates requires elevated pressure (P) and low temperature (T).

It was the first time in 1810 that gas hydrate was discovered and documented by Humphrey Davy (Davy, 1811).

> *"It is generally stated in chemical books, that oxymuriatic gas is capable of being condensed and crystallized at low temperature; I have found by several experiments that this is not the case. The solution of oxymuriatic gas in water freezes more readily than pure water, but the pure gas dried by muriate of lime undergoes no change whatever at a temperature of 40 below 0° of Fahrenheit."*

Since then, gas hydrate research experienced a long history until present and could be divided into three phases depending on the major points each stage focus on (Sloan and Koh, 2007):

The first phase: 1810s - present

Since the first time gas hydrate was discovered in 1810, it became a lab curiosity. Research on gas hydrates mainly focused on (1) looking for more gases which could form gas hydrates and (2) studying the physical properties and compositions of the gas hydrates. Many gases which are suitable for hydrate formation were found during this period and a detailed review is described within the book written by Sloan and Koh (2007).

The second phase: 1930s - present

In 1930s, gas hydrate was observed for the first time within natural gas pipelines that blocked gas transmission and caused industrial accident within permafrost areas (Hammerschmidt, 1934). Realizing the significance of this discovery, industries dedicated to understand the behavior of gas hydrate formation and to prevent gas hydrate crystallization in the pipelines which opened a new window of modern research in this subject.

The third phase: 1960s - present

In was recognized by Soviet scientists for the first time that methane-rich gas hydrates (methane hydrates) potentially exist within arctic permafrost regions (Makogon, 1965) as well as deep-sea sediment (Makogon et al., 1971) where temperature and pressure were favorable for hydrate formation. These hypotheses were proved first by natural gas hydrate discovery in Siberia permafrost regions (Makogon et al., 1971) then in Caspian Sea and Black Sea (Yefremova and Zhizhchenko, 1974). Since then more cruises were designed to

find natural gas hydrates, leading to the discovery of quite a few hydrate reservoirs worldwide (Figure 1.1).

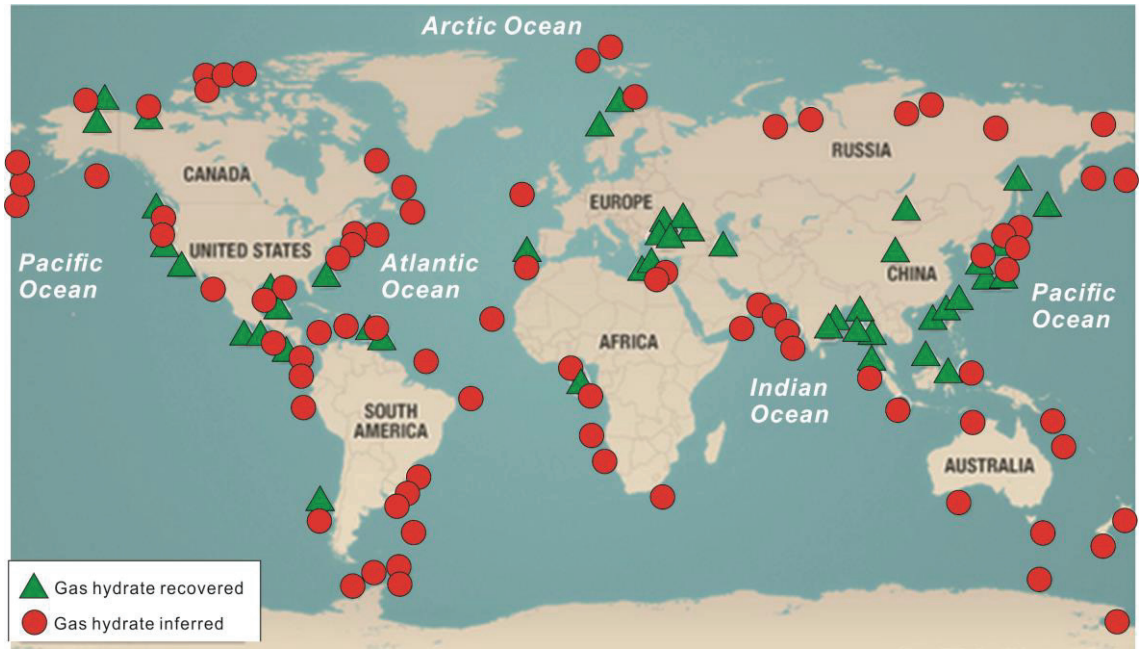

Figure 1.1 Gas hydrate deposits in the world (from http://www.naturalgaseurope.com/).

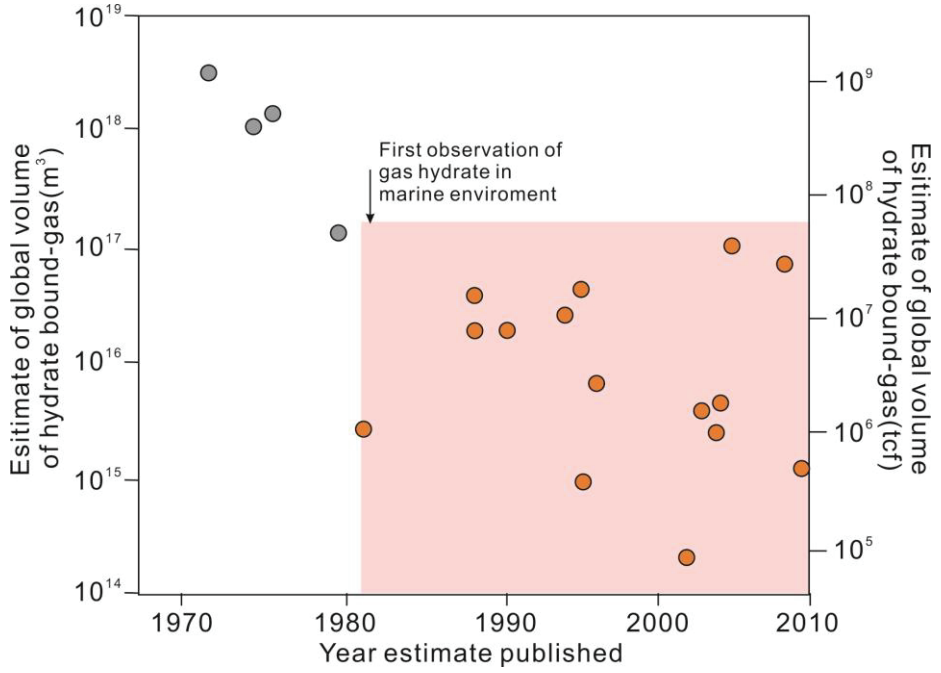

Figure 1.2 Estimation of global hydrate bonded gas with the publication date of the estimation (after Boswell and Collett, 2011).

In recent years, more scientists as well as industries contributed to the research and exploitation of gas hydrate, reflecting an increasing concern both national and international. Estimation of total amount of hydrate bonded gases decreased with time (Figure 1.2) in the past several decades because more physical data and other information were obtained to confine the conditions (Boswell and Collett, 2011). However, even conservative estimates of hydrate-bonded gases are tremendous, therefore, from a geological as well as economic

point of view, there are four fundamental questions which stimulate the research of natural gas hydrate:

1. Are the natural gas hydrate deposits exploitable and could they serve as potential future energy resources (Archer et al., 2009; Boswell et al., 2009; Lee and Holder, 2001; Moridis et al., 2013)?
2. Methane is the most prevalent gas in natural gas hydrates which is also a greenhouse gas. What is/was the impact of gas hydrate formation and dissociation on climate change in the past, at present as well as in the future (Dickens, 2003; Henriet and Mienert, 1998; Jahren et al., 2001; Jenkyns, 2003; Katz et al., 1999; Kennett et al., 2003; Reagan and Moridis, 2007)?
3. Gas hydrate formation and destabilization are sensitive to many factors, for instance, temperature and pressure. What is the effect of gas hydrate destabilization on the stability of continental slope (Kayen and Lee, 1991; Maslin et al., 1998; Mienert et al., 1998)?
4. What is the significance of natural gas hydrate on global carbon cycle (Archer et al., 2009; Dickens, 2003)?

This thesis focuses on understanding the distribution as well as basic characteristics, including gas composition and structure, of natural gas hydrates in shallow marine sediment. Impact of gas hydrates on fluid flow, seafloor morphology changes and chemosynthetic communities are also discussed.

1.2 Fundamental principles

1.2.1 Cages and crystal structures

Gas hydrates are non-stoichiometric solid compound which is similar to ice crystals (Sloan and Koh, 2007). Natural gas hydrates are mainly classified into three categories which are structure I (sI), II (sII) and H (sH) based on the crystallographic structure (Ripmeester et al., 1987; Stackelberg and Müller, 1951).

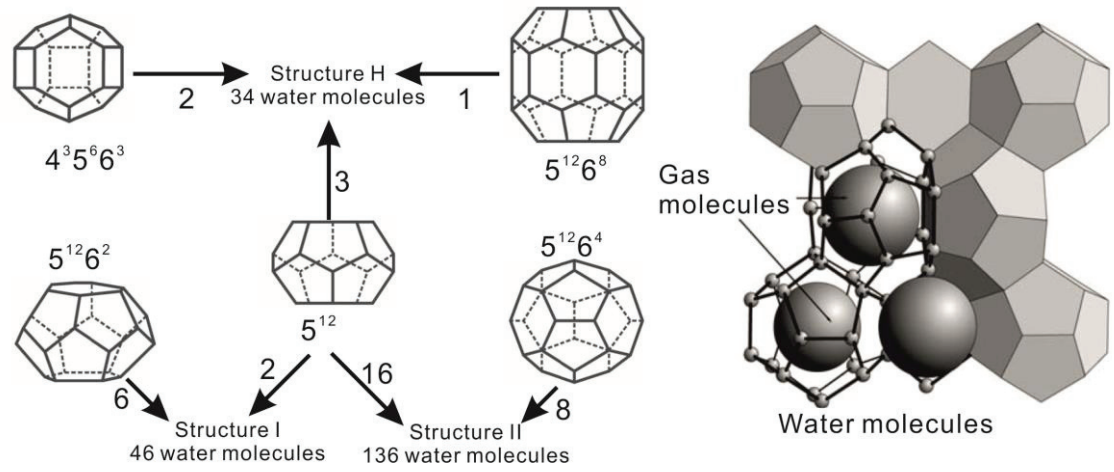

Figure 1.3 Relation of cages and crystal structure of gas hydrates (after Bohrmann and Torres, 2006).

Table 1.1 Ratio of gas molecule diameter with hydrate cavity diameter (from Sloan and Koh, 2007).

Molecule	Guest diameter Å	Structure I		Structure II	
		5^{12}	$5^{12}6^2$	5^{12}	$5^{12}6^4$
N_2	4.10	0.80	0.70	0.82	0.62
CH_4	4.36	0.86	0.74	0.87	0.65
H_2S	4.58	0.90	0.78	0.91	0.69
CO_2	5.12	1.00	0.83	1.02	0.77
C_2H_6	5.50	1.08	0.94	1.10	0.83
C_3H_8	6.28	1.23	1.07	1.25	0.94
i-C_4H_{10}	6.50	1.27	1.11	1.29	0.98
n-C_4H_{10}	7.10	1.39	1.21	1.41	1.07

Water molecules form different types of polyhedral cages in which low molecular weight gases are enclosed as guests. There are five types of cages (Figure 1.3) which could be described according to the number of faces and edges (Sloan and Koh, 2007). Small cages, known as pentagonal dodecahedra, are composed of twelve five-side polygons (5^{12}). Large cages, including tetrakaidecahedron ($5^{12}6^2$), hexakaidecahedron ($5^{12}6^4$) and icosahedron ($5^{12}6^8$), are formed by adding two, four and eight hexagonal faces, respectively. Medium cages, known as irregular dodecahedron ($4^35^66^3$), comprise three square, six pentagonal and three hexagonal faces. Different types of cages with certain combination form the unit cells of different hydrate structures. Hydrate structures are described according to the number of cages and the number of water molecules of the unit cell. For instance, structure I hydrate are described as ($2[5^{12}]$ $6[5^{12}6^2]$ $46H_2O$), which shows that the unit cell is composed of two small cages and six large cages with 46 water molecules. Structure II and H are described as ($16[5^{12}]$ $8[5^{12}6^4]136H_2O$) and ($3[5^{12}]$ $2[4^35^66^3]$ $1[5^{12}6^8]$ $34H_2O$), respectively.

1.2.2 Guest molecules

Sufficient gas molecules are the prerequisite condition for gas hydrate formation and stabilization. Which gas could be fitted into certain type of cage.is governed by the ratio of gas molecule size and cavity size For ratios greater than 1 (Table 1.1), it is unlikely for respective gases to be enclathrated naturally on earth, however, they were discovered under extreme conditions (P, T) in lab. Figure 1.4 shows guest molecules with size in a wide range from Ar to iso-C_4H_{10} which are known to fit in different type of cages (Sloan and Koh, 2007).

Because CH_4 is widely produced from microbial degradation of organic matters, methane hydrate is the most abundant hydrate discovered in marine sediment (Hester and Brewer, 2009; Kvenvolden, 1993). Methane molecule has diameter of 4.36Å and could be incorporated into the small cage of sI and sII, and in the large cage of sI. Small amount of other gas molecules, such as CO_2 and H_2S, are also found in sI hydrates (detailed

discussion in Chapter 4). These gases change the hydrate phase boundary significantly and help to stabilize gas hydrate (Swart et al., 2000). When larger gas molecules exist, such as C_3H_8 and C_4H_{10}, sII gas hydrate will form by enclathrating these gases into the large cages. Up to date, sH hydrate was only found at one site at the Cascadia margin which is an oily gas seepage site with complex composition of hydrocarbons (Lu et al., 2007).

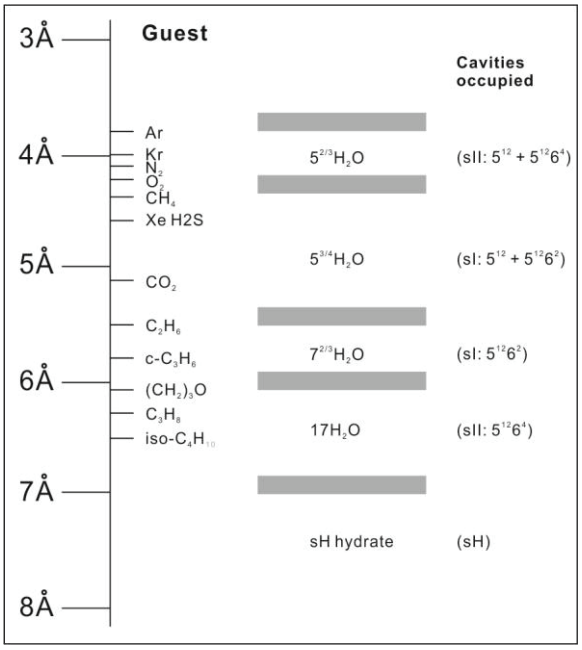

Figure 1.4 Diameter and the respective cages for specific gas (after Sloan and Koh, 2007).

In natural system, the feeding gas for hydrate formation is normally a mixture of two or more gases. Hydrate crystal structure is governed by both the largest gas molecule and the concentrations of gases. For instance, CH_4 could be enclathrated into small and large cage of sI, whereas C_2H_6 could be enclathrated into the small cages and large cages of both sI and sII. Therefore, the type of hydrate structure depends on the concentration of each gas component (Subramanian et al., 2000a; Subramanian et al., 2000b). For instance, sI will be the only crystal structure if CH_4 or C_2H_6 occurs alone. If CH_4 and C_2H_6 exist together, the hydrate structure is governed by the content of each component, and a mixture of sII and sI hydrate will form if CH_4 concentration is below 99.2-99.4% (Subramanian et al., 2000b).

1.3 Stability and phase boundary of gas hydrate

The stability of gas hydrate is thermodynamically governed by several key factors, including temperature, pressure, composition, and pore-water salinity (Sloan and Koh, 2007). These parameters are determined by lots of processes within marine environment, leading to the formation of a multiple dynamic system both spatially and temporally. The gas hydrate stability zone (GHSZ) is the area within the water column and sediments where gas hydrates are thermodynamically stable if sufficient gas is supplied. In this section, we will have a brief view of these parameters.

1.3.1 Pressure and temperature

Since methane is the most abundant gas in marine deposits, we will discuss the pressure and temperature parameters based on methane hydrate. Temperature and pressure that satisfy the condition of hydrate formation are widely located at the seabed where water depths exceed 300-600m, depending on the regional bottom water temperature. Figure 1.5 shows an example of hydrate phase diagram at the Nigerian continental margin. As shown in Figure 1.5, the upper and lower boundaries of the GHSZ are the intersections of hydrate phase boundary (calculated using software HWHYD) and geothermal gradient line as well as water temperature profile. Within a short timescale, pressure and temperature are considered as static parameters in marine environment, although they are slightly affected by tides, deep eddies, and currents. However, in a long timescale, they change dramatically due to the variation of sea level, tectonic activity, sedimentation and ocean currents, which accordingly influence the stability of gas hydrate.

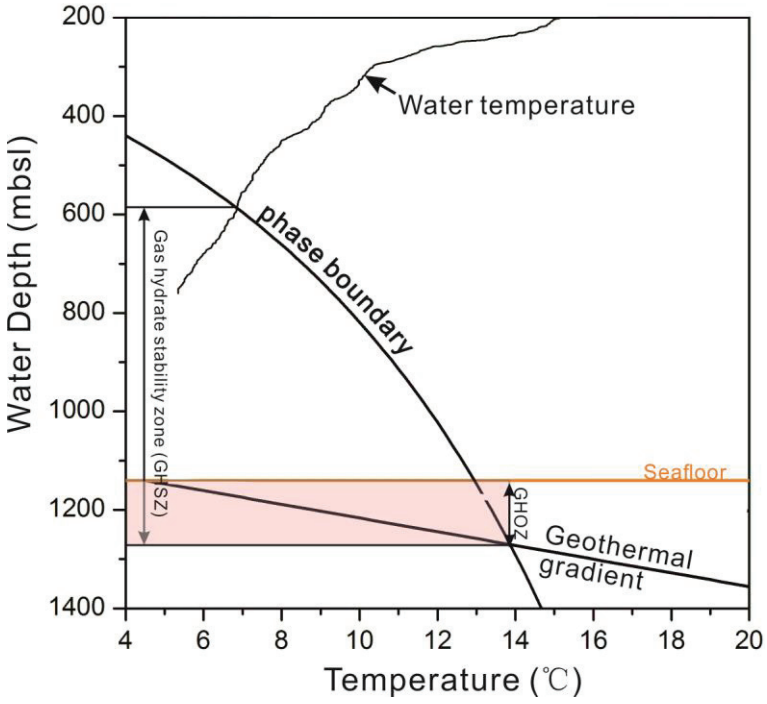

Figure 1.5 Phase diagram showing the stability field of sI methane hydrates at the Nigerian continental margin. GHSZ is short for gas hydrate stability zone.

1.3.2 Gas composition

Gas hydrate can not form without super saturation of hydrate-forming gases in pore water (Xu and Ruppel, 1999). Therefore, although pressure and temperature condition which is suitable for gas hydrate formation is almost everywhere in the ocean, gas hydrate occurrence are only restricted to continental margins and enclosed seas due to the insufficient methane supply in the wide ocean basin.

Figure 1.6 illustrates the relation between gas hydrate occurrence zone (GHOZ) and CH_4 solubility and concentration. In shallow sediments within the GHSZ, due to the methane consumption by AOM, CH_4 concentration is under saturated, leading to the absence of gas hydrate. As depth increases, CH_4 concentration in the pore water increases with depth due

to the absent of AOM. When CH_4 concentration reaches solubility, gas hydrate nucleation starts and defines the top of the GHOZ. When CH_4 concentration is lower than the solubility, the depth marks the base of the GHOZ. It could be inferred that when CH_4 flux increases or decreases, the GHOZ will expand or shrink accordingly. CH_4 flux in marine sediment is not constant, therefore, it affects CH_4 concentration in the pore water with time. When CH_4 concentration in the pore water decreases below solubility, gas hydrate will start dissolving, leading to the destabilization of gas hydrate (Sultan et al., 2010).

Gas composition does not only govern the hydrate structure, but also affects the stability of hydrate. The presences of CO_2, H_2S, and other light molecular weight hydrocarbons could shift the stability curve to higher temperature at a given pressure, increasing the stability of methane hydrate (Swart et al., 2000). Chapter 4 describes the impact of CO_2 and H_2S on enhancing hydrate stability.

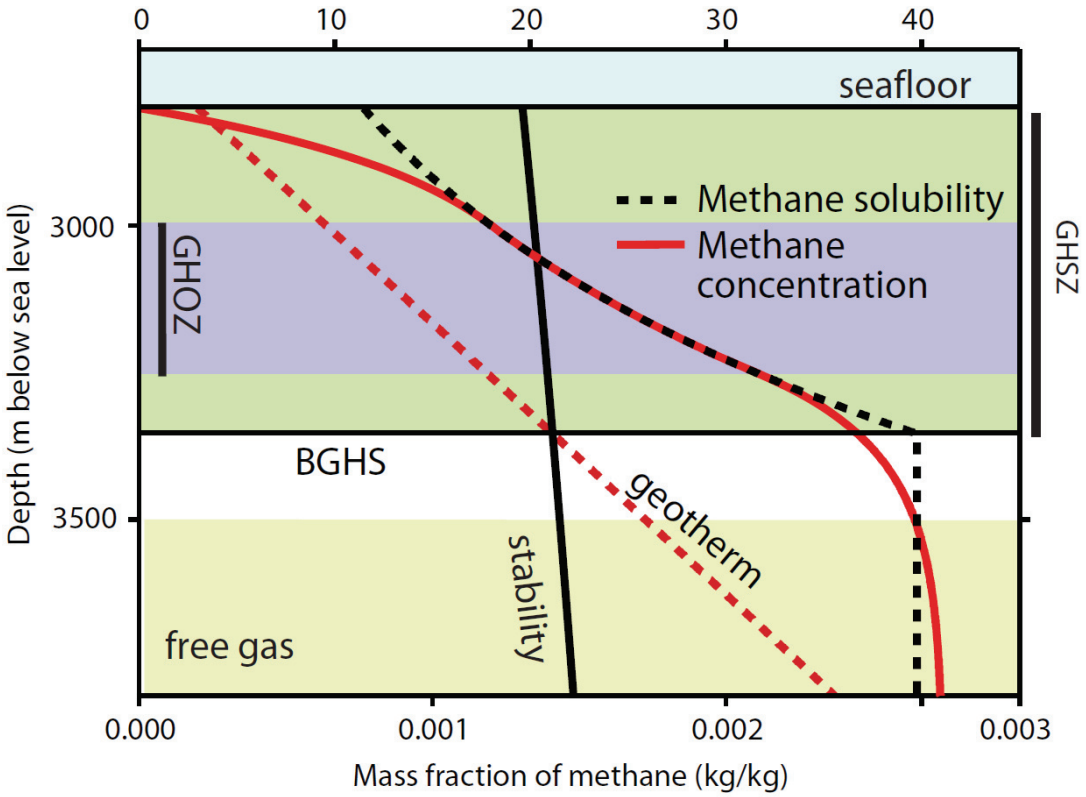

Figure 1.6 Methane hydrate occurrence and absence controlled by the methane concentration (from Trehu et al., 2006).

1.3.3 Influence of salinity

The stability of gas hydrates is influenced by ionic strength of the water. This is because the probability of water molecule arrangement within hydrate cage decreases due to the interchanging between ions and polar water molecules.

The elevation of dissolved ions concentration in the pore water shifts the phase boundary to left and inhibits the formation of hydrate. For instance, compare to the hydrate formation in pure water, there is a -1.1°C shift in dissociation temperature of methane hydrate in 33% NaCl solvent (Dickens and Quinby‐Hunt, 1994). Elevated pore water salinity sometimes

exerts a major effect on inhibiting hydrate formation, even system with sufficient gas supply and adequate P, T conditions is established.

A more complex situation is that since gas hydrate formation excludes ions into the surrounding pore water, elevated pore water salinity might inhibit hydrate formation (Liu and Flemings, 2007) as feedbacks which are a common case in areas featured by intensive methane flux.

1.4 Fabric and accumulation of gas hydrates in marine sediment

Gas hydrates precipitate as authigenic minerals in marine sediments. The fabric of gas hydrate varies significantly and is related to fluid flux, lithology and porosity of sediment, water content and overburden pressure (Bohrmann and Torres, 2006). Gas hydrate accumulation is defined as local occurrence of gas hydrates in marine sediments which is associated with geological structures and/or stratigraphic traps (Milkov and Sassen, 2002). The properties of the surrounding host sediment, especially grain size, have significant influence on the hydrate content in sediment.

1.4.1 Hydrate fabric and relation to burial depth

Gas hydrates can be classified into disseminated, nodular, layered and massive hydrates (Malone, 1985) according to the size and fabric of hydrate occurrences. The classification of Malone (1985) enables a uniform description of gas hydrate recovered from different sites in the world.

Hydrate ridge is one of the most well studied regions for natural gas hydrate. During the ODP Leg 204 drilling campaign, a relation between burial depth and fabric of gas hydrates was recognized at Hydrate Ridge (Abegg et al., 2007; Abegg et al., 2006). The fabric of gas hydrate could be classified into two major categories with respect to their burial depth (Abegg et al., 2007): 1) In shallow sediment, massive hydrates, hydrate nodules and hydrates which were intercalated with the sediments occurred. Hydrate layers formed (sub-) parallel to the bedding (Figure 1.7). The size of such hydrates varied from millimeters to decimeters. Accumulation and growth of hydrates within shallow sediments will displace the sediment particles in order to gain space. This is impossible at greater depth due to the overburden. Torres pointed out that at Hydrate Ridge the approximate sediment depth at which the force of gas hydrate crystallization can overcome the overburden pressure is 25 meters below seafloor (mbsf) (Torres et al., 2004b). Internal structure with bubble fabric is quite often observed within shallow gas hydrate. Such pores occur in variable sizes, and in some specimens very large pores of up to 3-4 cm in diameter can be observed. The fabric is similar to that of gas hydrates experimentally formed on the sea-floor (Brewer et al., 1997). There are several lines of evidence that support migration of methane gas from deep subsurface (Bohrmann and Torres, 2006), which either turns into such macroscopic porous gas hydrates or escapes at the seafloor. 2) At depths greater than 25mbsf, massive hydrates only occurred if large pore spaces (sand) and cavities were present in the sediments. Otherwise, hydrates were found in veins and veinlets with steep dipping angles (Figure 1.7). This is due to upwards-migrating gases and hydrate precipitation along fractures and

faults within the sediments (Abegg et al., 2007; Bohrmann and Torres, 2006; Torres et al., 2004b; Tréhu et al., 2004b).

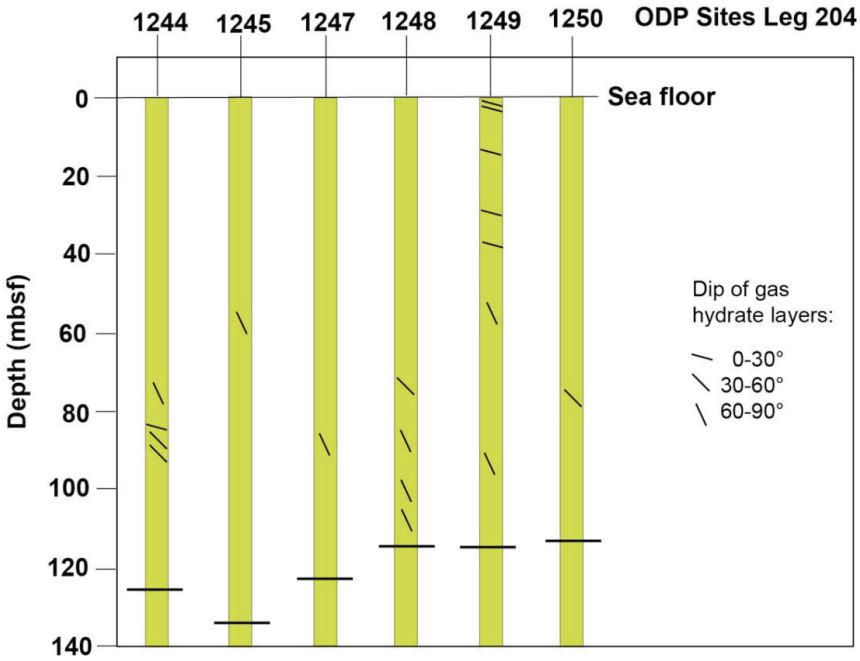

Figure 1.7 Relation between dipping angles and burial depth at ODP Leg 204 drilling sites (from Abegg et al., 2007).

1.4.2 Importance of sediment grain size

The porosity and permeability of clay are much lower than that of sands, therefore, the majority of naturally occurring hydrate in clay sediment either fills pore space or occurs in thin fractures, forming hydrate deposit with low saturation. Except in very shallow sediment, hydrate accumulations with high saturation have only been found in coarse sediment because of its high porosity and permeability.

Correlation between gas hydrate occurrence and grain size was investigated using IR thermal images and core observation during Ocean Drilling Program (ODP) Leg 204 to southern Hydrate Ridge (Figure 1.8). Weinberger (2005) pointed out that 70% of gas hydrate occurrences are related to the sand horizons at site 1250 in the crest. Down-dip from the ridge crest, the percentage of sand horizons hosting hydrate drops to 57% at site 1246, 46% at site 1244, 30% at site 1245 and 29% at site 1251. This decreasing trend implies that sand layers not only provide space for hydrate nucleation and accumulation but also serve as pathway of lateral fluid flow at Hydrate Ridge. The investigation of Expedition 311 of the Integrated Ocean Drilling Program (IODP) to the northern Cascadia shows that both drilling sites (U1325 and U1326) are characterized by abundant coarse-grained (sand) layers up to 23 cm in thickness, and are interspaced within fine-grained (clay and silty clay) detrital sediments. Average gas hydrate content is between 4% and 8% at the drill sites. The gas-hydrate distribution is punctuated by localized depth intervals of high gas-hydrate saturation, which preferentially occur in the coarse-grained horizons and occupy up to 60% of the pore space at Site U1325 and 80% at Site U1326 (Torres et al., 2008). Torres (2008) pointed out that there is positive correlation between gas-hydrate

content and sediment grain size. Detailed analyses of contiguous samples of different lithologies show that when enough methane is present, about 90% of the variance in gas-hydrate saturation can be explained by the sand (>63 μm) content of the sediments. Drilling at the site UBGH1-9, offshore Korea in 2007 also showed gas-hydrate saturation varies with sediment grain size (Bahk et al., 2011). Comparison of IR scan images and split-core lithology suggests that the cold spots (gas hydrate) generally correspond to turbidite sand beds. Positive correlations between gas hydrate content and sediment grain size were also found within the Krishna–Godavari Basin, East Coast off India during the India (Riedel et al., 2011). At Site NGHP-01-15 of the India National Gas Hydrate Program (NGHP), average of gas hydrate content was estimated to be 15% of the pore-space. However, highest hydrate content of almost 50% of the pore space was detected at a 5–8 m thick interval characterized by higher sand content than anywhere else at the site (Riedel et al., 2011). The drillings in the Shenhu area, South China Sea, showed that average gas hydrate content is less than 10% in the whole GHOZ (Wang et al., 2011). However, elevated gas hydrate content as high as 45% was detected within silt and silty clay sediments due to the increase of calcareous nannofossil and foraminifer.

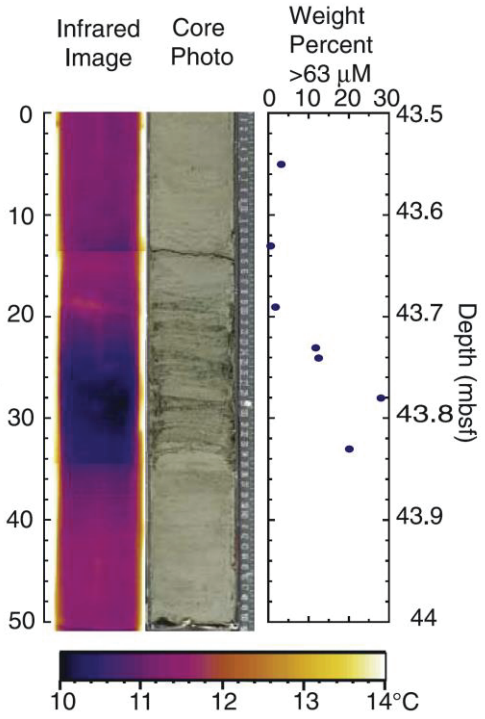

Figure 1.8 Comparison of IR thermal images and core lithology (1250C-6H-1, 100–150 cm, ODP Leg 204) show clearly that gas hydrate preferentially accumulated in sand layers at drilling site (after Weinberger et al., 2005).

1.5 Proxies of gas hydrate presence

Geophysical methods are a major tool for detecting gas hydrate in marine sediments and represent an important precursor for drilling expeditions. Geophysical data are used to identify suitable drilling targets and provide geological context for these sites. Drilling and logging data, in turn, are used to calibrate and validate models for gas hydrate distribution derived from remote sensing data.

Seismic profiling is one of the major geophysical surveys which allows detection and interpretation of gas hydrate occurrence in deeper sediment. Multibeam echosounder and sidescan sonar are also quite often employed for quick mapping of seepage sites in a broad area where gas hydrate normally occurs within shallow sediments. There are quite a few other remote sensing techniques which are available to detect gas hydrate and quantify its content within sediment including controlled-source electromagnetic sounding (Edwards, 1997; Weitemeyer et al., 2006; Yuan and Edwards, 2000), seafloor compliance (Willoughby et al., 2005), and ocean-bottom seismology (Hobro et al., 2005). Although these methods are not widely used for now, they show promising developments in gas hydrate detection and quantification over large areas.

Coring allows analysis of sediment samples which provides direct information of distribution and abundance of gas hydrate within marine sediments. Logging techniques provide in situ geophysical and geochemical properties of marine sediments along the borehole. Rapid dissociation starts when gas hydrate is recovered from the seafloor with non-pressurized conventional cores. Therefore, proxies are required for understanding the distribution and content of gas hydrate in the sediment. Proxies of in situ gas hydrate presence vary in resolution and accuracy and mainly include: (1) pore water chloride concentration; (2) core temperatures measured with infrared (IR) cameras; (3) pressure coring; (4) geophysical logs. Techniques (1) and (3) provide accurate gas hydrate content in low resolution because of the sophisticated and time-consuming operations. The other two techniques provide information in high resolution; however, the algorithms for calculation of hydrate content need to be calibrated by other proxies.

1.5.1 Seismic

Gas hydrate occurrence in marine sediment could be inferred from the bottom-simulating reflectors (BSRs) with reversed negative polarity of seismic reflection data (Figure 1.9) (Kvenvolden, 1985). BSRs are thought to represent the base of the GHSZ, which indicate the transition interface between free gas below and hydrate-bearing sediments above. Seismic amplitude is enhanced below the BSR due to free gas accumulation beneath the GHSZ which increases acoustic impedance contrasts between sedimentary layers. Gas hydrates within sediment pore space increase the sediment interval velocity in the GHSZ and may reduce interstate acoustic impedance contrasts significantly, leading to a remarkable seismic amplitude decrease above the BSR (Hyndman and Spence, 1992), which is known as amplitude blanking. In the past several decades, the BSRs have been found widely at deep seas and continental margins, such as Makran accretionary prism (Sain et al., 2000) Norwegian continental margin (Andreassen et al., 2000; Berndt et al., 2004), Nankai Trough (Foucher et al., 2002), Gulf of Mexico (Shedd et al., 2012), continental margin of the Beaufort Sea (Andreassen et al., 1995), Taiwan collision zone (Chi et al., 1998), south China sea (Wang et al., 2010), continental margins off New Zealand (Townend, 1997), Svalbard continental slope (Haacke et al., 2008), Black Sea (Zillmer et al., 2005), Ulleung Basin (Horozal et al., 2009), offshore Vancouver Island (Riedel et al., 2002), Peru margin (von Huene and Pecher, 1999), and Northern Cascadia

continental slope (Yuan et al., 1996). Gas hydrate, however, has also been recovered at areas where no BSR is observed (Holbrook et al., 2002; Holbrook et al., 1996; Mathews and VONHUENE, 1985; Shipboard Scientific Party, 1996). Therefore, although BSRs are an important indicator of gas hydrate presence, gas hydrate existence cannot be excluded without a distinct BSR.

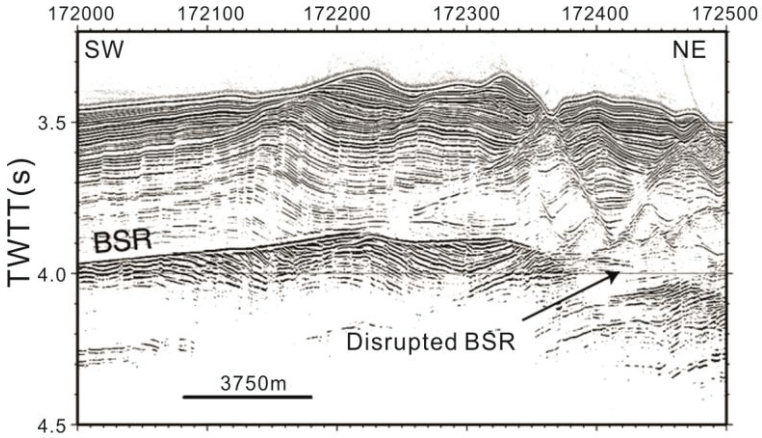

Figure 1.9 An example of bottom simulating reflector (BSR) of the Blake Ridge (after Holbrook et al., 2002)

BSR normally occurs very close to the base of the GHSZ which is governed by local geothermal gradients, pressure, gas hydrate crystal structure, pore water chemistry and hydrate-bonded gas composition (Sloan and Koh, 2007), therefore, it could potentially be used to calculate the local heat flow which is of great interest for geoscientists (Horozal et al., 2009; Kinoshita et al., 2011; Townend, 1997; Yamano et al., 1982). Continuous profiles of heat flows alongside seismic track lines could be calculated based on the depths of the BSR. The heat-flow distribution within a wide area could be easily and precisely derived from the BSR with much less biased than that from direct measurements (Grevemeyer and Villinger, 2001). In most cases, single BSR is observed in seismic data, however, double BSRs have also been found and are interpreted as ancient residual BSR (Foucher et al., 2002) or digenetic interface which is not related to gas hydrate (Andreassen et al., 2000).

Contents of gas hydrates above the BSR and free gas below have been estimated by using BSR waveforms in many different areas (Ecker et al., 2000; Holbrook et al., 1996; Lu and McMechan, 2002; Westbrook et al., 2008; Wood et al., 1994; Yuan et al., 1996), however, large uncertainties could be derived (Tréhu et al., 2006). Seismic velocity could be significantly affected by even adding a small number of free gas (Ostrander, 1984). Furthermore, gas hydrate distribution on a micro scale and its relation to the sediment grains could also exert strong effect on seismic velocity (Dvorkin and Nur, 1993; Helgerud et al., 1999). Only in a few areas, seismic velocity were calibrated by applying downhole logging and coring, which provide additional information of the heterogeneity of gas hydrate distribution in marine sediments (Holbrook et al., 1996; Tréhu et al., 2004b). Additional calibrations could also be provided by lab research of gas hydrate formation within marine sediments (Yun et al., 2005).

1.5.2 Indirect methods for shallow gas hydrate detection

Formation of shallow gas hydrate deposits requires specific geological structures that facilitate fast and sufficient methane supply. Therefore, shallow gas hydrate accumulation is normally related to marine seeps and is restricted to limited spatial extent which raises challenges for detection. Hydroacoustic methods, including side-scan sonar (Klaucke et al., 2006; Klaucke et al., 2012; Klaucke et al., 2005), parasound echosounder (Nikolovska et al., 2008; Römer et al., 2012) and multibeam echosounder (Greinert et al., 2006), provide a way of targeting local seeps in large areas based on their proxies. There are two major proxies that could be used for discovering seeps which are gas bubbles in water column (Römer et al., 2014a; Römer et al., 2014b) and high reflectivity patches on the seafloor (Bahk et al., 2009; Klaucke et al., 2012).

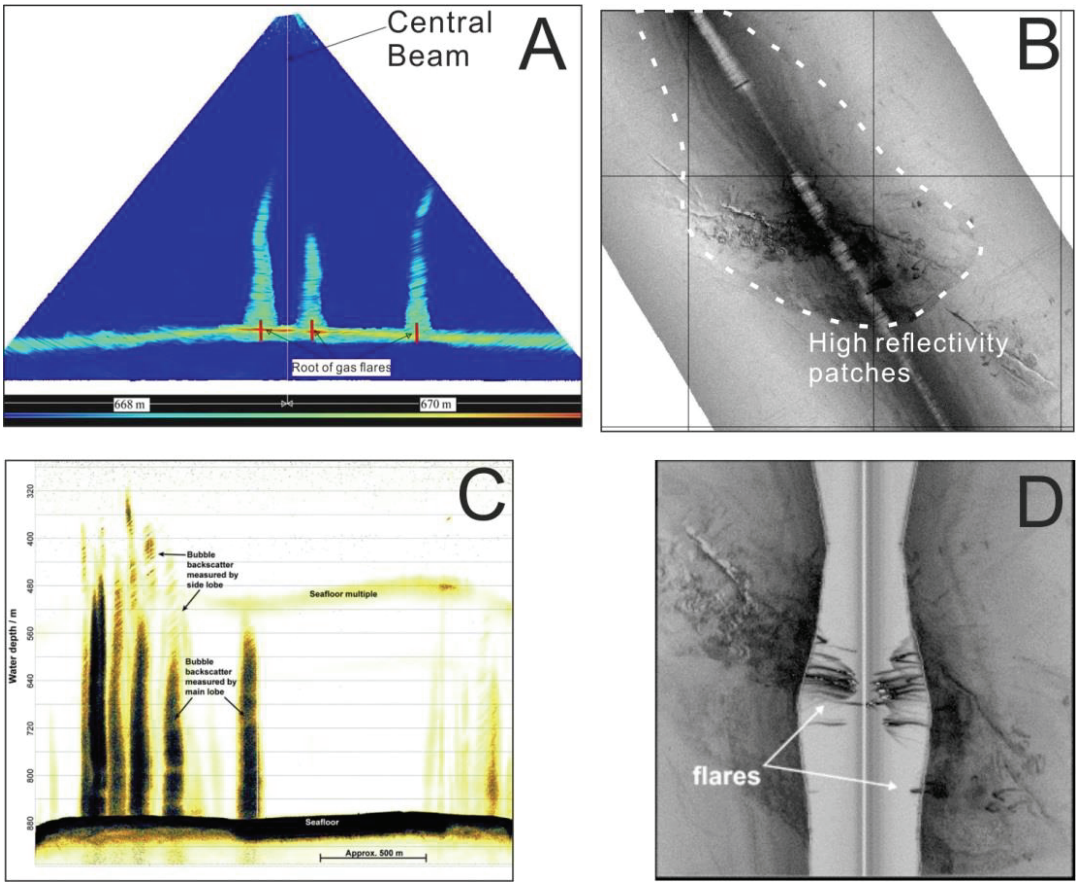

Figure 1.10 Examples of hydroacoustic investigation of Batumi gas seep in the eastern Black Sea. A: Gas flares imaged by EM710 multibeam echosounder (after Nikolovska et al., 2008). B: high reflective patches shown in sidescan sonar data (after Klaucke et al., 2006) C: Flares captured by parasound (after Nikolovska et al., 2008). D: Gas flares in water column shown in sidescan data (after Klaucke et al., 2006).

Gas escaping from the seafloor is a major feature of gas seeps. High amplitude reflection caused by gas bubbles due to the enhanced impedance contrast between the surrounding water and gas bubbles could be observed in the hydroacoustic profiles (Figure 1.10A, C and D) (Manasseh and Ooi, 2009). Rising gas bubbles from seabed are often detected as flare-shaped reflections in hydroacoustic profiles; consequently, these features are termed as “gas flare” by geologists (Greinert et al., 2006). Hydroacoustic evidence (gas flares) of

free gas release from seeps was obtained at numerous sites. High reflectivity patches on the seafloor are another proxy of marine seeps (Figure 1.10B). The patches are associated with changes in sediment type, seafloor topography, and seafloor mineral deposits (Römer et al., 2014a) which might be related to gas hydrate presence.

1.5.3 Pore water chloride concentration

Gas hydrate formation incorporates fresh water and excludes dissolved ions. Extra dissolved ions will diffuse away from the location of gas hydrate precipitation (Haeckel et al., 2004). When cores are recovered, gas hydrate will dissociate and release fresh water to the surrounding pore space and dilute chloride concentration. Therefore, discrete negative chloride anomalies are good indication for in situ gas hydrate presence and are currently the most widely used geochemical method for documenting gas hydrate distribution (Hesse, 2003; Torres et al., 2004a; Tréhu et al., 2004a).

However, there are several limitations to use this method for quantifying hydrate content in sediment. First, for areas where gas hydrates form recently, ions excluded in the pore water have not diffused away, therefore, chloride profiles usually show distinguish positive anomalies (Torres et al., 2011b; Torres et al., 2004b). Second, the background chloride concentration is hard to define, because it could be affected by many processes, for instance, elevation of Cl concentration due to alteration of volcanogenic sediments or decrease of Cl concentration caused by clay dehydration and opal formation (Bekins et al., 1994; Bekins et al., 1995; Hiruta et al., 2009). Third, the operation of sampling pore water and conducting the measurement is sophisticated and time consuming, therefore, pore water chloride can be obtained only in low resolution (Torres et al., 2011a; Tréhu et al., 2004a).

1.5.4 IR temperature measurements

Dissociation of gas hydrate is an endothermic reaction which absorbs heat from surroundings and decreases the temperature of the sediment cores containing gas hydrates. Thermistors were originally used to measure temperature directly at sporicidal points. Infrared camera scanning, however, provides the way to measure the core temperature fast and continuously. This method was first introduced during ODP Leg 201 (Ford et al., 2003) and was used since ODP Leg 204 to image all cores recovered from within or near the GHSZ (Riedel et al., 2005; Tréhu et al., 2006). It permits rapid, systematic scanning of all cores to identify gas-hydrate-bearing intervals and estimate gas hydrate distribution (Weinberger et al., 2005). The low temperature anomalies were helpful to locate and sample hydrate quickly from the cores for later lab analysis.

Temperature profiles obtained from IR scanning could also be used to quantify gas hydrate content (Long et al., 2004). For each of nine sites at southern Hydrate Ridge, offshore Oregon, USA (ODP Sites 1244-1252) during ODP Leg 204, temperature data extracted from the IR images were used to estimate hydrate abundance as a function of depth either by assuming simple parameterization of the relationship between IR anomalies and gas hydrate lenses or calibrated with chloride concentrations (Tréhu et al., 2004a).

1.5.5 Pressure cores for gas hydrate quantification

Pressure cores, which keep gas hydrate under high pressure condition during the core retrieve, provide a way of keeping all the gas in sediment, including free gas, gas dissolved in the pore water, and gas enclathrated in gas hydrate (Dickens et al., 1997). Assuming that various phase of gas are at equilibrium conditions prior to core retrieve, the amount of gas hydrates present in situ can be calculated by measuring the total amount of gas released during the core depressurization and comparing the in situ gas concentration to the in situ gas saturation (Pape et al., 2011). The first measurement of gas hydrate concentration using pressure core were conducted during ODP Leg 164 at Blake Ridge (Dickens et al., 1997). Similar measurements have been conducted from boreholes in other regions using the same tool (Milkov et al., 2003). In recent years, impact of gas hydrate on cold seeps and mud volcanos are of great interest to geologists, therefore, new generation of pressure coring tools were designed and produced, dedicating to the quantification of shallow gas hydrate (Heeschen et al., 2011; Heeschen et al., 2007; Pape et al., 2010).

As the only way to precisely estimate the total amount of gas, pressure core provides critical information to calibrate the estimation using other methods. However, it provides little information on length scales shorter than the core length. Information of hydrate distribution on a small scale is required for developing models to interpret remote sensing data and downhole geophysical logs (Dvorkin and Nur, 1993). Therefore, new pressure coring systems were developed recently which permit detailed analysis of physical properties at in situ conditions. Existing pressure coring tools are sophisticated and consume considerable time to deploy and depressurize. Accordingly, only a small percentage of the sediment column can be sampled using these tools (Tréhu et al., 2003).

1.5.6 Downhole logs

It was during the DSDP Leg 84 that downhole logs were used for the first time to understand hydrate distribution based on the ephemeral properties (Mathews, 1986). It has been conducted at all sites where gas hydrates was detected during ODP and IODP expeditions. Logging-while-drilling (LWD) technique, which conduct logging immediately follows drilling, eliminate the changes of sediment properties by thermal perturbations associated with coring and is especially useful for understanding distribution of hydrate and free gas within sediments (Goldberg, 1997) where core recovery might be poor. The LWD is also used as reconnaissance tool for identifying thin hydrate-bearing layers that are targeted for subsequent coring and sampling (Riedel et al., 2005). The most vigorous indicators of in situ hydrate presence are acoustic velocities and elevated electrical resistivity along with low gamma ray density (Goldberg and Saito, 1998; Hyndman et al., 1999; Waite et al., 2009). For remote-sensing techniques, quantitative estimation of hydrate content require log data to make assumptions about of the arrangement of gas hydrate and sediment grains on a micro scale (Helgerud et al., 1999). Spatial resolution of logging techniques is very high, therefore, they provide important information on the heterogeneous gas hydrate distribution by comparing data obtained laterally neighbor holes

and through the 360-degree images of physical parameters around the single borehole (Collett and Ladd, 2000).

1.6 Motivation and objective

The aim of this thesis is to understand the distribution and characteristics, including gas composition and structural information, of natural gas hydrates in shallow sediment of pockmarks and gas seepage sites.

How do gas hydrates distribute in the shallow sediment of pockmarks and what are the controlling factors of its distribution?

In previous cruises, shallow gas hydrates and athigenic carbonates were recovered from shallow sediments of a pockmark field on the Nigerian continental margin using gravity corer and piston corer. However, gas hydrate distribution in the deeper sediment is still unknown. In 2011, the French research vessel R/V '*Pourquoi pas?*' equipped with MeBo allowed deep drilling of the marine sediment. Twelve MeBo cores with maximum length of 58m were recovered from three pockmarks which provide a very good opportunity to understand hydrate distribution in deep sediment. Therefore, questions raised here are as follows: How do gas hydrates distribute in the sediment? Is there any horizontal or vertical variations? What controls the gas hydrate distribution? What is the impact of gas hydrate dynamic changes on pockmark formation and evolution?

Is it an occasional case or a common global case for H_2S-containing natural gas hydrates occurring in gas seeps? What is the significance?

When some gravity cores were opened, massive gas hydrates with smell of H_2S were noticed. Although the smell might come from the sediment, we decided to check whether H_2S also presents in gas hydrate. By using Raman spectroscopy analysis, H_2S was confirmed to be enclathrated in gas hydrate which is very a very exciting discovery because H_2S containing gas hydrates have only been found in Hydrate Ridge (Hester et al., 2007) and Niger Delta (Chazallon et al., 2007). In order to know whether this phenomenon also occurs in other areas, we investigated more samples from gas seeps in the Makran continental margin and the Black Sea. Surprisingly, we found more H_2S containing gas hydrates. Therefore, the questions raised here are: Where does H_2S in gas hydrate originate from? Does H_2S distribute homogenously or heterogeneously in gas hydrate? Does this type of gas hydrate occur in certain depths or all through the core, and what is the controlling factor? What is its significance on seafloor chemosynthetic communities and hydrate stability?

What is the structure and gas composition of gas hydrates? What are the impacts of small amount of CO_2 and H_2S on the hydrate structure?

By applying multiple methods, including gas chromatography, Raman scattering and X-ray diffraction, the structure and hydrate-bonding gas composition of gas hydrates recovered from pockmarks on Nigerian continental margin could be known. Therefore, questions

raised are: what are the other gas components other than hydrocarbons? Where do they come from? What are their effects on gas hydrate structure and hydrate phase boundary.

1.7 My contribution to the manuscripts

There are three manuscripts included in this thesis which are chapter 3, 4 and 5. In each manuscript, as the co-author and my supervisor, Prof. Bohrmann discussed the scientific questions with me at the very beginning. I wrote the main text including the discussion part independently based on the discussions. All co-authors commented on the first draft and I revised the manuscripts according to their comments. There are many lab work and data analysis involved in these manuscripts. The detail of the work is explained as follows:

In the first manuscript (chapter 3), I did all the work related to the infrared thermal scanning and sediment temperature measurement independently, including lab work, data analysis and interpretation. Carl A. Peters and Livio Ruffine did the measurement of pore water chloride concentration and I did the data analysis and interpretation.

In the second manuscript (chapter 4), I closely cooperated in lab work with Thomas Pape, Andrzej Falenty and Junfeng Qin, respectively. Data analysis and interpretation was done by me independently.

In the third manuscript (chapter 5), I did the sample preparation, data analysis and interpretation. I was also involved in the lab work related to Raman spectroscopy.

Reference

Abegg, F., Bohrmann, G., Freitag, J., and Kuhs, W., 2007, Fabric of gas hydrate in sediments from Hydrate Ridge—results from ODP Leg 204 samples: Geo-Marine Letters, v. 27, no. 2-4, p. 269-277.

Abegg, F., Bohrmann, G., and Kuhs, W., Data report: Shapes and structures of gas hydrates imaged by computed tomographic-analyses, ODP Leg 204, Hydrate Ridge, *in* Proceedings Proceedings of Ocean Drilling Program, Scientific Results2006, Volume 204, p. 1-11.

Andreassen, K., Hart, P., and Grantz, A., 1995, Seismic studies of a bottom simulating reflection related to gas hydrate beneath the continental margin of the Beaufort Sea: Journal of Geophysical Research: Solid Earth (1978–2012), v. 100, no. B7, p. 12659-12673.

Andreassen, K., Mienert, J., Bryn, P., and Singh, S. C., 2000, A double gas-hydrate related bottom simulating reflector at the Norwegian continental margin: Annals of the New York Academy of Sciences, v. 912, no. 1, p. 126-135.

Archer, D., Buffett, B., and Brovkin, V., 2009, Ocean methane hydrates as a slow tipping point in the global carbon cycle: Proceedings of the National Academy of Sciences, v. 106, no. 49, p. 20596-20601.

Bahk, J.-J., Kim, J.-H., Kong, G.-S., Park, Y., Lee, H., Park, Y., and Park, K. P., 2009, Occurrence of near-seafloor gas hydrates and associated cold vents in the Ulleung Basin, East Sea: Geosciences Journal, v. 13, no. 4, p. 371-385.

Bahk, J.-J., Um, I.-K., and Holland, M., 2011, Core lithologies and their constraints on gas-hydrate occurrence in the East Sea, offshore Korea: Results from the site UBGH1-9: Marine and Petroleum Geology, v. 28, no. 10, p. 1943-1952.

Bekins, B., McCaffrey, A. M., and Dreiss, S. J., 1994, Influence of kinetics on the smectite to illite transition in the Barbados accretionary prism: Journal of Geophysical Research: Solid Earth (1978–2012), v. 99, no. B9, p. 18147-18158.

Bekins, B. A., McCaffrey, A. M., and Dreiss, S. J., 1995, Episodic and constant flow models for the origin of low-chloride waters in a modern accretionary complex: Water Resources Research, v. 31, no. 12, p. 3205-3215.

Berndt, C., Bünz, S., Clayton, T., Mienert, J., and Saunders, M., 2004, Seismic character of bottom simulating reflectors: examples from the mid-Norwegian margin: Marine and Petroleum Geology, v. 21, no. 6, p. 723-733.

Bohrmann, G., and Torres, M. E., 2006, Gas hydrates in marine sediments, Marine Geochemistry, Springer, p. 481-512.

Boswell, R., Collett, T., McConnell, D., Frye, M., Shedd, B., Mrozewski, S., Guerin, G., Cook, A., Godfriaux, P., and Dufrene, R., 2009, Joint Industry Project Leg II discovers rich gas hydrate accumulations in sand reservoirs in the Gulf of Mexico: Natural Gas & Oil, v. 304, p. 285-4541.

Boswell, R., and Collett, T. S., 2011, Current perspectives on gas hydrate resources: Energy & environmental science, v. 4, no. 4, p. 1206-1215.

Brewer, P. G., Orr, F. M., Friederich, G., Kvenvolden, K. A., Orange, D. L., McFarlane, J., and Kirkwood, W., 1997, Deep-ocean field test of methane hydrate formation from a remotely operated vehicle: Geology, v. 25, no. 5, p. 407-410.

Chazallon, B., Focsa, C., Charlou, J.-L., Bourry, C., and Donval, J.-P., 2007, A comparative Raman spectroscopic study of natural gas hydrates collected at different geological sites: Chemical Geology, v. 244, no. 1–2, p. 175-185.

Chi, W.-C., Reed, D. L., Liu, C.-S., and Lundberg, N., 1998, Distribution of the bottom-simulating reflector in the offshore Taiwan collision zone: Terr. Atmos. Ocean. Sci, v. 9, no. 4, p. 779-794.

Collett, T. S., and Ladd, J., 19. Detection of gas hydrate with downhole logs and assessment of gas hydrate concentrations (saturations) and gas volumes on the Blake Ridge with electrical resistivity log data, *in* Proceedings Proceedings of the Ocean Drilling Program. Scientific results2000, Volume 164, Ocean Drilling Program, p. 179-191.

Davy, H., 1811, The Bakerian Lecture: On Some of the Combinations of Oxymuriatic Gas and Oxygene, and on the Chemical Relations of These Principles, to Inflammable Bodies: Philosophical Transactions of the Royal Society of London, v. 101, p. 1-35.

Dickens, G. R., 2003, Rethinking the global carbon cycle with a large, dynamic and microbially mediated gas hydrate capacitor: Earth and Planetary Science Letters, v. 213, no. 3, p. 169-183.

Dickens, G. R., Paull, C. K., and Wallace, P., 1997, Direct measurement of in situ methane quantities in a large gas-hydrate reservoir.

Dickens, G. R., and Quinby-Hunt, M. S., 1994, Methane hydrate stability in seawater: Geophysical Research Letters, v. 21, no. 19, p. 2115-2118.

Dvorkin, J., and Nur, A., 1993, Dynamic poroelasticity: A unified model with the squirt and the Biot mechanisms: Geophysics, v. 58, no. 4, p. 524-533.

Ecker, C., Dvorkin, J., and Nur, A. M., 2000, Estimating the amount of gas hydrate and free gas from marine seismic data: Geophysics, v. 65, no. 2, p. 565-573.

Edwards, R. N., 1997, On the resource evaluation of marine gas hydrate deposits using sea-floor transient electric dipole-dipole methods: Geophysics, v. 62, no. 1, p. 63-74.

Ford, K., Naehr, T., and Skilbeck, C., 2003, The use of infrared thermal imaging to identify gas hydrate in sediment cores.

Foucher, J.-P., Nouzé, H., and Henry, P., 2002, Observation and tentative interpretation of a double BSR on the Nankai slope: Marine Geology, v. 187, no. 1, p. 161-175.

Goldberg, D., 1997, The role of downhole measurements in marine geology and geophysics: Reviews of Geophysics, v. 35, no. 3, p. 315-342.

Goldberg, D., and Saito, S., 1998, Detection of gas hydrates using downhole logs: Geological Society, London, Special Publications, v. 137, no. 1, p. 129-132.

Greinert, J., Artemov, Y., Egorov, V., De Batist, M., and McGinnis, D., 2006, 1300-m-high rising bubbles from mud volcanoes at 2080m in the Black Sea: Hydroacoustic characteristics and temporal variability: Earth and Planetary Science Letters, v. 244, no. 1–2, p. 1-15.

Grevemeyer, I., and Villinger, H., 2001, Gas hydrate stability and the assessment of heat flow through continental margins: Geophysical Journal International, v. 145, no. 3, p. 647-660.

Haacke, R. R., Westbrook, G. K., and Riley, M. S., 2008, Controls on the formation and stability of gas hydrate-related bottom-simulating reflectors (BSRs): A case study from the west Svalbard continental slope: Journal of Geophysical Research: Solid Earth (1978–2012), v. 113, no. B5.

Haeckel, M., Suess, E., Wallmann, K., and Rickert, D., 2004, Rising methane gas bubbles form massive hydrate layers at the seafloor: Geochimica et Cosmochimica Acta, v. 68, no. 21, p. 4335-4345.

Hammerschmidt, E., 1934, Formation of gas hydrates in natural gas transmission lines: Industrial & Engineering Chemistry, v. 26, no. 8, p. 851-855.

Heeschen, K., Haeckel, M., Klaucke, I., Ivanov, M., and Bohrmann, G., 2011, Quantifying in-situ gas hydrates at active seep sites in the eastern Black Sea using pressure coring technique: Biogeosciences Discussions, v. 8, no. 3, p. 4529-4558.

Heeschen, K. U., Hohnberg, H. J., Haeckel, M., Abegg, F., Drews, M., and Bohrmann, G., 2007, In situ hydrocarbon concentrations from pressurized cores in surface sediments, Northern Gulf of Mexico: Marine Chemistry, v. 107, no. 4, p. 498-515.

Helgerud, M., Dvorkin, J., Nur, A., Sakai, A., and Collett, T., 1999, Elastic-wave velocity in marine sediments with gas hydrates: Effective medium modeling: Geophysical Research Letters, v. 26, no. 13, p. 2021-2024.

Henriet, J.-P., and Mienert, J., Gas hydrates: relevance to world margin stability and climate change1998, Geological Society of London.

Hesse, R., 2003, Pore water anomalies of submarine gas-hydrate zones as tool to assess hydrate abundance and distribution in the subsurface: What have we learned in the past decade?: Earth-Science Reviews, v. 61, no. 1–2, p. 149-179.

Hester, K. C., and Brewer, P. G., 2009, Clathrate hydrates in nature: Annual review of marine science, v. 1, p. 303-327.

Hester, K. C., Dunk, R. M., White, S. N., Brewer, P. G., Peltzer, E. T., and Sloan, E. D., 2007, Gas hydrate measurements at Hydrate Ridge using Raman spectroscopy: Geochimica et Cosmochimica Acta, v. 71, no. 12, p. 2947-2959.

Hiruta, A., Snyder, G. T., Tomaru, H., and Matsumoto, R., 2009, Geochemical constraints for the formation and dissociation of gas hydrate in an area of high methane flux, eastern margin of the Japan Sea: Earth and Planetary Science Letters, v. 279, no. 3, p. 326-339.

Hobro, J., Minshull, T., Singh, S., and Chand, S., 2005, A three-dimensional seismic tomographic study of the gas hydrate stability zone, offshore Vancouver Island: Journal of Geophysical Research: Solid Earth (1978–2012), v. 110, no. B9.

Holbrook, W., Lizarralde, D., Pecher, I., Gorman, A., Hackwith, K., Hornbach, M., and Saffer, D., 2002, Escape of methane gas through sediment waves in a large methane hydrate province: Geology, v. 30, no. 5, p. 467-470.

Holbrook, W. S., Hoskins, H., Wood, W. T., Stephen, R. A., and Lizarralde, D., 1996, Methane hydrate and free gas on the Blake Ridge from vertical seismic profiling: Science, v. 273, no. 5283, p. 1840-1843.

Horozal, S., Lee, G. H., Yi, B. Y., Yoo, D. G., Park, K. P., Lee, H. Y., Kim, W., Kim, H. J., and Lee, K., 2009, Seismic indicators of gas hydrate and associated gas in the Ulleung Basin, East Sea (Japan Sea) and implications of heat flows derived from depths of the bottom-simulating reflector: Marine Geology, v. 258, no. 1, p. 126-138.

Hyndman, R., and Spence, G., 1992, A seismic study of methane hydrate marine bottom simulating reflectors: Journal of Geophysical Research: Solid Earth (1978–2012), v. 97, no. B5, p. 6683-6698.

Hyndman, R., Yuan, T., and Moran, K., 1999, The concentration of deep sea gas hydrates from downhole electrical resistivity logs and laboratory data: Earth and Planetary Science Letters, v. 172, no. 1, p. 167-177.

Jahren, A. H., Arens, N. C., Sarmiento, G., Guerrero, J., and Amundson, R., 2001, Terrestrial record of methane hydrate dissociation in the Early Cretaceous: Geology, v. 29, no. 2, p. 159-162.

Jenkyns, H. C., 2003, Evidence for rapid climate change in the Mesozoic–Palaeogene greenhouse world: Philosophical Transactions of the Royal Society of London.

Series A: Mathematical, Physical and Engineering Sciences, v. 361, no. 1810, p. 1885-1916.

Katz, M. E., Pak, D. K., Dickens, G. R., and Miller, K. G., 1999, The source and fate of massive carbon input during the latest Paleocene thermal maximum: Science, v. 286, no. 5444, p. 1531-1533.

Kayen, R. E., and Lee, H. J., 1991, Pleistocene slope instability of gas hydrate-laden sediment on the Beaufort sea margin: Marine Georesources & Geotechnology, v. 10, no. 1-2, p. 125-141.

Kennett, J. P., Cannariato, K. G., Hendy, I. L., and Behl, R. J., 2003, Methane hydrates in Quaternary climate change: The clathrate gun hypothesis, American Geophysical Union.

Kinoshita, M., Moore, G. F., and Kido, Y. N., 2011, Heat flow estimated from BSR and IODP borehole data: Implication of recent uplift and erosion of the imbricate thrust zone in the Nankai Trough off Kumano: Geochemistry, Geophysics, Geosystems, v. 12, no. 9.

Klaucke, I., Sahling, H., Weinrebe, W., Blinova, V., Bürk, D., Lursmanashvili, N., and Bohrmann, G., 2006, Acoustic investigation of cold seeps offshore Georgia, eastern Black Sea: Marine Geology, v. 231, no. 1, p. 51-67.

Klaucke, I., Weinrebe, W., Linke, P., Kläschen, D., and Bialas, J., 2012, Sidescan sonar imagery of widespread fossil and active cold seeps along the central Chilean continental margin: Geo-Marine Letters, v. 32, no. 5-6, p. 489-499.

Klaucke, I., Weinrebe, W., Sahling, H., and Bohrmann, G., 2005, Mapping deep-water gas emissions with sidescan sonar: Eos, Transactions American Geophysical Union, v. 86, no. 38, p. 341-346.

Kvenvolden, K. A., 1985, 23. Gas hydrates of the middle America trench-deep sea drilling project Leg 84.

Kvenvolden, K. A., 1993, Gas hydrates—geological perspective and global change: Reviews of Geophysics, v. 31, no. 2, p. 173-187.

Lee, S.-Y., and Holder, G. D., 2001, Methane hydrates potential as a future energy source: Fuel Processing Technology, v. 71, no. 1, p. 181-186.

Liu, X., and Flemings, P. B., 2007, Dynamic multiphase flow model of hydrate formation in marine sediments: Journal of Geophysical Research: Solid Earth (1978–2012), v. 112, no. B3.

Long, P., Ussler III, W., Weinberger, J., Riedel, M., and Tréhu, A., Quantification of gas hydrate abundance from infrared imaging of sub-seafloor cores, *in* Proceedings AAPG Hedberg conference2004.

Lu, H., Seo, Y.-t., Lee, J.-w., Moudrakovski, I., Ripmeester, J. A., Chapman, N. R., Coffin, R. B., Gardner, G., and Pohlman, J., 2007, Complex gas hydrate from the Cascadia margin: Nature, v. 445, no. 7125, p. 303-306.

Lu, S., and McMechan, G. A., 2002, Estimation of gas hydrate and free gas saturation, concentration, and distribution from seismic data: Geophysics, v. 67, no. 2, p. 582-593.

Makogon, Y. F., 1965, Hydrate formation in the gas-bearing beds under permafrost conditions: Gazovaia Promyshlennost, v. 5, p. 14-15.

Makogon, Y. F., Trebin, F., Trofimuk, A., Tsarev, V., and Cherskiy, N., Detection of a pool of natural gas in a solid (hydrated gas) state, *in* Proceedings Doklady of the Academy of Sciences of the USSR-Earth Science Sections1971, Volume 196, p. 197.

Malone, R., 1985, Gas hydrates topical report: DOE/METC/SP-218, US Department of Energy, p. 33-50.

Manasseh, R., and Ooi, A., 2009, Frequencies of acoustically interacting bubbles: Bubble Science, Engineering & Technology, v. 1, no. 1-2, p. 58-74.

Maslin, M., Mikkelsen, N., Vilela, C., and Haq, B., 1998, Sea level and gas hydrate controlled catastrophic sediment failures of the Amazon Fan: Geology, v. 26, no. 12, p. 1107-1110.

Mathews, M., 1986, Logging characteristics of methane hydrate: The Log Analyst, v. 27, no. 03.

Mathews, M., and Vonhuene, R., 1985, site-570 Methane hydrate zone: Initial Reports of the Deep Sea Drilling Project, v. 84, no. May, p. 773-790.

Mienert, J., Posewang, J., and Baumann, M., 1998, Gas hydrates along the northeastern Atlantic margin: possible hydrate-bound margin instabilities and possible release of methane: Geological Society, London, Special Publications, v. 137, no. 1, p. 275-291.

Milkov, A. V., Claypool, G. E., Lee, Y.-J., Xu, W., Dickens, G. R., and Borowski, W. S., 2003, In situ methane concentrations at Hydrate Ridge, offshore Oregon: New constraints on the global gas hydrate inventory from an active margin: Geology, v. 31, no. 10, p. 833-836.

Milkov, A. V., and Sassen, R., 2002, Economic geology of offshore gas hydrate accumulations and provinces: Marine and Petroleum Geology, v. 19, no. 1, p. 1-11.

Moridis, G. J., Collett, T. S., Boswell, R., Hancock, S., Rutqvist, J., Santamarina, C., Kneafsey, T., Reagan, M. T., Pooladi-Darvish, M., and Kowalsky, M., 2013, Gas Hydrates as a Potential Energy Source: State of Knowledge and Challenges, Advanced Biofuels and Bioproducts, Springer, p. 977-1033.

Nikolovska, A., Sahling, H., and Bohrmann, G., 2008, Hydroacoustic methodology for detection, localization, and quantification of gas bubbles rising from the seafloor at gas seeps from the eastern Black Sea: Geochemistry, Geophysics, Geosystems, v. 9, no. 10.

Ostrander, W., 1984, Plane-wave reflection coefficients for gas sands at nonnormal angles of incidence: Geophysics, v. 49, no. 10, p. 1637-1648.

Pape, T., Bahr, A., Klapp, S. A., Abegg, F., and Bohrmann, G., 2011, High-intensity gas seepage causes rafting of shallow gas hydrates in the southeastern Black Sea: Earth and Planetary Science Letters, v. 307, no. 1, p. 35-46.

Pape, T., Bahr, A., Rethemeyer, J., Kessler, J. D., Sahling, H., Hinrichs, K.-U., Klapp, S. A., Reeburgh, W. S., and Bohrmann, G., 2010, Molecular and isotopic partitioning of low-molecular-weight hydrocarbons during migration and gas hydrate precipitation in deposits of a high-flux seepage site: Chemical Geology, v. 269, no. 3–4, p. 350-363.

Reagan, M. T., and Moridis, G. J., 2007, Oceanic gas hydrate instability and dissociation under climate change scenarios: Geophysical research letters, v. 34, no. 22.

Riedel, M., Collett, T., and Malone, M., 2005, Expedition 311 Scientists, Cascadia margin gas hydrates: Proc. IODP, v. 311.

Riedel, M., Collett, T. S., and Shankar, U., 2011, Documenting channel features associated with gas hydrates in the Krishna–Godavari Basin, offshore India: Marine Geology, v. 279, no. 1–4, p. 1-11.

Riedel, M., Spence, G., Chapman, N., and Hyndman, R., 2002, Seismic investigations of a vent field associated with gas hydrates, offshore Vancouver Island: Journal of Geophysical Research: Solid Earth (1978–2012), v. 107, no. B9, p. EPM 5-1-EPM 5-16.

Ripmeester, J. A., John, S. T., Ratcliffe, C. I., and Powell, B. M., 1987, A new clathrate hydrate structure: Nature, v. 325, no. 6100, p. 135-136.

Römer, M., Sahling, H., Pape, T., Bahr, A., Feseker, T., Wintersteller, P., and Bohrmann, G., 2012, Geological control and magnitude of methane ebullition from a high-flux seep area in the Black Sea—the Kerch seep area: Marine Geology, v. 319–322, no. 0, p. 57-74.

Römer, M., Sahling, H., Pape, T., dos Santos Ferreira, C., Wenzhöfer, F., Boetius, A., and Bohrmann, G., 2014a, Methane fluxes and carbonate deposits at a cold seep area of the Central Nile Deep Sea Fan, Eastern Mediterranean Sea: Marine Geology, v. 347, p. 27-42.

Römer, M., Torres, M., Kasten, S., Kuhn, G., Graham, A. G., Mau, S., Little, C. T., Linse, K., Pape, T., and Geprägs, P., 2014b, First evidence of widespread active methane

seepage in the Southern Ocean, off the sub-Antarctic island of South Georgia: Earth and Planetary Science Letters, v. 403, p. 166-177.

Sain, K., Minshull, T., Singh, S., and Hobbs, R., 2000, Evidence for a thick free gas layer beneath the bottom simulating reflector in the Makran accretionary prism: Marine Geology, v. 164, no. 1, p. 3-12.

Shedd, W., Boswell, R., Frye, M., Godfriaux, P., and Kramer, K., 2012, Occurrence and nature of "bottom simulating reflectors" in the northern Gulf of Mexico: Marine and Petroleum Geology, v. 34, no. 1, p. 31-40.

Shipboard Scientific Party, 1996, Sites 994, 995, and 997 (Leg 164): Proceedings of the Ocean Drilling Program, initial reports, v. 164, p. 99-623.

Sloan, E. D., and Koh, C., 2007, Clathrate hydrates of natural gases, CRC press.

Stackelberg, M. v., and Müller, H., 1951, On the structure of gas hydrates: The Journal of Chemical Physics, v. 19, no. 10, p. 1319-1320.

Subramanian, S., Ballard, A., Kini, R., Dec, S., and Sloan, E., 2000a, Structural transitions in methane+ ethane gas hydrates—part I: upper transition point and applications: Chemical Engineering Science, v. 55, no. 23, p. 5763-5771.

Subramanian, S., Kini, R. A., Dec, S. F., and Sloan Jr, E. D., 2000b, Evidence of structure II hydrate formation from methane+ethane mixtures: Chemical Engineering Science, v. 55, no. 11, p. 1981-1999.

Sultan, N., Marsset, B., Ker, S., Marsset, T., Voisset, M., Vernant, A. M., Bayon, G., Cauquil, E., Adamy, J., Colliat, J. L., and Drapeau, D., 2010, Hydrate dissolution as a potential mechanism for pockmark formation in the Niger delta: Journal of Geophysical Research: Solid Earth, v. 115, no. B8, p. B08101.

Swart, P. K., Wortmann, U. G., Mitterer, R. M., Malone, M. J., Smart, P. L., Feary, D. A., and Hine, A. C., 2000, Hydrogen sulfide–hydrates and saline fluids in the continental margin of South Australia: Geology, v. 28, no. 11, p. 1039-1042.

Torres, M., Collett, T., Rose, K., Sample, J., Agena, W., and Rosenbaum, E., 2011a, Pore fluid geochemistry from the Mount Elbert gas hydrate stratigraphic test well, Alaska North Slope: Marine and Petroleum Geology, v. 28, no. 2, p. 332-342.

Torres, M., Trehu, A. M., Cespedes, N., Kastner, M., Wortmann, U., Kim, J.-H., Long, P., Malinverno, A., Pohlman, J., and Riedel, M., 2008, Methane hydrate formation in turbidite sediments of northern Cascadia, IODP Expedition 311: Earth and Planetary Science Letters, v. 271, no. 1, p. 170-180.

Torres, M. E., Kim, J.-H., Choi, J.-Y., Ryu, B.-J., Bahk, J.-J., Riedel, M., Collett, T. S., Hong, W.-L., and Kastner, M., Occurrence of high salinity fluids associated with massive near-seafloor gas hydrate deposits, *in* Proceedings 7th International Conference on Gas Hydrates (ICGH 2011) 2011b.

Torres, M. E., Teichert, B. M. A., Tréhu, A. M., Borowski, W., and Tomaru, H., 2004a, Relationship of pore water freshening to accretionary processes in the Cascadia margin: Fluid sources and gas hydrate abundance: Geophysical Research Letters, v. 31, no. 22, p. L22305.

Torres, M. E., Wallmann, K., Tréhu, A. M., Bohrmann, G., Borowski, W. S., and Tomaru, H., 2004b, Gas hydrate growth, methane transport, and chloride enrichment at the southern summit of Hydrate Ridge, Cascadia margin off Oregon: Earth and Planetary Science Letters, v. 226, no. 1-2, p. 225-241.

Townend, J., 1997, Estimates of conductive heat flow through bottom-simulating reflectors on the Hikurangi and southwest Fiordland continental margins, New Zealand: Marine Geology, v. 141, no. 1, p. 209-220.

Tréhu, A., Ruppel, C., Holland, M., Dickens, G., Torres, M., Collett, T., Goldberg, D., Riedel, M., and Schultheiss, P., 2006, Gas hydrates in marine sediments: Lessons from scientific ocean drilling: Oceanography, v. 19, no. 4, p. 124-142.

Tréhu, A. M., Flemings, P. B., Bangs, N. L., Chevallier, J., Gràcia, E., Johnson, J. E., Liu, C. S., Liu, X., Riedel, M., and Torres, M. E., 2004a, Feeding methane vents and gas hydrate deposits at south Hydrate Ridge: Geophysical Research Letters, v. 31, no. 23.

Tréhu, A. M., Long, P. E., Torres, M. E., Bohrmann, G., Rack, F. R., Collett, T. S., Goldberg, D. S., Milkov, A. V., Riedel, M., Schultheiss, P., Bangs, N. L., Barr, S. R., Borowski, W. S., Claypool, G. E., Delwiche, M. E., Dickens, G. R., Gracia, E., Guerin, G., Holland, M., Johnson, J. E., Lee, Y. J., Liu, C. S., Su, X., Teichert, B., Tomaru, H., Vanneste, M., Watanabe, M., and Weinberger, J. L., 2004b, Three-dimensional distribution of gas hydrate beneath southern Hydrate Ridge: constraints from ODP Leg 204: Earth and Planetary Science Letters, v. 222, no. 3–4, p. 845-862.

Tréhu, A. M., Stakes, D. S., Bartlett, C. D., Chevallier, J., Duncan, R. A., Goffredi, S. K., Potter, S. M., and Salamy, K. A., 2003, Seismic and seafloor evidence for free gas, gas hydrates, and fluid seeps on the transform margin offshore Cape Mendocino: Journal of Geophysical Research: Solid Earth (1978–2012), v. 108, no. B5.

Trehu, A. M., Torres, M. E., Bohrmann, G., and Colwell, F., 2006, Leg 204 synthesis: Gas hydrate distribution and dynamics in the central Cascadia accretionary complex.

von Huene, R., and Pecher, I. A., 1999, Vertical tectonics and the origins of BSRs along the Peru margin: Earth and Planetary Science Letters, v. 166, no. 1, p. 47-55.

Waite, W. F., Santamarina, J. C., Cortes, D. D., Dugan, B., Espinoza, D., Germaine, J., Jang, J., Jung, J., Kneafsey, T. J., and Shin, H., 2009, Physical properties of hydrate-bearing sediments: Reviews of Geophysics, v. 47, no. 4.

Wang, X., Hutchinson, D. R., Wu, S., Yang, S., and Guo, Y., 2011, Elevated gas hydrate saturation within silt and silty clay sediments in the Shenhu area, South China Sea: Journal of Geophysical Research: Solid Earth, v. 116, no. B5, p. B05102.

Wang, X., Wu, S., Yuan, S., Wang, D., Ma, Y., Yao, G., Gong, Y., and Zhang, G., 2010, Geophysical signatures associated with fluid flow and gas hydrate occurrence in a tectonically quiescent sequence, Qiongdongnan Basin, South China Sea: Geofluids, v. 10, no. 3, p. 351-368.

Weinberger, J. L., Brown, K. M., and Long, P. E., 2005, Painting a picture of gas hydrate distribution with thermal images: Geophysical Research Letters, v. 32, no. 4.

Weitemeyer, K., Constable, S., Key, K., and Behrens, J., 2006, First results from a marine controlled-source electromagnetic survey to detect gas hydrates offshore Oregon: Geophysical Research Letters, v. 33, no. 3.

Westbrook, G., Chand, S., Rossi, G., Long, C., Bünz, S., Camerlenghi, A., Carcione, J., Dean, S., Foucher, J.-P., and Flueh, E., 2008, Estimation of gas hydrate concentration from multi-component seismic data at sites on the continental margins of NW Svalbard and the Storegga region of Norway: Marine and Petroleum Geology, v. 25, no. 8, p. 744-758.

Willoughby, E. C., Schwalenberg, K., Edwards, R. N., Spence, G. D., and Hyndman, R. D., Assessment of marine gas hydrate deposits: a comparative study of seismic, electromagnetic and seafloor compliance methods, *in* Proceedings International conference on gas hydrates, Trondheim, Norway2005.

Wood, W. T., Stoffa, P. L., and Shipley, T. H., 1994, Quantitative detection of methane hydrate through high-resolution seismic velocity analysis: Journal of Geophysical Research: Solid Earth (1978–2012), v. 99, no. B5, p. 9681-9695.

Xu, W., and Ruppel, C., 1999, Predicting the occurrence, distribution, and evolution of methane gas hydrate in porous marine sediments: Journal of Geophysical Research: Solid Earth (1978–2012), v. 104, no. B3, p. 5081-5095.

Yamano, M., Uyeda, S., Aoki, Y., and Shipley, T., 1982, Estimates of heat flow derived from gas hydrates: Geology, v. 10, no. 7, p. 339-343.

Yefremova, A., and Zhizhchenko, B., 1974, Occurrence of crystal hydrates of gases in the sediments of modern marine basins: Doklady Akademii Nauk SSSR, v. 214, no. 5, p. 1179-1181.

Yuan, J., and Edwards, R., 2000, The assessment of marine gas hydrates through electrical remote sounding: hydrate without a BSR?: Geophysical Research Letters, v. 27, no. 16, p. 2397-2400.

Yuan, T., Hyndman, R., Spence, G., and Desmons, B., 1996, Seismic velocity increase and deep-sea gas hydrate concentration above a bottom-simulating reflector on the

northern Cascadia continental slope: Journal of Geophysical Research: Solid Earth (1978–2012), v. 101, no. B6, p. 13655-13671.

Yun, T., Francisca, F., Santamarina, J., and Ruppel, C., 2005, Compressional and shear wave velocities in uncemented sediment containing gas hydrate: Geophysical Research Letters, v. 32, no. 10.

Zillmer, M., Flueh, E. R., and Petersen, J., 2005, Seismic investigation of a bottom simulating reflector and quantification of gas hydrate in the Black Sea: Geophysical Journal International, v. 161, no. 3, p. 662-678.

Chapter 2 Sampling sites, materials and methods

2.1 Sampling sites

Gas hydrates investigated in this thesis were sampled at seepage sites of the Nigerian continental margin, the Makran continental margin and Black Sea, respectively (Figure 2.1). Detailed information about the study areas are described in the following sections.

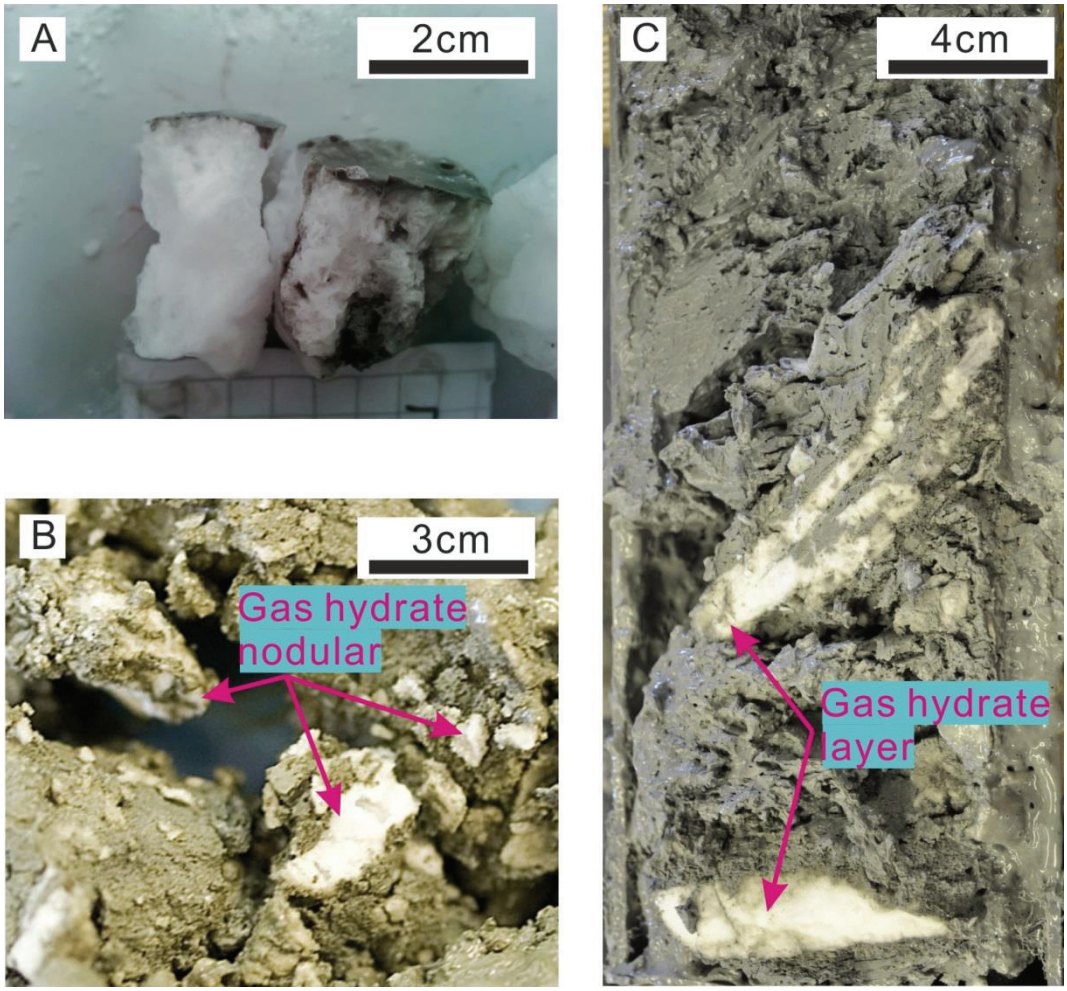

Figure 2.1 Representative gas hydrate occurrence at seepage sites of the Nigerian continental margin (A: GMGC17), the Makran continental margin (B: GeoB 12316-3) and the Black Sea (C: GeoB 15268-1).

2.1.1 The Nigerian continental margin

At the continental margin off Nigeria, sediment has been deformed by compressional gravity tectonism, leading to the formation of diapirism, faults and folding. Three regional structural styles are defined in this area (Damuth, 1994): (1) upper extensional region beneath the outer continental shelf characterized by deep rooted faults; (2) intermediate translational region beneath the continental slope characterized by shale diapirs; (3) lower compressional region beneath the lower continental slope characterized by toe thrusts.

These structural styles indicate that large part of the thick sediment deposits is moving slowly downslope driven by gravity which is similar to mega-landslides.

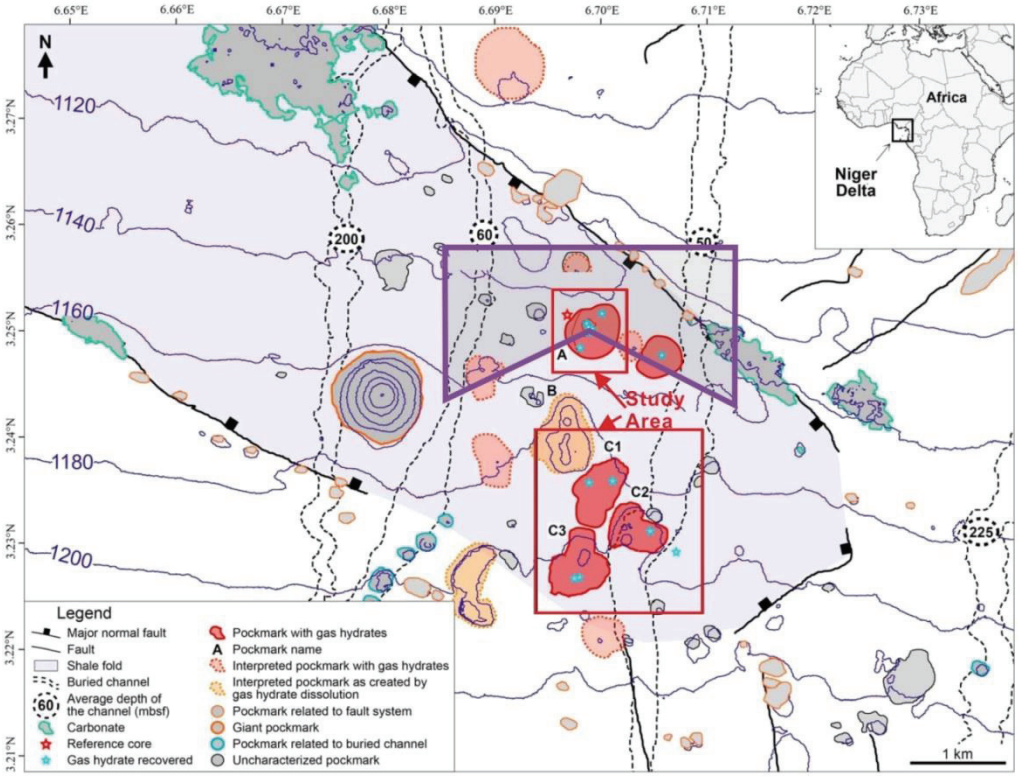

Figure 2.2 Location of pockmark field at the Nigerian continental margin with interpreted seafloor features (after Sultan et al., 2014). Purple box indicate the location of Figure 2.4.

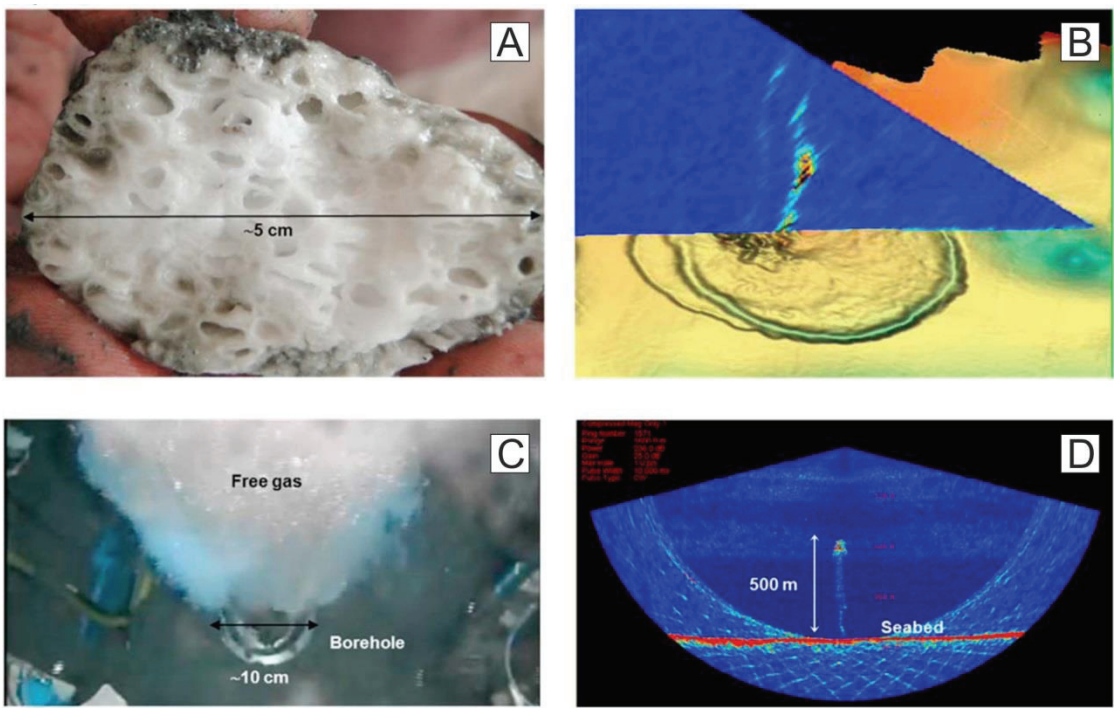

Figure 2.3 (A): Photograph of hydrate specimen with bubble fabric structure sampled from the central area of pockmark A. (B) and (D): Gas plumes sources in the central part of pockmark A detected using the multibeam echosounder (SeaBat 7150). Gas flares disappear completely 500m above the seabed

(around 600m below the sea surface) (C) Gas escape from a gas pocket at around 18 mbsf during the MeBo drilling of GMMB04 (after sultan et al., 2014).

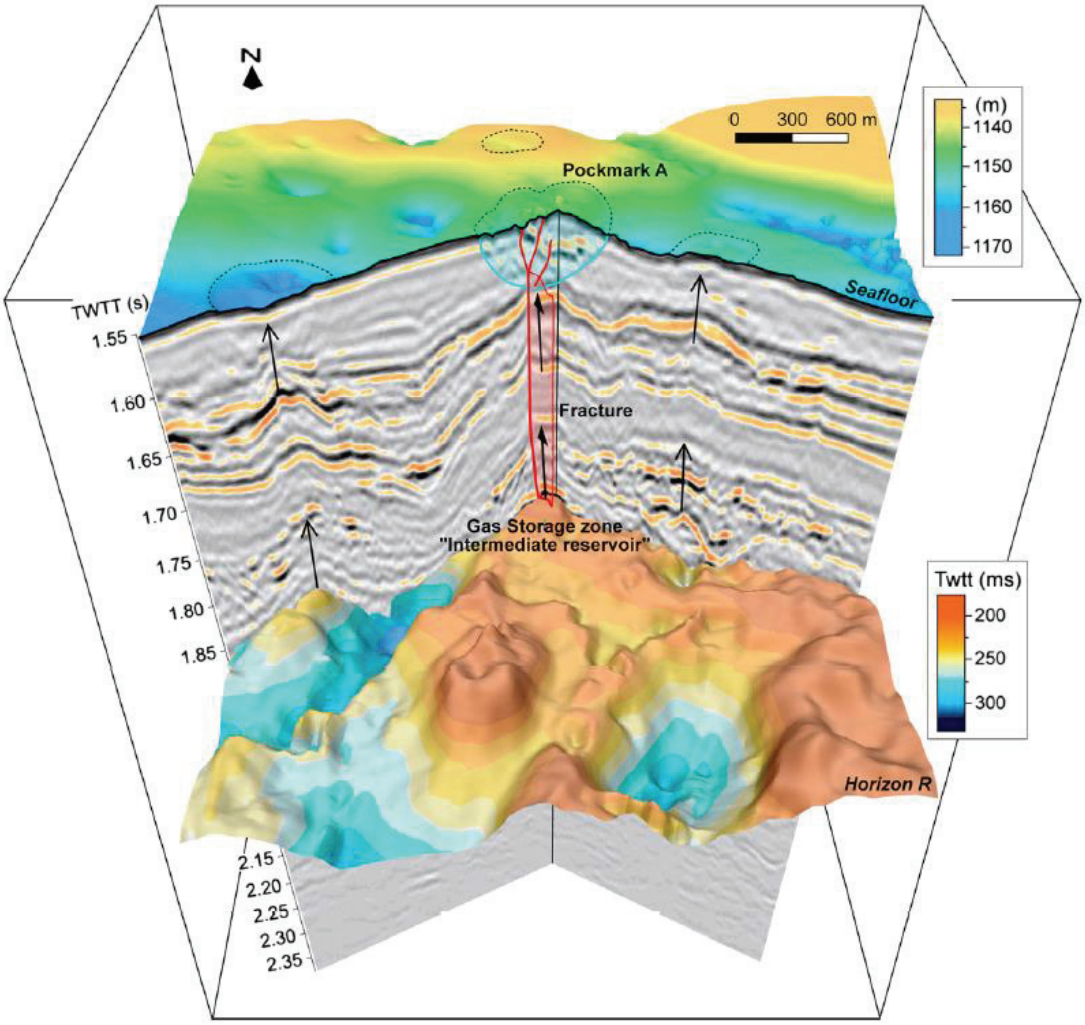

Figure 2.4 Gas migration pathways from gas reservoir to seafloor in pockmark A (after Sultan et al., 2014)

From a tectonic-stratigraphic point of view, the study area (a pockmark field) is located within the translational zone. The pockmark field comprises pockmarks A and C which lies at water depths between 1141 and 1199 m within a SE–NW trend area confined by two boundaries clearly shown on bathymetry map (Figure 2.2). The two boundaries correspond to normal faults, which define a collapsed zone related to a subsurface anticline structure. Pockmark A is a slightly NE-SW elongated seafloor feature with a hummocky topography in the center. The hummocky seafloor morphology corresponds to high backscatter of multibeam echosounder data (George and Cauquil, 2007) which might indicate the presence of shallow hydrates, authigenic carbonates and/or free gas (Sultan et al., 2014; Sultan et al., 2010). Gas emission from the central part of pockmark A (Figure 2.3 B and D) was observed by using multibeam echosounder (SeaBat 7150). Gas hydrates with bubble

fabric internal structure were recovered from the center of pockmark A which indicates hydrate formation directly from free gas bubbles trapped in the sediment during migration (Figure 2.3A). Figure 2.4 shows that vertical fractures underneath pockmark A serve as the conduit for fast fluid migration from deep reservoir to the seafloor. Pockmark C consists of at least three small pockmarks (C1 - C3). Within this pockmark field, gas hydrates in shallow sediment might contribute to the seafloor morphological changes and evolution of the pockmarks.

2.1.2 The Makran continental margin

The Makran accretionary wedge offshore Pakistan and Iran was formed by the Arabian subduction under the Eurasian Plate started since the Late Cretaceous (Figure 2.5) (De Jong, 1982). The average rate of convergence is about 4 cm/yr decreasing from east to west (DeMets et al., 1990). The deformation front is located 150 km seaward from the shoreline. A remarkable thick sediment deposit, up to 7 km, moves in the subduction zone. The upper 4 km of the entering sediment on the subducted plate becomes incorporated and offscraped in the Makran accretionary wedge, the lower part is underthrusted and partly underplated northward to the hinterland (Kopp et al., 2000). This causes substantial uplift of approximately 1.5 mm/yr (White and Louden, 1982) and the seaward movement of the coastline (Kopp et al., 2000).

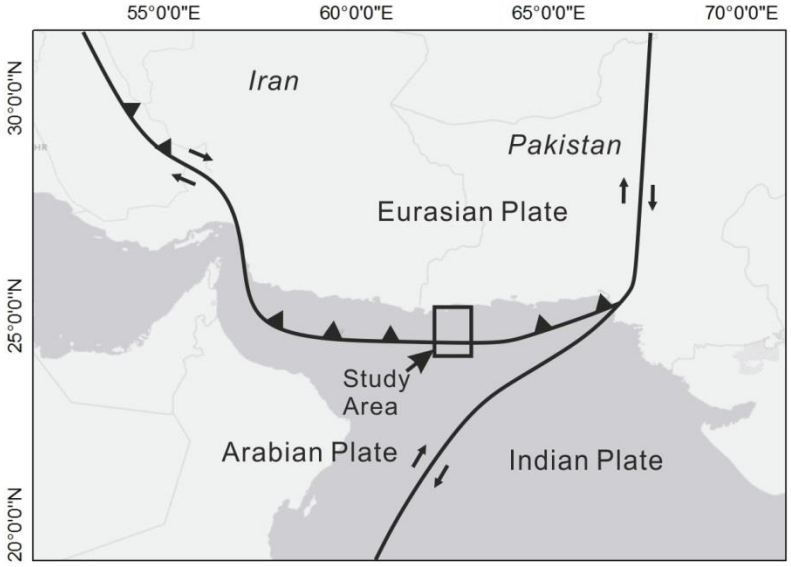

Figure 2.5 Location of the study area and simplified tectonic settings of the Makran continental margin.

High free gas content in sediments was first inferred from the spot of high amplitude reflection of seismic data (White, 1977). Bottom simulating reflector (BSR), which marks the lower boundary of the GHSZ, was further indicated by Seismic studies at approximately 500–800 mbsf throughout the continental slope (Minshull and White, 1989). Fluid seepage was directly observed for the first time in the 1990s featured by high methane concentration in water column, seep-related authigenic carbonate precipitation, and chemosynthetic clams (Von Rad et al., 2000).

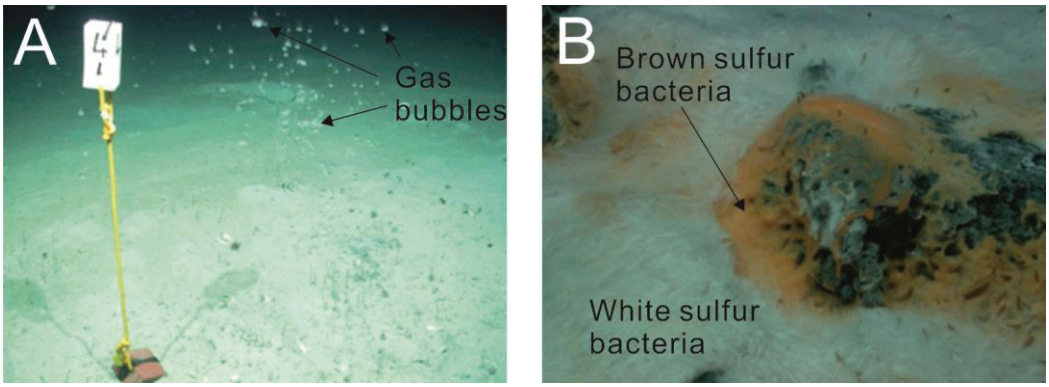

Figure 2.6 High quality images show gas bubbles in the water column and bacteria mat on the seafloor at the gas seeps of the Makran continental margin (Bohrmann, 2008).

Hydrates were sampled at water depths of 1019m and 2860m from the so-called Flare 2 and Flare 5 gas seeps, respectively, on the Makran continental margin. Chemosynthetic communities (Figure 2.6B) and gas bubble emissions (Figure 2.6A) were observed using ROV 'MARUM-QUEST 4000m' at both sites (Bohrmann, 2008).

2.1.3 The Black Sea

Black Sea, surrounded by Cenozoic mountain belts, is a marginal ocean with water depth of 2-2.2 km (Robinson and Kerusov, 1997). It is separated by Andrusov Ridge and Archangelsky Ridge into the eastern and western Black Sea basins (Figure 2.7). The Black Sea is underlain by thinned continental and oceanic crust with 10-19 km thick sediment deposits (Tugolesov et al., 1985).

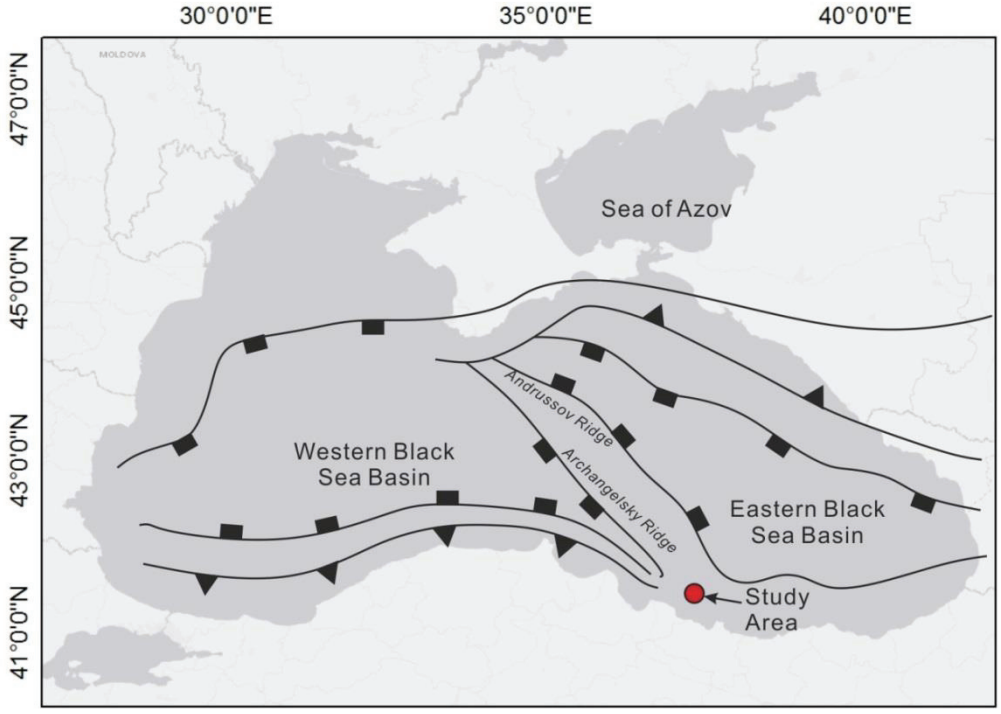

Figure 2.7 Location of study area and simplified tectonic settings of Black Sea (after Çifçi et al., 2003).

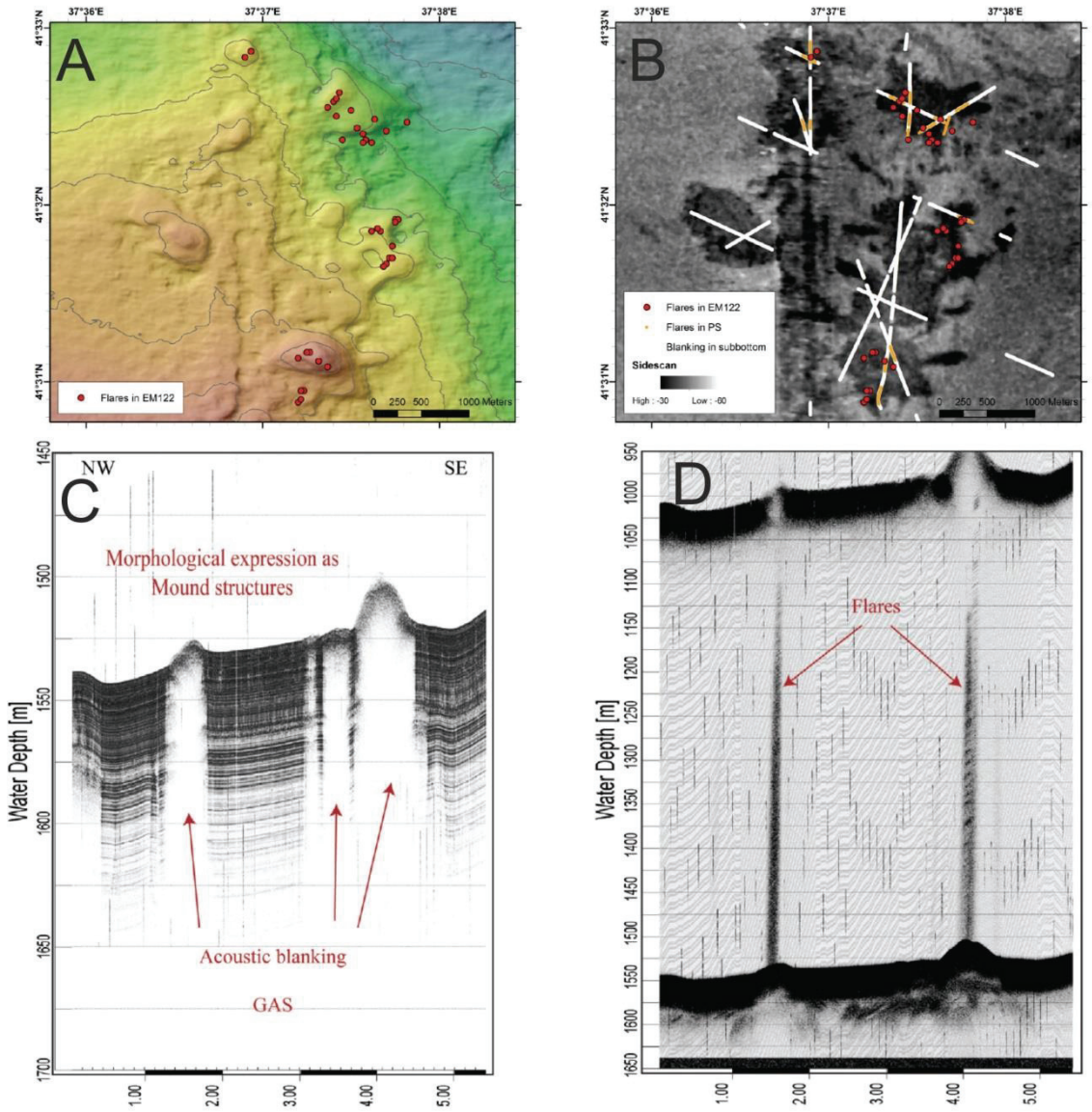

Figure 2.8 Mound structure at ordu ridge (A) which is characterized by high backscatter (B). Parasound echograms show clear evidence of gas accumulation in the shallow sediment and gas bubbles in water column (Bohrmann, 2011).

Ordu ridge is a small ridge which is located at water depth over 1000m at southeast of the Black Sea. This ridge was named during the M84-2 cruise. Several gas emissions sites were discovered at the Ordu Ridge, which are related to mounded structures. These positive elevations (Figure 2.8A) are featured by higher backscatter (Figure 2.8B) and show clearly dark patches on amplitude map. Gas accumulation in shallow sediment (Figure 2.8C) and gas emissions in the water column (Figure 2.8D) at the mound could be detected by using PARASOUND echograms (Bohrmann, 2011).

2.2 Field methods

2.2.1 MeBo

Conventional methods of sampling subsurface marine sediments include mainly gravity cores, piston cores and mini-cores. Although they are all robust and reliable coring

instruments, the coring depth are usually limited to very shallow sediment (Hebbeln, 2003). Additionally, when gas hydrate layers or hard rocks are encountered they might be broken.

Drilling ships are usually used for drilling long sediment cores or cores from hard-rock provinces (Hebbeln, 2003). Several hundreds to even thousands of meters long cores could be achieved by such ships. However, the expense of using drilling ships is high and it is not efficient for shallow drilling (McGinnis, 2009).

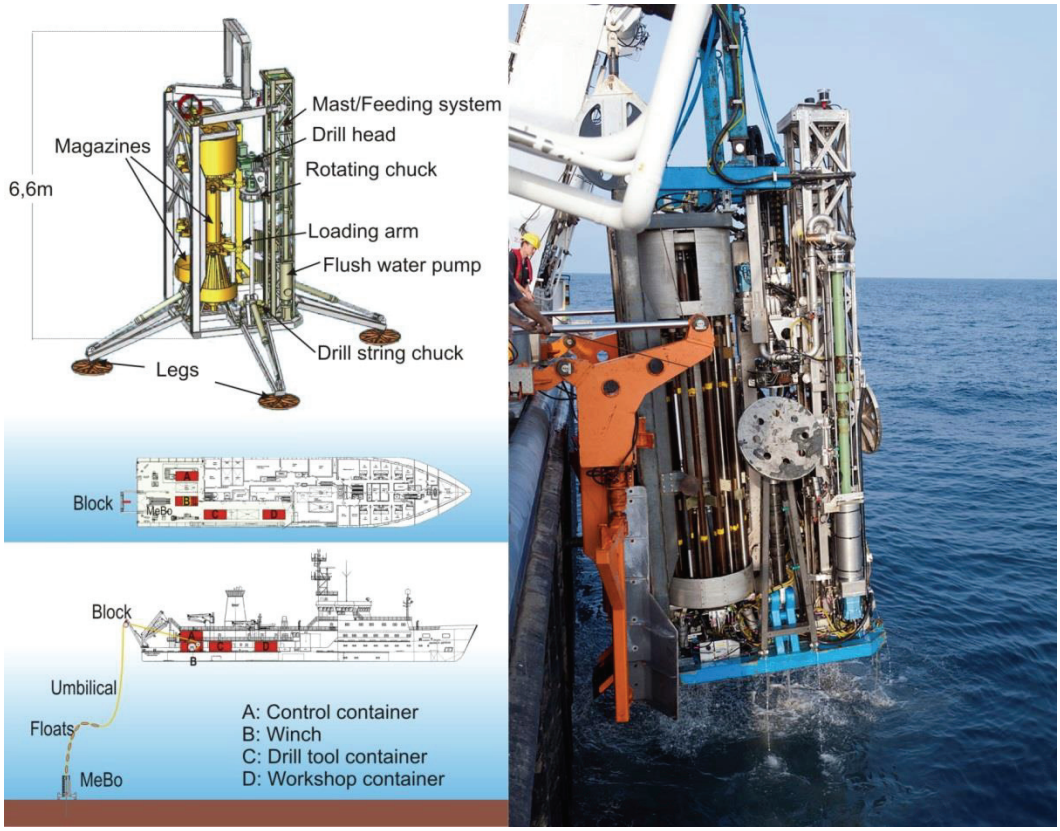

Figure 2.9 Simplified model and deployment of MeBo (after Freudenthal and Wefer, 2013).

The seafloor drill rig MeBo of MARUM compromises the high expense of drilling ships and the limited coring depth of conventional coring methods (Figure 2.9). This device is a robotic drill machine which could be deployed onto the seabed and controlled remotely from the ship. The maximum operation depth is 2000m water depth and the maximum sampling depth is 80 mbsf. Detailed parameters about MeBo could be found in (Freudenthal and Wefer, 2007; Freudenthal and Wefer, 2013). During RV 'Pourquoi Pas?' cruise, it was used for getting long sediment cores from a pockmark field at the Nigerian continental margin, where massive gas hydrates and carbonate concretions are expected. The advantage of MeBo is that the drilling mode could be switched from pushing coring to rotary drilling which is better suited for massive hydrates and carbonates.

MeBo was deployed 12 times in total during the entire cruise. Altogether, 374 m were drilled and about 278 m core was recovered.

2.2.2 Gravity coring and hydrate sampling

Gas hydrates were exclusively sampled from shallow sediments by using a 6-m long conventional gravity corer. When the gravity cores were on board, gas hydrates were immediately sampled and stored in liq. N_2 to prevent further dissociation.

2.2.3 Measurements of in situ sediment temperature

In-situ temperature measurements were conducted using temperature loggers (MTLs) manufactured by ANTARES Datensystem GmbH in Germany (Feseker et al., 2009). The accuracy of the sensors is better than 0.002 °C with a calibration range from -2 to 35°C. Five temperature sensors were mounted on the outriggers attached to the cutting barrel of a 6 m-long gravity corer (Figure 2.10). Distance between loggers was set to 100 cm and time resolution was set to 5 seconds. The absolute depths of the measurements below the seabed could be estimated from mud smear on the gravity corer or on the cable.

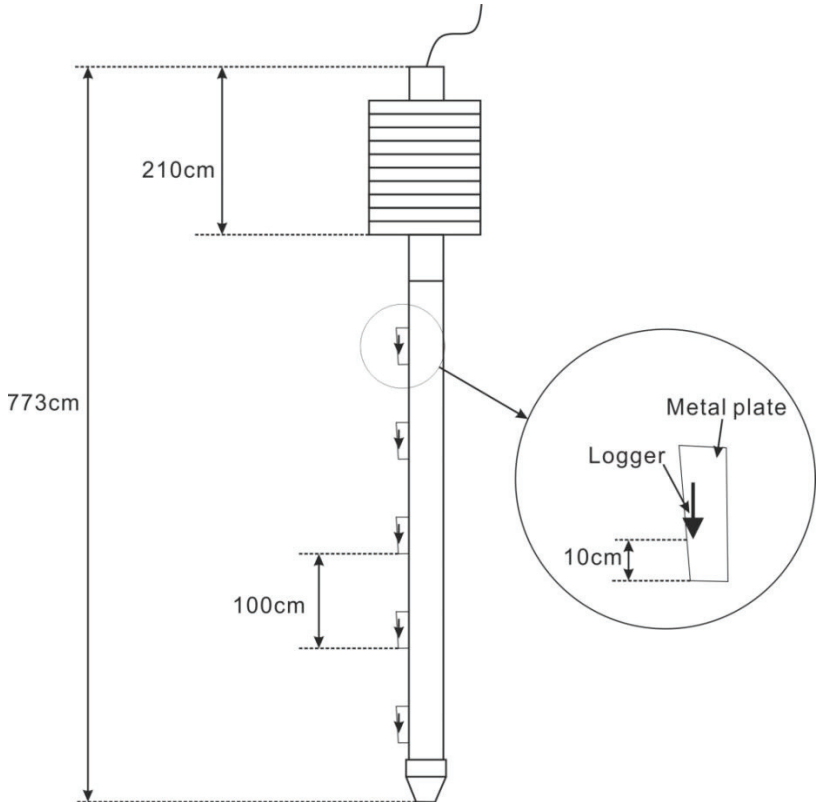

Figure 2.10 Temperature loggers attached to the 6-m gravity cutting barrel.

At each station, the loggers were left in the sediment for about 15 min after the penetration of the gravity corer, to adjust to the ambient sediment temperature. The recorded temperatures were used to calculate the geothermal gradients by using linear regression.

2.2.4 Infrared thermal imaging

Thermal radiation is electromagnetic radiation that is caused by thermal motion of charged particles in substance (Siegel and Howell, 1992). All substances with temperature higher than absolute zero emit thermal radiation to the surroundings. Electromagnetic spectrum is divided into a number of wavelength regions that are termed as bands (Figure 2.11) (Siegel

and Howell, 1992). There are no fundamental differences between radiations in the different bands of the electromagnetic spectrum.

Infrared spectral band is used for thermography. Infrared camera scanning measures and documents the thermal radiation from an object in the form of infrared spectral. Temperature of the object surface could be calculated and displayed because radiation is a function of object surface temperature.

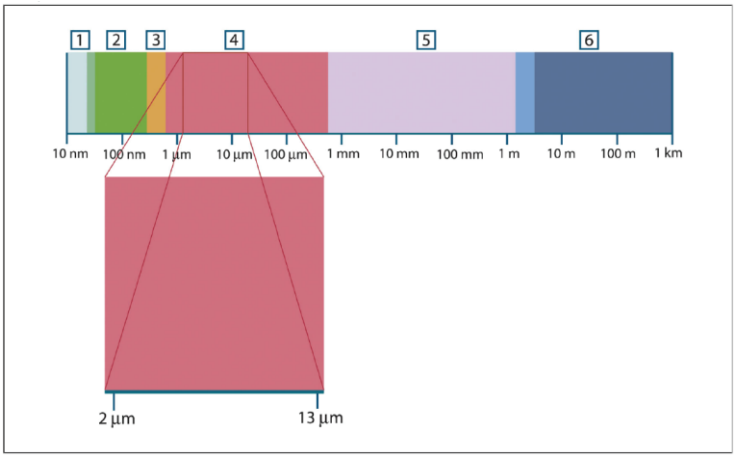

Figure 2.11 Electromagnetic spectrum. 1: X-ray; 2: UV; 3: Visible light; 4: IR; 5: Microwaves; 6: Radio waves (From Flir Manual).

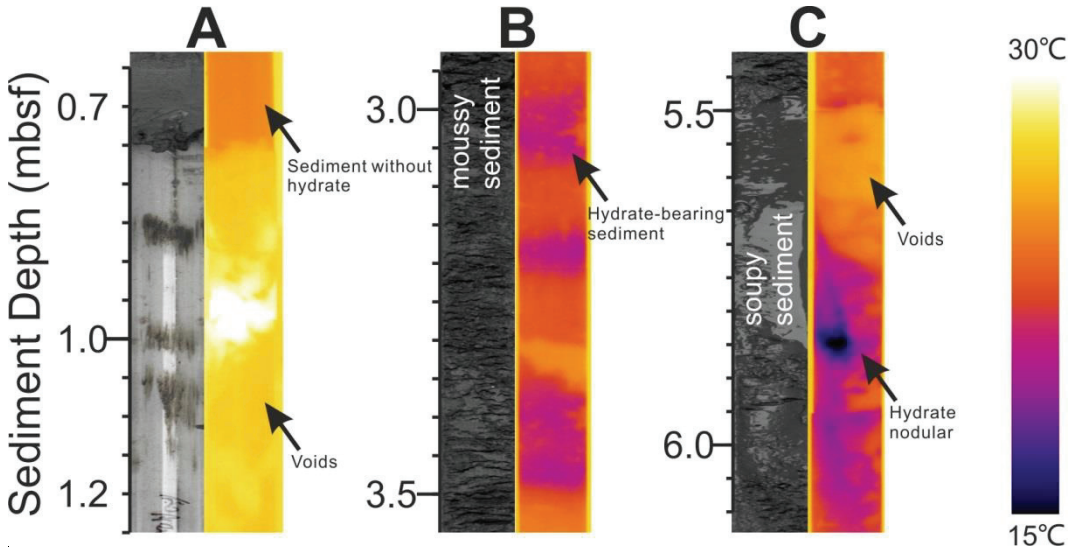

Figure 2.12 Comparison of IR images and cores of MeBo drill site GMMB06 at the Nigerian continental margin. High temperature corresponds to the voids which contain air or other gases (A). Low temperature corresponds to the moussy (B) and soupy (C) sediment caused by hydrate dissociation.

Because hydrate dissociation is an endothermic process, intervals in sediment cores where hydrate is currently dissociating, or dissociated recently, are relatively cold. These signals either can be felt by hand or measured with infrared (IR) thermal cameras. This technique was first used during ODP Leg 201 (Ford et al., 2003) for gas hydrate detection and was further developed during ODP Leg 204 (Tréhu et al., 2006).

Although other processes also potentially introduce IR temperature anomalies, it is proved that distinct and strong anomalies are a reliable proxy of in situ gas hydrate presence (Figure 2.12).

IR camera (ThermaCam SC 640 camera, FLIR Systems) was used to scan the core liners and record the core temperature for 10 drill sites. The temperature range of the IR system is between –40 °C and + 120 °C, the precision of the camera is 0.1 °C at 30 °C with the accuracy of ±2 °C.

Considering distinct hot or cold spots as reference points, all IR images were merged consecutively for each drilling. Temperatures alongside the central line of each core were extracted from the IR images to obtain a temperature log. Because there are differences of in situ sediment temperature and time of handling cores, the background temperatures of each linear varies slightly (1-2 °C) and are assigned to each core arbitrarily. In order to obtain a better visualization and to minimize the artifacts for further analysis, only the anomalies with $\Delta T > 1°C$ were considered as voids and $\Delta T < -2$ °C were considered as gas hydrate-bearing sediment.

2.3 Laboratory methods

2.3.1 Gas chromatography

A two-channel gas chromatography was used to determine the composition of hydrate-bonded gases. C_1-C_6 hydrocarbons were quantified with a capillary column (OPTIMA-5; 50 m length; 0.32 mm inside diameter) connected to a flame ionization detector. Other gases, including O_2, N_2, CO_2 as well as CH_4 and C_2H_6 were analyzed using a packed (molecular sieve) stainless steel column coupled with a thermal conductivity detector. More detailed information about the gas chromatography could be found in literatures (Pape et al., 2010).

The molar ratios of hydrocarbons (C_1/C_2+) were used to relate the hydrate-bound components to thermogenic or biogenic sources (Bernard et al., 1976) and to calculate the hydrate thermodynamic stability. That was accomplished by using the HWHYD software (HWHYD, 2005), which is a commercial product from Heriot-Watt-University.

2.3.2 X-ray diffraction

X-ray diffraction (XRD) was applied to analyze and quantify hydrate phases present in hydrate samples. For measurements in Göttingen, we use a Bragg-Brentano focusing Philips MRD (Materials Research Diffractometer) cryo-goniometer, which emit a wavelength of 0.7093 Å from a molybdenum anode (Klapp et al., 2010a). A detailed description of X-ray diffraction is referred to (Als-Nielsen and McMorrow, 2001). During the measurements, the gas hydrate samples were kept stable by using depressurized liquid nitrogen. The temperature was set to 80 K and was monitored by a temperature controller.

Phase fractions are calculated from Rietveld refinement using the EXPGUI user interface and the GSAS software (Toby, 2001).

2.3.3 Raman spectroscopy

Raman spectroscopy is widely used to identify hydrate-bonded gases, their relative cage occupancy and hydrate structure. Raman spectroscopy, unlike X-ray diffraction and gas chromatography, provides hydrate structure information on a small area and does not require big samples (Qin and Kuhs, 2013). Therefore, gas hydrate information on different scales could be obtained by combining Raman spectroscopy with other methods, such as gas chromatography and X-ray diffraction (Klapp et al., 2010b).

In this study, Raman spectra analysis was conducted by using a confocal Raman spectrometer LabRAM HR800 (France Jobin Yvon) equipped with a Peltier-cooled charge coupled device detector (DU 420A, Andor, 1024 × 256 pixels) and a 600 grooves/mm grating. Light with wavelength of 488nm emitted from an Ar+ laser (Innova 9C, Coherent) was used as the excitation source at the output power of 20.5 mW. Measurements were conducted by focusing the laser beam via a 50× long working distance objective (Numerical aperture = 0.55, brand Olympus). The backscattered mode was used and confocal aperture was set to 100 μm. The focus spot has a diameter of about 1.1 μm and the power of the laser beam is around 4.5 mW. Raman spectra was collected at a nominal resolution of 2.2 cm^{-1}, was obtained in two accumulations of 30 s exposure time within a range of 100 cm^{-1} to 4000 cm^{-1}. The temperature of the Raman laboratory was controlled to 295±1 K by an air-conditioner.

Raman analysis was conducted in a freezing stage (Linkam THMS600), which was placed under an Olympus microscope attached to the spectrometer. The device was operated at 113 K with an ambient pressure N_2 atmosphere to prevent gas hydrate decomposition. Sample stage can be moved laterally (X, Y) and horizontally (Z). Time interval between two consecutive Raman measurements of the separated samples of one loading was typically 4–6 min.

After the baseline correction, each spectrum was fitted in the region of interest by a Gaussian/Lorentzian mixed function using “dmfit” software.

2.3.4 Pore water chloride concentration

Gas hydrate formation extracts pore water from marine sediment and excludes dissolved ions. Water within the hydrate lattice is therefore fresher than that in surrounding pore water. When extra ions released to the pore water during hydrate formation diffuse away, concentration of ions in pore water decreases back to the level before hydrate formation (Figure 2.13). During core retrieving, hydrate dissociation releases fresh water to the pore water, therefore, sediment intervals containing gas hydrate will be recorded as low Cl anomalies in pore water. Therefore, discrete anomalies of pore water Cl concentration could be served as a proxy for determining in situ gas hydrate presence.

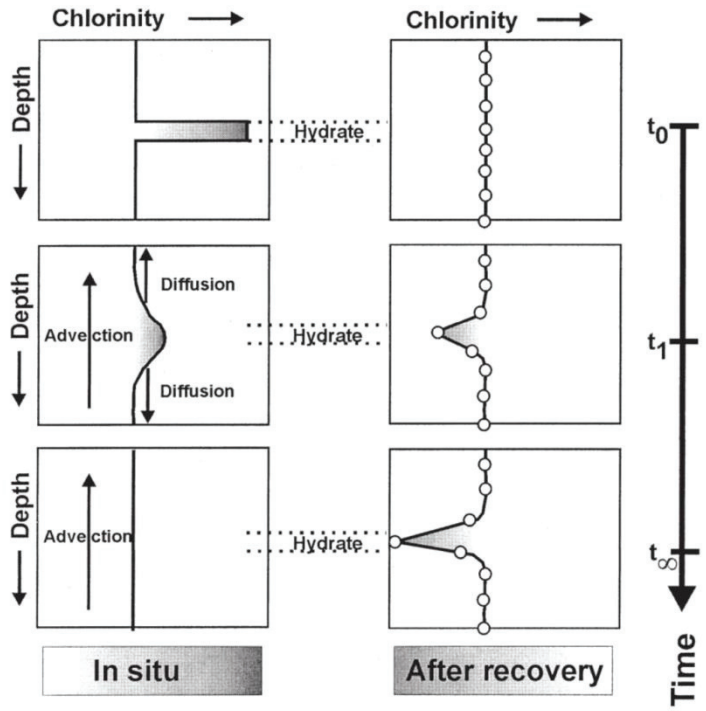

Figure 2.13 Chloride concentration anomalies in pore water caused by hydrate formation and dissociation (from Haeckel et al., 2004).

In this work, pore water was extracted using Rhizon sampler, which consists of a thin tube made up with hydrophilic porous polymer of pore diameter of approximate 0.2 µm. The Rhizon were pushed into sediment through holes drilled on the plastic liners. Syringes with volume of 10 or 20 ml were connected to the sampler to create a vacuum and collect the pore water. Chloride concentrations were detected by using ion chromatography (861 Advanced Compact IC, Metrohm). Since no sulfate was expected to be presented in pore water below the sulfate-methane interface (SMI), pore water constituents by the contamination values was recalculated. These small contaminations of the pore water probably result from smearing at the rim of the sediments. However, this does not influences the chloride values of the pore water significantly.

Reference

Als-Nielsen, J., and McMorrow, D., 2001, Elements of X-ray Physics, New York: John Wiley and Sons.

Bernard, B. B., Brooks, J. M., and Sackett, W. M., 1976, Natural gas seepage in the Gulf of Mexico: Earth and Planetary Science Letters, v. 31, no. 1, p. 48-54.

Bohrmann, G., 2008, Report and Preliminary Results of R/V Meteor Cruise M74/3, Fujairah-Male, 30 October-28 November, 2007: Cold Seeps of the Makran Subduction Zone (continental Margin of Pakistan);[cruise Within the Framework of the DFG Financed Research Center Ocean Margins, Project Aera E:" Fluid and Gas Seepage at Ocean Margins"], Fachbereich Geowiss., Univ.

Bohrmann, G., 2011, R/V METEOR Cruise Report M84/2: Origin and Distribution of Methane and Methane Hydrates in the Black Sea, DFG-Forschungszentrum MARUM, Universität Bremen.

Çifçi, G., Dondurur, D., and Ergün, M., 2003, Deep and shallow structures of large pockmarks in the Turkish shelf, Eastern Black Sea: Geo-Marine Letters, v. 23, no. 3-4, p. 311-322.

Damuth, J. E., 1994, Neogene gravity tectonics and depositional processes on the deep Niger Delta continental margin: Marine and Petroleum Geology, v. 11, no. 3, p. 320-346.

De Jong, K. A., 1982, Tectonics of the Persian Gulf, Gulf of Oman, and southern Pakistan region, The ocean basins and margins, Springer, p. 315-351.

DeMets, C., Gordon, R. G., Argus, D., and Stein, S., 1990, Current plate motions: Geophysical journal international, v. 101, no. 2, p. 425-478.

Feseker, T., Dählmann, A., Foucher, J.-P., and Harmegnies, F., 2009, In-situ sediment temperature measurements and geochemical porewater data suggest highly dynamic fluid flow at Isis mud volcano, eastern Mediterranean Sea: Marine Geology, v. 261, no. 1, p. 128-137.

Ford, K., Naehr, T., and Skilbeck, C., 2003, The use of infrared thermal imaging to identify gas hydrate in sediment cores.

Freudenthal, T., and Wefer, G., 2007, Scientific drilling with the sea floor drill rig MeBo: Scientific Drilling, v. 5, p. 63-66.

Freudenthal, T., and Wefer, G., 2013, Drilling cores on the sea floor with the remote-controlled sea-floor drilling rig MeBo: Geoscientific Instrumentation, Methods and Data Systems Discussions, v. 3, no. 2, p. 347-369.

George, R. A., and Cauquil, E., AUV Ultrahigh-Resolution 3D Seismic Technique for Detailed Subsurface Investigations, *in* Proceedings Offshore Technology Conference2007, Offshore Technology Conference.

Haeckel, M., Suess, E., Wallmann, K., and Rickert, D., 2004, Rising methane gas bubbles form massive hydrate layers at the seafloor: Geochimica et Cosmochimica Acta, v. 68, no. 21, p. 4335-4345.

Hebbeln, D., 2003, State of the art and future prospects of scientific coring and drilling of marine sediments, Ocean Margin Systems, Springer, p. 57-66.

Klapp, S. A., Bohrmann, G., Kuhs, W. F., Mangir Murshed, M., Pape, T., Klein, H., Techmer, K. S., Heeschen, K. U., and Abegg, F., 2010a, Microstructures of structure I and II gas hydrates from the Gulf of Mexico: Marine and Petroleum Geology, v. 27, no. 1, p. 116-125.

Klapp, S. A., Murshed, M. M., Pape, T., Klein, H., Bohrmann, G., Brewer, P. G., and Kuhs, W. F., 2010b, Mixed gas hydrate structures at the Chapopote Knoll, southern Gulf of Mexico: Earth and Planetary Science Letters, v. 299, no. 1, p. 207-217.

Kopp, C., Fruehn, J., Flueh, E., Reichert, C., Kukowski, N., Bialas, J., and Klaeschen, D., 2000, Structure of the Makran subduction zone from wide-angle and reflection seismic data: Tectonophysics, v. 329, no. 1, p. 171-191.

McGinnis, T., 2009, Seafloor drilling: Drilling in Extreme Environments: Penetration and Sampling on Earth and other Planets, p. 309-345.

Minshull, T., and White, R., 1989, Sediment compaction and fluid migration in the Makran accretionary prism: Journal of Geophysical Research: Solid Earth (1978–2012), v. 94, no. B6, p. 7387-7402.

Pape, T., Bahr, A., Rethemeyer, J., Kessler, J. D., Sahling, H., Hinrichs, K.-U., Klapp, S. A., Reeburgh, W. S., and Bohrmann, G., 2010, Molecular and isotopic partitioning of low-molecular-weight hydrocarbons during migration and gas hydrate precipitation in deposits of a high-flux seepage site: Chemical Geology, v. 269, no. 3–4, p. 350-363.

Qin, J., and Kuhs, W. F., 2013, Quantitative analysis of gas hydrates using Raman spectroscopy: AIChE Journal, v. 59, no. 6, p. 2155-2167.

Robinson, A. G., and Kerusov, E., 1997, AAPG Memoir 68: Regional and Petroleum Geology of the Black Sea and Surrounding Region. Chapter 19: Stratigraphic and Structural Development of the Gulf of Odessa, Ukrainian Black Sea: Implications for Petroleum Exploration.

Siegel, R., and Howell, J. R., 1992, Thermal radiation heat transfer: NASA STI/Recon Technical Report A, v. 93, p. 17522.

Sultan, N., Bohrmann, G., Ruffine, L., Pape, T., Riboulot, V., Colliat, J. L., De Prunelé, A., Dennielou, B., Garziglia, S., and Himmler, T., 2014, Pockmark formation and

evolution in deep water Nigeria: Rapid hydrate growth versus slow hydrate dissolution: Journal of Geophysical Research: Solid Earth, v. 119, no. 4, p. 2679-2694.

Sultan, N., Marsset, B., Ker, S., Marsset, T., Voisset, M., Vernant, A. M., Bayon, G., Cauquil, E., Adamy, J., Colliat, J. L., and Drapeau, D., 2010, Hydrate dissolution as a potential mechanism for pockmark formation in the Niger delta: Journal of Geophysical Research: Solid Earth, v. 115, no. B8, p. B08101.

Toby, B. H., 2001, EXPGUI, a graphical user interface for GSAS: Journal of Applied Crystallography, v. 34, no. 2, p. 210-213.

Tréhu, A., Ruppel, C., Holland, M., Dickens, G., Torres, M., Collett, T., Goldberg, D., Riedel, M., and Schultheiss, P., 2006, Gas hydrates in marine sediments: Lessons from scientific ocean drilling: Oceanography, v. 19, no. 4, p. 124-142.

Tugolesov, D., Gorshkov, A., Meisner, L., Solov'ev, V., and Khakhalev, E., 1985, Tectonics of Mesozoic-Cenozoic deposits of the Black Sea basin: Nedra, Moscow, p. 215.

Von Rad, U., Berner, U., Delisle, G., Doose-Rolinski, H., Fechner, N., Linke, P., Lückge, A., Roeser, H., Schmaljohann, R., and Wiedicke, M., 2000, Gas and fluid venting at the Makran accretionary wedge off Pakistan: Geo-Marine Letters, v. 20, no. 1, p. 10-19.

White, R. S., 1977, Seismic bright spots in the Gulf of Oman: Earth and Planetary Science Letters, v. 37, no. 1, p. 29-37.

White, R. S., and Louden, K. E., 1982, The Makran continental margin: structure of a thickly sedimented convergent plate boundary: Studies in continental margin geology, v. 34, p. 499-518.

Chapter 3

Gas hydrate distributions in sediments of pockmarks from the Nigerian continental margin - Results and interpretation from shallow drilling

Jiangong Wei[1*], Thomas Pape[1], Nabil Sultan[2], Jean-Louis Colliat[3], Tobias Himmler[1,2], Livio Ruffine[2], Alexis de Prunelé[2], Bernard Dennielou[2], Sebastien Garziglia[2], Tania Marsset[2], Carl A. Peters[1,5], Abdulkarim Rabiu[4], Gerhard Bohrmann[1]

1 MARUM, University of Bremen, Klagenfurter Str., 28359 Bremen, Germany

2 IFREMER, Département REM, Unité des Géosciences Marines, F- 29280 Plouzané, France

3 Total, Pau, av. Larribau, France

4 Nigeria Institute for Oceanography and Marine Research, Nigeria

5 Department of Earth and Planetary Sciences, Macquarie University, Sydney, NSW 2109, Australia

MANUSCRIPT 1

In press in Marine and petroleum geology, Vol. 59, 2015

3.1 Abstract

A joint research expedition between the French IFREMER and the German MARUM was conducted in 2011 using the R/V *Pourquoi pas?* to study gas hydrate distributions in a pockmark field (1141 – 1199 meters below sea surface) at the continental margin of Nigeria. The sea floor drill rig MeBo of MARUM was used to recover sediments as deep as 56.74 meters below seafloor. The presence of gas hydrates in specific core sections was deduced from temperature anomalies recorded during continuous records of infrared thermal scanning and anomalies in pore water chloride concentrations. *In situ* sediment temperature measurements showed elevated geothermal gradients of up to 258 °C/km in the center of the so-called pockmark A which is up to 4.6 times higher than that in the background sediment (72 °C/km). The gas hydrate distribution and thermal regime in the pockmark are largely controlled by the intensity, periodicity and direction of fluid flow. The joint interaction between fluid flow, gas hydrate formation and dissolution, and the thermal regime governs pockmark formation and evolution on the Nigerian continental margin.

Keywords: gas hydrate; pockmark; chloride profile; infrared thermal imaging; fluid flow, Nigerian continental margin, MeBo drill rig

3.2 Introduction

Pockmarks are circular to elongated seafloor depressions which are often associated with fluid flow from the subsurface (Judd and Hovland, 2007). Submarine pockmarks with various sizes, shapes and state of activity have been widely discovered at different water depths (e.g. Bünz et al., 2003; Chen et al., 2010; Dondurur et al., 2011; Pilcher and Argent, 2007; Pinet et al., 2010; Sahling et al., 2008; Sun et al., 2011; Ussler et al., 2003). In addition, buried paleo-pockmarks found during seismic investigations were proposed to be associated with periodic fluid flow activity in the past (Andresen et al., 2008).

Depending on the local geological conditions, several mechanisms have been suggested to explain the process of pockmark formation. Researchers tend to agree that pockmarks are directly or indirectly caused by upward fluid flow from the deep subsurface, through moderate to violent processes (Chand et al., 2012; Gay et al., 2006a; Gay et al., 2006b; Hartwig et al., 2012; Moss et al., 2012; Paull et al., 2008; Riboulot et al., 2013; Rise et al., 1999). In particular on continental margins, methane oversaturated in upward migrating fluids reacts under high pressure and low temperature in shallow sediment to form solid gas hydrate (Matsumoto et al., 2011; Sloan and Koh, 2007). The structural properties of gas hydrate, like its fabric, and the hydrate saturations in the sediment, are largely controlled by the intensity and distribution of fluid flow and by the sediment properties, including permeability and strength (Abegg et al., 2007). Moreover, fluid migration patterns are changed by pore space blocking caused by gas hydrate formation (Bangs et al., 2011; Riedel et al., 2006). The interaction between fluid flow, gas hydrates and host sediment increases the complexity of the pockmark system and is of significant importance when studying the formation and evolution of deep-water pockmark located in the gas hydrate stability zone (GHSZ).

Sultan et al. (2010) proposed an initial model for the formation of individual pockmarks on the Nigerian continental margin. Based on gas hydrate findings in shallow sediments and numerical modeling of the dynamic response of the gas hydrate to changes in gas concentrations underneath the gas hydrate occurrence zone (GHOZ), gas hydrate formation and dissolution was suggested to be the major control for the evolution of these pockmarks. In order to gain further insight, a joint research expedition (Guineco-MeBo) between the French IFREMER and the German MARUM with the R/V *Pourquoi pas?* and the portable sea floor drill-rig MeBo was conducted in 2011. The major objective of the expedition was to reveal gas hydrate distributions in even deeper sediments, which eluded sampling with common sampling techniques (e.g., long piston cores) before.

In this study, gas hydrate distributions in sediments of selected pockmarks were determined using infrared (IR) thermal scanning of core liners and pore water chloride analysis. Furthermore, the impact of fluid flow and gas hydrate formation/dissolution on controlling the geothermal regime and evolution of the pockmarks is discussed.

3.3 Geological settings

Our study area is a pockmark field located within the Gulf of Guinea on the continental margin offshore Nigeria (Fig 3.1). This continental margin is undergoing slow deformation by gravity tectonism that initiated in response to both, rapid seaward progradation and loading huge amount of sediment (Damuth, 1994). Damuth (1994) distinguished this area into three subareas based on the structural styles: 1) an upper extensional zone, 2) an intermediate translational zone, and 3) a lower compressional zone. The pockmark field studied in this paper is located in the translational zone which is characterized by diapirs underneath. Examples of seismic recordings of shale diapirs in this area can be found in Damuth (1994) and Cohen and McClay (1996).

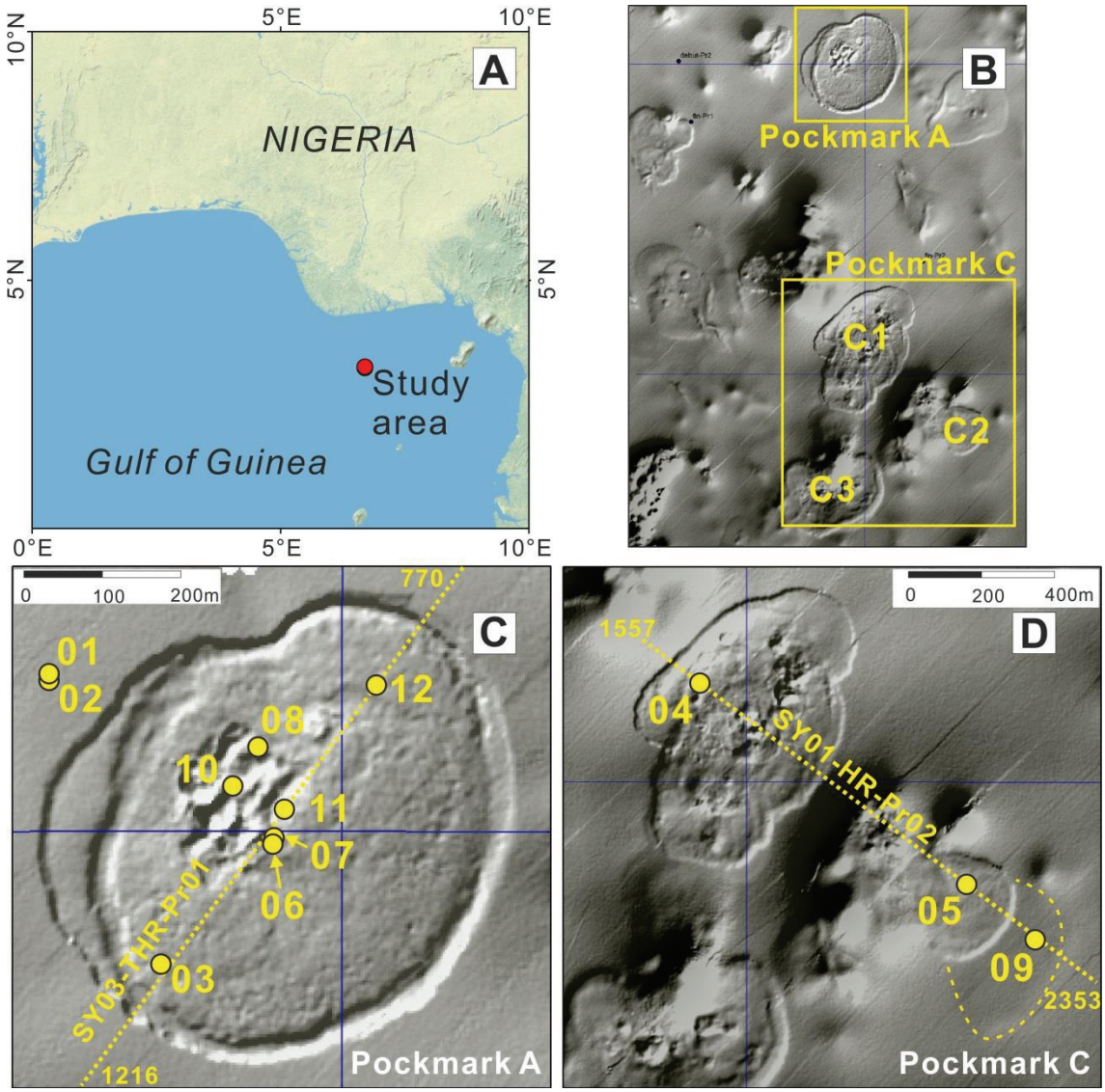

Figure 3.1: (A): Location of the pockmark field at the Nigerian continental margin. (B): Overview of the studied pockmark field. (C) and (D): MeBo drill sites (GMMB) in pockmarks A and C (C1 and C2), respectively. Numbers refer to individual MeBo station codes (i.e. No. 01 = station GMMB01, for example) Track lines of SYSIF seismic profiles SY03-THR-Pr01 and SY01-HR-Pr02 as well as the shot points are shown. For exact positions refer to Sultan et al. (2014).

The Nigerian continental margin is an active fluid flux area as indicated from various seafloor features, such as pockmarks, mud volcanoes, gas hydrates and carbonate concretions (Bayon et al., 2007; Brooks et al., 2000; Graue, 2000; Hovland et al., 1997). Formation of such authigenic carbonates is typically attributed to the anaerobic methane oxidation (AOM; Ritger 1987). Pronounced bottom simulating reflectors (BSR), demonstrating the boundary between the base of the GHSZ and free gas underneath, were reported (Cunningham and Lindholm, 2000). Such BSRs indicate the presence of gas hydrates related to high methane flux towards shallow sediments caused by fluid migration (Hovland et al., 1997). In addition, gas chimneys found in the subsurface were proposed to serve as pathways for fast hydrocarbon migration between reservoirs and the seafloor (Heggland, 2003).

The pockmark field, comprising the pockmarks A and C studied herein, lies at water depths between 1141 and 1199 m. Pockmark A (Fig 3.1C) is a slightly NE-SW elongated seafloor feature with a hummocky topography in the center. The hummocky area corresponds to high multibeam backscatter (George and Cauquil, 2007) which may indicate the occurrence of shallow gas hydrates, free gas and/or authigenic carbonates (Carson et al., 1994). Pockmark C (Fig 3.1D) is a pockmark cluster composed of at least three pockmarks (C1 – C3). Shallow gas hydrates were found widely in this pockmark field which might contribute to the formation of the pockmarks (Sultan et al., 2010). Authigenic carbonates were also recovered from different depths in these pockmarks (Sultan et al., 2010).

3.4 Material and methods

3.4.1 MeBo drilling

The mobile drilling system MeBo (Freudenthal and Wefer, 2013) was deployed from the R/V '*Pourquoi pas?'* to drill 12 cores of up to 56.74 m in length in the pockmark field between 1141 and 1199 m water depth (Fig 3.1; Table 3.1). Seven drill sites were located in and around pockmark A (Fig 3.1C), with five sites in the central part (GMMB06, 07, 08, 10 and 11) and two in the periphery (GMMB03 and 12). Two drill sites (GMMB01 and 02) were located outside (NW) pockmark A. Further three drill sites (Fig 3.1D) were located in pockmark C1 (GMMB04), pockmark C2 (GMMB05), and SE of pockmark C2 (GMMB09), respectively.

3.4.2 Infrared thermal imaging of MeBo cores

Infrared (IR) temperature profiles of the 2.52 m-long MeBo core liners were obtained for 10 drill sites in order to document the gas hydrate distribution in the MeBo cores. Images for GMMB10 were not interpreted due to their low quality. The core liners were removed from the core barrels immediately after recovery on deck. After a quick cleaning of the liner surfaces, pictures were taken with an IR camera (ThermaCam SC 640 camera, FLIR Systems) for documenting temperature variations. The temperature measurements of the IR system ranged from –40 °C to + 120 °C and the precision of the camera was 0.1 °C at

30 °C with the accuracy of ±2 °C. Each thermal scan covered approximately 60 cm depth range of the core. Five to six pictures including a spatial overlap of about 10 cm were taken from each liner in less than one minute.

For an individual drilling station, all IR images were combined in one figure to display the temperature distribution for the entire core surface. The raw data were converted and exported as bitmap format using the ThermaCAM™ Researcher Professional software. The bitmap files were processed using commercially available graphical software. All IR images were merged consecutively, considering distinct hot or cold spots as reference points. Temperatures along the central axis of the cores were extracted from the IR images to obtain temperature logs (Fig 3.2). Surface temperatures of core liners containing sediment devoid of gas hydrates were considered as background temperature. At each drilling station, background temperatures varied slightly (ca. 1–2 °C) between individual liners due to different *in situ* sediment temperatures and/or slightly different times required for individual liner handling (equilibration with ambient temperature of ≈30 °C on ship's deck). Thus, the specific background temperature was assigned to each core liner individually.

The difference between liner surface temperature and background temperature (ΔT) was calculated to interpret the content of the cores. In order to obtain a better visualization and to minimize the artifacts for further analysis, only anomalies with ΔT >+1°C were considered as voids in the liner and ΔT <–2 °C were considered to represent hydrate-bearing sediment, as hydrate dissociation is an endothermic process.

3.4.3 Pore water chloride and sulfate analysis

Pore water was extracted using Rhizon samplers (Seeberg-Elverfeldt et al., 2005), which consists of a thin tube made up with hydrophilic porous polymer with pore diameters of approximate 0.2 µm. The Rhizon samplers were pushed into the sediment through holes drilled through the plastic liners. 10 or 20 ml plastic syringes were connected to the sampler to create a vacuum and collect the pore water. Extracted pore water was split, prepared for various analyses, and stored in the refrigerator or reefer. Sulfate and chloride concentrations were measured on-board by using ion chromatography (861 Advanced Compact IC, 837 IC Eluent Degasser, and Advanced Sample Processor by Metrohm).

For several MeBo stations, seawater-derived sulfate in detectable concentrations was not only found in near-surface sediments but also in deeper layers. This was unexpected because sulfate is typically depleted below the sulfate-methane interface (SMI) due to AOM. Moreover, since measured sulfate concentrations below the SMI scattered considerably, we assumed that the presence of sulfate in these core sections were artifacts caused during the core drilling/handling procedure. Therefore, concentrations of chloride were re-calculated assuming the absence of sulfate below the SMI. This procedure caused changes in absolute chloride concentrations of <20% but affected trends in chloride profiles insignificantly.

3.4.4 In situ temperature measurements

In-situ temperature measurements were conducted in pockmark A using autonomous miniaturized temperature loggers (MTLs) from ANTARES Datensystem GmbH (Germany), which have already been used successfully during previousstudies (Römer et al., 2012; Feseker et al., 2009; Pape et al., 2011). Five temperature sensors were mounted on outriggers attached to the cutting barrel of a 6 m-long gravity corer according to Feseker et al. (2009). Distances between the loggers were 100 cm and the logging time interval was set to 5 sec. For each deployment, the gravity corer was held 50 meters above the seafloor for three to four minutes to measure the water temperature for calibration purposes of each MTL. Based on these measurements the standard deviation of the five loggers was calculated to be smaller than 0.008 °C (Table 3.2). At each station, the loggers were left in the sediment for about 15 minutes (Fig 3.5) after penetration of the gravity corer to adjust to the sediment temperature. The absolute penetration depths could be estimated from mud smear on the gravity corers or on the cable. By using linear regression individual temperatures recorded with the MTLs and assumed penetration depths were used to calculate the site-specific geothermal gradients.

3.5 Results

MeBo was deployed 12 times in total during the entire cruise. Depending on the lithology as well as on gas and gas hydrate contents, the recovery of the drill cores ranged between 60% and 94% with a mean of 81%. The cores comprised homogenous hemipelagic dark greyish clay with sporadic authigenic carbonate concretions. Distinct depth-changes or lateral variations of sediment grain sizes were not observed. Sediments with elevated water content, which was attributed to ex situ gas hydrate dissociation, were observed at different depths without regularity. No relation between gas hydrate distributions and sediment grain sizes became obvious.

3.5.1 Infrared thermal imaging

Infrared (IR) temperature profiles of core liners were established for most of the drill sites. The only exceptions were station GMMB01 and GMMB02 outside of pockmark A since indications for the presence of gas hydrates in sediments within the penetration depth (53.3 meters below seafloor (mbsf)) at these drill sites were missing in seismic profiles (Sultan et al., 2010). The assumption of the gas hydrates absence in these sediments was confirmed by the subsequent pore water chloride profiling (see chapter 4.2).

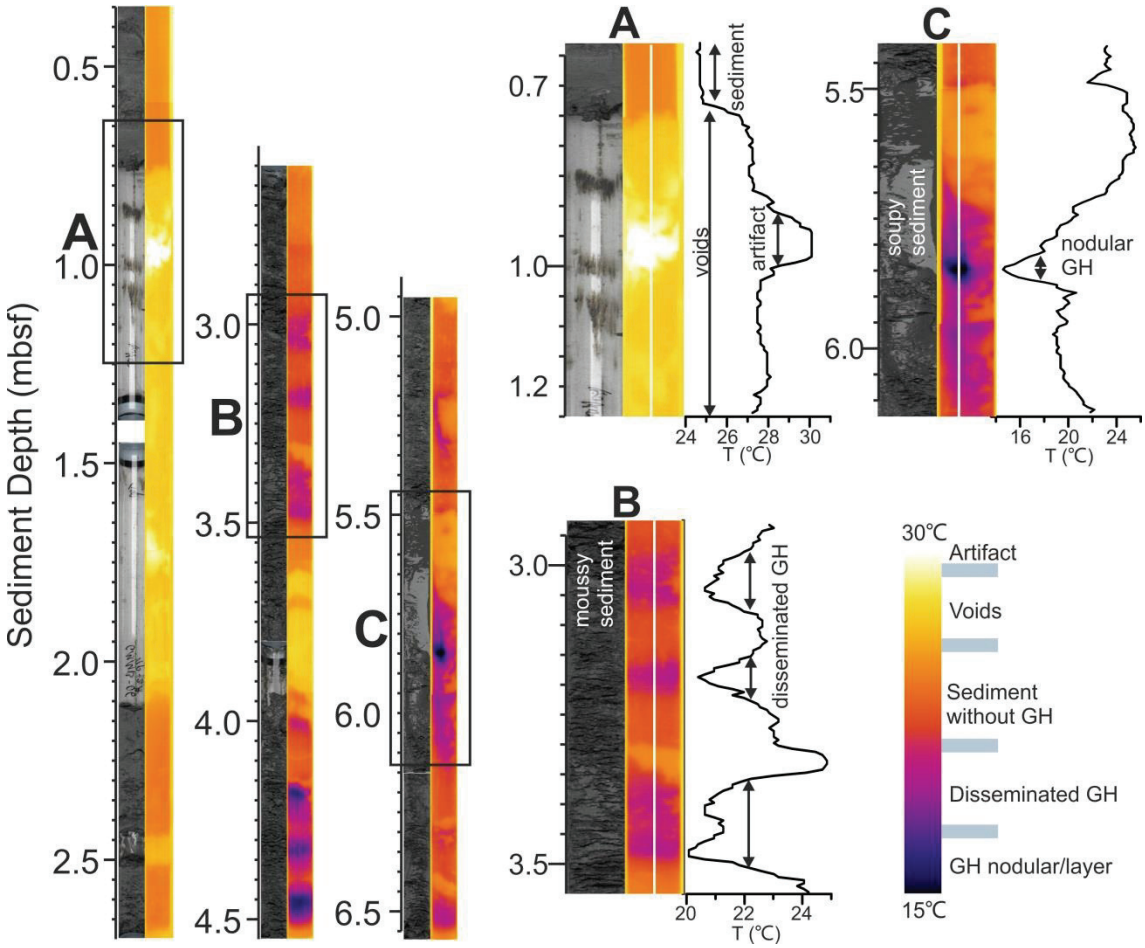

Figure 3.2: Combined illustration of core photographs (left) and IR images (right) of the 6.6 m-long MeBo drill core GMMB06. Representative intervals of the core (A, B and C) are shown in detail (right part of the figure). (A): normal hemi-pelagic sediment (upper part) and voids (lower part), which in the IR images correspond to the background temperature (orange) and high temperature (yellow), respectively. The bright spot (white) is an artifact generated during the core handling. (B): Moussy sediment with cracks, which in the IR image shows three cold temperature zones (light purple) caused by the dissociation of disseminated gas hydrates. (C): Soupy and fluidized sediments. The cold temperature interval below 5.70 mbsf contained gas hydrates including a nodular gas hydrate between 5.80 and 5.85 mbsf represented by an extremely cold spot (dark purple to black). GH = gas hydrate

Comparison of IR images with lithological core descriptions and high-resolution core photographs showed that thermal regimes of the MeBo cores were mainly determined by the core contents. This is exemplary shown for core GMMB06 (Fig 3.2). Since the *in situ* temperature of sediment (~4.5 °C) was significantly lower than that of the upper water column (up to ~28 °C) and the atmosphere (~30 °C), the cores were continuously warmed up during the core recovery and handling on deck. Liners filled with sediment exhibited intermediate temperatures of 23–25 °C (Fig 3.2A), depending mainly on the duration they were exposed to the water column and air before being imaged. These temperatures were considered as background.

Cores containing dissociating gas hydrates yielded prominent cold anomalies since hydrate dissociation happening during core recovery and handling is an endothermic process. The temperature decrease is mainly influenced by the volume of gas hydrate pieces and the

decomposition speed. The extent of cold temperature zones reflects in many ways the fabric of gas hydrates in the liners. Disseminated gas hydrates are prone to dissociation in a relatively short time. After a very short time of dissociation-induced cooling which occurs relatively homogenously throughout a respective core section temperature re-increases. Because of the relatively small amount of water released during decomposition of disseminated hydrates, residual sediments often show a moussy fabric (Weinberger et al., 2005) and exhibit moderate negative ΔT of –3 °C to –4 °C (Fig 3.2B). In contrast, nodular gas hydrates, massive hydrate layers or hydrate-filled fractures usually occurring in distinct intervals reveal stronger negative ΔT of up to –10 °C (Fig 3.2C). Decomposition of such hydrate fabrics principally takes much longer time than that of disseminated hydrates because of both, their comparably smaller surface area and the resulting higher efficiency of the self-preservation effect (Sloan and Koh, 2007). During decomposition of nodular/massive hydrates the residual sediment might become very soupy because of the high volume of hydrate water released.

Voids or gaps defined as empty intervals in the liners are often due to gas expansion. They are typically represented by positive ΔT of +2 °C to +4 °C (Fig 3.2A and 2C) because the effective heat capacity of the gas/air filled liner strongly differs from that of sediments and the temperature gets into equilibrium with the ambient air rapidly. Voids within gas hydrate-bearing sediments (Fig 3.2C) are generated by gas expansion likely caused by gas release from hydrate dissociation. In contrast, voids within non-hydrate sediment (Fig 3.2A), are likely caused by methane release from the dissolved phase due to the pressure drop during core recovery. High-temperature patches with absolute temperatures of more than 30 °C as shown in Fig 3.2A are core handling artifacts.

Since the IR thermal patterns of the cores are mainly controlled by their contents, they were classified into four groups (Fig 3.3).

IR-temperature pattern 1: Sediment without gas hydrates

Homogenous hemipelagic sediment was represented by moderate temperatures of 23–25 °C (Fig 3.2A). It was present in the top few meters of all cores (from 1.2 mbsf in GMMB11 to 38.5 mbsf in GMMB09). It also occurred at the bottom of some cores below the gas hydrate occurrence zone (GHOZ), including GMMB03, GMMB05, GMMB08 and GMMB12 (Fig 3.3).

IR-temperature pattern 2: Sediment with gas hydrate

Gas hydrate-bearing sediments showed relatively low temperatures (less than ~22 °C) of the liner surface (Fig 3.2B and 2C). Associated voids represented by positive ΔT were also observed. Since the voids are mainly caused by gas expansion during hydrate dissociation, which pushes the sediments apart, void intervals were included in pattern 2 as well.

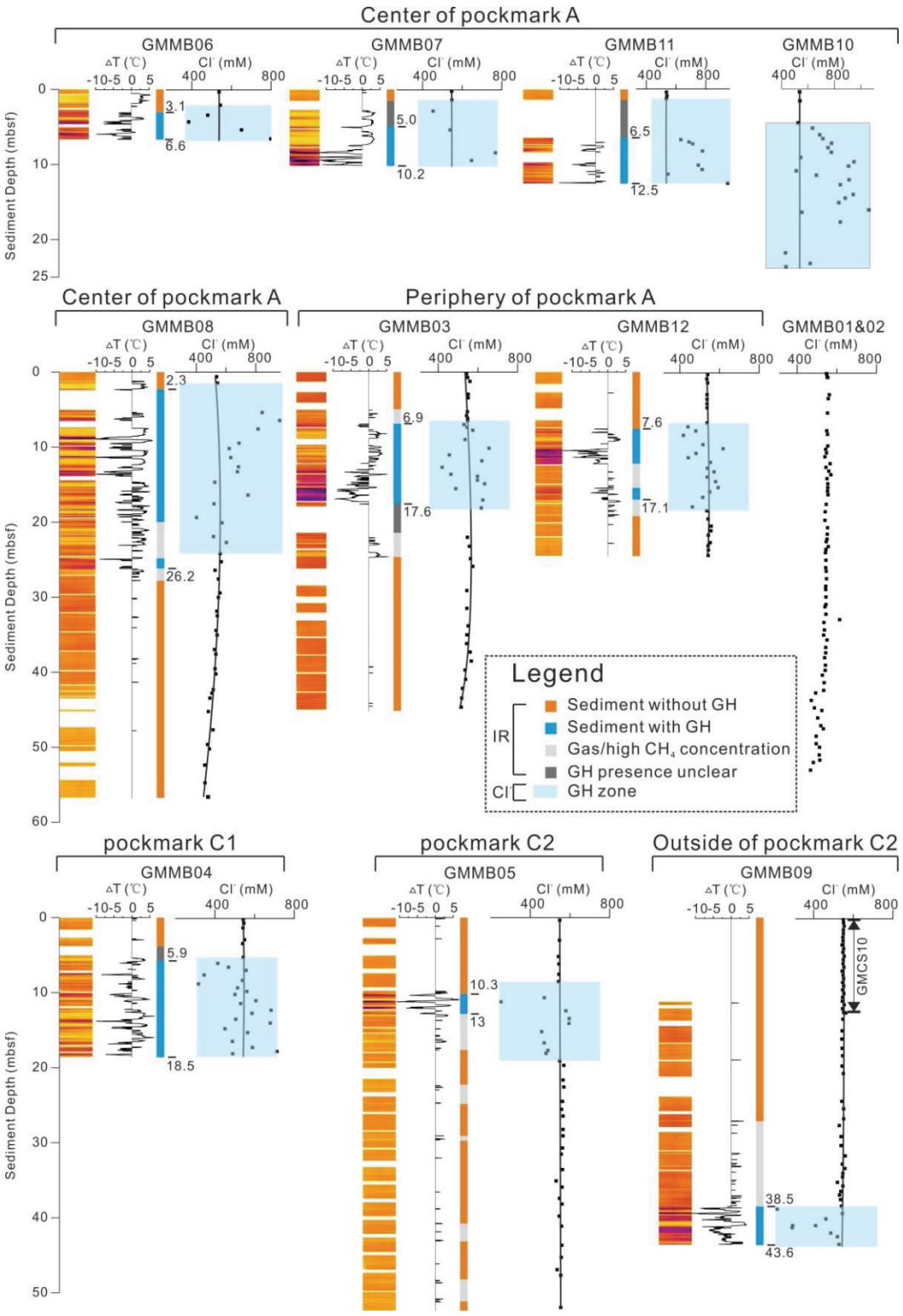

Figure 3.3: IR temperatures and pore water chloride concentration profiles of MeBo cores. Four data sets are shown for most drill sites: IR image colors, IR temperature profiles, interpreted gas hydrate distributions, and chloride profiles. The color bar of the IR images is consistent with Fig 3.2 and white intervals indicate gaps. Temperature profiles show the differences between the measured temperature and background temperatures of core liners, expressed as ΔT. Positive ΔT values correlate with voids in the cores and negative ΔT values represent decomposing gas hydrates. The approximate down-core gas hydrate presence interpreted from IR images is indicated by colored bars and indications for depth below seafloor (mbsf). Depths of gas hydrate-bearing intervals as inferred from chloride anomalies are highlighted in blue shading. Note that the chloride data of the upper 12.7 mbsf at station GMMB09 were derived from a piston core (GMCS10) taken at the same position.

IR-temperature pattern 3: High gas concentration

This temperature pattern was defined for core sections with relative moderate temperature between 23 and 25 °C, separated by distinct voids represented by slightly warmer temperatures of ~27 °C. In some gas hydrate-free sediment intervals, cm-scaled voids appeared in a dense pattern and revealed positive ΔT in the IR images (e.g. 30.0-38.5 mbsf in core GMMB09; Fig 3.3). Formation of voids is attributed to the expansion of methane gas excluded from the dissolved phase due to depressurization.

IR-temperature pattern 4: Intervals of unidentified liner content

Large unfilled sections adjacent to gas hydrate-bearing sediment were occasionally observed, for example in GMMB07 and GMMB11 (Fig 3.3). However, it remained unclear whether gas hydrates were present in these sections prior to IR imaging. Thus, we defined these core sections as intervals of unidentified liner content.

3.5.2 Pore water chloride concentrations

Chloride concentrations in pore waters of 12 MeBo cores were measured to study vertical gas hydrate distributions and to compare the results with those obtained by IR thermal scanning (Fig 3.3). Chloride concentrations in bottom waters were around 550 mM and were also measured in near-surface sediments. With increasing depth, Cl^- concentrations showed a slightly decreasing trend in some cores such as GMMB08 and GMMB03. By considering Cl^- = 550 mM as background, discrete positive and negative concentration anomalies were identified in the cores. Negative anomalies, with minimum concentrations of 213.1 mM at 38.83 mbsf in core GMMB09, were found widely distributed in gas hydrate-bearing sediments. These were caused by the dilution of pore water by Cl^--free water which is released by hydrate dissociation during core recovery (Torres et al., 2004a; Tréhu et al., 2004). Discrete positive Cl^- anomalies, of up to 1059.7 mM, in contrast are proposed to be associated with fast hydrate formation. During formation of gas hydrates ions are excluded from the hydrate lattice, which results in an increases in pore water chloride concentrations (Torres et al., 2011; Torres et al., 2004b). In previous studies it was observed that for chloride back diffusion to background concentrations takes a comparably long time (Haeckel et al., 2004). Therefore, positive anomalies existing *in situ* can still be detected by conventional pore water analysis in case quick sampling prevents pore water dilution by fresh water from dissociating hydrates. Since the pore water samples were taken immediately before the massive hydrates were totally decomposed, the elevated chloride concentrations are a proxy for relatively recent hydrate formation in sediments of the pockmarks.

3.5.3 Regional and depth variations in gas hydrate distributions

Both proxies, IR imaging and pore water chloride concentration profiling, revealed similar gas hydrate down core distributions and only for some small intervals results from both methods did not correlate (Table 3.1). Hydrates in pockmark A were present in the central

part at much shallower depth compared to the periphery (Fig 3.3, Table 3.1). Temperature anomalies captured by the IR images indicated that the top of the GHOZ in the central part (GMMB06, GMMB07, GMMB08 and GMMB11) ranges from 2.3 mbsf (GMMB08) to 6.5 mbsf (GMMB11), whereas chloride anomalies revealed hydrate presence from 1.2 mbsf (GMMB11) to 4.4 mbsf (GMMB10). Peripheral cores (GMMB03 and GMMB12) showed down core gas hydrate presence from 6.9 to 7.6 mbsf by using IR imaging and 6.1 to 6.7 mbsf based on chloride anomalies (Fig 3.3). These data sets substantiate a very shallow top of the GHOZ in the pockmark center which deepens towards its rim as already suggested by Sultan (2010). In core GMMB08, taken in the NW central part of pockmark A, the down core gas hydrate distribution was indicated by IR imaging down to 26.4 mbsf and by the chloride proxy down to 24.1 mbsf. In cores GMMB03 and GMMB12 taken at the periphery of pockmark A, gas hydrate occurrences were present from about 7 mbsf down to about 17 mbsf.

In pockmarks C1 and C2, the top of the GHOZ was determined to be positioned between 5.9 mbsf and 10.3 mbsf using IR imaging proxy, and 5.3 mbsf and 8.5 mbsf using chloride anomalies (Fig 3.3). Outside pockmark C2, core GMMB09 showed the deepest gas hydrate occurrence of all MeBo cores from about 38.5 mbsf down to its maximum penetration depth of 43.6 mbsf (Fig 3.3).

3.5.4 In situ sediment temperatures

In situ temperature measurements conducted at ten stations in pockmark A using MTLs showed slight variations in water temperatures ranging between 4.45 and 4.53 °C (Fig 3.4, Table 3.2). For the *in situ* sediment temperature measurements most geothermal gradients showed linear or sub-linear slopes. The thermal gradient established at station GMGCT22, which was performed outside pockmark A and is considered as reference station, was about 72 °C/km. Similar thermal gradients ranging between 51 and 79 °C/km were determined for four other stations (GMGCT23, 24, 41 and 49). At a cluster of five stations performed in the hummocky area elevated geothermal gradients were observed. Slightly elevated gradients of 112 and 119 °C/km were measured at stations GMGCT46 and -47, respectively. At stations GMGCT44, -45 and -40, the gradients were 198 and 330 °C/km, which is 2.8 and 4.6 times higher than the gradient at the background station, respectively. At station GMGCT40 a considerably elevated temperature deviating from the general trend established by the other MTLs was measured with TL-2 at a sediment depth of about 2 mbsf (Fig 3.4).

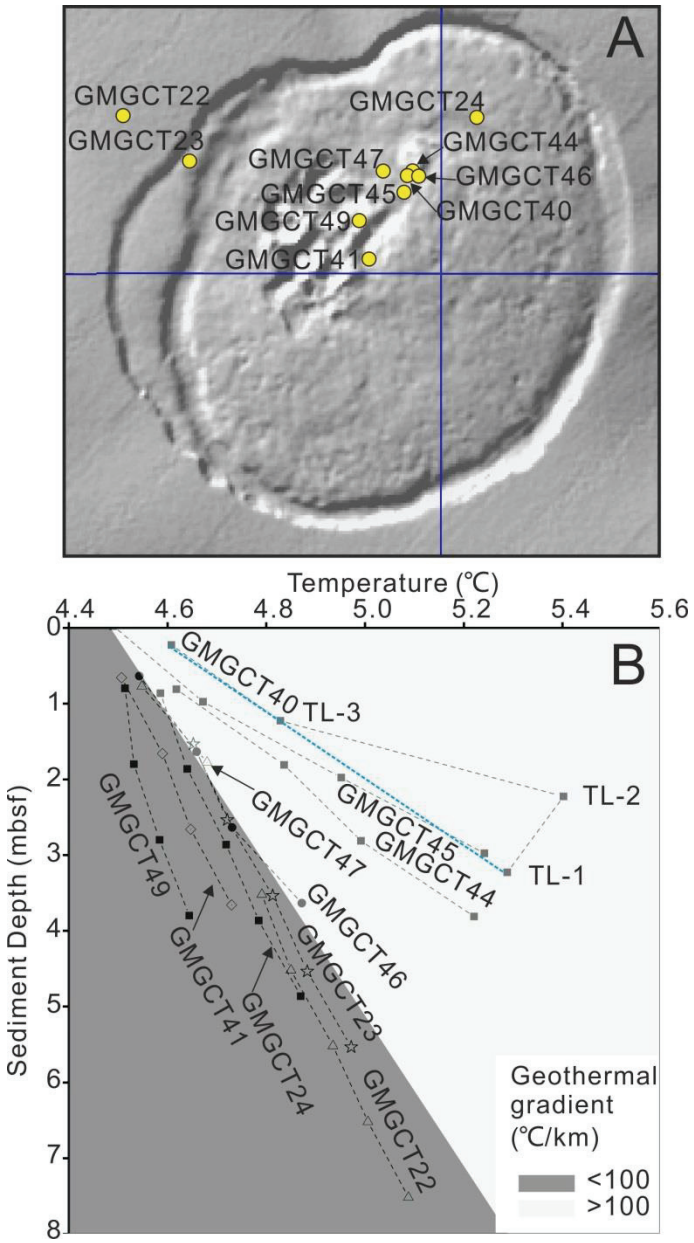

Figure 3.4: A: Position of sites chosen for temperature measurements in pockmark A. B: In situ sediment temperature measurements. Temperature gradients were classified into two clusters: (1) background gradients (around 72 °C/km) highlighted by the dark grey background, and (2) high gradients caused by fluid advection without background color.

3.6 Discussion

3.6.1 Thermal regime of pockmark A

The geothermal gradient in the central part of pockmark A was significantly higher than the local background gradient (Fig 3.4). Elevated temperatures in marine sediments caused by fluid flow have been widely reported from active mud volcanoes (e.g. Feseker et al., 2008; 2009a;b; Foucher et al., 2010) and other marine seep types (Römer et al., 2012). At pockmark A studied herein indications for mud flow activities such as mud breccia (Kopf, 2002) have not been found. However, free gas ebullition observed above the central part of pockmark A during the expedition (for location see Sultan et al., 2014) proves fluid

upward migration at this structure. Thus, the temperature elevation in shallow sediment is likely caused by fluid advection.

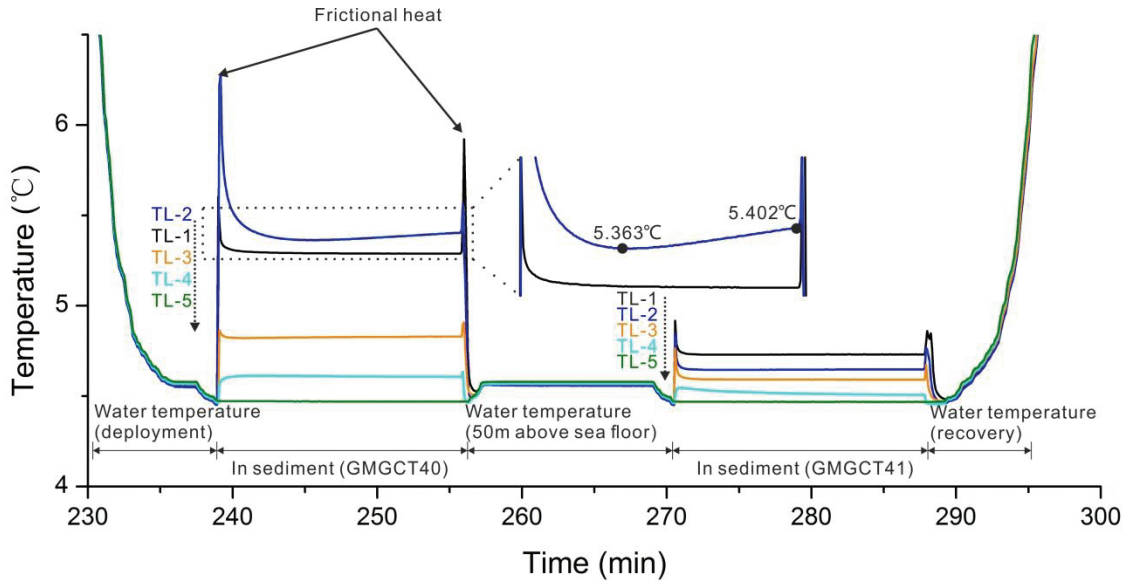

Figure 3.5: Temperature change with time at stations GMGCT40 and GMGCT41. TL-1 to TL-5 represents the temperature sensors attached to the corer from base to top. Remarkably, the temperature measured with TL-2 at station GMGCT40 increased continuously after penetration and was higher than that of TL-1, which penetrated deeper into the sediment. Note that TL-5 had no contact with sediment and, therefore, measured bottom water temperature.

It is worth noting that none of our measured geothermal profiles is strictly linear. We assume that besides the influence from heat convection induced by fluid flow, precipitation of gas hydrates in pore space contributes partially to this phenomenon. Several physical bulk sediment properties (i.e. thermal conductivity, heat capacity, density) are altered by gas hydrate precipitation in the pore space. In particular, gas hydrate formation is an exothermic reaction and heat is released when hydrate crystallizes (Sloan and Koh, 2007; Waite et al., 2007). Waite et al. (2007) pointed out that the thermal diffusivity of sediment with 60% porosity and 40% gas hydrate saturation increases by 20% compared to that of non-hydrate-bearing sediment. The gas hydrate saturation in the studied pockmarks is not quantified yet. Nevertheless, we conservatively estimate that gas hydrate saturations in specific sediment depths do not exceed 40% and that deviations of absolute temperatures caused by hydrates are <20% with respect to a hypothetical linear thermal gradient throughout the sediment.

At station GMGCT40 (Fig 3.4) an exceptionally high temperature was measured with TL-2 if compared to the other temperature loggers mounted below and above. This phenomenon was also observed at a high-flux seep area in the Black Sea (Römer et al., 2012). Fig 3.5 shows the continuous temperature change with time recorded with the loggers during stations GMGCT40 and 41 when the corer has not been lifted out of the water. It becomes obvious that at station GMGCT40 the absolute temperature measured with TL-2 was generally highest and that the temperature slope reversed after a while.

Temperatures determined with TL-1, -3, and -4 were lower and reached equilibrium in contrast to that of TL-2. During station GMGCT41 absolute temperatures changed according to the expected order which corresponded to the arrangement of loggers at the gravity corer.

The temperature difference between TL-1 and TL-2 is 0.127 °C which is two orders of magnitude higher than the logger accuracy (see Table 3.2). Thus, we conclude that the temperature measured with TL-2 was neither noise nor caused by wrong operation. However, if we ignore the temperature measured with TL-2, temperatures determined with the other three loggers show a linear regression with a slope similar to those of GMGCT44 (198°C/km) and GMGCT45 (258°C/km) (see Fig 3.4).

The exceptionally high temperature recorded at about 2 mbsf at station GMGCT40 can not be explained by vertical fluid advection and/or sediment thermal properties changed by hydrate formation. It is obvious that additional heat was generated at the depth between TL-1 and TL-3. In a 3D complex pockmark, spatially restricted temperature elevations might be caused by lateral heat advection from fluid flow along fractures or fast gas hydrate formation. Gas hydrate formation and dissociation are exothermic and endothermic processes, respectively, which subsequently change the thermal regime of pockmarks (Chen and Cathles, 2005). During the cruise, gas hydrate with bubble fabric, which is an indication of fast gas hydrate crystallization from methane bubbles (Bohrmann et al., 1998), was sampled with gravity cores. Since gas hydrate occurs widely in the center of pockmark A, its crystallization could release significant amounts of heat (Chen and Cathles, 2005). Although we did not further investigate the amount of freshly formed hydrate required to induce the relative temperature increase observed, we speculate that TL-2 might have intersected with a fracture in which either gas hydrate precipitated rapidly and/or fluid flowed happened facilitating lateral heat convection.

Because gas hydrates are sensitive to temperature variations (e.g. Feseker et al., 2009b; Pape et al., 2011; Römer et al., 2012; Berndt et al., 2014) thermal variations in the sediment impact gas hydrate distributions. At active seeps, temperature elevation in shallow sediments due to fluid advection lifts the base of the GHSZ (e.g. Ginsburg et al., 1999; Römer et al., 2012). Considering the maximum (258 °C/km) and minimum (72 °C/km) geothermal gradients determined in this study (Table 3.2), the base of the GHSZ under pockmark A should be situated between 35 mbsf and 130 mbsf, respectively (Fig 3.6). Since high thermal gradients were detected only in a restricted area NW of the geometrical center of the pockmark, we assume that distinct temperature elevations caused by fluid advection influence the GHSZ only on a small scale. In the water column, the top of the GHSZ is estimated to be at 587 mbsl which is consistent with the maximum height of gas flares observed above pockmark A during the cruise (Sultan et al., 2014).

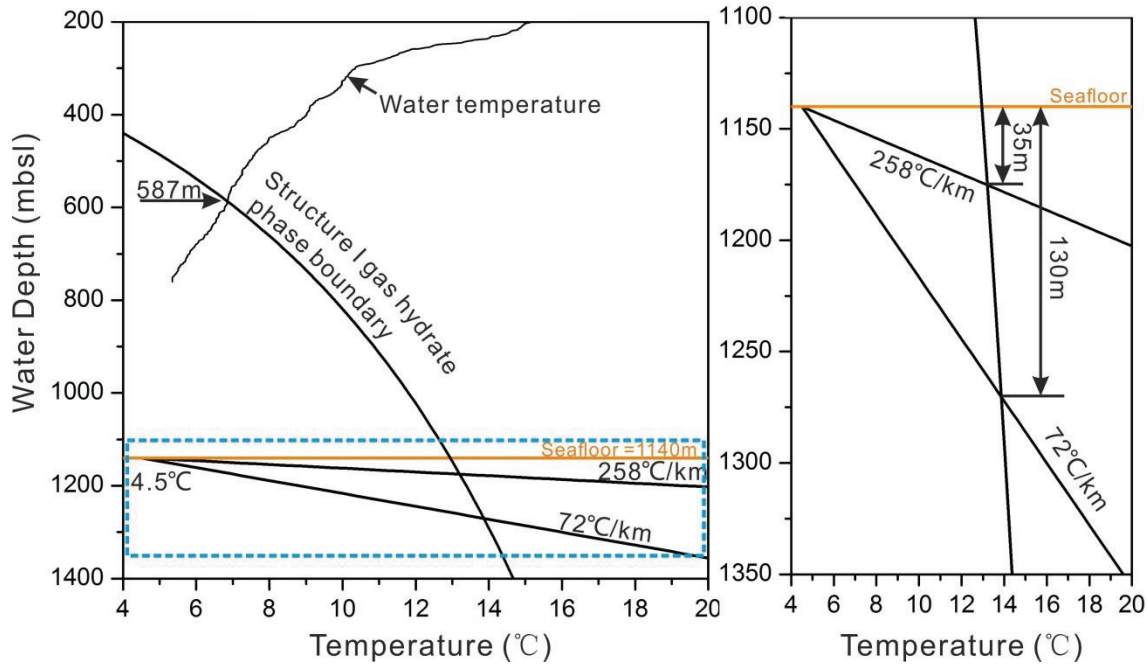

Figure 3.6: Phase diagram calculated for structure I gas hydrates with the HWHYD software (Masoudi and Tohidi, 2005) and using salinities and pure methane because methane concentration of hydrate-bounded gas is higher than 99.9% (unpublished data). A CTD record was used to show the water column temperature profile. 72 °C/km (GMGCT22) was used as the local background geothermal gradient outside the pockmarks, while 258 °C/km (GMGCT45) was measured close to a site at pockmark center which showed seafloor gas emission (see Sultan et al., 2014). The subsurface part (dash blue rectangle) of the diagram is enlarged in the right part of the figure.

3.6.2 Gas hydrate and fluid flow

Results from IR scanning and pore water chloride concentration analysis of the MeBo cores as well as recoveries substantiate gas hydrate presence in shallow (meters to tens of meters depth) sediments of the three studied pockmarks. It was shown that shallow gas hydrates at active marine seeps primarily form from free gas (Haeckel et al., 2004; Römer et al., 2012; Sahling et al., 2008; Torres et al., 2004b; Wallmann et al., 2006). Gas flares observed above pockmark A during the survey in 2011 are direct evidence of gas flow through the sediment (Sultan et al., 2014). Therefore, we assume that gas hydrates in the studied pockmarks are mainly formed from the free gas phase. Free gas captured in pockets within the GHOZ might contribute to the high amplitude reflectors observed in seismic records from that area (Figs .7). In particular, at station GMMB04 in pockmark C1 showed vigorous gas expulsion during drilling at ~18 mbsf, which corresponds to distinct high amplitude reflectors (Fig 3.7B) (Sultan et al., 2014).

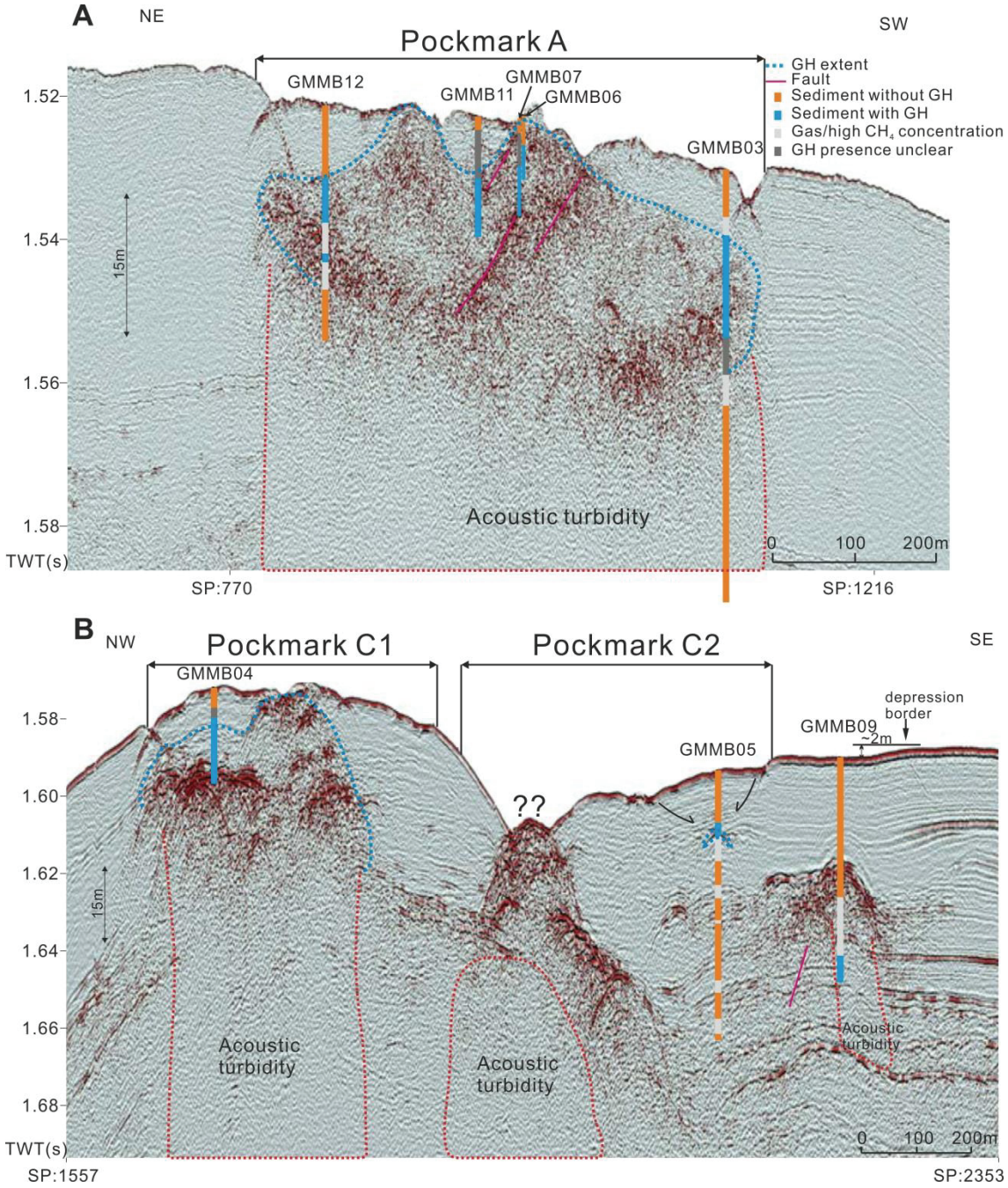

Figure 3.7: SYSIF seismic profiles SY03-THR-Pr01 crossing pockmark A and SY01-THR-Pr02 covering pockmark cluster C. Locations and orientations are shown in Fig 3.1. Interpretations from MeBo cores are projected on the seismic lines. High-amplitude reflectors are widespread in the seismic profile.

Free gas can migrate along fractures and gas hydrate can precipitate along fracture walls (Torres et al., 2004b; Flemings et al., 2003) where fluid pressure and crystallization forces are less than the effective overburden stress. In case free methane-rich gas migrates upward into shallow sediment, where fluid pressure and crystallization force exceed the effective overburden stress, it spreads out in the pore space and reacts with water, forming gas hydrate (Torres et al., 2004b). This assumption is supported by our observation of gas hydrates present within the upper ~30m (Figs. 2, 3, 7). Because the maximum depth of the

GHSZ at pockmark A is situated at around 130 mbsf (geothermal gradient: 72 °C/km; Table 3.2; Fig 3.6), we might assume that gas hydrate also forms at greater depth.

However, gas flow in a seep system is not under steady state (Bangs et al., 2011; Chand et al., 2012; Gay et al., 2006b; Greinert et al., 2006) and pressure drop in deep gas reservoirs (Bangs et al., 2011) and/or sealing of pathways by gas hydrate formation (Riedel et al., 2006) might result in a decrease, or even cease of gas flow. Thus, although no gas flares were recognized at pockmark C1 and C2 during this expedition, gas hydrates in these two pockmarks likely formed from active gas flow in the recent past.

Upward gas migration stimulates the anaerobic methane oxidation (AOM) mediated by methanotrophic archaea and sulfate reducing bacteria in near-surface sediments (Hoehler et al., 1994; Boetius et al., 2000), and the resulting end products, such as hydrogen sulfide, nourish a chemosynthesis-based ecosystem (Sahling et al., 2008). During our expedition living vesicomyid clams, which rely on sulfide oxidation, were recovered from the seafloor in the studied area, indicating a living chemosynthetic ecosystem. However, as mentioned above, gas flow at a seep system is a transient process. Bangs et al. (2011) pointed out that methane gas flow for a vent at Southern Hydrate Ridge has undergone significant reduction or complete interruption within just a few years, whereas the associated ecosystem has persisted for thousands of years. This observation raises the question, how the chemosynthesis-based species survive during periods of reduced gas flow. In a gas hydrate setting methane diffuses continuously from the shallow gas hydrate reservoir towards the methane-depleted sea water and sustains AOM. This is consistent with the assumption of Sultan et al. (2010) that many gas hydrate reservoirs in the study area are currently undergoing dissolution due to insufficient methane supply from greater depth. Similar conclusions of chemosynthetic-based macrofauna presumably relying on continuous methane supply from decomposing hydrates were already proposed for seep systems in other regions (e.g., Paull et al., 1995; Pape et al., 2014). Thus, we propose that gas hydrate reservoirs in shallow sediments serve as a capacitor (see e.g. Dickens, 2003), as they form rapidly during a high gas-flow phase, and sustain the seep ecosystem by slow methane diffusion when the gas flow from below is reduced.

3.6.3 Pockmark formation

It was initially proposed by Sultan et al. (2010) that gas hydrate dissolution caused by insufficient gas supply is the controlling factor for pockmark formation and evolution in the study area. New field data suggested that pockmark formation is not only controlled by slow gas hydrate dissolution but also by rapid hydrate formation (Sultan et al., 2014). Based on the data obtained from the MeBo cores in this study, an improved but simple model comprising five stages is suggested for the evolution of the pockmarks (Fig 3.8) in the studied area.

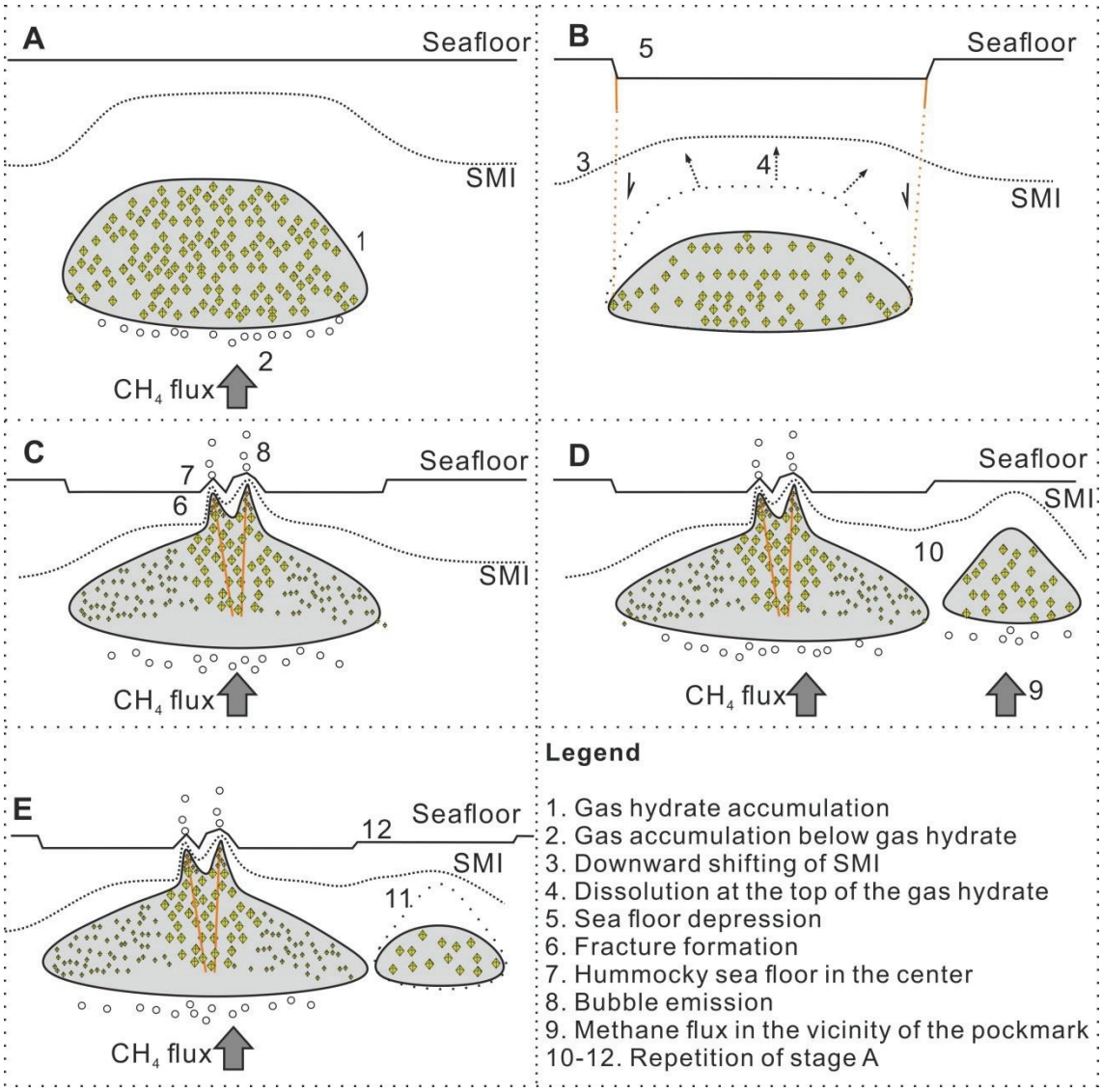

Figure 3.8: Schematic representations of the pockmark formation controlled by fluid flow and gas hydrate precipitation during different evolutionary stages (A-E).

Stage A: Gas migrates from a deep source. Within the GHSZ, when the hydrate crystallization force overcomes the burden of the overlying sediment, gas hydrate starts precipitating in the shallow sediment. Gas hydrate growth decreases the pore space availability and sediment permeability and clogs the pathways of fluid flow, which subsequently decreases or even ceases the fluid flow in uppermost sediments. During this stage, there is neither a distinct morphological change on the seafloor nor gas emission into the water column.

Stage B: In case of reduced gas flow to shallow sediments, sulfate can penetrate to greater depths, which leads to a downward shift of the SMI (see e.g. Borowski et al., 1996). Methane in the shallow sediment is likely depleted due to diffusion and AOM. As a result, gas hydrates dissolve from the top of the GHOZ (see Sultan et al., 2010). Subsequently, the overlying sediment is deformed due to the volume loss below and a seafloor depression is

created. This stage might explain the ~2 m depression observed for pockmark C2 (Figs. 1 and 7).

Stage C: Once the fluid flow is re-intensified, methane and shallow hydrate repeat the same procedure as described in Stage A. When pore pressure surpasses a threshold value, fractures are generated in the overlying sediment at the pockmark center (e.g. observed in pockmark A, Fig 3.7) which might serve as pathways for free gas to migrate to the seafloor. Since these fractures form within the GHSZ, gas hydrates might accumulate along the fracture walls which efficiently prevent the contact between pore water and gases. Fast gas hydrate formation will significantly increase the salinity of the surrounding pore water due to ion exclusion and the resulting brine might locally prevent gas hydrate formation (Ussler & Paull, 1995; Torres et al., 2011). Massive gas hydrate accumulating in the shallow sediment expands the mass volume and creates convex-shaped elevations as well as a rough seafloor, like observed close to the center of pockmark A (Fig 3.1). This can explain the cones and hummocky structure at the centers of pockmarks A and C1 (Fig 3.7).

Stage D: In case the methane flux is redirected towards shallow sediments in the vicinity of the initial pockmark, a new pockmark might be created and might repeat stages A-C.

Stage E: The complexity and size of a pockmark might increase significantly in case more and more new pockmarks morphologically combine (Marcon et al., 2014). It might be assumed that pockmark C1, which exhibits a roughly NE-SW seafloor expression and complex seafloor morphology, is composed of several small pockmarks at different stages.

3.7 Conclusion

Gas hydrate distributions in the sediment of three pockmarks on the Nigerian continental margin were investigated by applying infrared (IR) thermal imaging and pore water chloride and sulfate concentration measurements on cores recovered with the portable MeBo drill rig. In addition, ten in situ sediment temperature measurements were performed to study the geothermal regime of the individual pockmark A. Based on the temperature and chloride anomalies, the following conclusions are drawn:

1. Negative temperature anomalies detected by IR thermal scanning as well as positive and negative chloride anomalies in pore waters indicated the presence of gas hydrate in shallow pockmark sediments. Distributions of gas hydrate-bearing sediments as inferred from both methods match each other.

2. Geothermal gradients up to 5 times higher in the center of pockmark A than the background were interpreted to result from enhanced heat advection caused in the course of fluid flow and potentially also to fast growth of gas hydrates.

3. Recent hydrate formation is inferred from positive chloride anomalies.

4. Gas hydrate precipitation and dissolution caused by the variation of fluid flow exert significant impact on the formation and evolution of pockmarks on the Nigerian continental margin.

Acknowledgement

We thank the captain and crew of R/V Pourquoi pas? for support during the Guineco-MeBo cruise in 2011. We thank also the MeBo team from MARUM and the staff of IFREMER for the excellent help during the cruise. We are thankful for the constructive comments from C. Berndt and an anonymous reviewer which helped to improve the manuscript significantly.

This work was partly funded through the DFG-Research Center/Excellence Cluster "The Ocean in the Earth System" MARUM – Center for Marine Environmental Sciences. A major financial contribution came from BMBF-project 03G0824A.

Data used in the present paper are covered by a confidentiality agreement between Total, IFREMER and MARUM that restrict access; interested readers can contact the authors for more information. J. Wei was sponsored by the China Scholarship Council (CSC).

Reference

Abegg, F., Bohrmann, G., Freitag, J., and Kuhs, W., 2007, Fabric of gas hydrate in sediments from Hydrate Ridge—results from ODP Leg 204 samples: Geo-Marine Letters, v. 27, no. 2-4, p. 269-277.

Andresen, K. J., Huuse, M., and Clausen, O. R., 2008, Morphology and distribution of Oligocene and Miocene pockmarks in the Danish North Sea - implications for bottom current: Basin Research, v. 20, no. 3, p. 445-466.

Bangs, N. L. B., Hornbach, M. J., and Berndt, C., 2011, The mechanics of intermittent methane venting at South Hydrate Ridge inferred from 4D seismic surveying: Earth and Planetary Science Letters, v. 310, no. 1–2, p. 105-112.

Bayon, G., Pierre, C., Etoubleau, J., Voisset, M., Cauquil, E., Marsset, T., Sultan, N., Le Drezen, E., and Fouquet, Y., 2007, Sr/Ca and Mg/Ca ratios in Niger Delta sediments: Implications for authigenic carbonate genesis in cold seep environments: Marine Geology, v. 241, no. 1–4, p. 93-109.

Berndt, C., Feseker, T., Treude, T., Krastel, S., Liebetrau, V., Niemann, H., Bertics, V. J., Dumke, I., Dünnbier, K., Ferré, B., Graves, C., Gross, F., Hissmann, K., Hühnerbach, V., Krause, S., Lieser, K., Schauer, J., and Steinle, L., 2014, Temporal Constraints on Hydrate-Controlled Methane Seepage off Svalbard: Science, v. 343, no. 6168, p. 284-287.

Boetius, A., Ravenschlag, K., Schubert, C. J., Rickert, D., Widdel, F., Gieseke, A., Amann, R., Jorgensen, B. B., Witte, U., and Pfannkuche, O., 2000, A marine microbial consortium apparently mediating anaerobic oxidation of methane: Nature, v. 407, no. 6804, p. 623-626.

Bohrmann, G., Greinert, J., Suess, E., and Torres, M., 1998, Authigenic carbonates from the Cascadia subduction zone and their relation to gas hydrate stability: Geology, v. 26, no. 7, p. 647-650.

Borowski, W.S., Paull, C.K., Ussler III, W., (1996) Marine pore-water sulfate profiles indicate in situ methane flux from underlying gas hydrate. Geology, 24(7), 655-658.

Brooks, J. M., Bryant, W. R., Bernard, B. B., and Cameron, N. R., 2000, The Nature of Gas Hydrates on the Nigerian Continental Slope: Annals of the New York Academy of Sciences, v. 912, no. 1, p. 76-93.

Bünz, S., Mienert, J., and Berndt, C., 2003, Geological controls on the Storegga gas-hydrate system of the mid-Norwegian continental margin: Earth and Planetary Science Letters, v. 209, no. 3–4, p. 291-307.

Carson, B., Seke, E., Paskevich, V., Holmes, M.L., (1994) Fluid expulsion sites on the Cascadia accretionary prism: Mapping diagenetic deposits with processed GLORIA imagery. J. Geophys. Res., 99(B6), 11959-11969.

Chand, S., Thorsnes, T., Rise, L., Brunstad, H., Stoddart, D., Bøe, R., Lågstad, P., and Svolsbru, T., 2012, Multiple episodes of fluid flow in the SW Barents Sea (Loppa High) evidenced by gas flares, pockmarks and gas hydrate accumulation: Earth and Planetary Science Letters, v. 331–332, no. 0, p. 305-314.

Chen, D. F., and Cathles, L. M., 2005, On the thermal impact of gas venting and hydrate crystallization: Journal of Geophysical Research: Solid Earth, v. 110, no. B11, p. B11204.

Chen, S.-C., Hsu, S.-K., Tsai, C.-H., Ku, C.-Y., Yeh, Y.-C., and Wang, Y., 2010, Gas seepage, pockmarks and mud volcanoes in the near shore of SW Taiwan: Marine Geophysical Researches, v. 31, no. 1-2, p. 133-147.

Cohen, H. A., and McClay, K., 1996, Sedimentation and shale tectonics of the northwestern Niger Delta front: Marine and Petroleum Geology, v. 13, no. 3, p. 313-328.

Cunningham, R., and Lindholm, R. M., 2000, AAPG Memoir 73, Chapter 8: Seismic Evidence for Widespread Gas Hydrate Formation, Offshore West Africa.Damuth, J. E., 1994, Neogene gravity tectonics and depositional processes on the deep Niger Delta continental margin: Marine and Petroleum Geology, v. 11, no. 3, p. 320-346.

Dickens, G.R., (2003) Rethinking the global carbon cycle with a large, dynamic and microbially mediated gas hydrate capacitor. Earth and Planetary Science Letters, 213(3-4), 169-183.

Dondurur, D., Çifçi, G., Drahor, M. G., and Coşkun, S., 2011, Acoustic evidence of shallow gas accumulations and active pockmarks in the Izmir Gulf, Aegean sea: Marine and Petroleum Geology, v. 28, no. 8, p. 1505-1516.

Feseker, T., Dählmann, A., Foucher, J. P., and Harmegnies, F., 2009a, In-situ sediment temperature measurements and geochemical porewater data suggest highly dynamic fluid flow at Isis mud volcano, eastern Mediterranean Sea: Marine Geology, v. 261, no. 1–4, p. 128-137.

Feseker, T., Foucher, J. P., and Harmegnies, F., 2008, Fluid flow or mud eruptions? Sediment temperature distributions on Håkon Mosby mud volcano, SW Barents Sea slope: Marine Geology, v. 247, no. 3–4, p. 194-207.

Feseker, T., Pape, T., Wallmann, K., Klapp, S.A., Schmidt-Schierhorn, F., Bohrmann, G., (2009b) The thermal structure of the Dvurechenskii mud volcano and its implications for gas hydrate stability and eruption dynamics. Marine and Petroleum Geology, 26(9), 1812-1823.

Flemings, P. B., Liu, X., and Winters, W. J., 2003, Critical pressure and multiphase flow in Blake Ridge gas hydrates: Geology, v. 31, no. 12, p. 1057-1060.

Foucher, J.-P., Dupré, S., Scalabrin, C., Feseker, T., Harmegnies, F., and Nouzé, H., 2010, Changes in seabed morphology, mud temperature and free gas venting at the Håkon Mosby mud volcano, offshore northern Norway, over the time period 2003–2006: Geo-Marine Letters, v. 30, no. 3-4, p. 157-167.

Freudenthal, T., and Wefer, G., 2013, Drilling cores on the sea floor with the remote-controlled sea-floor drilling rig MeBo: Geosci. Instrum. Method. Data Syst. Discuss., v. 3, no. 2, p. 347-369.

Gay, A., Lopez, M., Cochonat, P., Levaché, D., Sermondadaz, G., and Seranne, M., 2006a, Evidences of early to late fluid migration from an upper Miocene turbiditic channel revealed by 3D seismic coupled to geochemical sampling within seafloor pockmarks, Lower Congo Basin: Marine and Petroleum Geology, v. 23, no. 3, p. 387-399.

Gay, A., Lopez, M., Ondreas, H., Charlou, J. L., Sermondadaz, G., and Cochonat, P., 2006b, Seafloor facies related to upward methane flux within a Giant Pockmark of the Lower Congo Basin: Marine Geology, v. 226, no. 1–2, p. 81-95.

George, R. A., and Cauquil, E., AUV Ultrahigh-Resolution 3D Seismic Technique for Detailed Subsurface Investigations, *in* Proceedings Offshore Technology Conference2007, Offshore Technology Conference.

Ginsburg, G. D., Milkov, A. V., Soloviev, V. A., Egorov, A. V., Cherkashev, G. A., Vogt, P. R., Crane, K., Lorenson, T. D., and Khutorskoy, M. D., 1999, Gas hydrate accumulation at the Håkon Mosby Mud Volcano: Geo-Marine Letters, v. 19, no. 1-2, p. 57-67.

Graue, K., 2000, Mud volcanoes in deepwater Nigeria: Marine and Petroleum Geology, v. 17, no. 8, p. 959-974.

Greinert, J., Artemov, Y., Egorov, V., De Batist, M., and McGinnis, D., 2006, 1300-m-high rising bubbles from mud volcanoes at 2080m in the Black Sea: Hydroacoustic characteristics and temporal variability: Earth and Planetary Science Letters, v. 244, no. 1–2, p. 1-15.

Haeckel, M., Suess, E., Wallmann, K., and Rickert, D., 2004, Rising methane gas bubbles form massive hydrate layers at the seafloor: Geochimica et Cosmochimica Acta, v. 68, no. 21, p. 4335-4345.

Hartwig, A., Anka, Z., and di Primio, R., 2012, Evidence of a widespread paleo-pockmarked field in the Orange Basin: An indication of an early Eocene massive fluid escape event offshore South Africa: Marine Geology, v. 332-334, p. 222-234.

Heggland, R., Vertical hydrocarbon migration at the Nigerian continental slope: applications of seismic mapping techniques, *in* Proceedings AAPG Annual Meeting, Salt Lake City, May2003, p. 11-14.

Hoehler, T.M., Alperin, M.J., Albert, D.B., Martens, C.S., (1994) Field and laboratory studies of methane oxidation in an anoxic marine sediment: Evidence for a methanogen-sulfate reducer consortium. Global Biogeochemical Cycles, 8(4), 451-463.

Hovland, M., Gallagher, J. W., Clennell, M. B., and Lekvam, K., 1997, Gas hydrate and free gas volumes in marine sediments: Example from the Niger Delta front: Marine and Petroleum Geology, v. 14, no. 3, p. 245-255.

Judd, A. A. G., and Hovland, M., 2007, Seabed fluid flow: the impact of geology, biology and the marine environment, Cambridge University Press.

Kopf, A. J., 2002, Significance of mud volcanism: Reviews of Geophysics, v. 40, no. 2, p. 1005.

Marcon, Y., Ondréas, H., Sahling, H., Bohrmann, G., and Olu, K., 2014, Fluid flow regimes and growth of a giant pockmark: Geology, v. 42, no. 1, p. 63-66.

Masoudi, R., Tohidi, B., (2005) Estimating the hydrate stability zone in the presence of salts and/or organic inhibitors using water partial pressure. Journal of Petroleum Science and Engineering, 46(1-2), 23-36.

Matsumoto, R., Ryu, B.-J., Lee, S.-R., Lin, S., Wu, S., Sain, K., Pecher, I., and Riedel, M., 2011, Occurrence and exploration of gas hydrate in the marginal seas and continental margin of the Asia and Oceania region: Marine and Petroleum Geology, v. 28, no. 10, p. 1751-1767.

Moss, J. L., Cartwright, J., and Moore, R., 2012, Evidence for fluid migration following pockmark formation: Examples from the Nile Deep Sea Fan: Marine Geology, v. 303-306, p. 1-13.

Pape, T., Feseker, T., Kasten, S., Fischer, D., Bohrmann, G., (2011) Distribution and abundance of gas hydrates in near-surface deposits of the Håkon Mosby Mud Volcano, SW Barents Sea. Geochemistry, Geophysics, Geosystems, 12(9), Q09009.

Pape, T., Geprägs, P., Hammerschmidt, S., Wintersteller, P., Wei, J., Fleischmann, T., Bohrmann, G., Kopf, A.J., (2014) Hydrocarbon seepage and its sources at mud volcanoes of the Kumano forearc basin, Nankai Trough subduction zone. Geochemistry, Geophysics, Geosystems, 15(6), 2180-2194.

Paull, C.K., Ussler III, W., Borowski, W.S., Spiess, F.N., (1995) Methane-rich plumes on the Carolina continental rise: Associations with gas hydrates. Geology, 23(1), 89-92.

Paull, C. K., Ussler, W., Holbrook, W. S., Hill, T. M., Keaten, R., Mienert, J., Haflidason, H., Johnson, J. E., Winters, W. J., and Lorenson, T. D., 2008, Origin of pockmarks and chimney structures on the flanks of the Storegga Slide, offshore Norway: Geo-Marine Letters, v. 28, no. 1, p. 43-51.

Pilcher, R., and Argent, J., 2007, Mega-pockmarks and linear pockmark trains on the West African continental margin: Marine Geology, v. 244, no. 1-4, p. 15-32.

Pinet, N., Duchesne, M., and Lavoie, D., 2010, Linking a linear pockmark train with a buried Palaeozoic structure: a case study from the St. Lawrence Estuary: Geo-Marine Letters, v. 30, no. 5, p. 517-522.

Riboulot, V., Cattaneo, A., Sultan, N., Garziglia, S., Ker, S., Imbert, P., and Voisset, M., 2013, Sea-level change and free gas occurrence influencing a submarine landslide and pockmark formation and distribution in deepwater Nigeria: Earth and Planetary Science Letters, v. In Press, Corrected Proof.

Riedel, M., Novosel, I., Spence, G. D., Hyndman, R. D., Chapman, R. N., Solem, R. C., and Lewis, T., 2006, Geophysical and geochemical signatures associated with gas hydrate–related venting in the northern Cascadia margin: Geological Society of America Bulletin, v. 118, no. 1-2, p. 23-38.

Rise, L., Sættem, J., Fanavoll, S., Thorsnes, T., Ottesen, D., and Bøe, R., 1999, Sea-bed pockmarks related to fluid migration from Mesozoic bedrock strata in the Skagerrak offshore Norway: Marine and Petroleum Geology, v. 16, no. 7, p. 619-631.

Ritger, S., Carson, B., Suess, E., (1987) Methane-derived authigenic carbonates formed by subduction-induced pore-water expulsion along the Oregon/Washington margin. Geological Society of America Bulletin, 98, 147-156.

Römer, M., Sahling, H., Pape, T., Bahr, A., Feseker, T., Wintersteller, P., and Bohrmann, G., 2012, Geological control and magnitude of methane ebullition from a high-flux seep area in the Black Sea—the Kerch seep area: Marine Geology, v. 319–322, no. 0, p. 57-74.

Sahling, H., Bohrmann, G., Spiess, V., Bialas, J., Breitzke, M., Ivanov, M., Kasten, S., Krastel, S., and Schneider, R., 2008, Pockmarks in the Northern Congo Fan area, SW Africa: Complex seafloor features shaped by fluid flow: Marine Geology, v. 249, no. 3-4, p. 206-225.

Seeberg-Elverfeldt, J., Schlüter, M., Feseker, T., Kölling, M., (2005) Rhizon sampling of porewaters near the sediment-water interface of aquatic systems. Limnology and Oceanography: Methods, 3, 361-371.

Sloan, E. D., and Koh, C., 2007, Clathrate hydrates of natural gases, CRC press.

Sultan, N., Bohrmann, G., Ruffine, L., Pape, T., Riboulot, V., Colliat, J. L., De Prunelé, A., Dennielou, B., Garziglia, S., Himmler, T., Marsset, T., Peters, C. A., Rabiu, A., and Wei, J., 2014, Pockmark formation and evolution in deep water Nigeria: Rapid hydrate growth versus slow hydrate dissolution: Journal of Geophysical Research: Solid Earth, v. 119, no. 4, p. 2013JB010546.

Sultan, N., Marsset, B., Ker, S., Marsset, T., Voisset, M., Vernant, A.-M., Bayon, G., Cauquil, E., Adamy, J., and Colliat, J., 2010, Hydrate dissolution as a potential mechanism for pockmark formation in the Niger delta: Journal of geophysical research, v. 115, no. B8, p. B08101.

Sun, Q., Wu, S., Hovland, M., Luo, P., Lu, Y., and Qu, T., 2011, The morphologies and genesis of mega-pockmarks near the Xisha Uplift, South China Sea: Marine and Petroleum Geology, v. 28, no. 6, p. 1146-1156.

Torres, M. E., Kim, J.-H., Choi, J.-Y., Ryu, B.-J., Bahk, J.-J., Riedel, M., Collett, T. S., Hong, W.-L., and Kastner, M., Occurrence of high salinity fluids associated with massive near-seafloor gas hydrate deposits, *in* Proceedings 7th International Conference on Gas Hydrates (ICGH 2011)2011.

Torres, M. E., Teichert, B. M. A., Tréhu, A. M., Borowski, W., and Tomaru, H., 2004a, Relationship of pore water freshening to accretionary processes in the Cascadia

margin: Fluid sources and gas hydrate abundance: Geophysical Research Letters, v. 31, no. 22, p. L22305.

Torres, M. E., Wallmann, K., Tréhu, A. M., Bohrmann, G., Borowski, W. S., and Tomaru, H., 2004b, Gas hydrate growth, methane transport, and chloride enrichment at the southern summit of Hydrate Ridge, Cascadia margin off Oregon: Earth and Planetary Science Letters, v. 226, no. 1-2, p. 225-241.

Tréhu, A. M., Long, P. E., Torres, M. E., Bohrmann, G., Rack, F. R., Collett, T. S., Goldberg, D. S., Milkov, A. V., Riedel, M., Schultheiss, P., Bangs, N. L., Barr, S. R., Borowski, W. S., Claypool, G. E., Delwiche, M. E., Dickens, G. R., Gracia, E., Guerin, G., Holland, M., Johnson, J. E., Lee, Y. J., Liu, C. S., Su, X., Teichert, B., Tomaru, H., Vanneste, M., Watanabe, M., and Weinberger, J. L., 2004, Three-dimensional distribution of gas hydrate beneath southern Hydrate Ridge: constraints from ODP Leg 204: Earth and Planetary Science Letters, v. 222, no. 3-4, p. 845-862.

Ussler III, W., Paull, C.K., (1995) Effects of ion exclusion and isotopic fractionation on pore water geochemistry during gas hydrate formation and decomposition. Geo-Marine Letters, 15(1), 37-44.

Ussler, W., III, Paull, C. K., Boucher, J., Friederich, G. E., and Thomas, D. J., 2003, Submarine pockmarks: a case study from Belfast Bay, Maine: Marine Geology, v. 202, no. 3-4, p. 175-192.

Waite, W. F., Stern, L. A., Kirby, S. H., Winters, W. J., and Mason, D. H., 2007, Simultaneous determination of thermal conductivity, thermal diffusivity and specific heat in sI methane hydrate: Geophysical Journal International, v. 169, no. 2, p. 767-774.

Wallmann, K., Aloisi, G., Haeckel, M., Obzhirov, A., Pavlova, G., and Tishchenko, P., 2006, Kinetics of organic matter degradation, microbial methane generation, and gas hydrate formation in anoxic marine sediments: Geochimica et Cosmochimica Acta, v. 70, no. 15, p. 3905-3927.

Weinberger, J. L., Brown, K. M., and Long, P. E., 2005, Painting a picture of gas hydrate distribution with thermal images: Geophysical Research Letters, v. 32, no. 4, p. L04609.

Chapter 4

Occurrence and characteristics of gas hydrates in the shallow sediments of the pockmark field at the Nigeria continental margin

Jiangong Wei[1*], Thomas Pape[1], Andrzej Falenty[2], Werner Kuhs[2], Gerhard Bohrmann[1]

1 MARUM, University of Bremen, Klagenfurter Str., 28359 Bremen, Germany

2 GZG, Abteilung Kristallographie, University of Goettingen, Goldschmidtstrasse 1, 37077 Goettingen, Germany

MANUSCRIPT 2

To be submitted to Marine and petroleum geology

4.1 Abstract

Knowledge of gas composition and crystal structure of natural gas hydrates is important for determining their stability, which is a key factor to understand the fate of methane gas bubbles and hydrate bulks in the water column and the size of the hydrate reservoir in the sediment. We ran experiments of powder X-ray diffraction (PXRD), Raman spectroscopy and gas chromatography (GC) analysis to study the structure and gas compositions of hydrate samples recovered from shallow sediment of pockmarks at water depths between1140 m and 1280 m on the Nigeria continental margin. The results show that well preserved hydrate samples are exclusively structure I hydrate, with methane as the dominant gas (96.87-98.49%) with small amount of CO_2 (0.35-1.65%), H_2S (0.48-2.73%) and trace C_2H_6 (0.02-0.03%). Other higher order hydrocarbon gases were below the detection limit. Raman analysis shows clear evidence that H_2S and CO_2 are enclathrated within gas hydrate cages. Experimentally calculated methane cage occupancy ratios (1.03-1.06) are slightly lower than the theoretical value of 1.10 which is explained by the preferential of CO_2 into large cages. Based on the physical conditions as well as gas hydrate characteristics, we calculated the gas hydrate stability. The results show that the gas hydrate stability zone (GHSZ) expands remarkably both upward in the water column and downward in the sediment due to the small amount of other gases, especially H_2S. This effect might significantly increase the size of the hydrate reservoir in the sediment as well as the possibility of methane bubbles and/or hydrate bulks into the winter mixed layer and even into the atmosphere.

Keywords: gas hydrate, Raman spectra, XRD, gas composition, gas hydrate stability

4.2 Introduction

Natural gas hydrates, composed of water and gas molecules, could be formed under high pressure and low temperature conditions, and were found widely in the sediment of the continental margins as well as permafrost regions (Hester and Brewer, 2009). Although the estimation of the global storage of natural gas hydrates in marine sediments varies several orders in magnitude (Klauda and Sandler, 2005; Milkov, 2004; Piñero et al., 2013), even conservative estimation suggests that natural gas hydrates might be a promising unconventional fuel energy resource (Lee and Holder, 2001; Moridis et al., 2013), and potentially play an important role in climate change (Dickens et al., 1997; Katz et al., 1999), continental slope stability (Maslin et al., 1998; Mienert et al., 1998) and global carbon cycle (Archer et al., 2009; Dickens, 2003).

Depending on the gas composition, three gas hydrate structures were found in nature which are cubic structure I (sI), cubic structure II (sII) and hexagonal structure H (sH) (Sloan, 2003). sI gas hydrate contains mainly methane with small amount of H_2S, CO_2 and other small molecule gases which are normally associated with biogenic origins. Since microbial biogenic methane is dominated in the sediment on the continental margin where sedimentation rate and total organic carbon (TOC) are relative high, sI methane hydrate is thought to be most abundant in marine sediment (Bohrmann et al., 2007; Chazallon et al., 2007; Liu et al., 2012; Lu et al., 2005; Stern et al., 2011). Structure II and H gas hydrates, which contain considerable amount of higher order hydrocarbons beside CH_4, were also found in marine sediment (Kida et al., 2006; Klapp et al., 2010; Lu et al., 2007).

The size of gas hydrate reservoir is a function of the thickness of GHSZ and gas hydrate saturation in marine sediments (Milkov, 2004). Additionally, the fate of methane emitted from seafloor via gas bubbles (De Beukelaer et al., 2003; Milkov et al., 2003; Römer et al., 2012) and hydrate pieces rafted from the seafloor is still in debate (MacDonald et al., 1994; Pape et al., 2011). Methane bubbles are coated by gas hydrate skins in the GHSZ in the water column, which decrease the methane dissolution rate significantly (Rehder et al., 2002). Therefore, it is important to know the gas composition and structure of gas hydrate, because they are very important factors for determining gas hydrate stability in both sediment and water column.

In 2011, a joint research cruise between Marum and Ifremer were conducted to investigate a pockmark field on the Nigerian continental margin (Figure 4.1). The so-called Pockmark C1 and A are two prominent pockmarks which are located at water depths between 1140 and 1280 m. The Bottom water temperature is around 4.5 °C, and the background geothermal gradient is approximately 80 °C/km (Sultan et al., 2010).

In this study, we described the occurrence as well as characteristics, including gas hydrate structure and gas composition, of gas hydrates recovered in four gravity cores. We further discussed the impact of minor gases on changing methane cage occupancy, gas hydrate stability, and ecosystem at seeps.

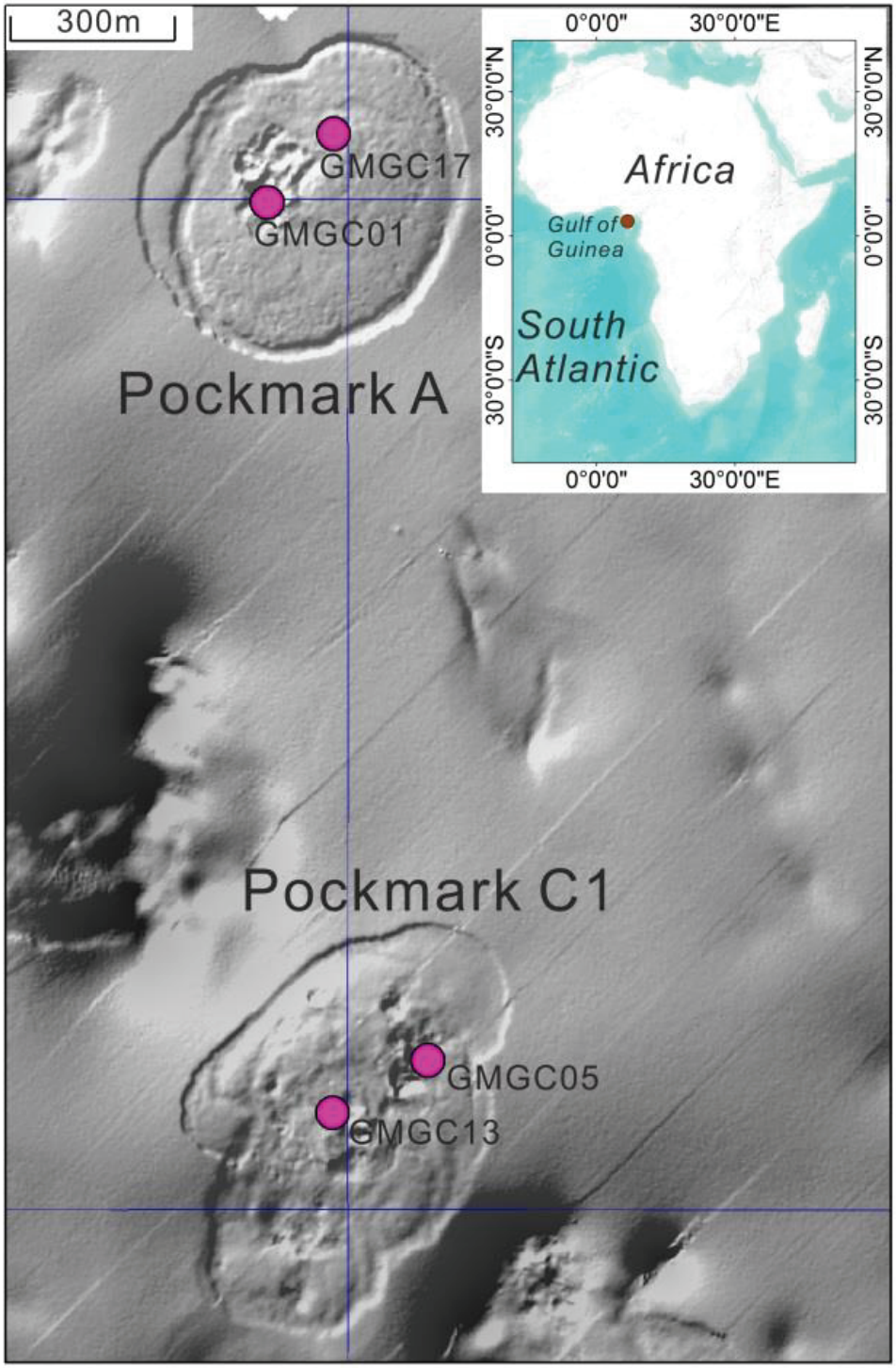

Figure 4.1 Locations of gravity cores from which gas hydrates were sampled. Inset shows the location of the study area at Gulf of Guinea.

4.3 Materials and methods

4.3.1 Coring and sampling

Gas hydrate pieces were sampled from four individual gravity cores. In order to sample the gas hydrates quickly, plastic bags were put inside the 6-m long cutting barrels. When the gravity cores were on deck, plastic bags with sediment core inside were withdrawn immediately from the cutting barrels. The plastic bags were then opened with knife, and

the cores were split into halves. Big gas hydrate pieces were sampled and preserved in the liquid nitrogen immediately to prevent further dissociation. It usually took less than 20 minutes between cores passing through the top of GHSZ and gas hydrate samples emerged in the liquid nitrogen. The core was then scanned with Infrared Thermal Camera to document its surface temperature which is a useful proxy of gas hydrate occurrence.

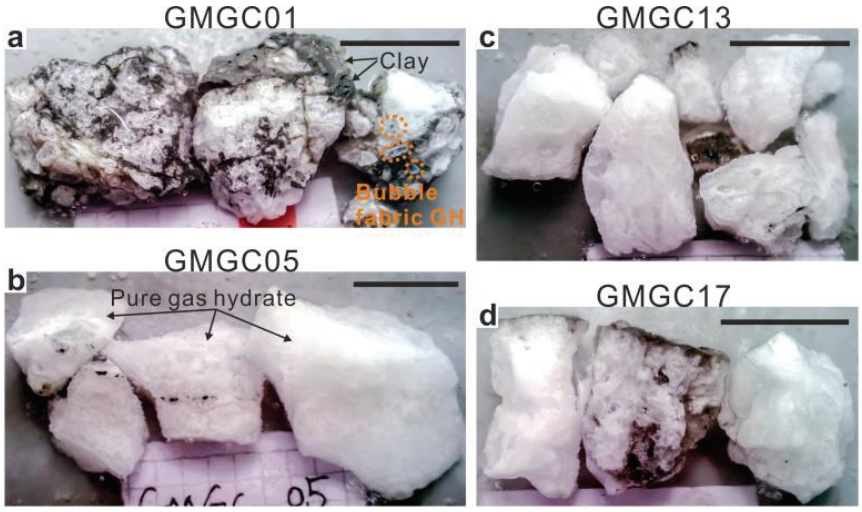

Figure 4.2 Recovered gas hydrate samples from the sediment cores. Most of the samples are pure white gas hydrate (b, c, and d). Small fractions are embedded in the hemi-pelagic clay (a). The scale bars are 2cm.

In order to keep it simple and consistent, GMGC was used to represent both the gas hydrate samples and gravity cores. Great efforts have been made to sample the inner part of massive pure white gas hydrate (Figure 4.2b, c, and d) to minimize the contamination of the sediment and pore water. However, when gas hydrate is mixed with clay matrix and frozen in liquid nitrogen, it is impossible to eliminate the clay thoroughly (Figure 4.2a). Fortunately, the small content of clay has very limit effect on the experimental results. Figure 4.2 shows the samples prepared for all the analysis in this study.

4.3.2 Sulfate concentrations

Interstitial pore water was extracted using Rhizon sampler, which consists of a thin tube made up with hydrophilic porous polymer with pore diameter of approximate 0.2 μm. Syringes with volume of 10 or 20 ml were connected to the sampler to create a vacuum and collect the pore water. Pore water was then split and prepared for different analyses and stored in the refrigerator or reefer. Sulfate concentrations were detected by using ion chromatography (861 Advanced Compact IC, 837 IC Eluent Degasser, and Advanced Sample Processor by Metrohm).

4.3.3 Gas chromatography

A two-channel gas chromatography was used to determine the composition of hydrate-bonded gases. C_1-C_6 hydrocarbons were quantified with a capillary column (OPTIMA-5; 50 m length; 0.32 mm inside diameter) connected to a flame ionization detector. Other gases, including O_2, N_2, CO_2 as well as CH_4 and C_2H_6 were analyzed using a packed (molecular sieve) stainless steel column coupled with a thermal conductivity detector.

4.3.4 XRD

For XRD measurements in Göttingen, a Bragg-Brentano focusing Philips MRD (Materials Research Diffractometer) cryo-goniometer was applied, which employs light of a wavelength of 0.7093 Å from a molybdenum anode (Klapp et al., 2010). Phase content of the samples was calculated based on Rietveld refinement using the GSAS software and the EXPGUI user interface (Toby, 2001).

4.3.5 Raman (area integration)

Raman spectra over a wide range of 0-4000 cm^{-1} were acquired using a LabRAM HR800 (Horiba Jobin Yvon) Raman spectrometer equipped with a Peltier-cooled CCD detector and 600 grooves/mm grating. A 488 nm line emitted by an Ar^{+} laser was used at an output power of 20 mW. The detailed instrumental settings and peak analysis can be found in the reference of (Qin and Kuhs, 2013).

4.4 Results

4.4.1 Sediment lithology and gas hydrate occurrence

The sediment cores are between 2.0 m and 4.5 m in length (Figure 4.3). Strong rotten egg odor, which is a typical feature of H_2S, was noticed when the cores were opened. The upper parts of the cores are dominated by hemipelagic clays with dispersed authigenic carbonate concretions derived from sulfate reduction-anaerobic methane oxidation (SR-AOM). In the lower parts of the cores, occurrence of massive/layered white gas hydrates were observed and recorded using IR thermal scanning which shows cold anomalies down to ~0 °C (Figure 4.3). The top of GHOZ observed by core description and estimated from IR thermal scanning are generally identical. In the center of pockmark A, it is estimated to be at 1.1 and 1.0 mbsf for GMGC01 and GMGC17, respectively. In pockmark C1, it is estimated to be at 1.5 and 2.5 mbsf for GMGC05 and GMGC13, respectively.

In sample GMGC01 (Figure 4.2a), ~mm size elongated hydrate coated bubbles were observed; indicating gas bubble migration and fast hydrate formation and accumulation in the shallow sediment (Bohrmann et al., 1998; Torres et al., 2004).

4.4.2 Sulfate concentration

Sulfate concentrations in the pore water were measured for GMGC01 and GMGC05 with non-uniform intervals between 20 and 50 cm (Figure 4.3). The concentrations decrease from ~28 mM at the water-sediment interface to 2-3 mM at 0.6 mbsf within GMGC01 and at 0.8 mbsf within GMGC05, respectively. These depths were inferred to be the sulfate-methane interface (SMI) below which sulfate concentrations show values between 0 and 5 mM.

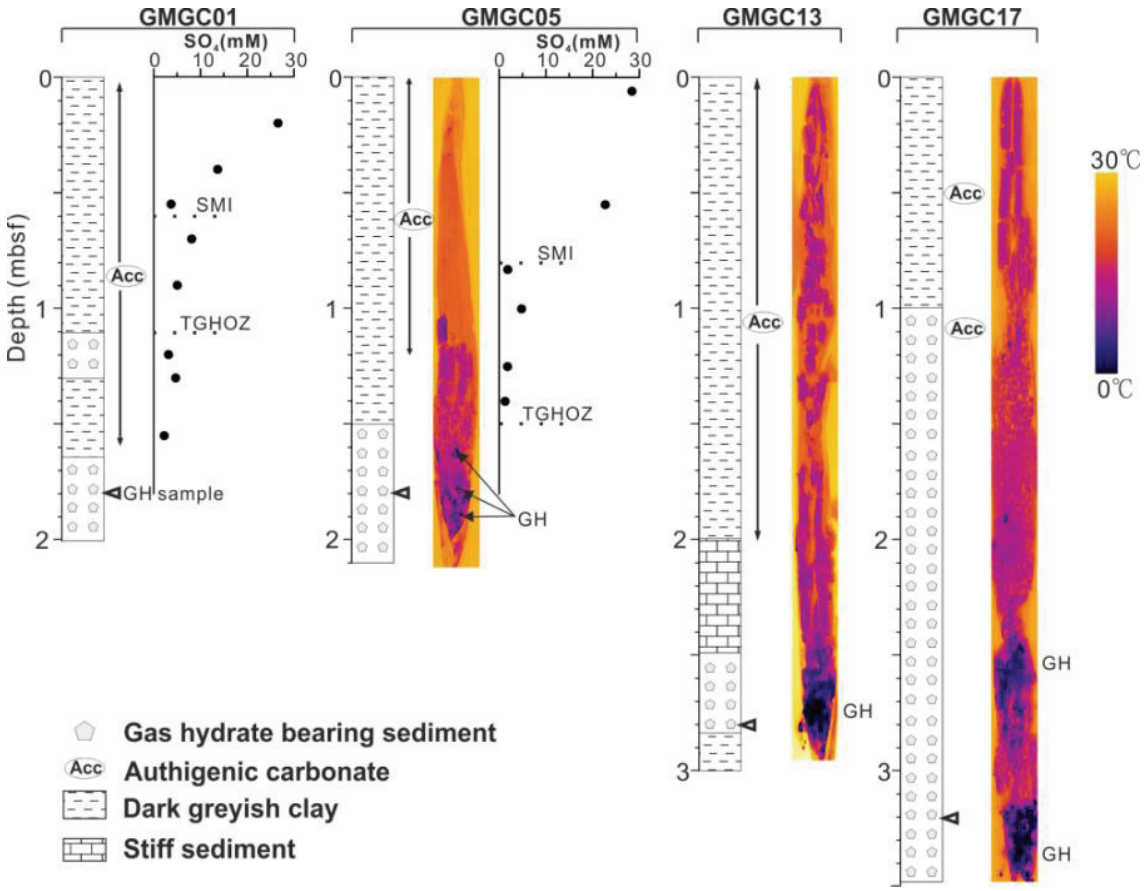

Figure 4.3 Sediment lithology, sulfate profiles and IR thermal scanning of the sediment cores. Gas hydrates show cold anomalies in IR thermal scanning. The depths of gas hydrate samples were noted with triangles.

4.4.3 Gas composition

The composition of low-molecular weight hydrocarbons (LMWHC) and CO_2 of the gas hydrate samples were analyzed using gas chromatography. The results were listed in (Table 4.1). Methane is the dominant gas in each sample ranging between 98.31% and 99.62%. Slight variation of methane concentration is mainly attributed to the variation of small amounts of CO_2 ranging between 0.35% and 1.66%. Trace C_2H_6 (0.02%-0.03%) was also detected in each sample, whereas other higher order hydrocarbon are below the detection level and were not detected. Ratios of methane to ethane are between 3908 and 5297.

Table 4.1 Content of low-molecular weight hydrocarbons and CO2 measured using gas chromatography. Gas hydrate fraction is an indicator of quality of hydrate preservation and were calculated based on the XRD measurements using Rietveld analysis. ND: no detection.

Samples	GH fraction	Gas compositions [$C_i/\sum(C_1\text{-}C_5, CO_2)$, mol%]				C_1/C_2
		C_1	C_2	C_3+	CO_2	
GMGC01	32.0 ± 2.0	98.31	0.02	ND	1.66	3971
GMGC05	91.8 ± 1.8	99.62	0.03	ND	0.35	3908
GMGC13	87.3 ± 5.0	99.59	0.02	ND	0.39	5176
GMGC17	72.7 ± 5.2	99.37	0.02	ND	0.61	5297

4.4.4 X-ray diffraction

Powder X-ray diffraction measurements revealed that all gas hydrate samples are exclusively structure I hydrate (sI), with a portion of hexagonal ice (Ih) (Figure 4.4). sI hydrate is demonstrated by the three intensive peaks (222), (320) and (321) in the 2Θ scans, whereas ice are represented by peaks (100), (002) and (101).

Gas hydrate fractions of the constituents were quantitatively calculated using PXRD data Rietveld analysis (Table 4.1). GMGC05, 13 and 17 show very high contents of sI hydrates between 73% and 92%, which could also be graphically observed from the extremely intensive sI peaks compared to the Ih peaks (Figure 4.4a). GMGC01 is the only one that shows low hydrate content of 32%. High gas hydrate content indicates that samples were sampled efficiently for the gas composition and structure analysis.

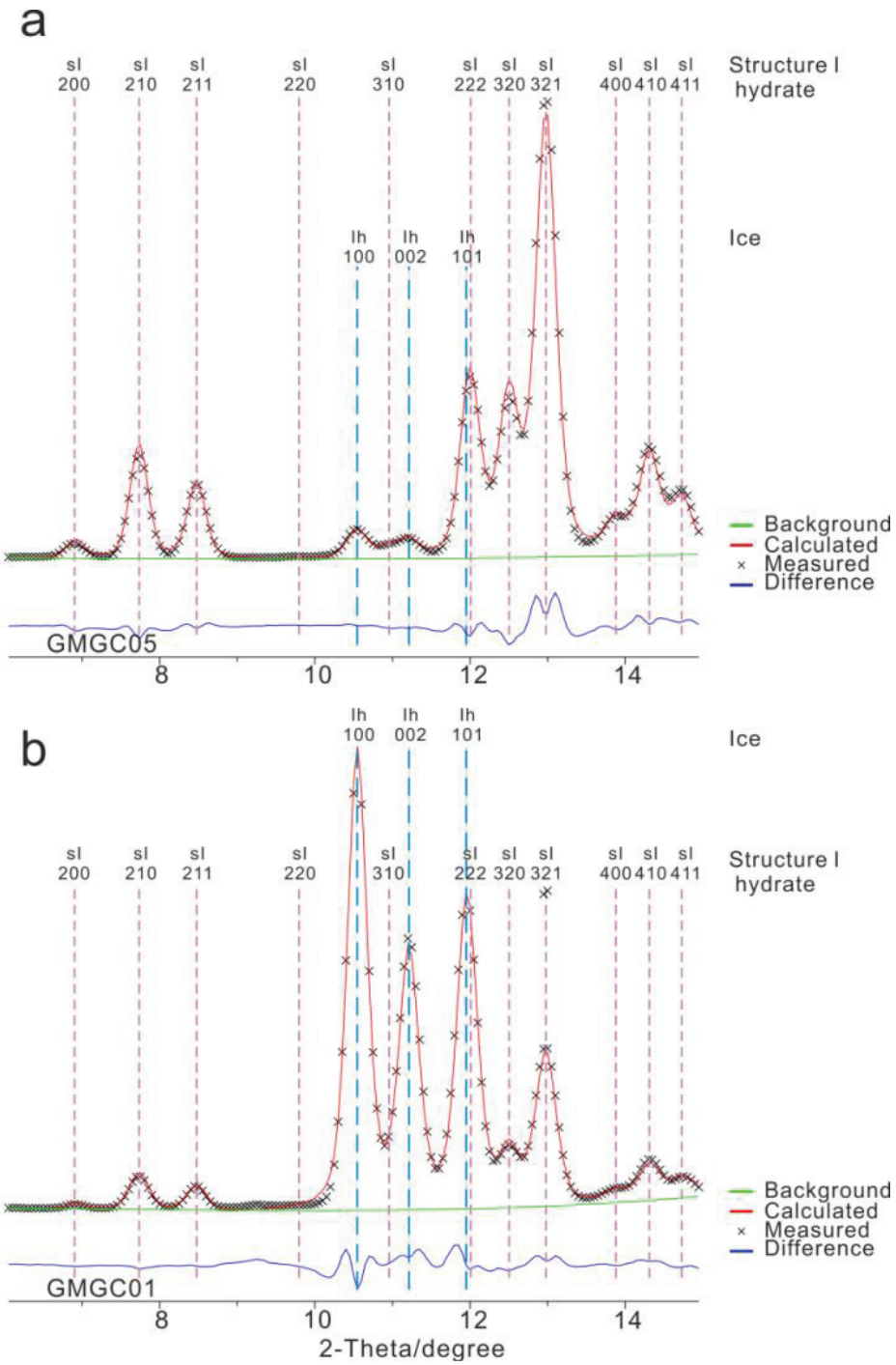

Figure 4.4 Representative plots of X-ray diffraction measurements and Rietveld analysis of samples with different gas hydrate contents (a: 92% and b: 32%, shown in Table 4.1). Only two phases (structure I gas hydrate and ice) were identified by their majors peaks noted in the figure.

4.4.5 Raman spectroscopy

Raman spectroscopic analysis revealed that hydrate bonded gas mainly consist of methane, with small amounts of CO_2 and H_2S (Figure 4.5). Other hydrocarbons are below the limit of the detection.

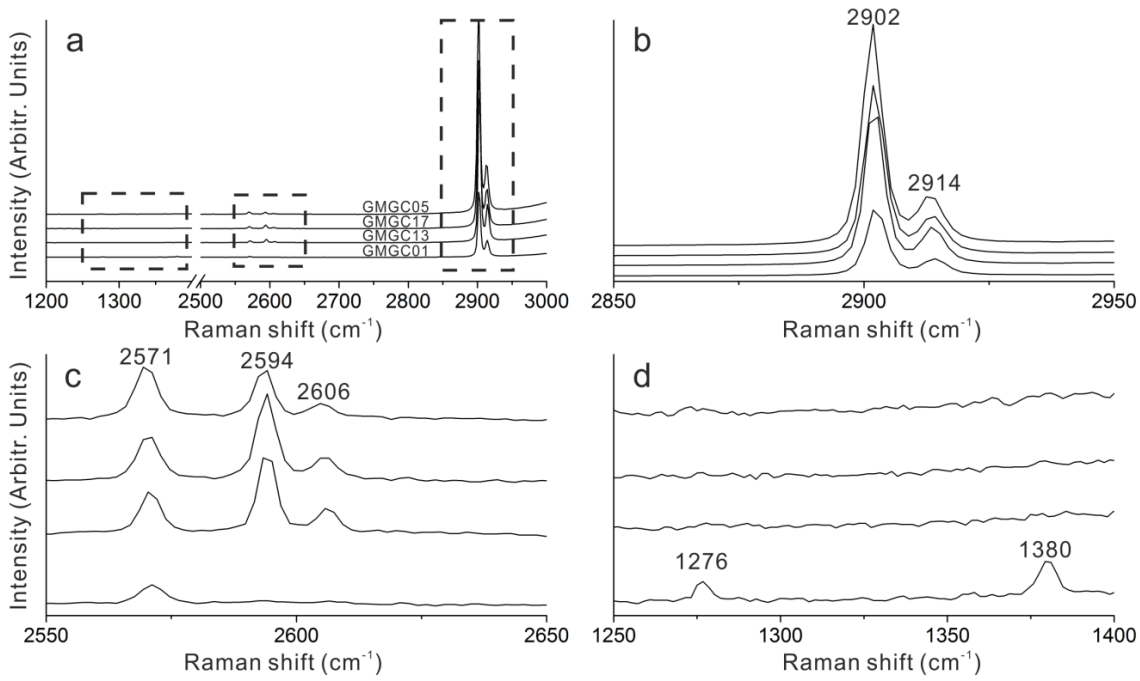

Figure 4.5 (a): Representative Raman spectra of gas hydrates. (b): C-H spectral region of methane. Peaks at 2902cm^{-1} and 2914 cm^{-1} represent CH_4 in large and small cages of sI gas hydrate, respectively. (c): H-S spectral region. Peaks at 2594cm^{-1} and 2606 cm^{-1} represent H_2S in large and small cages of sI gas hydrate, respectively. (d): Peaks at 1276cm^{-1} and 1380cm^{-1} represent the ν_1 and $2\nu_2$ stretching of CO_2 hydrate.

Methane is the dominant gas in all the samples. The ν_1 peaks of methane at approximately 2902 cm^{-1} and 2914 cm^{-1} (Figure 4.5b), represent methane in large cages ($5^{12}6^2$) and small cages (5^{12}) of sI hydrate, respectively (Sum et al., 1997). The other two minor methane peaks were also observed at 2571 cm^{-1} and 3050 cm^{-1}. Two relatively weak peaks at 2594 cm^{-1} and 2606 cm^{-1} (Figure 4.5c) confirm the presence of H_2S as the guest molecules in large ($5^{12}6^2$) and small cages (5^{12}) of sI hydrate, respectively (Chazallon et al., 2007). Raman signature of CO_2 in the hydrate (peaks at 1380 cm^{-1} and 1276 cm^{-1}) was identified in some measurements of GMGC01, GMGC05 and GMGC17 (Figure 4.5d and Table 4.2) (Sum et al., 1997).

Table 4.2 Existence of CO_2 and H_2S in gas hydrate and the experimentally measured methane cage occupancy ratios ($\Theta L/\Theta S$). Ratios of H_2S to CH_4 (nH_2S/nCH_4) calculated by correcting their identical peaks using their Raman cross sections. N: total number of Raman measurements. NCO2: number of measurements that CO_2 were observed. NH_2S: number of measurements that H_2S were observed.

Samples	N	N_{CO2}	N_{CO2}/N	N_{H2S}	N_{H2S}/N	n_{H2S}/n_{CH4}(%)	Θ_L/Θ_S	Θ_S	Θ_L	Hydration number
GMGC01	11	8	73%	2	18%	0.49±0.04	1.06±0.03	0.93±0.02	0.99±0.01	5.91±0.04
GMGC05	12	3	25%	10	83%	1.15±0.51	1.04±0.04	0.94±0.02	0.98±0.01	5.93±0.04
GMGC13	6	0	0%	6	100%	2.82±0.03	1.03±0.02	0.95±0.01	0.98±0.01	5.91±0.02
GMGC17	12	6	50%	6	50%	1.27±0.38	1.06±0.03	0.93±0.02	0.99±0.01	5.91±0.02
Total	41	17	41%	24	59%	-	1.05±0.03	0.94±0.02	0.98±0.01	5.91±0.04

H_2S and CO_2 only present in some of the measurements (Table 4.2), indicating a heterogeneous distribution of these two molecules in the gas hydrate on a decimeter scale. It should also be noted that CO_2 and H_2S were hardly detected co-existing in a single measurement (Table 4.2 and Figure 4.5c and d).

4.5 Discussions

4.5.1 Methane flux within the pockmark

As the pressure decreases during the core retrieval, the solubility of methane also decreases which leads to the precipitation of methane from pore water. Thus, it is impossible to measure in situ methane concentration by using conventional coring techniques. However, methane flux could be inferred from the pore water sulfate profiles if methane is totally consumed by sulfate via SR-AOM (Borowski et al., 1996). According to Fick's first law of diffusion, the diffusive flux is proportional to the concentration gradient under steady state. Diffusion processes within the sediment can only take place in pore water, thus, Fick's first law is modified as follows to calculate the flux within the sediment (Schulz, 2006):

$$J_{sed} = -\emptyset \cdot D_{sed} \cdot \frac{\partial c}{\partial x}$$

$$D_{sed} = \frac{D_{sw}}{\theta^2}$$

Where J_{sed} is the diffusive flux in the sediment, $\emptyset$ is the porosity of the sediment. In this study, $\emptyset$ was set to be 0.82 which is the average porosity of sediment in the upper 3 meters (Sultan et al., 2007). D_{sed} is the diffusion coefficient in the pore water of sediment which is a function of diffusion coefficient D_{sw} and tortuosity θ. D_{sw} is 5.72E-10 m^2 s^{-1} at 5 °C in sea water (Schulz, 2006). Tortuosity is a function of porosity and is 1.4 for this study (Schulz, 2006). Simplification was made to calculate the gradient of sulfate concentration ($\frac{\partial c}{\partial x}$) which is the division of 28 mM by the distances between seafloor and SMI (Figure 4.2).

If upward methane flux is stoichiometrically consumed by sulfate, methane fluxes in GMGC01 and GMGC05 are 1.4 mmol m^{-2} day^{-1} and 1 mmol m^{-2} day^{-1}, respectively. These values in this study are comparable to that at the clam sites of hydrate ridge (1mmol m^{-2} day^{-1}) in the Cascadia margin accretionary complex (Torres et al., 2002). In the mat-covered sites of hydrate ridge, the flux ranges between 30 and 90 mmol m^{-2} day^{-1} which is one order of magnitude higher than the clam sites, indicating a very inhomogeneous methane flux in the cold seeps (Torres et al., 2002). In the center of pockmark A where gas emission was observed in the center of pockmark A (Sultan et al., 2014), the methane fluxes are potentially more intensive than the coring sites. Increased methane flux potentially shifts both the SMI and the top of GHOZ upward to a shallower depth (Borowski et al., 1999), increasing the size of the gas hydrate reservoir in the pockmark.

4.5.2 Methane occupancy ratios and hydration numbers

Relative methane cage occupancy ratio expresses the distribution of methane filling in the hydrate cages, indicating the preferential of methane into large cages and small cages. In sI gas hydrate, the number of large cages are three times as many as small cages, thus, the ratio could be obtained by (Sum et al., 1997):

$$\frac{\theta_L}{\theta_S} = \frac{A_L}{3A_S}\frac{\sigma_S}{\sigma_L}$$

where θ_L, θ_S and σ_L ,σ_S are the absolute cage occupancies and Raman scattering cross sections of methane in the large and small cages, respectively . A_L and A_S are the integrated areas of the ν_1 methane peaks of the large and small cages, respectively. If we assume the Raman scattering cross sections of methane in large and small cages are identical, the equation could be simplified as follows (Sum et al., 1997; Uchida et al., 1999):

$$\frac{\theta_L}{\theta_S} = \frac{A_L}{3A_S}$$

The calculated cage occupancy ratios of the four gas hydrate pieces are listed in Table 4.2. The values are generally consistent for all the samples, with a minor variation between 1.03 and 1.06.

The relative methane cage occupancy ratios are larger than 1 in this study, indicating that methane molecules prefer to be enclathrated into the large cages rather than into the small cages. These values are in the same range as other lab studies (1.01-1.28) of both synthetic and natural methane hydrate (Chazallon et al., 2007; Liu et al., 2012; Lu et al., 2005; Uchida et al., 1999). However, the experimentally derived ratios are slightly lower than theoretical values of 1.10 for pure methane hydrate using CSMGem software at in situ condition. Same phenomenon was also observed for hydrates recovered from the West African margin (Chazallon et al., 2007). In this work, gas hydrate samples contain small amount of CO_2, H_2S and C_2H_6. Since CO_2 is preferentially trapped in large cages, the amount of CH_4 in large cages was reduced (Udachin et al., 2001). Therefore, we inferred that the differences between theoretical and experimental values might be caused by the small amount of CO2.

Estimation of hydration number of sI hydrate as well as absolute occupancies of methane in large and small cages could be obtained by solving the following equations (Sum et al., 1997):

$$\mu_w(h) - \mu_w(h_0) = -\mathrm{RT}[3\ln(1-\theta_L) + \ln(1-\theta_S)]/23$$

$$\mu_w(h) - \mu_w(h_0) = \Delta\mu_w^0$$

$$n = \frac{23}{3\theta_L + \theta_S}$$

Where $\mu_w(h)$ is the chemical potential of water molecules in the lattice of empty hydrate, $\mu_w(h_0)$ is the chemical potential of water molecules in the reference state. $\Delta\mu_w^0$ is the chemical potential difference between the water in the empty hydrate lattice and ice. An experimental value of $\Delta\mu_w^0$ was found to be 1297 J/mol under standard conditions which is in agreement with values obtained by fitting thermodynamic data (Davidson et al., 1986). n is the hydration number for sI hydrate.

Absolute occupancies of methane in large cages and small cages and the hydration number of the four samples are very similar to each other with average values of 5.91, 0.98 and 0.94, respectively. The hydration number drops well within the lower part of the ranges of previous studies of natural gas hydrates between 5.9 and 6.3 (Liu et al., 2012). High absolute occupancies indicate that hydrates are richer in methane than previous studies.

4.5.3 H_2S concentration

As a minor gas component, H_2S was detected in each gas hydrate sample using Raman spectroscopy. Since methane is the dominant gas (Table 4.1), the contents of H_2S could be potentially expressed as H_2S/CH_4 ratio. The ratio was calculated as follows (Sum et al., 1997),

$$\frac{c_1}{c_2} = \frac{A_1}{A_2}\frac{\sigma_2}{\sigma_1}$$

where A_1 and A_2 are the integrated areas of the ν_1 peaks of H_2S and CH_4, respectively. As a first approximation, 7 and 8.55 were set for σ_1 and σ_2 which are the Raman scattering cross sections of the ν_1 peaks of H_2S and CH_4, respectively (Hester et al., 2008). H_2S were detected in all the samples except GMGC13 (Table 4.2). The mean values of H_2S/CH_4 ratio range between 0.49% and 2.82% with large standard deviations of 0.51% and 0.38% in GMGC05 and GMGC17, respectively (Table 4.2). Inhomogeneous distribution of H_2S could be inferred from (1) H_2S absence of some measurements (2) large variations of H_2S contents between gas hydrate samples, and (3) large standard deviations.

CH_4-H_2S gas hydrates have also been found at Hydrate Ridge using Raman spectroscopy (Hester et al., 2007), and the contents of H_2S reported by Hester range between 1.94% and 2.47% which are comparable to our result in this study (Hester et al., 2008).

4.5.4 Composition and source of hydrate hounded gases

Since gas chromatograph analysis only gives the composition of LMWHC and CO_2, therefore, we combine the H_2S/CH_4 ratios of Raman measurements to make a full description of compositions of hydrate-bounded gases (Table 4.3). Compared with the results of gas chromatograph analysis, CH_4 is still the dominate gas but with a slightly decrease in amount due to the consideration of H_2S (0.48%-2.73%). Compositions of CO_2 and C_2H_6 have no significant change.

Table 4.3 Recalculated gas compositions considering the content of H_2S in gas hydrates as listed in Table 4.2.

Samples	Gas compositions [$C_i/\sum(C_1\text{-}C_5, CO_2, H_2S)$, mol%]				
	C_1	C_2	C_3+	CO_2	H_2S
GMGC01	97.85	0.02	ND	1.65	0.48
GMGC05	98.49	0.03	ND	0.35	1.13
GMGC13	96.87	0.02	ND	0.38	2.73
GMGC17	98.13	0.02	ND	0.60	1.25

C1/C2 ratio of the hydrate is a useful indicator to distinguish thermo-genic gas and biogenic gas. Gases with C1/C2 ratio greater than 100 are considered to be biogenic, while those smaller than 100 are potentially thermogenic gases (Bernard et al., 1976). The values in this study are between 3908 and 5297 what are far greater than 100 (Table 4.1), indicating that gases in the gas hydrates are likely to be of biogenic origin.

Sulfate reduction is supposed to be the major process that produces H_2S in the shallow marine sediment of cold seeps (Jørgensen and Kasten, 2006). Shallow SMI, gas ebullition from the seafloor, and widespread shallow gas hydrates in the shallow sediment indicate sufficient and intensive methane flux from subsurface within the pockmark field. Additionally, H_2S containing hydrate was recovered in adjacent to the SMI where the rate of AOM is the highest through the sediment column (Iversen, 1985). Thus, we infer that H_2S in gas hydrates are predominately formed through SR-AOM. Methane fluxes and H_2S production within the cold seeps are inhomogeneous which might lead to a spatial and temporal heterogeneous H_2S distribution (Fischer et al., 2012). Variation of H_2S contents in the gas hydrate is potentially associated with spatial and temporal variation of methane flux.

4.5.5 H_2S-induced increased gas hydrate stability and its impact

Knowing gas hydrate stability is crucial for estimating the gas hydrate reservoir and understanding the fate of methane gas bubbles and gas hydrate chucks in ocean water column released from the seafloor. Gas hydrate stability is determined by many factors, including temperature, pressure, salinity, gas hydrate structure types as well as gas composition. The GHSZ of the four gas hydrate samples with different gas constitutes as well as pure methane hydrate was calculated under local conditions. The results were shown in Figure 4.6. Prominent depth variation of the top and bottom of the GHSZ are associated with small contents of minor gases. The top and bottom of the GHSZ for pure methane hydrate are at water depths of 601 m and 1253 m (113 mbsf), which correspond to a thicknesses of GHSZ of 539 m in the water column and 113 m in the sediment, respectively. Compared with pure methane hydrate, GMGC13 shows the greatest enhancement of gas hydrate stability. The thicknesses of the GHSZ of GMGC13 within water column and sediment increased 30% to 700 m and 37% to 155 m, respectively. The GHSZ of GMGC17 (1.25% H_2S and 0.6% CO_2) increased by 18%-19%, which is

approximately twice as large as that of GMGC01 (0.48% H_2S and 1.65% CO_2), indicating that H_2S exerts a much larger effect on increasing gas hydrate stability than CO_2. Largely increased GHSZ in the sediment due to the addition of minor gases, mainly H_2S, potentially increases the size of the gas hydrate reservoir in marine sediment. Thus, the effect of H_2S on increasing GHSZ should not be ignored when estimating the size of the gas hydrate reservoir. The increased gas hydrate stability in the water column is likely to prolong the lifetime of gas hydrate. Consequently, the possibility of methane transported to atmosphere through water column via gas hydrate coated bubbles and gas hydrate chucks rafted from the seafloor are potentially increased.

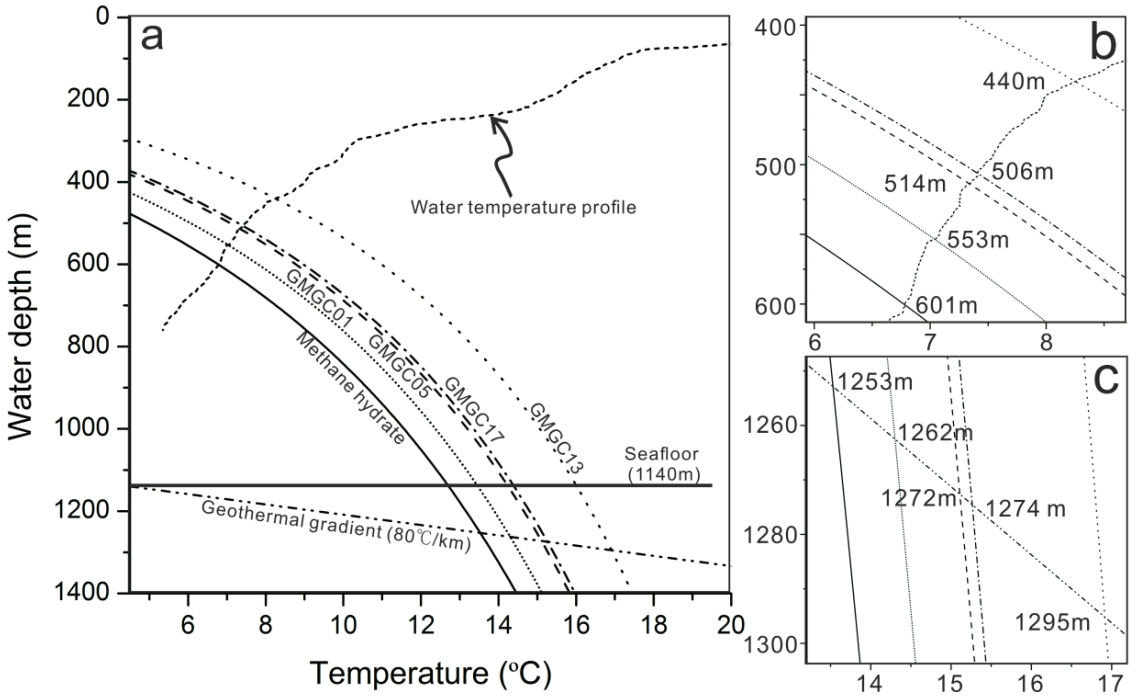

Figure 4.6 Gas hydrate stability fields calculated using Heriot-Watt-Hydrate software with gas compositions listed in Table 4.3. (b) and (c) are the enlarged plots of the upper boundary in the water column and lower boundary in the sediment of the GHSZ, respectively.

It has been known for a long time that chemosynthetic communities which are fed on H_2S occur widely at seep sites (Olu et al., 1997). The distribution of the fauna species are strongly related and controlled by the intensity of methane flux (Fischer et al., 2012). Since cold seeps are highly dynamic thermal and geochemical systems due to the spatial and temporal variation of fluid flow, H_2S released and absorbed during gas hydrate formation, dissociation and dissolution might is likely to affect the local ecosystem.

4.6 Conclusions

We investigated the gas composition and structure of the gas hydrate samples recovered from the shallow sediment of the pockmarks on the Nigerian continental margin with laboratory measurements of power X-ray diffraction, Raman spectroscopy and gas chromatography. The major conclusions are drawn as follows:

1. Power X-ray diffraction measurements show that all samples are composed of exclusively sI hydrate and a portion of ice which is derived from the dissociation and refreezing during the gas hydrate sampling and storage.

2. Hydrate bonded gases are mainly composed of CH_4, with a small amount of CO_2 and trace C_2H_6. Other hydrocarbons were below the detection limit.

3. CH_4, H_2S and CO_2 in gas hydrates were also detected by their identical peaks in Raman spectral. CO_2 and H_2S distribute heterogeneously and hardly co-exist in any Raman measurements. We propose that this phenomenon is caused by their concentration variation in the pore water which is likely influenced by temporal and spatial variation of upward methane flux.

4. The contents of the hydrated bonded gases were calculated as follows: methane (96.87-98.49%), CO_2 (0.35-1.65%), H_2S (0.48-2.73%) and C_2H_6 (0.02-0.03%).

5. Methane cage occupancy ratios range between 1.03 and 1.06, and are slightly lower than the theoretical value of 1.10. This effect ascribed to the presence of CO_2 which is preferentially occupying large cages. Hydration number is estimated to be 5.91 for gas hydrate in these two pockmarks.

6. Compared with pure methane hydrate, the stability field is significantly enlarged due to the presence of other gases, especially H_2S. This impact potentially increases the size of gas hydrate reservoirs in the marine sediment, and also increases the possibility of methane in gas bubbles and hydrate bulks transporting into the atmosphere.

Acknowledgements

We greatly thank Junfeng Qin for the Raman scattering analysis. We thank the captain and crew of R/V Pourquoi pas? for support during the Guineco-MeBo cruise in 2011. This work was partly funded through the DFG-Research Center/Excellence Cluster "The Ocean in the Earth System" MARUM – Center for Marine Environmental Sciences. A major financial contribution came from BMBF-project 03G0824A. J. Wei was sponsored by the China Scholarship Council (CSC).

Reference

Archer, D., Buffett, B., and Brovkin, V., 2009, Ocean methane hydrates as a slow tipping point in the global carbon cycle: Proceedings of the National Academy of Sciences, v. 106, no. 49, p. 20596-20601.

Bernard, B. B., Brooks, J. M., and Sackett, W. M., 1976, Natural gas seepage in the Gulf of Mexico: Earth and Planetary Science Letters, v. 31, no. 1, p. 48-54.

Bohrmann, G., Greinert, J., Suess, E., and Torres, M., 1998, Authigenic carbonates from the Cascadia subduction zone and their relation to gas hydrate stability: Geology, v. 26, no. 7, p. 647-650.

Bohrmann, G., Kuhs, W. F., Klapp, S. A., Techmer, K. S., Klein, H., Murshed, M. M., and Abegg, F., 2007, Appearance and preservation of natural gas hydrate from Hydrate Ridge sampled during ODP Leg 204 drilling: Marine Geology, v. 244, no. 1–4, p. 1-14.

Borowski, W. S., Paull, C. K., and Ussler Iii, W., 1999, Global and local variations of interstitial sulfate gradients in deep-water, continental margin sediments: Sensitivity to underlying methane and gas hydrates: Marine Geology, v. 159, no. 1–4, p. 131-154.

Borowski, W. S., Paull, C. K., and Ussler, W., 1996, Marine pore-water sulfate profiles indicate in situ methane flux from underlying gas hydrate: Geology, v. 24, no. 7, p. 655-658.

Chazallon, B., Focsa, C., Charlou, J.-L., Bourry, C., and Donval, J.-P., 2007, A comparative Raman spectroscopic study of natural gas hydrates collected at different geological sites: Chemical Geology, v. 244, no. 1–2, p. 175-185.

Davidson, D. W., Handa, Y. P., and Ripmeester, J. A., 1986, Xenon-129 NMR and the thermodynamic parameters of xenon hydrate: The Journal of Physical Chemistry, v. 90, no. 24, p. 6549-6552.

De Beukelaer, S. M., MacDonald, I. R., Guinnasso, N. L., Jr., and Murray, J. A., 2003, Distinct side-scan sonar, RADARSAT SAR, and acoustic profiler signatures of gas and oil seeps on the Gulf of Mexico slope: Geo-Marine Letters, v. 23, no. 3-4, p. 177-186.

Dickens, G. R., 2003, Rethinking the global carbon cycle with a large, dynamic and microbially mediated gas hydrate capacitor: Earth and Planetary Science Letters, v. 213, no. 3–4, p. 169-183.

Dickens, G. R., Castillo, M. M., and Walker, J. C., 1997, A blast of gas in the latest Paleocene: Simulating first-order effects of massive dissociation of oceanic methane hydrate: Geology, v. 25, no. 3, p. 259-262.

Fischer, D., Sahling, H., Nöthen, K., Bohrmann, G., Zabel, M., and Kasten, S., 2012, Interaction between hydrocarbon seepage, chemosynthetic communities, and bottom water redox at cold seeps of the Makran accretionary prism: insights from habitat-specific pore water sampling and modeling: Biogeosciences, v. 9, no. 6, p. 2013-2031.

Hester, K., Koh, C., Dec, S., and Sloan, E., Data report: Gas hydrate structural and compositional characterization by spectroscopic analysis, IODP Expedition 311, *in* Proceedings Proc. IODP| Volume2008, Volume 311, p. 2.

Hester, K. C., and Brewer, P. G., 2009, Clathrate Hydrates in Nature: Annual Review of Marine Science, v. 1, no. 1, p. 303-327.

Hester, K. C., Dunk, R. M., White, S. N., Brewer, P. G., Peltzer, E. T., and Sloan, E. D., 2007, Gas hydrate measurements at Hydrate Ridge using Raman spectroscopy: Geochimica et Cosmochimica Acta, v. 71, no. 12, p. 2947-2959.

Iversen, N., 1985, Anaerobic methane oxidation rates at the sulfate-methane transition in marine sediments from Kattegat and Skagerrak (Denmark): Limnol. Oceanogr, v. 30, no. 5, p. 944-955.

Jørgensen, B., and Kasten, S., 2006, Sulfur Cycling and Methane Oxidation, *in* Schulz, H., and Zabel, M., eds., Marine Geochemistry, Springer Berlin Heidelberg, p. 271-309.

Katz, M. E., Pak, D. K., Dickens, G. R., and Miller, K. G., 1999, The source and fate of massive carbon input during the latest Paleocene thermal maximum: Science, v. 286, no. 5444, p. 1531-1533.

Kida, M., Khlystov, O., Zemskaya, T., Takahashi, N., Minami, H., Sakagami, H., Krylov, A., Hachikubo, A., Yamashita, S., Shoji, H., Poort, J., and Naudts, L., 2006, Coexistence of structure I and II gas hydrates in Lake Baikal suggesting gas sources from microbial and thermogenic origin: Geophysical Research Letters, v. 33, no. 24, p. L24603.

Klapp, S. A., Murshed, M. M., Pape, T., Klein, H., Bohrmann, G., Brewer, P. G., and Kuhs, W. F., 2010, Mixed gas hydrate structures at the Chapopote Knoll, southern Gulf of Mexico: Earth and Planetary Science Letters, v. 299, no. 1–2, p. 207-217.

Klauda, J. B., and Sandler, S. I., 2005, Global Distribution of Methane Hydrate in Ocean Sediment: Energy & Fuels, v. 19, no. 2, p. 459-470.

Lee, S.-Y., and Holder, G. D., 2001, Methane hydrates potential as a future energy source: Fuel Processing Technology, v. 71, no. 1, p. 181-186.

Liu, C., Ye, Y., Meng, Q., He, X., Lu, H., Zhang, J., Liu, J., and Yang, S., 2012, The Characteristics of Gas Hydrates Recovered from Shenhu Area in the South China Sea: Marine Geology, v. 307–310, no. 0, p. 22-27.

Lu, H., Moudrakovski, I., Riedel, M., Spence, G., Dutrisac, R., Ripmeester, J., Wright, F., and Dallimore, S., 2005, Occurrence and structural characterization of gas hydrates

associated with a cold vent field, offshore Vancouver Island: Journal of Geophysical Research: Solid Earth, v. 110, no. B10, p. B10204.

Lu, H., Seo, Y.-t., Lee, J.-w., Moudrakovski, I., Ripmeester, J. A., Chapman, N. R., Coffin, R. B., Gardner, G., and Pohlman, J., 2007, Complex gas hydrate from the Cascadia margin: Nature, v. 445, no. 7125, p. 303-306.

MacDonald, I. R., Guinasso , N. L., Sassen, R., Brooks, J. M., Lee, L., and Scott, K. T., 1994, Gas hydrate that breaches the sea floor on the continental slope of the Gulf of Mexico: Geology, v. 22, no. 8, p. 699-702.

Maslin, M., Mikkelsen, N., Vilela, C., and Haq, B., 1998, Sea level and gas hydrate controlled catastrophic sediment failures of the Amazon Fan: Geology, v. 26, no. 12, p. 1107-1110.

Mienert, J., Posewang, J., and Baumann, M., 1998, Gas hydrates along the northeastern Atlantic margin: possible hydrate-bound margin instabilities and possible release of methane: Geological Society, London, Special Publications, v. 137, no. 1, p. 275-291.

Milkov, A. V., 2004, Global estimates of hydrate-bound gas in marine sediments: how much is really out there?: Earth-Science Reviews, v. 66, no. 3–4, p. 183-197.

Milkov, A. V., Sassen, R., Apanasovich, T. V., and Dadashev, F. G., 2003, Global gas flux from mud volcanoes: A significant source of fossil methane in the atmosphere and the ocean: Geophysical Research Letters, v. 30, no. 2, p. 1037.

Moridis, G. J., Collett, T. S., Boswell, R., Hancock, S., Rutqvist, J., Santamarina, C., Kneafsey, T., Reagan, M. T., Pooladi-Darvish, M., and Kowalsky, M., 2013, Gas Hydrates as a Potential Energy Source: State of Knowledge and Challenges, Advanced Biofuels and Bioproducts, Springer, p. 977-1033.

Olu, K., Lance, S., Sibuet, M., Henry, P., Fiala-Médioni, A., and Dinet, A., 1997, Cold seep communities as indicators of fluid expulsion patterns through mud volcanoes seaward of the Barbados accretionary prism: Deep Sea Research Part I: Oceanographic Research Papers, v. 44, no. 5, p. 811-841.

Pape, T., Bahr, A., Klapp, S. A., Abegg, F., and Bohrmann, G., 2011, High-intensity gas seepage causes rafting of shallow gas hydrates in the southeastern Black Sea: Earth and Planetary Science Letters, v. 307, no. 1–2, p. 35-46.

Piñero, E., Marquardt, M., Hensen, C., Haeckel, M., and Wallmann, K., 2013, Estimation of the global inventory of methane hydrates in marine sediments using transfer functions: Biogeosciences, v. 10, no. 2, p. 959-975.

Rehder, G., Brewer, P. W., Peltzer, E. T., and Friederich, G., 2002, Enhanced lifetime of methane bubble streams within the deep ocean: Geophysical Research Letters, v. 29, no. 15, p. 21-21-21-24.

Römer, M., Sahling, H., Pape, T., Bohrmann, G., and Spieß, V., 2012, Quantification of gas bubble emissions from submarine hydrocarbon seeps at the Makran continental margin (offshore Pakistan): Journal of Geophysical Research: Oceans, v. 117, no. C10, p. C10015.

Schulz, H., 2006, Quantification of Early Diagenesis: Dissolved Constituents in Pore Water and Signals in the Solid Phase, *in* Schulz, H., and Zabel, M., eds., Marine Geochemistry, Springer Berlin Heidelberg, p. 73-124.

Sloan, E. D., 2003, Fundamental principles and applications of natural gas hydrates: Nature, v. 426, no. 6964, p. 353-363.

Stern, L. A., Lorenson, T. D., and Pinkston, J. C., 2011, Gas hydrate characterization and grain-scale imaging of recovered cores from the Mount Elbert Gas Hydrate Stratigraphic Test Well, Alaska North Slope: Marine and Petroleum Geology, v. 28, no. 2, p. 394-403.

Sultan, N., Bohrmann, G., Ruffine, L., Pape, T., Riboulot, V., Colliat, J. L., De Prunelé, A., Dennielou, B., Garziglia, S., Himmler, T., Marsset, T., Peters, C. A., Rabiu, A., and Wei, J., 2014, Pockmark formation and evolution in deep water Nigeria: Rapid hydrate growth versus slow hydrate dissolution: Journal of Geophysical Research: Solid Earth, v. 119, no. 4, p. 2013JB010546.

Sultan, N., Marsset, B., Ker, S., Marsset, T., Voisset, M., Vernant, A. M., Bayon, G., Cauquil, E., Adamy, J., Colliat, J. L., and Drapeau, D., 2010, Hydrate dissolution as a potential mechanism for pockmark formation in the Niger delta: Journal of Geophysical Research: Solid Earth, v. 115, no. B8, p. B08101.

Sultan, N., Voisset, M., Marsset, T., Vernant, A. M., Cauquil, E., Colliat, J. L., and Curinier, V., 2007, Detection of free gas and gas hydrate based on 3D seismic data and cone penetration testing: An example from the Nigerian Continental Slope: Marine Geology, v. 240, no. 1–4, p. 235-255.

Sum, A. K., Burruss, R. C., and Sloan, E. D., 1997, Measurement of Clathrate Hydrates via Raman Spectroscopy: The Journal of Physical Chemistry B, v. 101, no. 38, p. 7371-7377.

Torres, M. E., McManus, J., Hammond, D. E., de Angelis, M. A., Heeschen, K. U., Colbert, S. L., Tryon, M. D., Brown, K. M., and Suess, E., 2002, Fluid and chemical fluxes in and out of sediments hosting methane hydrate deposits on Hydrate Ridge, OR, I: Hydrological provinces: Earth and Planetary Science Letters, v. 201, no. 3–4, p. 525-540.

Torres, M. E., Wallmann, K., Tréhu, A. M., Bohrmann, G., Borowski, W. S., and Tomaru, H., 2004, Gas hydrate growth, methane transport, and chloride enrichment at the southern summit of Hydrate Ridge, Cascadia margin off Oregon: Earth and Planetary Science Letters, v. 226, no. 1–2, p. 225-241.

Uchida, T., Hirano, T., Ebinuma, T., Narita, H., Gohara, K., Mae, S., and Matsumoto, R., 1999, Raman spectroscopic determination of hydration number of methane hydrates: AIChE Journal, v. 45, no. 12, p. 2641-2645.

Udachin, K. A., Ratcliffe, C. I., and Ripmeester, J. A., 2001, Structure, Composition, and Thermal Expansion of CO2 Hydrate from Single Crystal X-ray Diffraction Measurements†: The Journal of Physical Chemistry B, v. 105, no. 19, p. 4200-4204.

Chapter 5

Hydrogen sulfide in natural gas hydrates: Importance for local sulfur cycle and hydrate stability

Jiangong Wei[1*], David Fischer[1], Junfeng Qin[2], Thomas Pape[1], Gerhard Bohrmann[1], Werner F. Kuhs[2]

1 MARUM, University of Bremen, Klagenfurter Str., 28359 Bremen, Germany

2 GZG, Abteilung Kristallographie, Georg-August-Universität Göttingen,, Goldschmidtstrasse 1, 37077 Göttingen, Germany

MANUSCRIPT 3

To be submitted to Geology

5.1 Abstract

We recovered gas hydrate samples from shallow sediments of gas seeps in three different areas globally, including the Nigerian continental margin (NCM), the Makran continental margin (MCM) and the southeastern Black Sea (BS). Raman spectroscopy was employed to study the gas compositions as well as crystallographic structure of these hydrates. The result shows that all samples were exclusively structure I hydrate, with guest molecules dominated by methane. Besides methane, minor amounts of hydrogen sulfide (H_2S) were detected at all locations with mean concentrations between 0.53-1.34 mol% and sometimes large variations on a microscopic scale. Based on the strong methane flux evidenced by gas ebullition from the seafloor, H_2S in the hydrate phase is inferred to be produced through sulfate reduction and anaerobic oxidation of methane (SR-AOM). The observed inhomogeneous H_2S distribution is suggested to be the result of a spatial and temporal heterogeneity of methane flux. Considering the limitations of H_2S availability in non-seepage areas, H_2S-containing hydrate may not be as widespread as methane hydrate on a global scale; nevertheless, its presence is likely to be more common than thought before, especially at seep sites. Enhanced hydrate stability, due to the addition of H_2S, potentially increases the possibility of methane to reach the upper mixed layer of water column via bubbles and raising hydrate pieces. In addition, dynamic hydrate formation and dissolution/dissociation is likely to change the H_2S flux and distribution at seep sites, consequently influences the sulfur cycle and local ecosystem.

Keywords: hydrogen sulfate, anaerobic methane oxidation, gas hydrate, gas seeps, pockmarks, sulfur cycle

5.2 Introduction

Gas hydrates (GH) are crystalline compounds composed of water and guest molecules, and present widely in the sediment at continental margins and in permafrost regions (Sloan, 1998). Most attention has been paid on methane and hydrocarbon gas hydrates since they are promising energy resources (Ruppel, 2007), and play an important role in the global carbon cycle (Dickens, 2003), potentially contributing to past and present climate changes (Bratton, 1999). Other guest molecules in natural gas hydrates, for example hydrogen sulfide, are known, but were often ignored or overlooked.

Gas Chromatography is an efficient method to study the H_2S concentration in the samples (Kastner et al., 1998; Swart et al., 2000); however, it cannot distinguish the source of H_2S, whether it is derived from the pore water or from gas hydrate. Raman spectroscopy was also used to study the hydrate characteristics, including cage occupancy of guest, gas composition and hydrate structure (Qin and Kuhs, 2013; Sum et al., 1997). In comparison with gas chromatography, the major advantage of Raman scattering is that it can distinguish H_2S in the water-rich phase from GH-based H_2S (Dubessy et al., 1992). So far, H_2S-contaning hydrates were found at Hydrate Ridge (Hester et al., 2007) and Nigerian Margin (Chazallon et al., 2007) which were confirmed by using Raman spectroscopy. H_2S admixtures to gas hydrates potentially affect gas hydrate stability, the sulfur cycle in the ocean and local ecosystem (Kastner et al., 1998). However, little is known about H_2S distribution or their contribution to natural marine gas hydrates, nor has the amount of H_2S been quantified in earlier studies.

In this study, we analyzed guest gas compositions of hydrate samples from three different seep areas using Raman spectroscopy. We found that H_2S in gas hydrates is distributed heterogeneously on a microscopic scale, and we provide a first estimation of its concentration. Based on these results, we discuss the source of H_2S as well as the impact of H_2S on chemosynthetic communities and enhancing hydrate stability. Furthermore, we discuss the reason for the heterogeneous distribution of H_2S in gas hydrates.

5.3 Materials and methods

Five gas hydrate pieces were sampled from sediments of marine gas seeps in different areas using gravity corer during three cruises: Guineco-MeBo cruise in 2011, M74-3 cruise in 2007 and M84-2 cruise in 2011 (Figure 5.1a). To make it convenient and consistent, we use the same names for both gas hydrate samples and gravity cores. When the gravity cores were on board, gas hydrates were immediately sampled and stored in liq. N_2 to prevent further dissociation.

Raman spectra over a wide range of 0-4000 cm^{-1} were acquired using a LabRAM HR800 (Horiba Jobin Yvon) Raman spectrometer equipped with a Peltier-cooled CCD detector and 600 grooves/mm grating. A 488 nm line emitted by an Ar^+ laser was used at an output power of 20 mW. The detailed instrumental settings and peak analysis can be found in the reference of (Qin and Kuhs, 2013). Each sample was measured for 5-10 illumined spots at the temperature of 113 K and the ambient pressure of liq. N_2.

The corresponding gas-hydrate stability field was calculated using HWHYD software (Østergaard et al., 2005) based on the water temperature, hydrate structure, gas composition and salinity. Water temperature and salinity were obtained by using CTD.

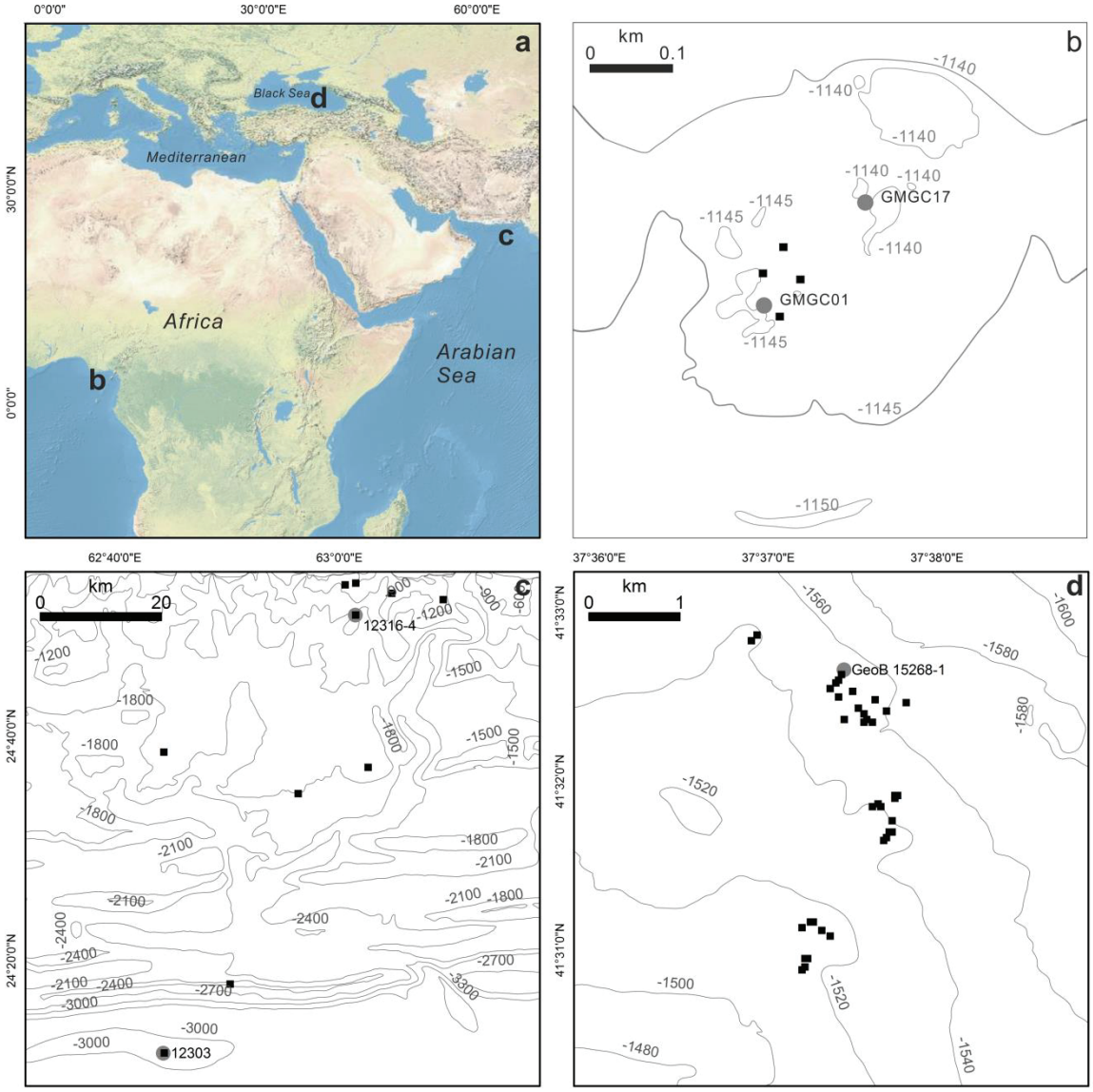

Figure 5.1 a: overview of the study areas. b-d: The detailed bathymetric contour maps of seep sites located in the different areas, the Nigerian continental margin (NCM), the Makran continental margin (MCM) and the Black Sea (BS), respectively. The locations of gas hydrate samples (grey circles) and gas plumes (black squares) in the water column documented by using acoustic methods are shown.

5.4 Seep sites description

Gas hydrate samples GMGC01 and GMGC17 were sampled from shallow sediments in the center of the so-called pockmark A at water depth of around 1140m on the Nigerian continental margin (Figure 5.1b). Gas ebullition from the center of the pockmark was observed in hydroacoustic images. Strong H_2S odor was noticed with authigenic carbonates dispersed within the hemiplegic sediment when the gravity cores were opened.

GeoB12316-4 and GeoB12303 were sampled at water depths of 1019m and 2860m from the so-called Flare 2 and Flare 5 gas seeps, respectively, on the Makran continental margin

(Figure 5.1c). Chemosynthetic communities were observed using ROV 'MARUM-QUEST 4000m' at the seafloor at both sites. Gas ebullition was detected using both ROV and hydroacoustic methods (Römer et al., 2012). Carbonates, which are presumably a product of anaerobic methane oxidation (AOM), were observed directly underneath the bacterial mats at Flare 2, whereas no carbonate was found in Flare 5. Hydrates in the sediments varied in size and shape, and there were two major hydrate fabrics: tube-like hydrates (several centimeters in length and 1~2 cm in diameter) and platy chip-like hydrates (1-3 cm in diameter and a few millimeters in thickness).

GeoB15268-1 was recovered from Ordu ridge (Figure 5.1d). This ridge, named during the M84-2 cruise, is composed of several slightly mounded structures, and is located at water depth around 1534 m in the southeastern Black Sea. Gas accumulation in the shallow sediment and gas emission in the water column at the mound were inferred using hydroacoustic methods (Bohrmann, 2011). Gas hydrate occurred in the unit-3 of the typical Black Sea sediment in gravity core GeoB15268-1, until a depth of 2.5 mbsf.

5.5 Results and discussion

5.5.1 Raman evidence of H_2S in gas hydrate

Gas hydrate samples and their representative Raman spectra of guest molecules, H_2S and CH_4, are shown in Figure 5.2a and Figure 5.2b, respectively. In general, methane was the dominant guest molecule in all the hydrate samples, with minor amounts of H_2S.

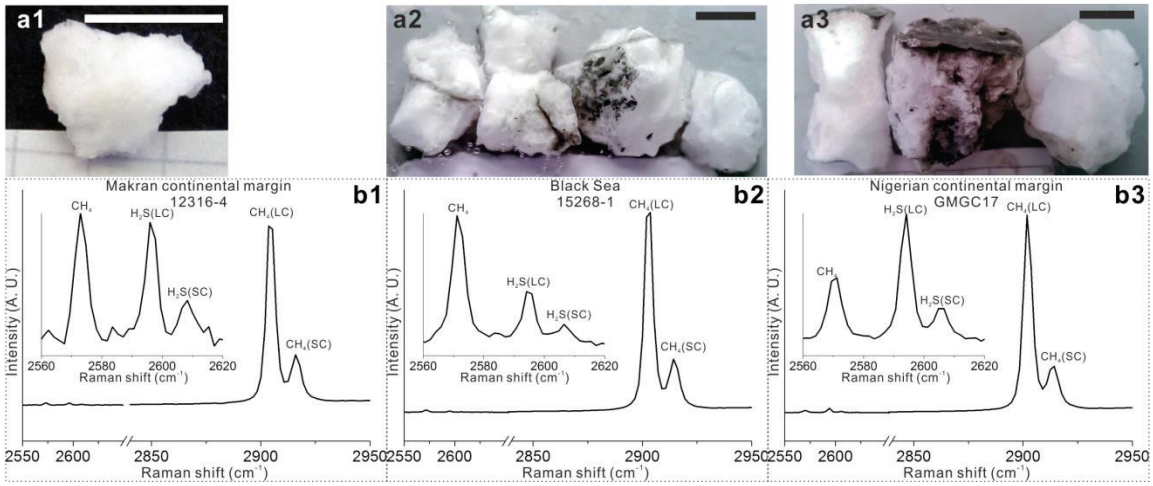

Figure 5.2 Above (a1-a3): Hydrate samples for Raman spectra analysis before being crushed. The scale bar is 1cm. Below (b1-b3): The corresponding representative Raman spectra of the samples. The Raman shift between 2560 cm^{-1} and 2620 cm^{-1} were enlarged in the insert figures to have a close view of the H_2S bands. LC and SC represent large and small hydrate cages, respectively.

Two peaks at about 2901 cm^{-1} and 2913 cm^{-1} were assigned to the symmetric C-H stretching-vibrational mode (v_1) of methane molecules in the large cages ($5^{12}6^2$, LC) and small cages (5^{12}, SC), respectively (Chazallon et al., 2007; Qin and Kuhs, 2013). The other two Raman bands of methane are at 3049 cm^{-1} and 2570 cm^{-1} (Qin and Kuhs, 2013). In all analyzed gas hydrate samples small amounts of H_2S were detected. The H-S symmetric stretching band for H_2S has been reported at 2593-2595 cm^{-1} for H_2S in the large cages and

at 2605 cm^{-1} for small cages in sI H_2S-containing hydrate (Chazallon et al., 2007; Dubessy et al., 1992). In this study, two weak peaks measured at 2594 and 2605 cm^{-1} (Figure 5.2) confirmed that H_2S is present as a guest gas in both large and small cavities, which are around 4 and 15 cm^{-1} higher than the Raman peak of H_2S dissolved in water (Dubessy et al., 1992).

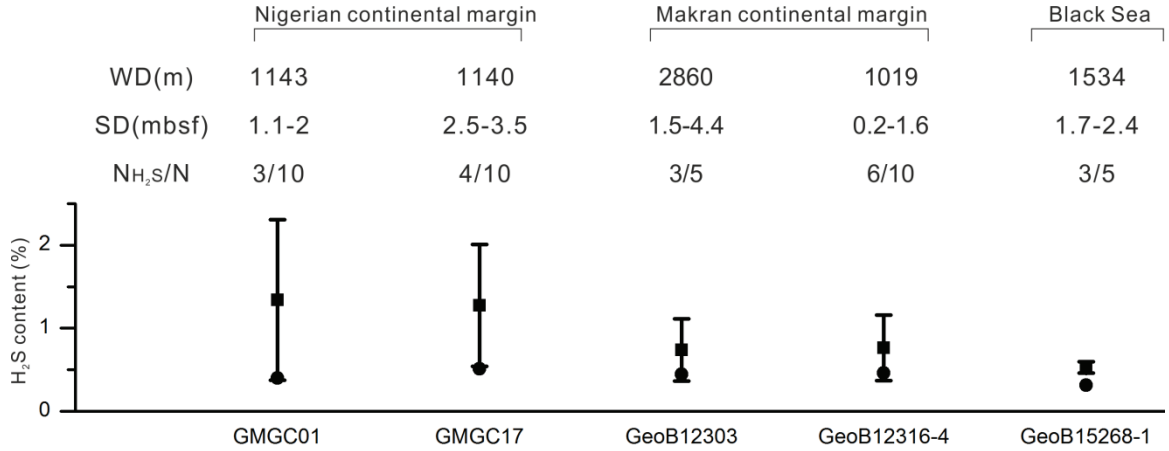

Figure 5.3 Basic information for the samples (WD: water depth, SD: sample depth), and the H_2S contents calculated based on the Raman spectra. The mean values were calculated based on the number of both all measurements (N, circle, mean1) and those in which H_2S occurs (NH_2S, square, mean2). The error bars shows one standard deviation (deviation from the mean).

The concentration of H_2S in natural gas hydrates can be derived from the relative peak intensities of H_2S to CH_4 and their Raman quantification factor ratios calibrated using the crystallographically established absolute cage occupancies of a pure H_2S sample (Qin & Kuhs 2014, personal communication), in analogy to the procedures described in (Qin and Kuhs, 2013) for methane hydrate. As shown in Figure 5.3, the mean values of the concentration of encaged H_2S of all the measurements (mean1) are ~ 0.32-0.51 mol%, assuming that content of H_2S in the sampled spots without any detectable H_2S peak is 0. The mean values of concentration of encaged H_2S for H_2S-containing samples (mean2) ranges between 0.53±0.07 mol% and 1.34±0.97 mol%. Intermittent H_2S occurrence in the measurements and the high standard deviations for each sample indicate a spatial inhomogeneous distribution of H_2S on a microscopic scale in the samples. This heterogeneous H_2S distribution has also been observed in the gas hydrates of Hydrate Ridge (Schicks et al., 2010).

5.5.2 Source of H_2S

In marine sediments, H_2S is formed by sulfate reduction driven by either organic matter degradation or AOM (Froelich et al., 1979; Hoehler et al., 1994). AOM is responsible for the majority of sulfate reduction in the gas seep areas, and has been confirmed in several marine gas seeps (Borowski et al., 1996). In our study areas, the coincidence of H_2S-containing hydrate and strong methane bubble ebullition in the water column indicates that H_2S in the gas hydrate was mainly formed by sulfate reduction driven by AOM. This is confirmed by pore water profiles indicating a co-depletion of sulfate and methane strongly pointing at AOM as the sulfate-consuming process (Fischer et al., 2013).

5.5.3 Impact of H_2S in gas hydrate

Addition of small amounts of H_2S has a significant impact on enhancing the gas hydrate stability (Kastner et al., 1998). In comparison with pure methane hydrate, the shifts of the upper boundaries of the gas hydrate stability zone (GHSZ) in the water column ranges between 67 m and 102 m depending on the measured H_2S contents in the hydrate samples of the three study areas (Figure 5.4). This indicates that the GHSZ is significantly expanded by adding even relatively small amount of H_2S; as a result, the potential lifetime of gas hydrate is likely to be significantly enhanced in the water column. Based on these considerations, we argue that methane transported to the upper mixed water layers and even to the atmosphere through gas bubbles coated with hydrate skins (Rehder et al., 2002) or hydrate chunks rafting from the seafloor (Pape et al., 2011) might be underestimated, if H_2S contributes to the guest molecule fraction.

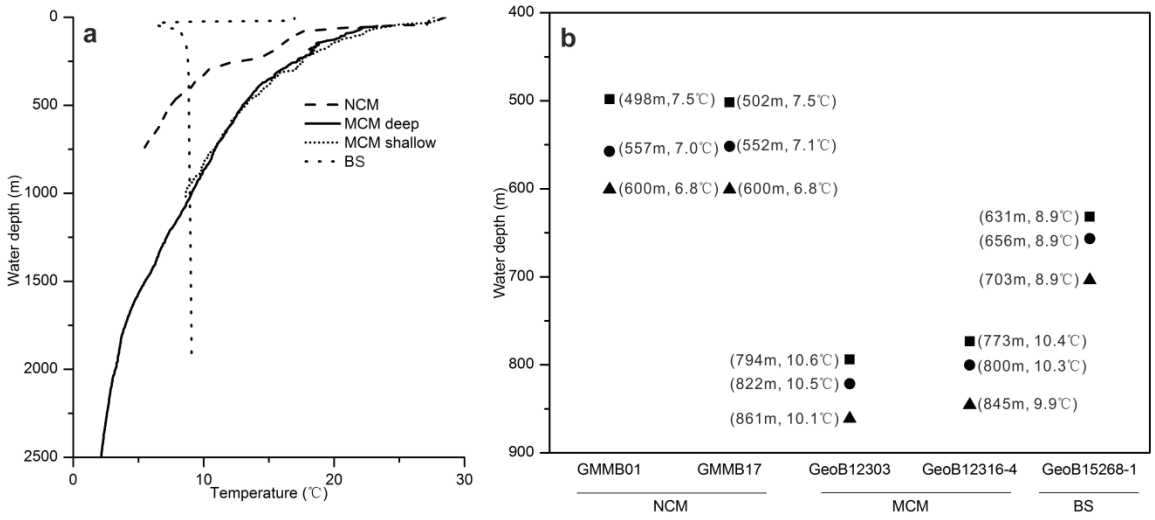

Figure 5.4 a: Water column temperature in the vicinity of the sampling sites measured by using CTD. b: The upper boundaries of sI hydrate (triangle: pure methane hydrate; circle: methane+H_2S (mean1); square: methane+H_2S (mean2)) at each site were calculated using HWHYD software. The salinities of seawater were set to 32 PSU, 35.5 PSU and 21 PSU for seeps sites of NCM, MCM and BS, respectively.

Chemosynthetic communities of several groups of macrofaunal species feeding on H_2S as energy source are a common feature of marine gas seeps (Olu et al., 1997). The intensity of methane flux normally decreases from the center of the seeps to the surroundings (Fischer et al., 2012). Different organisms have their own suitable growing conditions, which are mainly confined by the intensity of methane flux. Thus, the distribution of the organisms often exhibits concentric habitats. The H_2S fluxes might be affected by gas hydrate dissociation and dissolution if H_2S is contained in the hydrates. The sudden variation of H_2S fluxes is likely to change the local condition and have a dramatic impact on the seep related chemosynthetic communities. If gas hydrates are to decompose or dissolve, for example, due to warming of bottom water or insufficient methane supply, H_2S released to the sediment/water environment may be enhanced, which would certainly affect chemosynthetic communities.

5.5.4 Model of CH_4-H_2S hydrate formation

Based on our calculation (Figure 5.4), the temperature and pressure conditions of all the study regions are within the gas hydrate stability field. Thus, the only condition which hinders the formation of H_2S-containing hydrate is the availability of H_2S from the pore water. The intermittent H_2S occurrence and large variation of H_2S content on a microscopic scale indicate a heterogeneous distribution of H_2S; consequently, we argue the availability of H_2S is related to the spatial and temporal methane flux variation in the cold seeps. The sketch shown in Figure 5.5 explains this process.

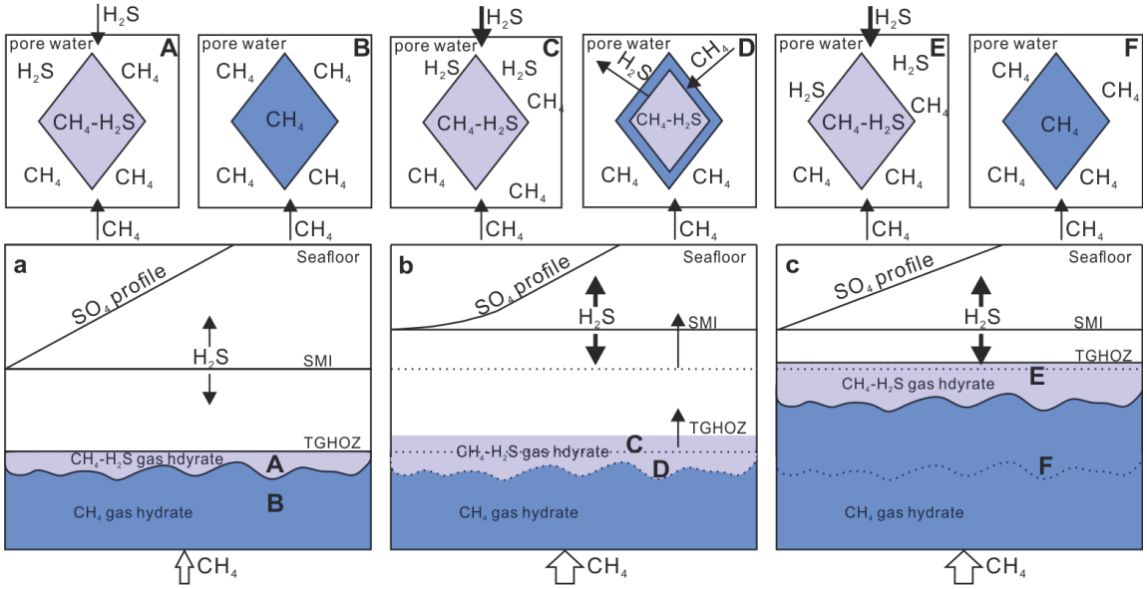

Figure 5.5 Model explaining the relation between the heterogeneous distribution of H_2S in the gas hydrate and the spatial and temporal variation of methane flux.

Stage 1 (Figure 5.5a): At the beginning, when the methane flux is stable, H_2S produced by SR-AOM diffuses from the sulfate methane interface (SMI) both upward and downward (Figure 5.5a). The concentration of H_2S at the top of gas hydrate occurrence zone (TGHOZ) is the most possible region to reach the criteria of CH_4-H_2S hydrate formation (Figure 5.5A). However, in the relative deeper sediment (Figure 5.5B) where H_2S can not transport that far, only pure methane hydrate occurs.

Stage 2 (Figure 5.5b): When methane fluxes increase, both SMI and TGHOZ were shifted upward (Borowski et al., 1999). The H_2S concentration in the gas hydrate might increase through two aspects. On one hand, the oversupplied methane stimulates the SR-AOM, consequently increases H_2S production rate and leads to a higher H_2S concentration in the pore water. On the other hand, CH_4-H_2S gas hydrate formed close to the former depth of SMI where H_2S were enriched in the pore water. The increased H_2S content in the sediment could finally increase the H_2S content in the gas hydrate (Figure 5.5C). H_2S in the CH_4-H_2S gas hydrate formed at the old TGHOZ and SMI tends to be replaced by CH_4 gradually due to the increased methane flux and decreased H_2S concentration in the pore water (Figure 5.5D).

Stage 3 (Figure 5.5c): In the third stage, when the methane flux is stable, a new SMI and TGHOZ will form. CH_4-H_2S gas hydrate formed at the old TGHOZ and SMI will be totally transformed to methane hydrates (Figure 5.5E), whereas H_2S are enriched in the hydrates at the TGHOZ (Figure 5.5F).

Thus, when the gas hydrates were sampled at different stages and depths, H_2S exhibit heterogamous distribution in the gas hydrate.

5.6 Future work

In this work, the existence and content of H_2S in shallow gas hydrates from cold seeps of three different areas are reported, which indicates that H_2S-containing hydrate is likely to be more common than we thought before, especially at cold seeps. However, on which spatial scales H_2S gas hydrate occurs in the sediment, which is an important factor to evaluate its impact on local ecosystems, is still unknown. For the future, it would be helpful to study the distribution of H_2S in gas hydrates from different depths in the same core to confine the limit of its occurrence depths. In order to evaluate the importance of H_2S in gas hydrates and its impact on the sulfur cycle, further work is necessary.

Acknowledgements

We thank the captain and crew of R/V ‘Pourquoi pas?’ and R/V ‘Meteor’ for the support during the cruises of ‘Guineco-MeBo’, M74-3 and M84-2. Jiangong Wei was sponsored by the China Scholarship Council (CSC).

Reference

Bohrmann, G., 2011, R/V METEOR Cruise Report M84/2: Origin and Distribution of Methane and Methane Hydrates in the Black Sea: M84, Leg 2, Istanbul-Istanbul, 26 February-02 April, 2011, DFG-Forschungszentrum MARUM, Universität Bremen.

Borowski, W. S., Paull, C. K., and Ussler Iii, W., 1999, Global and local variations of interstitial sulfate gradients in deep-water, continental margin sediments: Sensitivity to underlying methane and gas hydrates: Marine Geology, v. 159, no. 1–4, p. 131-154.

Borowski, W. S., Paull, C. K., and Ussler, W., 1996, Marine pore-water sulfate profiles indicate in situ methane flux from underlying gas hydrate: Geology, v. 24, no. 7, p. 655-658.

Bratton, J. F., 1999, Clathrate eustasy: Methane hydrate melting as a mechanism for geologically rapid sea-level fall: Geology, v. 27, no. 10, p. 915-918.

Chazallon, B., Focsa, C., Charlou, J.-L., Bourry, C., and Donval, J.-P., 2007, A comparative Raman spectroscopic study of natural gas hydrates collected at different geological sites: Chemical Geology, v. 244, no. 1–2, p. 175-185.

Dickens, G. R., 2003, Rethinking the global carbon cycle with a large, dynamic and microbially mediated gas hydrate capacitor: Earth and Planetary Science Letters, v. 213, no. 3–4, p. 169-183.

Dubessy, J., Boiron, M.-C., Moissette, A., Monnin, C., and Sretenskaya, N., 1992, Determinations of water, hydrates and pH in fluid inclusions by micro-Raman spectrometry: European journal of mineralogy, v. 4, no. 5, p. 885-894.

Fischer, D., Mogollon, J. M., Strasser, M., Pape, T., Bohrmann, G., Fekete, N., Spiess, V., and Kasten, S., 2013, Subduction zone earthquake as potential trigger of submarine hydrocarbon seepage: Nature Geosci, v. 6, no. 8, p. 647-651.

Fischer, D., Sahling, H., Nöthen, K., Bohrmann, G., Zabel, M., and Kasten, S., 2012, Interaction between hydrocarbon seepage, chemosynthetic communities, and bottom water redox at cold seeps of the Makran accretionary prism: insights from habitat-specific pore water sampling and modeling: Biogeosciences, v. 9, no. 6, p. 2013-2031.

Froelich, P. N., Klinkhammer, G. P., Bender, M. L., Luedtke, N. A., Heath, G. R., Cullen, D., Dauphin, P., Hammond, D., Hartman, B., and Maynard, V., 1979, Early oxidation of organic matter in pelagic sediments of the eastern equatorial Atlantic: suboxic diagenesis: Geochimica et Cosmochimica Acta, v. 43, no. 7, p. 1075-1090.

Hester, K. C., Dunk, R. M., White, S. N., Brewer, P. G., Peltzer, E. T., and Sloan, E. D., 2007, Gas hydrate measurements at Hydrate Ridge using Raman spectroscopy: Geochimica et Cosmochimica Acta, v. 71, no. 12, p. 2947-2959.

Hoehler, T. M., Alperin, M. J., Albert, D. B., and Martens, C. S., 1994, Field and laboratory studies of methane oxidation in an anoxic marine sediment: Evidence for a methanogen-sulfate reducer consortium: Global Biogeochemical Cycles, v. 8, no. 4, p. 451-463.

Kastner, M., Kvenvolden, K. A., and Lorenson, T. D., 1998, Chemistry, isotopic composition, and origin of a methane-hydrogen sulfide hydrate at the Cascadia subduction zone: Earth and Planetary Science Letters, v. 156, no. 3–4, p. 173-183.

Olu, K., Lance, S., Sibuet, M., Henry, P., Fiala-Médioni, A., and Dinet, A., 1997, Cold seep communities as indicators of fluid expulsion patterns through mud volcanoes seaward of the Barbados accretionary prism: Deep Sea Research Part I: Oceanographic Research Papers, v. 44, no. 5, p. 811-841.

Østergaard, K. K., Masoudi, R., Tohidi, B., Danesh, A., and Todd, A. C., 2005, A general correlation for predicting the suppression of hydrate dissociation temperature in the presence of thermodynamic inhibitors: Journal of Petroleum Science and Engineering, v. 48, no. 1–2, p. 70-80.

Pape, T., Bahr, A., Klapp, S. A., Abegg, F., and Bohrmann, G., 2011, High-intensity gas seepage causes rafting of shallow gas hydrates in the southeastern Black Sea: Earth and Planetary Science Letters, v. 307, no. 1–2, p. 35-46.

Qin, J., and Kuhs, W. F., 2013, Quantitative analysis of gas hydrates using Raman spectroscopy: AIChE Journal, v. 59, no. 6, p. 2155-2167.

Rehder, G., Brewer, P. W., Peltzer, E. T., and Friederich, G., 2002, Enhanced lifetime of methane bubble streams within the deep ocean: Geophysical Research Letters, v. 29, no. 15, p. 21-24.

Römer, M., Sahling, H., Pape, T., Bohrmann, G., and Spieß, V., 2012, Quantification of gas bubble emissions from submarine hydrocarbon seeps at the Makran continental margin (offshore Pakistan): Journal of Geophysical Research: Oceans, v. 117, no. C10, p. C10015.

Ruppel, C., 2007, Tapping Methane Hydrates for Unconventional Natural Gas: Elements, v. 3, no. 3, p. 193-199.

Schicks, J. M., Ziemann, M. A., Lu, H., and Ripmeester, J. A., 2010, Raman spectroscopic investigations on natural samples from the Integrated Ocean Drilling Program (IODP) Expedition 311: Indications for heterogeneous compositions in hydrate crystals: Spectrochimica Acta Part A: Molecular and Biomolecular Spectroscopy, v. 77, no. 5, p. 973-977.

Sloan, E. D., 1998, Clathrate Hydrates of Natural Gases, CRC Press.

Sum, A. K., Burruss, R. C., and Sloan, E. D., 1997, Measurement of Clathrate Hydrates via Raman Spectroscopy: The Journal of Physical Chemistry B, v. 101, no. 38, p. 7371-7377.

Swart, P. K., Wortmann, U. G., Mitterer, R. M., Malone, M. J., Smart, P. L., Feary, D. A., and Hine, A. C., 2000, Hydrogen sulfide–hydrates and saline fluids in the continental margin of South Australia: Geology, v. 28, no. 11, p. 1039-1042.

Chapter 6 Conclusion and outlook

6.1 Conclusion

In manuscript 1, we made a comprehensive investigation on hydrate distribution at the pockmark field at the Nigerian continental margin. In manuscript 2, Characteristics of the hydrates, including crystallographic structure and composition of hydrate bonded gas were analyzed. In manuscript 3, significance of H_2S containing hydrate were discussed based the analysis of samples from gas seeps of different areas. In this chapter, we will conclude the whole thesis by answering the questions proposed in the section of 'motivation and objective'.

How do gas hydrates distribute in the shallow sediment of pockmarks and what are the controlling factors of its distribution?

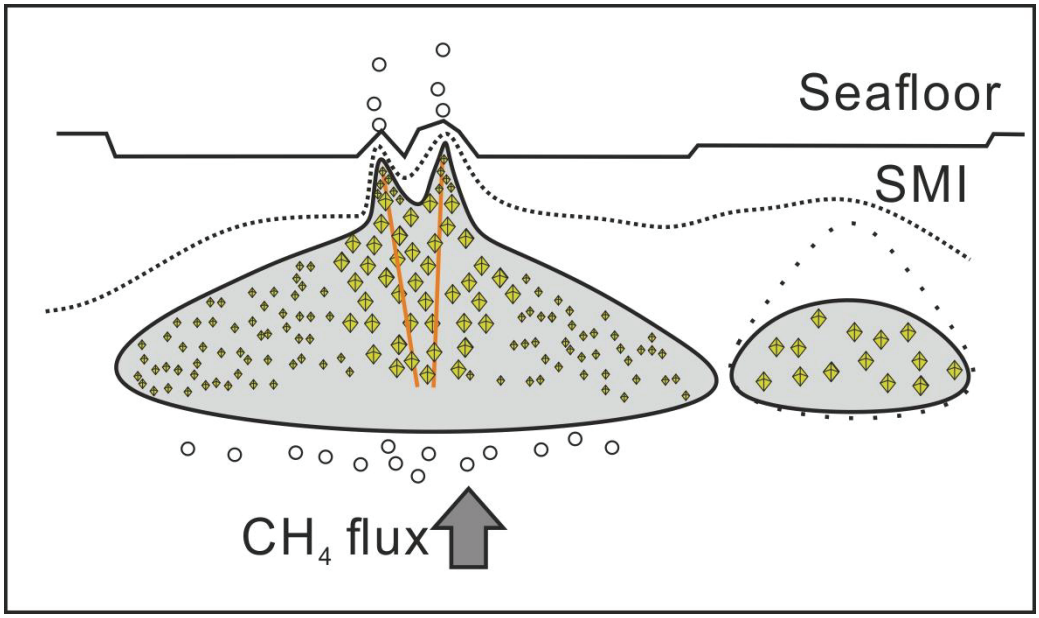

Figure 6.1 Model of pockmark evolution caused by hydrate formation and dissolution.

By applying infrared thermal imaging and pore water chloride concentration analysis on the MeBo drilling cores, gas hydrate distribution within the pockmark field were comprehensively interpreted. Gas hydrate occurrence is horizontally restricted in the sediment column whose boundary is confined by the pockmark shape. Vertically, gas hydrate occurs in the shallow sediment of 1.2 to 4.4 mbsf in the center of pockmark. Hydrate occurring depth increase dramatically from the center to the periphery and outside the pockmark. The distribution of gas hydrate is mainly controlled by fluid flow. Elevated geothermal gradient and free gas in the water column were observed in the center of pockmark, indicating the fluid flow is mainly controlled by advection through fractures. At the periphery, no obvious temperature elevation or free gas escape was observed, indicating a diffusion controlled fluid flow. Fluid advection is more efficiently in transporting methane to shallow sediment which compensates the methane consumed by AOM, therefore, gas hydrate could form in shallow sediments in the center than that at the

periphery. Hydrate formation might plug the fracture and cease methane supply or redirect the path of methane migration, causing hydrate dissolution due to the under saturated methane in the pore water. Alternately happened hydrate formation and dissolution due to variation of methane supply potentially influence the seafloor morphology of the pockmarks in this area (Figure 6.1).

What is the structure and gas composition of gas hydrates? What are the impacts of small amount of CO_2 and H_2S on the hydrate structure?

Samples from pockmarks at the Nigerian continental margin are exclusively structure I hydrate. Hydrate bonded gas is dominated by methane with small amount of CO_2, H_2S and C_2H_6. CO_2 and H_2S distributed heterogeneously and hardly co-exist by any Raman measurements. We propose that this phenomenon is caused by their concentration variation in the pore water, and might reflect the temporal and spatial variation of upward fluid flow. Since CO_2 preferentially occupies large cages, methane cage occupancy ratios decrease from 1.10 (pure methane hydrate, theoretical value) to 1.03. This phenomenon is ascribed to the presence of CO_2 which is preferentially occupying large cages.

Is it an occasional case or a common global case for H_2S-containing natural gas hydrates occurring in gas seeps? What is the significance?

H_2S is a potential guest for the small cage of sI hydrate. However, its existence in nature has only been confirmed at Hydrate ridge and Niger delta before this study. In this study, H_2S content within the hydrate samples from the Nigerian continental margin, the Makran continental margin and the Black Sea are estimated to be ranged between 0.53-1.34%. Therefore, we add three more locations to this database which indicate that H_2S containing hydrate is not restricted to specific places, but potentially occur within in the gas seeps worldwide where sufficient methane is available for fast AOM which produces H_2S. Although the content of H_2S is relatively small, the hydrate stability is dramatically increased, which potentially increases the possibility of methane to reach the upper mixed layer of water column via bubbles and raising hydrate pieces. In addition, dynamic hydrate formation and dissolution/dissociation is likely to change the H_2S flux and distribution at seep sites, consequently influences the sulfur cycle and local ecosystem.

6.2 Outlook

Can we improve or calibrate the infrared thermal scanning to estimate the hydrate content within marine sediment?

Compared with other methods for detecting hydrate distribution in cores, such as pore water chloride concentration, the biggest advantage of infrared thermal scanning is its high resolution and fast operation. In this study, we only used it for hydrate detection and documentation. However, it could be potentially used for estimating hydrate content with calibration from other proxies, such as pore water chloride concentration. In the future, algorithm should be developed to estimate the continuous hydrate content within sediment cores based on the temperature anomalies imaged by infrared camera.

How does H_2S containing hydrate distribute within the sediment of the cold seeps? Is it restricted to the SMI, or could it be expanded to both directions to some extent?

In this study, we know that H_2S containing hydrate potentially occurred worldwide in the gas seeps. However, we did not get the accurate depth of hydrate samples and the depth of SMI. Therefore, the spatial relation between H_2S containing hydrate and SMI cannot be defined. In the future, accurate sampling of hydrate could be done with remotely operating vehicle and SMI depth could be accurately detected. Based on these data, numerical model of H_2S diffusion and advection model coupled AOM will give inside view of the relation between the formation of H_2S containing hydrate, H_2S transportation, rate of AOM and methane flux.

Acknowledgements

I feel lucky and grateful that so many people helped me and encouraged me during the four year study. I can't reach that far without their help.

The deepest thanks go to my supervisor, Prof. Dr. Gerhard Bohrmann. I thank him for providing me the opportunity to be a PhD student in his group. He fully supported my work in the past four years and led me to the fascinating world of marine gas hydrate and cold seeps. I thank him especially for giving me the chance to participate four research cruises as well as international conferences from which I benefit a lot.

I greatly thank Dr. Thomas Pape and Dr. David Fischer for their advices and guidance during the whole project. Both of them helped me with improving the manuscripts significantly from general structure to detailed grammar mistakes and typos.

I thank Hella for her technique support of the analysis of computerized tomography. I thank Prof. Dr. Werner F.Kuhs, Dr. Junfeng Qin and Dr. Andrzej Falenty from University of Goettingen for their help on hydrate analysis.

I thank all my colleagues (ordered alphabetically):

Christian dos Santos Ferreira, Chieh-Wei Hsu, David Fischer, Henry Wu, Heiko Sahling, Iversen Morten, Jan-Hendrik Körber, Miriam Römer, Michal Tomczyk, Patrizia Geprägs, Paul Wintersteller, Sven Klüber, Susan Mau, Tobias Himmler, Thomas Pape, Xiting Liu, Yann Marcon who were always available to help. It is a pleasure to work with all of them. Further, I would like to thank Angelika Rinkel and Greta Ohling for their constant support; otherwise I would die in the administrative paperwork. I especially thank Paul for providing me a six month mini job.

I thank all my friends for all the good time we spend together.

I thank China Scholarship Council (CSC) and Ocean University of China for providing me the scholarship to study in Germany. I also thank my pre supervisor Xiuli Feng at Ocean University of China for her kind support and encouragement.

My greatest thanks go to my parents and my sister for their understanding and encouragement.

Finally, my very special thanks go to Tingting who support and encourage me and never questioned my choice.

感谢中国国家留学基金管理委员会给我提供四年的奖学金让我能有机会在德国完成博士学业。感谢母校中国海洋大学，感谢冯秀丽教授在我留学期间给我的支持和鼓励。

深深的感谢我的父母和姐姐在我低谷的时候给我的鼓励支撑我继续向前，感谢他们无私的包容，谅解和支持。

最后，衷心感谢四年来一直陪伴和支持我的爱人吴婷婷。

Jiangong Wei

Luisental 29A 4205

28359 Bremen

Erklärung

Erklärung gemäß § 6 Abs. 5 der Promotionsordnung der Universität Bremen für die mathematischen, natur- und ingenieurwissenschaftlichen Fachbereiche. Hiermit versichere ich, dass ich

1. die vorliegende Arbeit ohne unerlaubte fremde Hilfe angefertigt habe,

2. keine anderen als die von mir angegebenen Quellen und Hilfsmittel benutzt habe,

3. die den benutzen Werken wörtlich oder inhaltlich entnommenen Stellen als solche kenntlich gemacht habe.

Bremen, den 29.12.2014

Appendix

Appendix I: Pape et al., 2014

Appendix II: Sultan et al., 2014

AGU PUBLICATIONS

Geochemistry, Geophysics, Geosystems

RESEARCH ARTICLE
10.1002/2013GC005057

Hydrocarbon seepage and its sources at mud volcanoes of the Kumano forearc basin, Nankai Trough subduction zone

Thomas Pape[1], Patrizia Geprägs[1], Sebastian Hammerschmidt[1], Paul Wintersteller[1], Jiangong Wei[1], Timo Fleischmann[1], Gerhard Bohrmann[1], and Achim J. Kopf[1]

[1]MARUM – Center for Marine Environmental Sciences, Department of Geosciences, University of Bremen, Bremen, Germany

Key Points:
- Hydrocarbons (HC) at mud volcanoes (MVs) in the Kumano basin are thermogenic
- HCs most likely originate from the old accretionary prism deeper than 2300 m
- Except for MVs 2 and 5 seepage activity of MVs is low compared to former times

Supporting Information:
- Readme
- Auxiliary Material

Correspondence to:
T. Pape,
tpape@marum.de

Citation:
Pape, T., P. Geprägs, S. Hammerschmidt, P. Wintersteller, J. Wei, T. Fleischmann, G. Bohrmann, and A. J. Kopf (2014), Hydrocarbon seepage and its sources at mud volcanoes of the Kumano forearc basin, Nankai Trough subduction zone, *Geochem. Geophys. Geosyst.*, *15*, doi:10.1002/2013GC005057.

Received 23 SEP 2013
Accepted 30 APR 2014
Accepted article online 3 MAY 2014

Abstract Twelve submarine mud volcanoes (MV) in the Kumano forearc basin within the Nankai Trough subduction zone were investigated for hydrocarbon origins and fluid dynamics. Gas hydrates diagnostic for methane concentrations exceeding solubilities were recovered from MVs 2, 4, 5, and 10. Molecular ratios ($C_1/C_2 < 250$) and stable carbon isotopic compositions ($\delta^{13}C\text{-}CH_4 > -40‰$ V-PDB) indicate that hydrate-bound hydrocarbons (HCs) at MVs 2, 4, and 10 are derived from thermal cracking of organic matter. Considering thermal gradients at the nearby IODP Sites C0009 and C0002, the likely formation depth of such HCs ranges between 2300 and 4300 m below seafloor (mbsf). With respect to basin sediment thickness and the minimum distance to the top of the plate boundary thrust we propose that the majority of HCs fueling the MVs is derived from sediments of the Cretaceous to Tertiary Shimanto belt below Pliocene/Pleistocene to recent basin sediments. Considering their sizes and appearances hydrates are suggested to be relicts of higher MV activity in the past, although the sporadic presence of vesicomyid clams at MV 2 showed that fluid migration is sufficient to nourish chemosynthesis-based organisms in places. Distributions of dissolved methane at MVs 3, 4, 5, and 8 pointed at fluid supply through one or few MV conduits and effective methane oxidation in the immediate subsurface. The aged nature of the hydrates suggests that the major portion of methane immediately below the top of the methane-containing sediment interval is fueled by current hydrate dissolution rather than active migration from greater depth.

1. Introduction

Submarine mud volcanoes (MVs) are seafloor expressions of localized outflow of sediment and warm fluids mobilized in the subsurface typically several kilometers in depth [*Dimitrov*, 2002; *Kopf*, 2002]. Subduction-related liquid and gaseous fluids form in the deep subsurface as a consequence of sediment consolidation, mineral alteration, and organic matter decomposition [*Moore et al.*, 2001; *Moore and Vrolijk*, 1992]. Light hydrocarbons are typically formed during thermal cracking of organic matter at temperatures exceeding about 100°C in the deep subsurface [*Selley*, 1998; *Seewald*, 2003]. In contrast, microbial methane formation is thought to occur at temperatures less than ca. 90°C which usually exist at shallower sediment depths. It is well documented that MVs can show transient fluid discharge activities, which may be evaluated by interpreting concentration profiles of fluids having migrated into the pore space of shallow sediments. For instance, the depth of the sulfate-methane interface (SMI), i.e., the zone where upward migrating methane and seawater-derived sulfate are converted through the anaerobic oxidation of methane [e.g., *Hoehler et al.*, 1994], was proposed as a measure for the relative methane flux intensity [*Bhatnagar et al.*, 2011; *Borowski et al.*, 1996; *Castellini et al.*, 2006].

Submarine MVs are widespread at active continental margins because the buoyant upward migration of fluids is promoted by high pore-fluid pressure at depth caused by the overburden of overlying sediments and the general compressional regime induced by plate convergence. Subduction-related MVs predominantly located in forearc basins were reported from various regions including the Makran accretionary wedge [*Schlüter et al.*, 2002], the Mediterranean accretionary wedge [*Camerlenghi et al.*, 1995; *Kopf*, 1999], off Costa Rica [*Bohrmann et al.*, 2002], the Barbados Ridge complex [*Westbrook and Smith*, 1983], the eastern Indonesian accretionary complex [*Barber et al.*, 1986], and the Nankai accretionary wedge of Japan [*Kuramoto et al.*, 2001; *Morita et al.*, 2004].

In case the MV is located within the gas hydrate stability zone (GHSZ), hydrates might form a capacious reservoir of light hydrocarbons from the ascending fluids in shallow sediments [e.g., *Bohrmann et al.*, 2003;

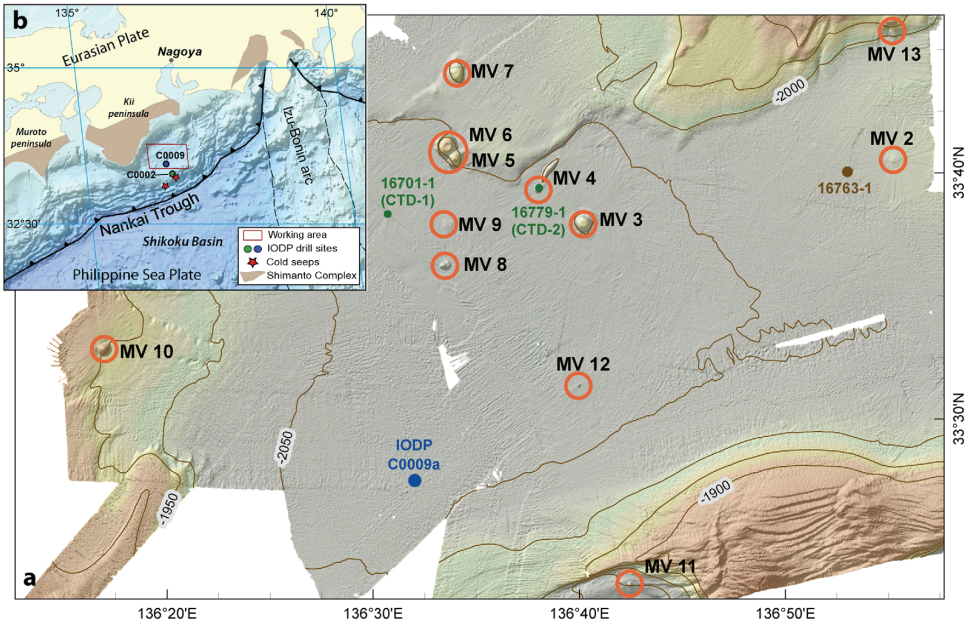

Figure 1. (a) Bathymetric map of the study area indicating positions of individual mud volcanoes investigated in this study. (b) Relief map and regional tectonic setting of the subduction zone of southwest Japan indicating the position of the working area in the Kumano forearc basin. Distributions of the Shimanto complex according to *Moore and Saffer* [2001].

Feseker et al., 2009; *Milkov*, 2000; *Pape et al*., 2010b, 2011b; *Sahling et al*., 2009]. Despite biotic and abiotic molecular and isotopic modifications known to occur during fluid migration and hydrate formation [e.g., *Hachikubo et al*., 2007; *James and Burns*, 1984; *Pape et al*., 2010a; *Sassen et al*., 1999], the chemical characteristics of those hydrates bear information on the geochemistry of the hydrocarbon source. For instance, a predominance of thermogenic hydrocarbons was reported from MVs in the Nile deep sea fan [*Mastalerz et al*., 2007], in the Anaximander Mountains [*Pape et al*., 2010b], or in the Gulf of Cadiz [*Hensen et al*., 2007]. A prevalence of microbial hydrocarbons was proposed for the Dvurechenskii and Vodyanitskii MV in the Black Sea [*Feseker et al*., 2009; *Sahling et al*., 2009], and the Håkon Mosby MV in the Barents Sea [*Pape et al*., 2011b].

More than a dozen of MVs are known from above the seismogenic zone in the Kumano forearc basin at the Nankai Trough subduction zone offshore SW Japan (Figure 1a). The region is characterized by destructive and tsunamigenic earthquakes and nonvolcanic tremors [*Ito and Obara*, 2006; *Obana and Kodaira*, 2009; *Shelly et al*., 2006]. Although several sites at the Nankai Trough subduction zone have already been explored in the frame of IODP drilling campaigns [see *Henry et al*., 2012; *Kinoshita et al*., 2009; *Kopf et al*., 2011; *Moore et al*., 2013; *Saffer et al*., 2010; *Saito*, 2009], causes for the MV activity in the Kumano forearc basin and the fluid sources have been poorly constraint so far. In the present study, we analyzed hydrate-bound gases and dissolved methane in shallow deposits of 12 MVs in order to assign fluid formation depths and processes, and potential source rocks, respectively. Current stages of activity at individual MVs were evaluated by conducting hydroacoustic water column surveys, seafloor inspections, and geochemical profiling.

2. Tectonic and Geological Setting

The Nankai Trough accretionary subduction zone is the active convergent plate boundary between the subducting Shikoku basin on the Philippine Sea Plate and the Eurasian Plate (Figure 1b). For the Philippine Sea Plate, minimum ages of 20–21 Myr (early Miocene) were estimated [*Marcaillou et al*., 2012]. Nowadays, the deformation front is located about 80–160 km southeast off the Kii Peninsula, SW Japan [*Moore et al*., 2001]. In our working area in the Kumano forearc basin the top of the subducting plate was proposed to be located at depths between about 10 and 20 kmbsf [*Marcaillou et al*., 2012; *Moore and Saffer*, 2001].

The landward subduction zone margin consists of the >100 km wide Nankai accretionary prism [e.g., *Taira et al*., 1992]. At present, predominantly hemipelagic sediments of the Shikoku basin are being accreted [*Henry et al*., 2012; *Saito*, 2009]. The landward succession of the toe of the prism is formed by sediments underlying the Kumano basin fill that are believed to belong to the Cretaceous and Tertiary Shimanto Belt (Figures 1a and 1b); [*Taira et al*., 1992]. The Kumano forearc basin is located east of the Kii peninsula and extends about 100 km in E–W and 70 km in N–S direction. It forms a low-topography seafloor basin approaching water depths of approx. 2100 m. Terrigenous and hemipelagic sediments in that basin are up to 2 km in thickness [*Morita et al*., 2004; *Tobin and Kinoshita*, 2006]. Age assignments for rocks at the bases of IODP Sites C0002 and C0009, that penetrated the boundary between basin sediments and old accreted sediments, suggest that basin formation commenced in the late Miocene [*Hayman et al*., 2012; *Kinoshita et al*., 2009; *McNeill et al*., 2010; *Saffer et al*., 2010].

A landward dipping system of out-of-sequence splay (OOSS) faults commences from the plate boundary thrust fault at ca. 50–55 km landward of the prism toe, migrates through the accretionary prism and surfaces at the seafloor [*Moore et al*., 2007; *Park et al*., 2002]. A megasplay, which apparently intersects the Nankai accretionary prism between the currently formed accretionary prism and the older accreted belt [*Moore et al*., 2007], branches upward from the plate-boundary interface at a depth of about 10 kmbsf and about 50–55 km landward to the deformation front [*Gulick et al*., 2010; *Strasser et al*., 2009]. The OOSSs are believed to branch from the up-dip limit of the seismogenic zone, and thus, to potentially serve as migration pathway for rapid fluid ascent to the seafloor [*Park et al*., 2002; *Tobin and Saffer*, 2009], but indications for deep-sourced fluids are missing yet [e.g., *Screaton et al*., 2009].

In the Kumano forearc basin, more than a dozen of MVs evolved with basal diameters of up to 2 km [*Kopf*, 2002; *Kuramoto et al*., 2001; *Morita et al*., 2004] (Figure 1a). Typically, they form conically shaped domes indicative for a relatively low viscosity of the expelled mud with several MVs protruding >100 m into the water column. Clasts ejected from the MVs are predominantly Late early Miocene to Early middle Miocene in age [*Morita et al*., 2004].

Seismic studies show that the MVs are situated above anticlines [*Morita et al*., 2004]. Also, most bottom-simulating seismic reflectors indicative for the presence of hydrates and free gas were associated with buried anticlines in our study area [*Baba and Yamada*, 2004]. Seismic studies, seafloor observations, as well as sedimentological and microbial investigations suggested different and varying dynamics of the individual MVs [*Kuramoto et al*., 2001; *Morita et al*., 2004]. For instance, enrichments in dissolved methane above MV 5 in 2004 were attributed to methane release into the water column [*Tsunogai et al*., 2012]. Indications for elevated methane concentrations in shallow sediments and/or methane seepage from the summit area were also reported for MV 8 in 2006 [*Miyazaki et al*., 2009].

3. Material and Methods

Twelve MVs in the Kumano forearc basin (Figures 1 and 2 and supporting information Table 1) were inspected in summer 2012 by means of hydroacoustic surveys, visual seafloor inspections and groundtruthing [*Kopf et al*., 2013]. For methodological details see supporting information.

3.1. Seafloor Inspection, Sampling, and Sample Preparation

Bathymetric mapping was conducted with the hull-mounted Kongsberg EM120 multibeam echosounder. A TV-grab was used for online seafloor inspection and sampling of near-surface sediments at MVs 2, 3, 4, and 10. Additional seafloor inspections and hydroacoustic bottom water investigations were carried out with the remotely operated vehicle (ROV) "QUEST4000m" (MARUM) equipped with a forward-looking sonar [*Nikolovska et al*., 2008] at MVs 3 and 4.

In total, 34 nonpressurized gravity cores of shallow sediments from 12 MVs were investigated (supporting information Table 1). Hydrate-bound gas was prepared from hydrate pieces [*Pape et al*., 2010a] and transferred into glass serum vials prefilled with saturated NaCl solution for storage until analysis. For vertical profiling of methane concentrations in gravity cores, a modified headspace technique [*Kvenvolden and McDonald*, 1986] was used. Three milliliter of sediment were taken with cut-off syringes immediately after core recovery, when concentrations of light hydrocarbons have still not equilibrated to atmospheric

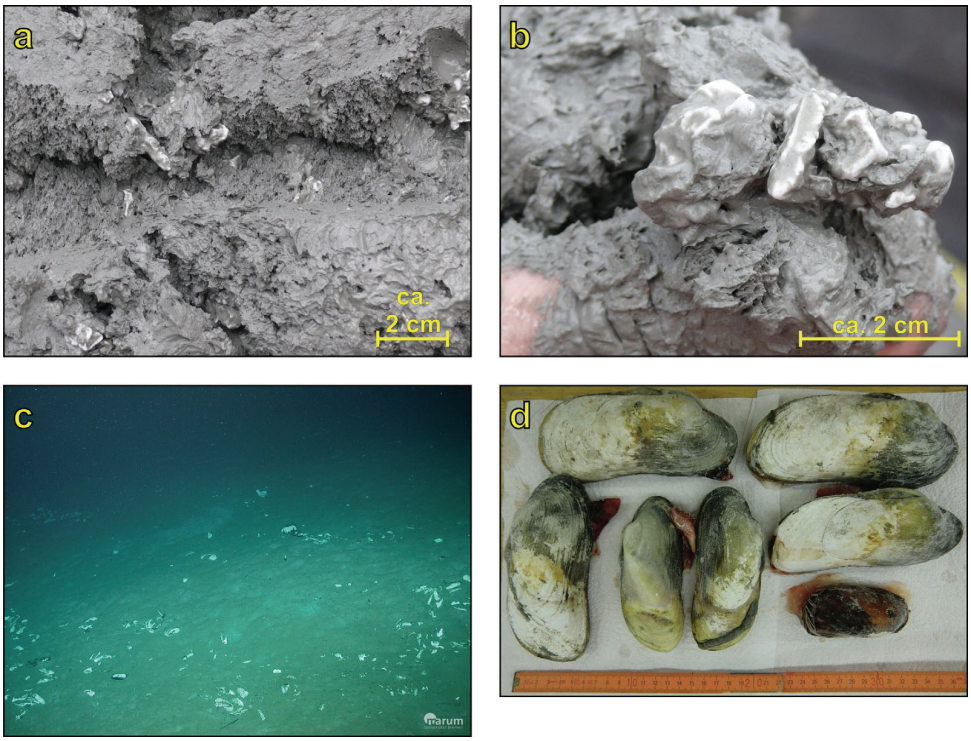

Figure 2. (a and b) Disseminated, millimeter-sized gas hydrate specimen in homogenous sediments (mud breccia) retrieved from MV 2. (c) Seafloor picture showing clam shells tentatively assigned to the genus Calyptogena at MV 3 taken during ROV dive 321 (GeoB16767-1). (d) Picture of live clams sampled from MV 2 during station TVG-5 (GeoB16793-1).

pressure, at defined depths and transferred into 20 mL glass vials prefilled with 5 mL of 1 M NaOH. The samples were stored at $+4^{\circ}$C until analysis onshore.

3.2. Analytical Methods

Gas samples were analyzed for their molecular compositions and methane concentrations by gas chromatography (GC) [*Pape et al.*, 2010a]. Stable carbon isotope ratios ($^{13}C/^{12}C$) of CH_4 in hydrate-bound gas and in lowermost headspace samples were determined by GC-isotope ratio mass spectrometry (GC-IRMS). Carbon isotopic ratios are reported in δ-notation in parts permil (‰) relative to the Vienna PeeDee Belemnite (V-PDB).

4. Results

4.1. Sediments and Associated Gas Hydrates

For all gravity core stations conducted at MVs, a penetration $<$6 m (Figure 3) indicated the presence of relatively hard substrate such as mud clasts, stiff sediments, and/or gas hydrates. The main lithologies detected were mud breccia with mudstone, siltstone, and sandstone clasts and background sediment, including shell fragments, nannofossils and microfossils. The background sediment had intercalations of layers with varying grain size, which, due to their fining upward behavior, were interpreted as turbidites. Background sediment overlying the mud breccia at the investigated MVs remained undetected, indicating their (sub-)recent activity. Several gas escape structures (e.g. voids, perforated appearance) and smell of H_2S indicated gas enrichments. In places, the mud breccia had regular gas voids, giving the entire lithology a mousse-like texture. The majority of the clasts were mudstones, most likely derived from within the old accreted sediments underlying the basin fill.

Hydrates were sampled in multiple gravity cores recovered from MVs 2, and 4, and in single cores each from MVs 5 and 10 (Figures 1 and 2 and Table 1). They were present in cores from the summit areas and in

cores GeoB16772-1 and 16722-2 that were taken from the slopes of MVs 2 and 4, respectively. In all cores, hydrates occurred below about 0.5 mbsf as disseminated specimen less than ca. 1 cm in diameter (Figures 2a and 2b).

Gases prepared from hydrates recovered from MVs 2, 4, and 10 were strongly dominated by methane ($CH_4 \geq 92.787$ mol% $\Sigma(C_1$ to n-$C_4 + CO_2)$; Table 1), followed by CO_2 (3.837–4.509 mol%) and C_2H_6 ($\leq$2.725 mol%). Higher hydrocarbons occurred in much smaller portions or were below detection limit (ca. 2 ppm). For all hydrate pieces, δ^{13}C-values of hydrate-bound methane were $\geq -40.5‰$ V-PDB.

4.2. Vertical Distributions and Stable Carbon Isotope Ratios of Dissolved Methane

Vertical ex situ concentration profiles of methane dissolved in pore waters of shallow sediments recovered from the summit areas and partially from the slopes were established for all MVs investigated (Figure 3). These profiles signify considerable methane enrichments with the top of the methane-bearing sediment interval ("methane zone") being situated shallower than ca. 350 cm below seafloor (cmbsf) in central areas of several MVs (Table 2). The shallowest sulfate-methane interface (SMI) was found for a core from MV 5 (ca. 15 cmbsf), which also showed highest ex situ concentrations of dissolved methane (ca. 35 mmol L^{-1} at 230 cmbsf). This was followed by cores from MVs 2, 4, and 13. As exemplified for MVs 3 and 4 (Figure 3), methane concentrations decreased significantly with increasing distance to the summit and the SMI could not be penetrated at the edges of the MVs. At stations positioned at the slopes of certain MVs (e.g., 3, 4, 5, and 8) concentrations were at least one order of magnitude higher compared to those measured at station GeoB16763-1 in the NE part of the study area (Figure 1a), where background samples ($<$1.0 μmol L^{-1} throughout the core) were taken. Methane was virtually absent in cores from MVs 6 and 7.

Stable carbon isotope ratios of dissolved methane in lowermost headspace samples varied from $-59.0‰$ (MV 10) to $-29.3‰$ (MV 2; Figure 3). Differences in stable carbon isotope signatures ($\Delta\delta^{13}$C) between dissolved methane in lowermost samples and of hydrate-bound methane ranged between $-1.7‰$ and $+3.3‰$ (Table 1). For cores from MVs 2 and 5 relative enrichments in ^{13}C with decreasing depth were observed for dissolved methane, while for cores from MVs 4 and 10 depletions in ^{13}C were found for shallower samples.

4.3. Water Column and Seafloor Characteristics

During SO222 hydroacoustic anomalies in the water column ("gas flares") diagnostic for gas bubble release from the seafloor were not observed above the MVs using the hull-mounted ATLAS Hydrographic PARASOUND sediment echosounder P70 [*Kopf et al*., 2013]. During the five TV-grab surveys and two ROV dives at MVs 2, 3, 4, and 10, gas bubble emissions were neither observed visually nor detected with the ROV-mounted sonar. During the ROV dive at MV 3 relative bottom water temperature elevations by up to ca. 1.75°C indicative for heat flow through MV activity, were recorded. Dense microbial mats, usually observed at active hydrocarbon-seeps, became not obvious. However, shells of clams inferred to belong to the genus Calyptogena (Vesicomyidae) and thought to indicate H_2S enrichments in the immediate subsurface [*Sahling et al*., 2002] were sporadically observed on the seafloor at the summit areas of MVs 2, 3, 4, and 10 (e.g., Figure 2c). On the summit of MV 2 live Calyptogena clams were sticking in the sediment in places (Figure 2d).

5. Discussion

5.1. Origin of Volatiles

Although molecular and isotopic compositions of gases might be altered during migration through the sediment and incorporation into gas hydrates, hydrates provide information on sources of hydrocarbons formed at greater depth [e.g., *Hachikubo et al*., 2007; *Pape et al*., 2010a; *Sassen et al*., 1999]. Relatively low C_1/C_2 ratios of hydrate-bound hydrocarbons ranging between 35 and 254 and δ^{13}C-CH_4-values $>-40‰$ V-PDB (Table 1) substantiate that light hydrocarbons expelled from MVs 2, 4, and 10 are predominantly generated by thermal cracking of type II kerogen, which typically originates from marine organic matter (Figure 4). In contrast, a significantly higher C_1/C_2 ratio of approx. 1630 determined for hydrocarbons bound in the single hydrate piece recovered from MV 5 may be explained by microbial production as additional hydrocarbon source and/or preferred incorporation of methane into the hydrate phase. A microbial hydrocarbon source would be consistent with stronger enrichments in ^{12}C (δ^{13}C $-52.0 \pm 2‰$) determined for dissolved methane in shallow pore waters at the center of MV 5 in 2000/2001 [*Tsunogai et al*., 2012]. By contrast,

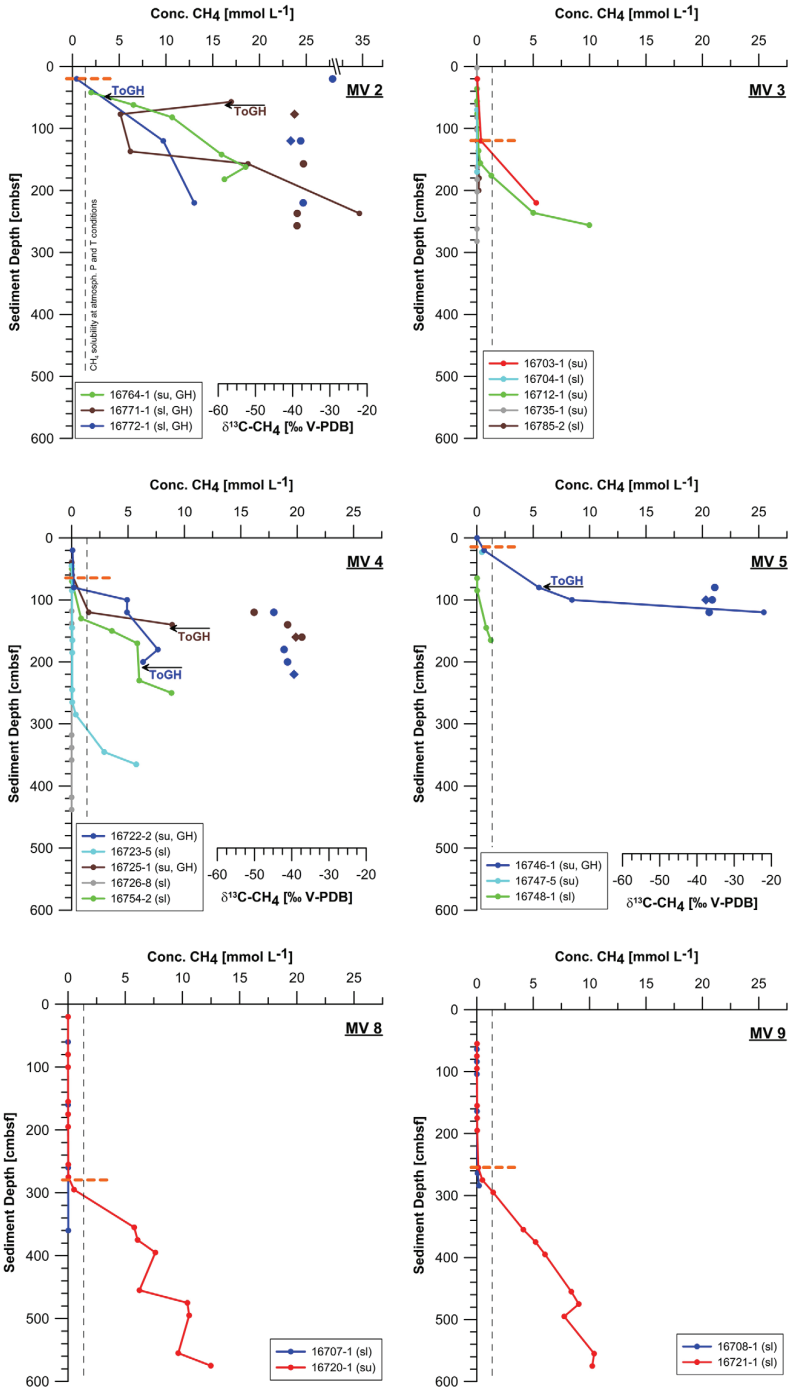

Figure 3. Vertical concentration profiles of methane dissolved in pore waters (solid line and filled circles) recovered from the MVs. Numbers in legends indicate GeoB core codes. Gas hydrate presence ("GH") in cores from MVs 2, 4, 5, and 10 as well as positions of cores at the summit ("su") or slope ("sl") of individual MVs are indicated (except for MVs 11 and12). For cores from MVs 2, 4, 5, and 10, δ^{13}C-values of dissolved methane (filled circles) and of hydrate-bound methane (filled diamonds) are added. The dashed horizontal orange-colored lines indicate the shallowest top of the methane zone observed at an individual MV during cruise SO222. Because of rapid sample preparation upon core recovery on ship's deck, methane concentrations in deeper core sections still exceeded methane solubility under atmospheric pressure (ca. 1.35 mmol L^{-1}, dashed vertical line) [*Duan and Mao*, 2006]. Irregularly shaped methane concentration profiles in the bottom parts of some cores, as observed for example, at MVs 4, 11, and 13 are, therefore, due to inhomogenous degassing at atmospheric pressure and/or dissociation of hydrate pieces. In situ methane solubility under presence of a sI hydrate phase would be ca. 55.5 mmol L^{-1} (at 1.7°C and 30 PSU salinity) [*Kopf et al.*, 2013].

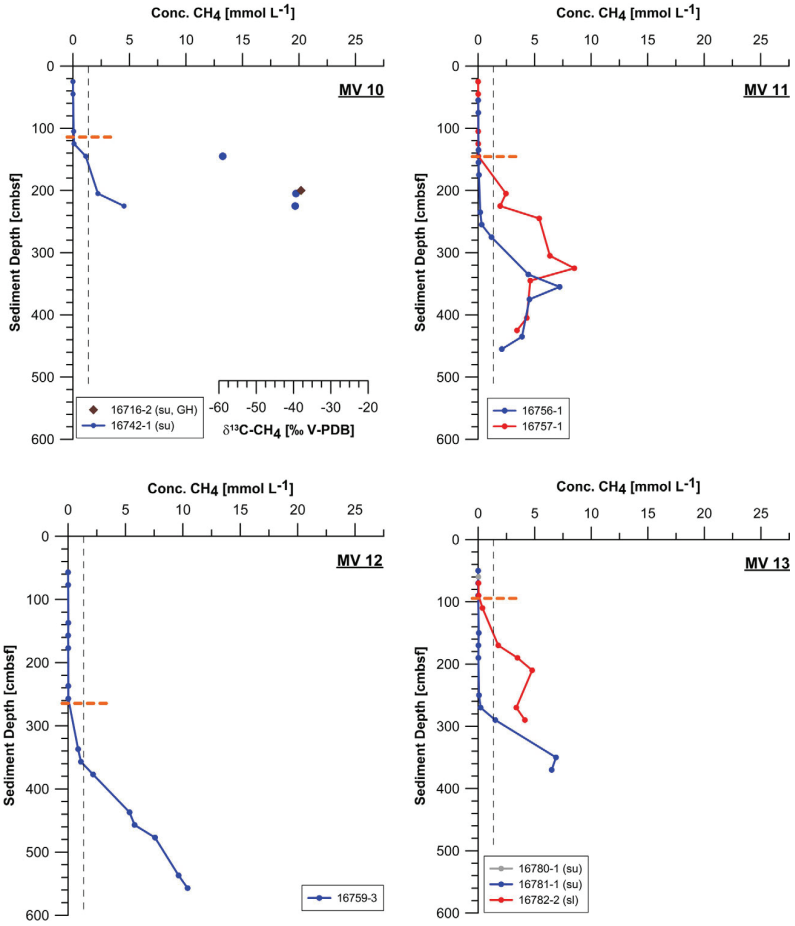

Figure 3. (Continued)

preferential incorporation of methane into hydrates [*Pape et al*., 2010a] causing the comparably high C_1/C_2 ratios would be plausible with respect to the similarities in δ^{13}C-CH_4-values (Table 1 and Figure 4) for all MVs investigated.

Thermogenic gases are typically characterized by relative high proportions of C_{3+} hydrocarbons [*Claypool and Kvenvolden*, 1983; *Sassen et al*., 1999], which in our study were only found in detectable amounts at MVs 4 and 10 (Table 1). In previous studies, depletions of hydrate-bound gases in C_{3+} hydrocarbons relative to the source gas were attributed to selective removal during migration or to size exclusion during hydrate precipitation [*James and Burns*, 1984; *Pape et al*., 2010a; *Sassen et al*., 2000]. With respect to the comparably low C_1/C_2 ratios and the likely formation of sII hydrates at least at MV 10 (chapter 5.2) that would allow for incorporation of C_{3+} hydrocarbons [*Sloan and Koh*, 2007], we assume higher amounts in the source gas, which have been depleted during migration. However, as migrated gas was not analyzed in this study, the specific effects of processes having led to potential removal of C_{3+} hydrocarbons are undetermined yet.

Whereas microbial light hydrocarbons are believed to be formed at temperatures below about 90°C [*Orphan et al*., 2000], formation of thermogenic hydrocarbons peaks in the 100–150°C range [*Claypool and Kvenvolden*, 1983; *Selley*, 1998; *Seewald, 2003*]. Analysis of in situ temperatures in shallow sediments at MVs 2, 3, 4, 9, 10, and 13 concurrent to our present study revealed slightly elevated temperature gradients compared to background values in shallow sediments only at the centers of MV 2 (max. 0.29°C m^{-1}) and MV 3 (max. 0.12°C m^{-1}) [*Kopf et al*., 2013]. Therefore, the temperature gradients determined at IODP Holes C0009 (approx. 0.035°C m^{-1}) [*Saffer et al*., 2010] and C0002 (ca. 0.043°C m^{-1}) [*Kinoshita et al*., 2009; *Harris et al*., 2011], which are located close to our study area, were used for a depth estimate of the hydrocarbon source

Table 1. Distributions of Light Hydrocarbons and CO_2 (in mol% $\sum$[C_1 to n-C_4 + CO_2]), C_1/C_2 Ratios, and Stable C Isotope Signatures of CH_4 (in ‰ V-PDB) in Hydrate-Bound Gas (Hyd.) and Dissolved Gas (Diss.)[a]

GeoB	C_1	C_2	C_3	i-C_4	C_4 n. Ident.	CO_2	n	C_1/C_2	δ^{13}C-CH_4 (Hyd.)	δ^{13}C-CH_4 (Diss.)[a]	$\Delta\delta^{13}$C (CH_4 Hyd.-Diss.)
MV #2											
16764-1	95.4837	0.4230	tr.	tr.	tr.	3.9944	*1*	226			
16771-1	95.3569	0.6120	tr.	tr.	tr.	3.9336	*2*	156	−39.5	−38.8	−0.7
16772-1	95.4521	0.5860	tr.	tr.	tr.	3.8649	*2*	163	−40.5	−37.2	−3.3
16788-1	95.5311	0.4318	tr.	tr.	tr.	3.9408	*2*	221	−39.7		
16788-2	95.5640	0.4854	tr.	tr.	tr.	3.8534	*2*	197	−39.9		
Average	95.4776	0.5076	tr.	tr.	tr.	3.9174		188	−39.9		
MV #4											
16722-2	92.7873	2.7252	tr.	tr.	tr.	4.3911	*2*	34	−39.4	−41.1	+1.7
16725-1	93.7949	1.7243	tr.	tr.	tr.	4.3817	*2*	54	−38.9	−37.3	−1.6
16736-1	94.0164	1.3663	0.0412	tr.	tr.	4.5087	*4*	69	−39.3		
Average	93.5329	1.9386	tr.	tr.	tr.	4.4275		48	−39.2		
MV #5											
16746-1	95.9588	0.1065	tr.	tr.	tr.	3.8371	*6*	901	−37.6	−36.7	−0.9
MV #10											
16716-2	94.7519	0.8170	0.4285	0.1107	tr.	3.8565	*7*	116	−38.0	−39.6	+1.6

[a]Values of δ^{13}C-CH_4 (diss.) are given for lowermost sample in profile. n = number of samples analyzed for molecular composition (mean value); tr. = trace (≤0.04 mol%).

Table 2. Depths of the SMI and Gas Hydrate Occurrences at Individual MVs

MV #	No. of Cores Retrieved From Summit Area	Estimated Depth of SMI at Summit [cmbsf]	Gas Hydrates/Top of Gas Hydrates
2	3	20	Gas hydrates/ca. 50 cmbsf
4	2	65	Gas hydrates/ca. 145 cmbsf
5	1	15	Gas hydrates/ca. 75 cmbsf
10	1	115	Gas hydrates/n. doc.
3	2	120	
8	1	280	
11	n. assign.	145 (?)	
12	n. assign.	265 (?)	
13	2	95	

n. doc. = not documented; n. assign. = not assigned.

rocks fueling the MVs. Assuming that the gradient follows a linear trend with depth, temperatures required to induce thermogenic hydrocarbon formation likely occur at depths between about 2300 mbsf (100°C, 43°C km^{-1}) and 4300 mbsf (150°C, 35°C km^{-1}). The higher C_1/C_2 ratio observed for hydrate-bound hydrocarbons at MV 5 compared to those from MVs 2, 4, and 10 might be explained by additional microbial hydrocarbon generation in the upper 2100–2600 mbsf.

The minimum formation depths calculated here for light hydrocarbons expelled from MVs 2, 4, and 10 imply that the fluids are mainly generated below the ca. max. 2 km thick Pliocene to recent basin sediments [*Hayman et al.*, 2012; *Tobin and Kinoshita*, 2006]. Consequently, the MVs should root either in the old accretionary wedge or even deeper. This assumption is corroborated by the exclusive occurrence of thermogenic hydrocarbons (as interpreted from C_1/C_{2+} ratios) in accreted sediments (Sites C0002, 1176, 1178), hemipelagic sediments (Site 808), and the oceanic basement (Sites C0011, C0012, 1173, 1174) drilled within the frame of ODP

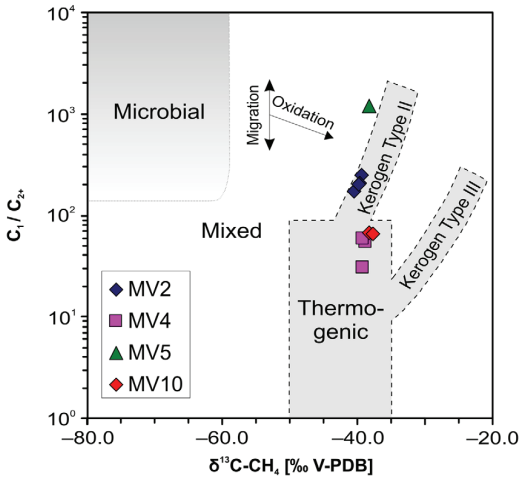

Figure 4. "Bernard diagram" modified after *Whiticar* [1990] showing δ^{13}C-values of methane versus molecular hydrocarbon ratios in hydrate-bound gas at MVs 2, 4, 5, and 10 and inferred hydrocarbon sources.

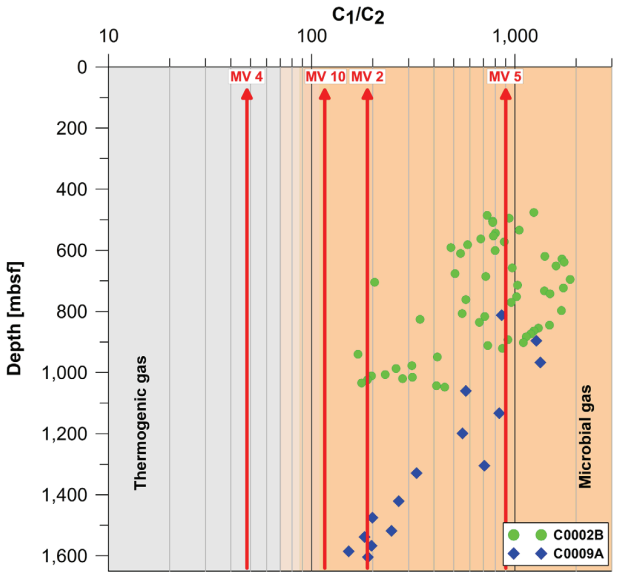

Figure 5. Depth profiles of C_1/C_2 ratios in headspace samples from IODP Holes C0002B and C0002D (green circles) [*Tobin and Kinoshita*, 2006] and in drilling cuttings from Hole C0009A (blue diamonds) [*Saffer et al.*, 2010]. C_1/C_2 ratios of hydrate-bound hydrocarbons at MVs 2, 4, 5, and 10 (red vertical lines) are shown for comparison.

and IODP campaigns off the Kii Peninsula and off Cape Muroto, respectively (Figures 1b and 5) [*Hill et al.*, 1993; *Mikada et al.*, 2005]. Moreover, recent drilling mud gas monitoring at Hole C0002F revealed a prevalence of thermogenic hydrocarbons below approx. 1700 mbsf with δ^{13}C-$CH_4 \geq -60‰$ and C_1/C_{2+} ratios ranging between 300 and 400 [*Moore et al.*, 2013]. In contrast, at Hole C0009A that is positioned close to the MVs studied herein (Figure 5) and likely was drilled through the forearc basin sediments into the top of the old accretionary prism (total depth ca. 1600 mbsf), a predominance of microbial hydrocarbons (C_1/C_{2+} ratios >100) was found at all depths investigated [*Saffer et al.*, 2010].

In our study area, the plate boundary thrust dips from about 10 km depth (SE edge) to >20 km depth (NW edge) and thermal modeling revealed temperatures between about 150 and 350°C at respective depths [*Marcaillou et al.*, 2012; *Moore and Saffer*, 2001]. With respect to (i) temperatures at the interplate boundary, (ii) the distance between its top and the seafloor, and (iii) the assumed preferential nonvertical transport of fluids generated at the interplate boundary via OOSSs to more seaward sites, it appears most probable that hydrocarbons mobilized during MV activity are derived from the old accreted sediments overlying the seismogenic zone (Figure 6). A supportive conclusion was drawn by *Moore and Saffer* [2001] who proposed that the fluid production potential is vastly reduced at burial depths exceeding about 4000 mbsf. With respect to age assignments for the top of the old accreted sediments at Sites C0002 and C0009 fluid source rocks must be older than Late Miocene age [*Kinoshita et al.*, 2009; *McNeill et al.*, 2010; *Saffer et al.*, 2010]. Although age models are apparently not available for the old accreted sediments, source rocks might be related to the Cretaceous to Tertiary Shimanto Belt [*Taira et al.*, 1992].

5.2. Gas Hydrates and Their Physical State

Gas hydrates in general and specifically those associated to MVs are a dynamic methane reservoir [*Dickens*, 2003; *Feseker et al.*, 2009]. The top of hydrates and also the top of the methane zone in MV deposits usually deepens with increasing distance to the MV conduit [*Castellini et al.*, 2006; *Egorov et al.*, 1999; *Pape et al.*, 2011b]. The presence of gas hydrates at MVs 2, 4, 5, and 10 (Table 2) demonstrates that upward methane flux was sufficient to induce hydrate formation at depths shallower than 1.5 mbsf in the recent past. However, in contrast to the massive, centimeter sized and sometimes porous hydrates frequently collected at intense gas emission sites [*Pape et al.*, 2011a; *Sassen et al.*, 1999; *Suess et al.*, 1999; *Torres et al.*, 2004], hydrate chips recovered from the Kumano basin MVs were dispersed and relatively small in size (Figures 2a and 2b). This, along with the virtual lack of free gas emissions (i.e., the absence of gas flares during hydroacoustic surveys), suggests that hydrate formation is not ongoing at present and that the hydrates found are subject to decomposition.

It is known that warm (>20°C) fluids can be injected into near-surface deposits and induce thermal hydrate dissociation in case the hydrate dissociation temperature is surpassed [*Feseker et al.*, 2009; *Pape et al.*, 2011b; *Römer et al.*, 2012]. Because of the differences in the stability conditions between both crystallographic hydrate structures widespread in nature (sI and sII), the hydrate crystal structure has to be known for calculating actual hydrate dissociation temperatures. However, analysis of hydrate crystal structures has

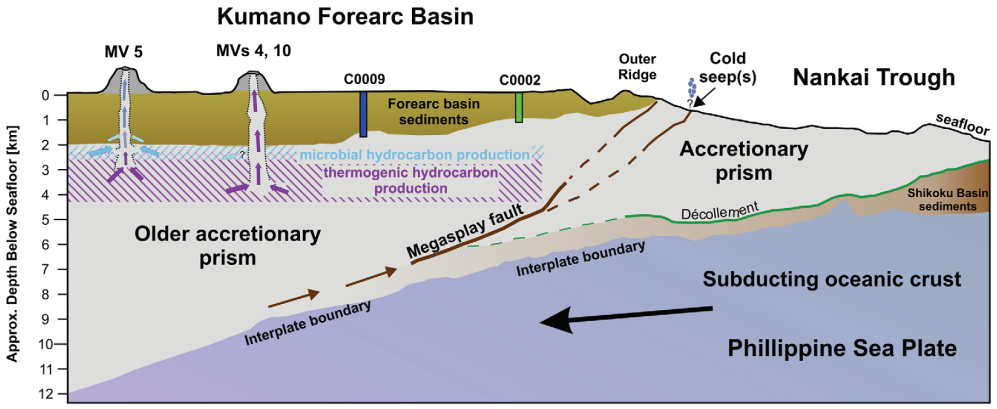

Figure 6. Sketch illustrating origins and migration pathways of fluids in the Nankai Trough subduction zone [adapted from *Park et al.*, 2002; *Saffer et al.*, 2010; *Strasser et al.*, 2009; *Toki et al.*, 2004]. Hydrocarbons expelled from MVs in the Kumano forearc basin originate from older accreted sediments below the forearc basin, whereas fluids generated at the interplate boundary are most likely transported along faults to seepage sites at the outer ridge. Note: Positions of MVs 5, 4, and 10 displayed as examples relative to IODP Sites C0009 and C0002 only. Horizontal distances not for scale.

not been conducted for hydrates recovered during cruise SO222, so far. The virtual absence of hydrocarbons $>C_3$ in hydrates recovered from MVs 2, 4, and 5 suggests that sI is the dominant hydrate phase at these sites. In contrast, a prevalence of sII hydrates at MV 10 might be inferred from the presence of C_3 and C_4-isomers. Calculations of phase boundaries substantiate that both, sI and sII hydrates, would in principle be stable at the MVs in the Kumano basin investigated (Figure 7) and would start to decompose when sediment temperatures exceed ca. 16.7–17.6°C. During the time of investigation both, bottom water temperatures (ca. 1.7–2.1°C, Figure 7) and in situ temperatures in shallow sediments at MVs 2, 3, 4, 5, 10, and 13 [*Kopf et al.*, 2013], were lower than the calculated hydrate dissociation temperatures of sI and sII hydrates. Exceptions were MVs 2 and 3 where sediment geothermal gradients were raised significantly above the background level and ranged between 0.03 and 0.06°C m^{-1}. The bottom water temperatures measured matched those reported by *Kinoshita et al.* [2011] and annual temperature variations <0.2°C were stated for a time period of about 900 days [*Hamamoto et al.*, 2011]. Therefore, the assumed hydrate decay at MVs lacking elevated temperatures in uppermost sediments is likely caused by dissolution due to pore water methane undersaturation resulting from currently insufficient methane supply rather than by thermal dissociation. This might be supported by the presence of similar looking hydrates on the slopes of MVs 2 (cores GeoB16771-1 and GeoB16772-1) and 4 (GeoB16722-2) where the impact of heat impulses from below should be comparably low.

Moreover, the stable carbon isotope signatures of hydrate-bound and dissolved methane at similar depth varied only slightly ($\Delta\delta^{13}$C between $-1.7‰$ and $+3.3‰$, Table 1). In theory, matching $^{13}C/^{12}C$ ratios of hydrate-bound methane and of methane dissolved in the immediate pore waters should either be found (i) during phases of high MV activity, when methane concentrations in the pore water exceed solubility and hydrates form, or (ii) during phases of low fluid flux from below, when hydrates decompose and substantial methane amounts are released. Considering our various observations (lack of seafloor gas emissions, sparse seafloor settlement by chemosynthesis-based organisms, dispersed state of hydrates recovered), we propose that similar δ^{13}C-values of hydrate-bound methane and dissolved methane determined for our samples result from current hydrate dissolution.

Considering the magnitude of dissolution rates (0.5–30 mm yr^{-1}) calculated for buried hydrates surrounded by methane-undersaturated pore water [*Lapham et al.*, 2010], we propose that hydrate dissolution at MVs 2, 4, 5, and 10 was already ongoing for several months at least at the time of our investigation. Very low methane concentrations (<1 μmol L^{-1}) in the uppermost sediments demonstrate that methane released during hydrate decomposition is effectively consumed by AOM [*Hoehler et al.*, 1994; *Miyazaki et al.*, 2009] in overlying sediments (Figure 3). As exemplified for MV 10, where hydrates were found at shallow depth, methane concentrations at the seafloor are consequently too low to enable significant chemosynthesis-based benthic life at the time of sampling.

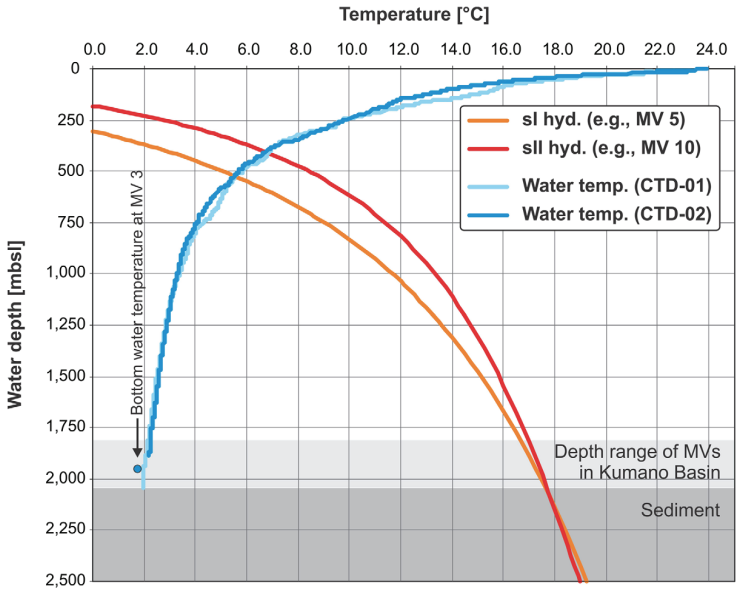

Figure 7. Phase boundaries calculated for MV-associated gas hydrates in the Kumano basin using the HWHYD U.K. software [*Masoudi and Tohidi*, 2005], molecular compositions of hydrate-bound gases determined for MV 5 and MV 10 (Table 1), and bottom water salinities of 34.59 PSU (CTD-02, GeoB16779-1 at 2,070 m below sealevel). Those MVs were selected because different hydrate crystal structures were inferred from gas compositions. Calculated dissociation pressures at individual temperatures were converted into actual water depths considering algorithms given in the UNESCO Technical Paper in Marine Science No. 44 [*Fofonoff and Millard*, 1983]. Water temperatures were determined at stations CTD-01 (GeoB16701-1) ca. 4.4 km W of MV 9 and CTD-02 above MV 4. Bottom water temperatures at MV 3 were recorded during ROV dive GeoB16767-1.

5.3. Current Activities of Individual MVs

Active submarine mud volcanism is usually accompanied by flow of heat and fluids into shallow sediments and potentially also into bottom waters. In general, an increase in methane concentration with increasing depth along with the top of the methane zone being positioned in the upper few meters is a significant feature of (sub-)recent hydrocarbon seepage activity [e.g., *Bhatnagar et al*., 2011; *Borowski et al*., 1996; *Castellini et al*., 2006; *Coffin et al*., 2008; *Wallmann et al*., 2006]. In contrast, the SMI at nonseep sites is typically positioned at several tens of meters depth. In previous studies, methane enrichments detected above MV 5 in 2004 were suggested to be caused by earthquake-induced mud volcanic activity [*Tsunogai et al*., 2012] and relatively high heat fluxes were measured at MV 8 [*Hamamoto et al*., 2011].

Although we only achieved an incomplete water column and seafloor coverage during hydroacoustic surveys and seafloor inspections in this study, it seemed that emissions of significant amounts of free, bubble-forming methane from the MVs into the hydrosphere did not occur during our time of investigation. Support for this assumption comes from the relatively moderate to low fluxes of MV-associated fluids in shallow sediments as indicated by the virtual absence of dense microbial mats (e.g., *Beggiatoa* sp.), the sparse distribution of chemosynthesis-based clams, and the SMI being positioned deeper than approx. 1 m in most cores investigated (Figure 3).

However, the discovery of assemblages of living Calyptogena individuals substantiates that at the summit area of MV 2 (Figure 2d) fluids are present in amounts sufficient to nourish chemosynthesis-based macrofauna [e.g., *Paull et al*., 1995; *Sahling et al*., 2002]. Furthermore, the presence of Calyptogena shells at the summits of MVs 3 and 10 and accumulations of hydrates at MVs 2, 4, 5, and 10 signify that high methane concentrations must have existed in the recent past. In conclusion, compared to gas fluxes observed at MVs in other regions, where virulent gas emission from the seafloor was observed [e.g., *Greinert et al*., 2006; *Sahling et al*., 2009; *Sauter et al*., 2006], the Kumano basin MVs appear to be in comparably low-activity or even dormant phases at present.

Comparison of dissolved methane concentration profiles from the summit areas and slopes of individual MVs (Figure 3) demonstrates that, similar to MVs in other regions, methane is principally provided through one or few conduits situated in the geographic center of the MV structure [*Dimitrov*, 2002; *Kopf*, 2002; *Pape*

et al., 2011b]. The depth of the SMI may spatially vary across the MV summit since for instance it is controlled by the number and capacity of fluid migration pathways, the thickness of mud deposited on top of the sediments during recent MV eruptions and the time elapsed since MV activities. Nevertheless, different depths of the SMI and shapes of methane concentration profiles along with the occurrence of shallow hydrates restricted to some MVs suggest that the structures investigated differ in their intensity of methane flux from below.

In this study, at least one gravity core was retrieved from the summit area of most of the investigated MVs (supporting information Table 1). Methane concentration profiles of these cores were used for rough assignments of relative methane flux intensities (Table 2). The SMI was generally situated above ca. 3.5 m at most MVs studied except for MVs 6 and 7. This indicates that methane upward flux was still sufficient to hamper seawater-derived sulfate to penetrate deeper into the sediments at most MVs. The very shallow SMI ($<$1 mbsf) and highest concentrations of dissolved methane on the summits of MVs 2, 4, and 5 (Table 2) correspond to the findings of hydrate pieces at those MVs. In contrast, the fluid flux providing concentrations of dissolved methane <10 μmol L^{-1} at the summits of MVs 6 and 7 was too low to induce hydrate formation in the recent past. Because of the virtual lack of bubble emissions it seems unlikely that a great portion of methane in the uppermost sediments was derived from gas migration through the GHSZ. Due to efficient AOM, methane concentrations in the immediate subsurface might be, at present, too low to sustain settlement by chemosynthesis-based organisms. Our classification of methane flux intensities in shallow sediments generally agrees with previous interpretations of MV activities at MVs 3, 4, 5, and 6 [*Kuramoto et al*., 2001; *Morita et al*., 2004; *Tsunogai et al*., 2012], but differs from observations at MV 8 where at its edge regions living Calyptogena colonies were observed in 2006 [*Miyazaki et al*., 2009] and steep thermal gradients were reported in 2011 [*Hamamoto et al*., 2011]. Based on our results, it appears that currently highest methane fluxes occur at MVs 2, 3, 4, 5, 10, and 13 located in the northern Kumano basin.

The geological causes for varying methane fluxes at the individual MVs remains subject to future studies. Remarkably, subduction-related earthquakes are frequent in the region investigated [*Ito and Obara*, 2006; *Moore et al*., 2007; *Obana and Kodaira*, 2009; *Shelly et al*., 2006] and a coincidence of seismic events and hydrocarbon seepage activity has already been proposed for other regions, such as MVs in Azerbeijan [*Mellors et al*., 2007] and Indonesia [*Mazzini et al*., 2007], cold seeps off Pakistan [*Fischer et al*., 2013] and also for MV 5 in our study area [*Tsunogai et al*., 2012]. Therefore, it is tempting to assume that seismic activity below the old accreted sediments affects or even triggers the MV activity in the Kumano basin. Long-term borehole observatories partly installed with the seafloor drill rig MeBo [*Freudenthal and Wefer*, 2013; *Kopf et al*., 2013] at MVs 3 and 4 during cruise SO222 will give information about the relationship between seismic activity at the seismogenic zone and MV activity in the overlying older accretionary prism.

6. Conclusions

Twelve mud volcanoes (MVs) in the Kumano forearc basin close to the Nankai subduction zone off Japan were investigated with regard to origins and flux intensities of hydrocarbons expelled in 2012. These MVs are well located within the gas hydrate stability zone and disseminated hydrates were recovered from MVs 2, 4, 5, and 10.

For hydrates from MVs 2, 4, and 10, significant amounts of C_{2+} hydrocarbons (C_1/C_2 ratios as low as 35) along with enrichments in ^{13}C-CH_4 ($\delta^{13}C$-CH_4-values between $-39.9‰$ and $-37.6‰$ V-PDB) substantiate that upward migrating hydrocarbons are predominantly of thermogenic origin. Considering geothermal gradients established at the adjacent IODP Sites C0009 and C0002, thickness of basin sediments, and minimum depth of the plate boundary, those hydrocarbons are most probably generated in old accreted sediments between about 2300 and 4300 mbsf. Much higher C_1/C_2 ratios (ca. 900) of hydrate-bound hydrocarbons recovered from MV 5 hint to additional ascent of comparably methane-rich hydrocarbons potentially formed in the basin sediments overlying the accretionary prism. These results may help to elucidate the provenance of hydrocarbons expelled from mud volcanoes at other subduction zones worldwide.

For all MVs investigated, steepest gradients in methane concentrations and shallowest depths ($<$1 mbsf) of the sulfate-methane interface, indicating present methane ascent, were found at MVs 2, 4, 5, and 13. Larger accumulations of alive chemosynthetic organisms diagnostic for ongoing fluid flow from below were only found at MV 2, while randomly distributed clam shells were found at MVs 2, 3, 4, and 10. With respect to the virtual lack of free gas emissions at any of the MVs and the comparably small size of recovered hydrates

it is proposed that these are remnants of more intense MV activity in the past and subject to dissolution at present. Except for MVs 2 and 5, we consequently regard current MV activities in the Kumano basin as moderate to low if compared to former times or to fluid discharge intensities of submarine MVs in other regions.

Acknowledgments

We thank the captain and crew of R/V Sonne cruise SO222 Legs A and B for their excellent support. The support by the teams of the seafloor drill rig "MeBo" and the ROV QUEST 4000m (MARUM, University of Bremen) is gratefully acknowledged. M. Lange (MARUM) and others are thanked for their support during work on deck. We wish to thank E. Schefuss (MARUM) for the help with the stable isotope analysis of volatiles and T. Wiersberg (GFZ Potsdam, Germany) for providing gas data from Hole C0009A. This paper has benefited considerably from the constructive comments of U. Tsunogai (Hokkaido University), an anonymous reviewer and the editor L. A. Derry. This study was funded through BMBF Grant 03G0222A and through DFG-Research Center/Excellence Cluster "MARUM—The Ocean in the Earth System." All data reported are made publicly available through the PANGAEA information system sustained by the World Data Center for Marine Environmental Sciences (WDC-MARE).

References

Baba, K., and Y. Yamada (2004), BSRs and associated reflections as an indicator of gas hydrate and free gas accumulation: An example of accretionary prism and forearc basin system along the Nankai Trough, off Central Japan, *Resour. Geol.*, *54*(1), 11–24, doi:10.1111/j.1751-3928.2004.tb00183.x.

Barber, A. J., S. Tjokrosapoetro, and T. R. Charlton (1986), Mud volcanoes, shale diapirs, wrench faults, and melanges in accretionary complexes, Eastern Indonesia, *AAPG Bull.*, *70*(11), 1729–1741.

Bhatnagar, G., S. Chatterjee, W. G. Chapman, B. Dugan, G. R. Dickens, and G. J. Hirasaki (2011), Analytical theory relating the depth of the sulfate-methane transition to gas hydrate distribution and saturation, *Geochem. Geophys. Geosyst.*, *12*, Q03003, doi:10.1029/2010gc003397.

Bohrmann, G., et al. (2002), Widespread fluid expulsion along the seafloor of the Costa Rica convergent margin, *Terra Nova*, *14*, 69–79.

Bohrmann, G., et al. (2003), Mud volcanoes and gas hydrates in the Black Sea: New data from Dvurechenskii and Odessa mud volcanoes, *Geo Mar. Lett.*, *23*(3–4), 239–249, doi:10.1007/s00367-003-0157-7.

Borowski, W. S., C. K. Paull, and W. Ussler III (1996), Marine pore-water sulfate profiles indicate in situ methane flux from underlying gas hydrate, *Geology*, *24*(7), 655–658.

Camerlenghi, A., M. B. Cita, B. Della Vedova, N. Fusi, L. Mirabile, and G. Pellis (1995), Geophysical evidence of mud diapirism on the Mediterranean Ridge accretionary complex, *Mar. Geophys. Res.*, *17*, 115–141.

Castellini, D. G., G. R. Dickens, G. T. Snyder, and C. D. Ruppel (2006), Barium cycling in shallow sediment above active mud volcanoes in the Gulf of Mexico, *Chem. Geol.*, *226*, 1–30.

Claypool, G. E., and K. A. Kvenvolden (1983), Methane and other hydrocarbon gases in marine sediment, *Annu. Rev. Earth Planet. Sci.*, *11*(1), 299–327, doi:10.1146/annurev.ea.11.050183.001503.

Coffin, R., L. Hamdan, R. Plummer, J. Smith, J. Gardner, R. Hagen, and W. Wood (2008), Analysis of methane and sulfate flux in methane-charged sediments from the Mississippi Canyon, *Gulf of Mexico, Mar. Pet. Geol.*, *25*(9), 977–987, doi:10.1016/j.marpetgeo.2008.01.014.

Dickens, G. R. (2003), Rethinking the global carbon cycle with a large, dynamic and microbially mediated gas hydrate capacitor, *Earth. Planet. Sci. Lett.*, *213*(3–4), 169–183, doi:10.1016/S0012-821X(03)00325-X.

Dimitrov, L. I. (2002), Mud volcanoes: The most important pathway for degassing deeply buried sediments, *Earth Sci. Rev.*, *59*(1–4), 49–76.

Duan, Z., and S. Mao (2006), A thermodynamic model for calculating methane solubility, density and gas phase composition of methane-bearing aqueous fluids from 273 to 523 K and from 1 to 2000 bar, *Geochim. Cosmochim. Acta*, *70*(13), 3369–3386.

Egorov, A. V., K. Crane, P. R. Vogt, A. N. Rozhkov, and P. P. Shirshov (1999), Gas hydrates that outcrop on the sea floor: Stability models, *Geo Mar. Lett.*, *19*(1–2), 68–75.

Feseker, T., T. Pape, K. Wallmann, S. A. Klapp, F. Schmidt-Schierhorn, and G. Bohrmann (2009), The thermal structure of the Dvurechenskii mud volcano and its implications for gas hydrate stability and eruption dynamics, *Mar. Pet. Geol.*, *26*(9), 1812–1823, doi:10.1016/j.marpetgeo.2009.01.021.

Fischer, D., J. M. Mogollón, M. Strasser, T. Pape, G. Bohrmann, N. Fekete, V. Spiess, and S. Kasten (2013), Subduction zone earthquake as potential trigger of submarine hydrocarbon seepage, *Nat. Geosci.*, *6*(8), 647–651, doi:10.1038/ngeo1886.

Fofonoff, N. P., and R. C. Millard (1983), Algorithms for computation of fundamental properties of seawater. *UNESCO Technical paper in Marine Science, 44*.

Freudenthal, T., and G. Wefer (2013), Drilling cores on the sea floor with the remote-controlled sea-floor drilling rig MeBo, *Geosci. Instrum. Methods Data Syst. Discuss.*, *3*(2), 347–369, doi:10.5194/gid-3-347-2013.

Greinert, J., Y. Artemov, V. Egorov, M. De Batist, and D. McGinnis (2006), 1300-m-high rising bubbles from mud volcanoes at 2080 m in the Black Sea: Hydroacoustic characteristics and temporal variability, *Earth. Planet. Sci. Lett.*, *244*(1–2), 1–15, doi:10.1016/j.epsl.2006.02.011.

Gulick, S. P. S., N. L. B. Bangs, G. F. Moore, J. Ashi, K. M. Martin, D. S. Sawyer, H. J. Tobin, S. Kuramoto, and A. Taira (2010), Rapid forearc basin uplift and megasplay fault development from 3D seismic images of Nankai Margin off Kii Peninsula, *Japan*, Earth. Planet. Sci. Lett., *300*(1–2), 55–62, doi:10.1016/j.epsl.2010.09.034.

Hachikubo, A., T. Kosaka, M. Kida, A. Krylov, H. Sakagami, H. Minami, N. Takahashi, and H. Shoji (2007), Isotopic fractionation of methane and ethane hydrates between gas and hydrate phases, *Geophys. Res. Lett.*, *34*, L21502, doi:10.1029/2007GL030557.

Hamamoto, H., M. Yamano, S. Goto, M. Kinoshita, K. Fujino, and K. Wang (2011), Heat flow distribution and thermal structure of the Nankai subduction zone off the Kii Peninsula, *Geochem. Geophys. Geosyst.*, *12*, Q0AD20, doi:10.1029/2011gc003623.

Harris, R. N., F. Schmidt-Schierhorn, and G. Spinelli (2011), Heat flow along the NanTroSEIZE transect: Results from IODP Expeditions 315 and 316 offshore the Kii Peninsula, Japan, *Geochem. Geophys. Geosyst.*, *12*, Q0AD16, doi:10.1029/2011gc003593.

Hayman, N. W., T. B. Byrne, L. C. McNeill, K. Kanagawa, T. Kanamatsu, C. M. Browne, A. M. Schleicher, and G. J. Huftile (2012), Structural evolution of an inner accretionary wedge and forearc basin initiation, Nankai margin, Japan, *Earth. Planet. Sci. Lett.*, *353–354*, 163–172, doi:10.1016/j.epsl.2012.07.040.

Henry, P., T. Kanamatsu, K. Moe, and the Expedition 333 Scientists (2012), NanTroSEIZE Stage 2: Subduction Inputs 2 and Heat Flow, *Proc. Integrated Ocean Drill. Program*, *333*.

Hensen, C., M. Nuzzo, E. Hornibrook, L. M. Pinheiro, B. Bock, V. H. Magalhaes, and W. Bruckmann (2007), Sources of mud volcano fluids in the Gulf of Cadiz–indications for hydrothermal imprint, *Geochim. Cosmochim. Acta*, *71*(5), 1232–1248, doi:10.1016/j.gca.2006.11.022.

Hill, I. A., et al. (1993), *Proc. Ocean Drill. Program, Sci. Results.*, *131*.

Hoehler, T. M., M. J. Alperin, D. B. Albert, and C. S. Martens (1994), Field and laboratory studies of methane oxidation in an anoxic marine sediment: Evidence for a methanogen-sulfate reducer consortium, *Global Biogeochem. Cycles*, *8*(4), 451–463.

Ito, Y., and K. Obara (2006), Dynamic deformation of the accretionary prism excites very low frequency earthquakes, *Geophys. Res. Lett.*, *33*, L02311, doi:10.1029/2005gl025270.

James, A. T., and B. J. Burns (1984), Microbial alteration of subsurface natural gas accumulations, *AAPG Bull.*, *68*(8), 957–960.

Kinoshita, M., H. Tobin, J. Ashi, G. Kimura, S. Lallemant, E. J. Screaton, D. Curewitz, H. Masago, K. T. Moe, and the Expedition 314/315/316 Scientists (2009), NanTroSEIZE Stage 1: Investigations of seismogenesis, Nankai Trough, Japan, *Proc. Integrated Ocean Drill. Program*, *314/315/316*.

Kinoshita, M., G. F. Moore, and Y. N. Kido (2011), Heat flow estimated from BSR and IODP borehole data: Implication of recent uplift and erosion of the imbricate thrust zone in the Nankai Trough off Kumano, *Geochem. Geophys. Geosyst.*, *12*, Q0AD18, doi:10.1029/2011gc003609.

Kopf, A., E. Araki, S. Toczko, and the Expedition 332 Scientists (2011), NanTroSEIZE Stage 2: Riserless Observatory, *Proc. Integrated Ocean Drill. Program*, *332*.

Kopf, A., et al. (2013), Report and preliminary results of RV Sonne cruise SO222: MEMO—MeBo drilling and in situ long-term monitoring in the Nankai Trough accretionary complex, Japan. Berichte, MARUM—Zentrum für Marine Umweltwissenschaften, Fachbereich Geowissenschaften, Universität Bremen, 297, 121 pp.

Kopf, A. J. (1999), Fate of sediment during plate convergence at the Mediterranean Ridge accretionary complex: Volume balance of mud extrusion versus subduction and/or accretion, *Geology*, *27*, 87–90.

Kopf, A. J. (2002), Significance of mud volcanism, *Rev. Geophys.*, *40*(2), 1005, doi:10.1029/2000RG000093.

Kuramoto, S., et al. (2001), Surface observations of subduction related mud volcanoes and large thrust sheets in the Nankai subduction margin: Report on YK00-10 and YK01-04 cruises, *JAMSTEC J. Deep Sea Res.*, *19*, 131–139.

Kvenvolden, K. A., and T. J. McDonald (1986), Organic geochemistry on the Joides Resolution: An Assay, *Tech. Note 6*, 147 pp., Ocean Drill. Prog., Texas A&M Univ, College Station, Tex.

Lapham, L. L., J. P. Chanton, R. Chapman, and C. S. Martens (2010), Methane under-saturated fluids in deep-sea sediments: Implications for gas hydrate stability and rates of dissolution, *Earth. Planet. Sci. Lett.*, *298*(3–4), 275–285, doi:10.1016/j.epsl.2010.07.016.

Marcaillou, B., et al. (2012), Seismogenic zone temperatures and heat-flow anomalies in the To-nankai margin segment based on temperature data from IODP expedition 333 and thermal model, *Earth. Planet. Sci. Lett.*, *349–350*, 171–185, doi:10.1016/j.epsl.2012.06.048.

Masoudi, R., and B. Tohidi (2005), Estimating the hydrate stability zone in the presence of salts and/or organic inhibitors using water partial pressure, *J. Pet. Sci. Eng.*, *46*(1–2), 23–36, doi:10.1016/j.petrol.2004.10.002.

Mastalerz, V., G. J. de Lange, A. Dählmann, and T. Feseker (2007), Active venting at the Isis mud volcano, offshore Egypt: Origin and migration of hydrocarbons, *Chem. Geol.*, *246*(1–2), 87–106, doi:10.1016/j.chemgeo.2007.09.005.

Mazzini, A., H. Svensen, G. G. Akhmanov, G. Aloisi, S. Planke, A. Malthe-Sorenssen, and B. Istadi (2007), Triggering and dynamic evolution of the LUSI mud volcano, Indonesia, *Earth. Planet. Sci. Lett.*, *261*(3–4), 375–388, doi:10.1016/j.epsl.2007.07.001.

McNeill, L., D. Saffer, T. Byrne, E. Araki, S. Toczko, N. Eguchi, K. Takahashi, and IODP Expedition 319 Scientists (2010), IODP Expedition 319, NanTroSEIZE Stage 2: First IODP riser drilling operations and observatory installation towards understanding subduction zone seismogenesis, *Sci. Drill.*, *10*, 4–13.

Mellors, R., D. Kilb, A. Aliyev, A. Gasanov, and G. Yetirmishli (2007), Correlations between earthquakes and large mud volcano eruptions, *J. Geophys. Res.*, *112*, B04304, doi:10.1029/2006jb004489.

Mikada, H., G. F. Moore, A. Taira, K. Becker, J. C. Moore, and A. Klaus (2005), *Proc. Ocean Drill. Program, Sci. Results*, *190/196*.

Milkov, A. V. (2000), Worldwide distribution of submarine mud volcanoes and associated gas hydrates, *Mar. Geol.*, *167*(1–2), 29–42.

Miyazaki, J., R. Higa, T. Toki, J. Ashi, U. Tsunogai, T. Nunoura, H. Imachi, and K. Takai (2009), Molecular characterization of potential nitrogen fixation by anaerobic methane-oxidizing archaea in the methane seep sediments at the number 8 Kumano Knoll in the Kumano Basin, offshore of Japan, *Appl. Environ. Microbiol.*, *75*(22), 7153–7162, doi:10.1128/aem.01184-09.

Moore, G. F., et al. (2001), New insights into deformation and fluid flow processes in the Nankai Trough accretionary prism: Results of Ocean Drilling Program Leg 190, *Geochem. Geophys. Geosyst.*, *2*(10), 1058, doi:10.1029/2001gc000166.

Moore, G. F., N. L. Bangs, A. Taira, S. Kuramoto, E. Pangborn, and H. J. Tobin (2007), Three-dimensional splay fault geometry and implications for tsunami generation, *Science*, *318*(5853), 1128–1131, doi:10.1126/science.1147195.

Moore, G. F., K. Kanagawa, M. Strasser, B. Dugan, L. Maeda, S. Toczko, and the Expedition 338 Scientists (2013), NanTroSEIZE Stage 3: NanTroSEIZE plate boundary deep riser 2, *Prelim. Rep. Integrated Ocean Drill. Program*, *338*.

Moore, J. C., and D. Saffer (2001), Updip limit of the seismogenic zone beneath the accretionary prism of southwest Japan: An effect of diagenetic to low-grade metamorphic processes and increasing effective stress, *Geology*, *29*(2), 183–186, doi:10.1130/0091-7613(2001)029<0183:ulotsz>2.0.co;2.

Moore, J. C., and P. Vrolijk (1992), Fluids in accretionary prisms, *Rev. Geophys.*, *30*(2), 113–135, doi:10.1029/92rg00201.

Morita, S., J. Ashi, K. Aoike, and S. Kuramoto (2004), Evolution of Kumano basin and sources of clastic ejecta and pore fluid in Kumano mud volcanoes, Eastern Nanaki Trough, In: Proceedings of the International Symposium on Methane Hydrates and Fluid Flow in Upper Accretionary Prisms, Engineering Geology Laboratory, Department of Civil & Earth Resources Engineering, Kyoto University, Kyoto, pp. 92–99.

Nikolovska, A., H. Sahling, and G. Bohrmann (2008), Novel hydro-acoustic methodology for detection, localization and quantification of gas bubbles rising from the seafloor at gas seeps from the eastern Black Sea, *Geochem. Geophys. Geosyst.*, *9*, Q10010, doi:10.1029/2008GC002118.

Obana, K., and S. Kodaira (2009), Low-frequency tremors associated with reverse faults in a shallow accretionary prism, *Earth. Planet. Sci. Lett.*, *287*(1–2), 168–174, doi:10.1016/j.epsl.2009.08.005.

Orphan, V. J., L. T. Taylor, D. Hafenbradl, and E. F. Delong (2000), Culture-dependent and culture-independent characterization of microbial assemblages associated with high-temperature petroleum reservoirs, *Appl. Environ. Microbiol.*, *66*(2), 700–711.

Pape, T., A. Bahr, J. Rethemeyer, J. D. Kessler, H. Sahling, K. U. Hinrichs, S. A. Klapp, W. S. Reeburgh, and G. Bohrmann (2010a), Molecular and isotopic partitioning of low-molecular weight hydrocarbons during migration and gas hydrate precipitation in deposits of a high-flux seepage site, *Chem. Geol.*, *269*(3–4), 350–363, doi:10.1016/j.chemgeo.2009.10.009.

Pape, T., S. Kasten, M. Zabel, A. Bahr, F. Abegg, H.-J. Hohnberg, and G. Bohrmann (2010b), Gas hydrates in shallow deposits of the Amsterdam mud volcano, Anaximander Mountains, Northeastern Mediterranean Sea, *Geo Mar. Lett.*, *30*(3–4), 187–206, doi:10.1007/s00367-010-0197-8.

Pape, T., A. Bahr, S. A. Klapp, F. Abegg, and G. Bohrmann (2011a), High-intensity gas seepage causes rafting of shallow gas hydrates in the southeastern Black Sea, *Earth. Planet. Sci. Lett.*, *307*, 35–46, doi:10.1016/j.epsl.2011.04.030.

Pape, T., T. Feseker, S. Kasten, D. Fischer, and G. Bohrmann (2011b), Distribution and abundance of gas hydrates in near-surface deposits of the Håkon Mosby Mud Volcano, SW Barents Sea, *Geochem. Geophys. Geosyst.*, *12*, Q09009, doi:10.1029/2011gc003575.

Park, J.-O., T. Tsuru, S. Kodaira, P. R. Cummins, and Y. Kaneda (2002), Splay fault branching along the Nankai subduction zone, *Science*, *297*(5584), 1157–1160, doi:10.1126/science.1074111.

Paull, C. K., W. Ussler III, W. S. Borowski, and F. N. Spiess (1995), Methane-rich plumes on the Carolina continental rise: Associations with gas hydrates, *Geology*, *23*(1), 89–92.

Römer, M., H. Sahling, T. Pape, A. Bahr, T. Feseker, P. Wintersteller, and G. Bohrmann (2012), Geological control and magnitude of methane ebullition from a high-flux seep area in the Black Sea: The Kerch seep area, *Mar. Geol.*, *319–322*, 57–74, doi:10.1016/j.margeo.2012.07.005.

Saffer, D., L. McNeill, T. Byrne, E. Araki, S. Toczko, N. Eguchi, K. Takahashi, and the Expedition 319 Scientists (2010), NanTroSEIZE Stage 2: NanTroSEIZE riser/riserless observatory, *Proc. Integrated Ocean Drill. Program*, *319*.

Sahling, H., D. Rickert, R. Lee, W., P. Linke, and E. Suess (2002), Macrofaunal community structure and sulfide flux at gas hydrate deposits from the Cascadia convergent margin, NE Pacific, *Mar. Ecol. Prog. Ser.*, *231*, 121–138.

Sahling, H., et al. (2009), Vodyanitskii Mud Volcano, Sorokin Trough, Black Sea: Geological characterization and quantification of gas bubble streams, *Mar. Pet. Geol.*, *26*(9), 1799–1811, doi:10.1016/j.marpetgeo.2009.01.010.

Saito, S., M. B. Underwood, Y. Kubo, and the Expedition 322 Scientists (2009), NanTroSEIZE Stage 2: Subduction Inputs, *Proc. Integrated Ocean Drill. Program*, *322*.

Sassen, R., S. Joye, S. T. Sweet, D. A. DeFreitas, A. V. Milkov, and I. R. MacDonald (1999), Thermogenic gas hydrates and hydrocarbon gases in complex chemosynthetic communities, Gulf of Mexico continental slope, *Org. Geochem.*, *30*(7), 485–497.

Sassen, R., S. T. Sweet, D. A. DeFreitas, and A. V. Milkov (2000), Exclusion of 2-methy lbutane (isopentane) during crystallization of structure II gas hydrate in sea-floor sediment, Gulf of Mexico, *Org. Geochem.*, *31*(11), 1257–1262.

Sauter, E. J., S. I. Muyakshin, J.-L. Charlou, M. Schlüter, A. Boetius, K. Jerosch, E. Damm, J.-P. Foucher, and M. Klages (2006), Methane discharge from a deep-sea submarine mud volcano into the upper water column by gas hydrate-coated methane bubbles, *Earth. Planet. Sci. Lett.*, *243*(3–4), 354–365, doi:10.1016/j.epsl.2006.01.041.

Schlüter, H. U., A. Prexl, C. Gaedicke, H. Roeser, C. Reichert, H. Meyer, and C. von Daniels (2002), The Makran accretionary wedge: Sediment thicknesses and ages and the origin of mud volcanoes, *Mar. Geol.*, *185*(3–4), 219–232.

Screaton, E., et al. (2009), Interactions between deformation and fluids in the frontal thrust region of the NanTroSEIZE transect offshore the Kii Peninsula, Japan: Results from IODP Expedition 316 Sites C0006 and C0007, *Geochem. Geophys. Geosyst.*, *10*, Q0AD01, doi:10.1029/2009gc002713.

Seewald, J. S. (2003), Organic-inorganic interactions in petroleum-producing sedimentary basins, *Nature*, *426*(6964), 327–333.

Selley, R. C. (1998), *Elements of Petroleum Geology*, 2nd ed., 470 pp., Academic, San Diego, Calif.

Shelly, D. R., G. C. Beroza, S. Ide, and S. Nakamula (2006), Low-frequency earthquakes in Shikoku, Japan, and their relationship to episodic tremor and slip, *Nature*, *442*(7099), 188–191, doi:10.1038/nature04931.

Sloan, E. D., and C. A. Koh (2007), *Clathrate Hydrates of Natural Gases*, 3rd ed., 752 pp., CRC Press, Boca Raton, Fla.

Strasser, M., et al. (2009), Origin and evolution of a splay fault in the Nankai accretionary wedge, *Nat. Geosci.*, *2*(9), 648–652, doi:10.1038/ngeo609.

Suess, E., et al. (1999), Gas hydrate destabilization: Enhanced dewatering, benthic material turnover and large methane plumes at the Cascadia convergent margin, *Earth. Planet. Sci. Lett.*, *170*(1–2), 1–15.

Taira, A., et al. (1992), Sediment deformation and hydrogeology of the Nankai Trough accretionary prism: Synthesis of shipboard results of ODP Leg 131, *Earth. Planet. Sci. Lett.*, *109*(3–4), 431–450.

Tobin, H. J., and M. Kinoshita (2006), NanTroSEIZE: The IODP Nankai trough seismogenic zone experiment, *Sci. Drill.*, *2*, 23–27.

Tobin, H. J., and D. M. Saffer (2009), Elevated fluid pressure and extreme mechanical weakness of a plate boundary thrust, Nankai Trough subduction zone, *Geology*, *37*(8), 679–682, doi:10.1130/g25752a.1.

Toki, T., U. Tsunogai, T. Gamo, S. Kuramoto, and J. Ashi (2004), Detection of low-chloride fluids beneath a cold seep field on the Nankai accretionary wedge off Kumano, south of Japan, *Earth. Planet. Sci. Lett.*, *228*(1–2), 37–47, doi:10.1016/j.epsl.2004.09.007.

Torres, M. E., K. Wallmann, A. M. Tréhu, G. Bohrmann, W. S. Borowski, and H. Tomaru (2004), Gas hydrate growth, methane transport, and chloride enrichment at the southern summit of Hydrate Ridge, Cascadia margin off Oregon, Earth. *Planet. Sci. Lett.*, *226*(1–2), 225–241, doi:10.1016/j.epsl.2004.07.029.

Tsunogai, U., K. Maegawa, S. Sato, D. D. Komatsu, F. Nakagawa, T. Toki, and J. Ashi (2012), Coseimic massive methane release from a submarine mud volcano, *Earth. Planet. Sci. Lett.*, *341–344*, 79–85, doi:10.1016/j.epsl.2012.06.004.

Wallmann, K., M. Drews, G. Aloisi, and G. Bohrmann (2006), Methane discharge into the Black Sea and the global ocean via fluid flow through submarine mud volcanoes, *Earth. Planet. Sci. Lett.*, *248*(1–2), 544–559, doi:10.1016/j.epsl.2006.06.026.

Westbrook, G. K., and M. J. Smith (1983), Long decollements and mud volcanoes: Evidence from the Barbados Ridge Complex for the role of high pore-fluid pressure in the development of an accretionary complex, *Geology*, *11*(5), 279–283.

Whiticar, M. J. (1990), A geochemical perspective of natural gas and atmospheric methane, *Org. Geochem.*, *16*(1–3), 531–547.

AGU PUBLICATIONS

JGR

Journal of Geophysical Research: Solid Earth

RESEARCH ARTICLE
10.1002/2013JB010546

This article is a companion to *Sultan et al.* [2010], doi:10.1029/2010JB007453.

Key Points:
- Free gas trapped in shallow micro-fractures near the seafloor
- Very low methane concentrations above the top of the gas hydrate occurrence zone
- Pockmark formation controlled by rapid hydrate growth and hydrate dissolution

Correspondence to:
N. Sultan,
nabil.sultan@ifremer.fr

Citation:
Sultan, N., et al. (2014), Pockmark formation and evolution in deep water Nigeria: Rapid hydrate growth versus slow hydrate dissolution, *J. Geophys. Res. Solid Earth*, *119*, 2679–2694, doi:10.1002/2013JB010546.

Received 22 JUL 2013
Accepted 13 MAR 2014
Accepted article online 18 MAR 2014
Published online 28 APR 2014

Pockmark formation and evolution in deep water Nigeria: Rapid hydrate growth versus slow hydrate dissolution

N. Sultan[1], G. Bohrmann[2], L. Ruffine[1], T. Pape[2], V. Riboulot[1], J.-L. Colliat[3], A. De Prunelé[1], B. Dennielou[1], S. Garziglia[1], T. Himmler[1,2], T. Marsset[1], C.A. Peters[2], A. Rabiu[4], and J. Wei[2]

[1]Ifremer, REM/GM/LES, Plouzané, France, [2]MARUM - Center for Marine Environmental Sciences, University of Bremen, Bremen, Germany, [3]TOTAL, Pau, France, [4]NIOMR, Victoria Island, Nigeria

Abstract In previous works, it has been suggested that dissolution of gas hydrate can be responsible for pockmark formation and evolution in deep water Nigeria. It was shown that those pockmarks which are at different stages of maturation are characterized by a common internal architecture associated to gas hydrate dynamics. New results obtained by drilling into gas hydrate-bearing sediments with the MeBo seafloor drill rig in concert with geotechnical in situ measurements and pore water analyses indicate that pockmark formation and evolution in the study area are mainly controlled by rapid hydrate growth opposed to slow hydrate dissolution. On one hand, positive temperature anomalies, free gas trapped in shallow microfractures near the seafloor and coexistence of free gas and gas hydrate indicate rapid hydrate growth. On the other hand, slow hydrate dissolution is evident by low methane concentrations and almost constant sulfate values 2 m above the Gas Hydrate Occurrence Zone.

1. Study Area and Main Objective

The investigated area is located in deep water of Nigeria. Bathymetry in the area ranges from 1100 to 1250 m (Figure 1). This area was previously shown to host a field of (sub) circular pockmarks [*Georges and Cauquil*, 2007]. These range in shape from a slightly depressed, hummocky seafloor to a much more pronounced depression and each of them is several tens to a few hundreds of meters wide (Figure 1). The various morphologies of the pockmarks suggest either distinct modes of formation or different evolutionary stages [*Sultan et al.*, 2010]. Most of the pockmarks are located in an area bounded by two NW-SE trending deep-rooted normal faults, which delineate a graben linked to the axis of anticline in the subsurface. Several deep and shallow faults and three N-S trending buried channels were recognized with high-resolution 3-D seismic data (Figure 1). The buried channels, which are situated between 80 ms and 180 ms (two-way travel time, TWTT) below the seabed, may have the potential of accumulating amounts of free gas and play therefore an important role for the gas hydrate distributions.

Based on geophysical and sedimentological data, and in situ piezocone measurements, *Sultan et al.* [2007] have shown that pockmark-associated gas hydrate accumulated within a few meters thick sediment layers at shallow depth. In addition, *Sultan et al.* [2010] proposed that the formation of a circular depression around the gas hydrate occurrence zone (GHOZ) is related to multiple steps in the pockmark evolution. The sequence is starting with hydrate formation induced by upward migration of fluids oversaturated in gas through fracture systems followed by decrease of fluid flow resulting in gas undersaturation, hydrate dissolution, generation of excess pore pressure, and by concurrent collapse of the gas hydrate-bearing sediment structures. Respective analyses were mainly based on subseabed approaches, using piston cores and in situ piezocone geotechnical measurements with a maximum penetration of 30 m below seafloor (mbsf). However, the gas hydrate stability zone (GHSZ) in this area is expected to expand from 90 to 120 mbsf [*Sultan et al.*, 2010, Figure 20] and several relatively deep structures (buried channels, microfaults and fractures) and intermediate reservoirs are located below the previously investigated shallow subseabed area.

In order to better understand processes that control not only the formation but also the evolution of pockmarks, longer cores of gas hydrate-bearing sediments were drilled using the MeBo seafloor drill rig [*Freudenthal et al.*, 2009] during the French-German Guineco-MeBo expedition in December 2011 on board

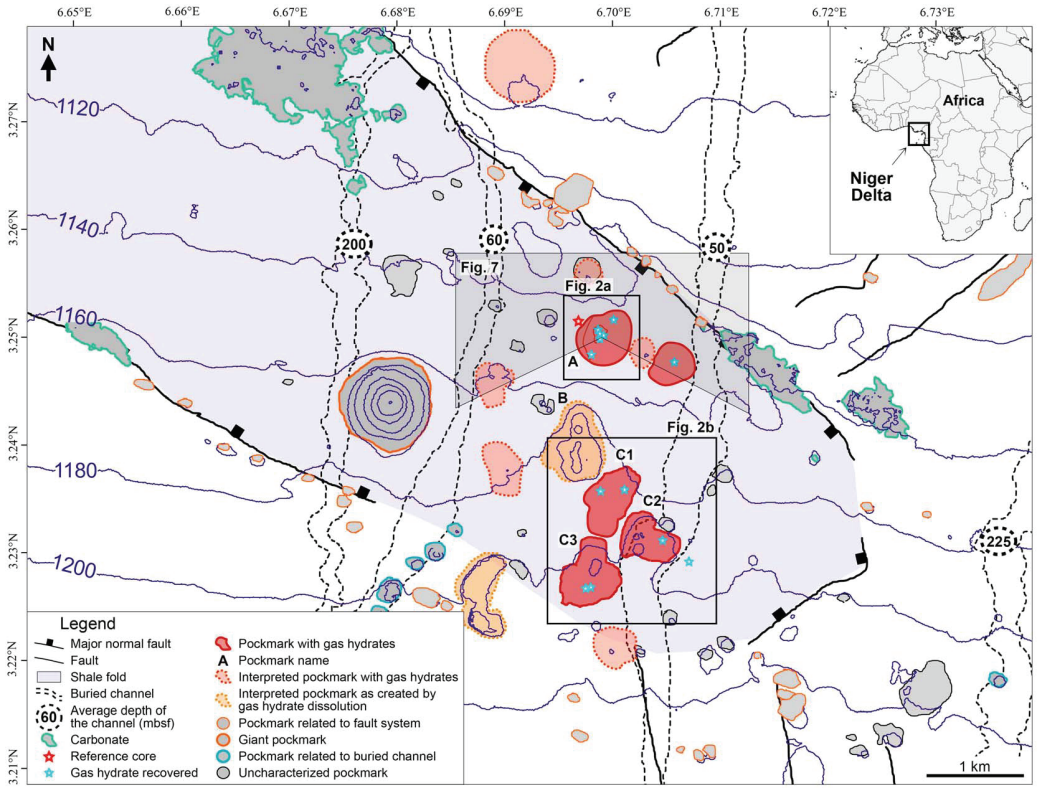

Figure 1. Interpreted bathymetry map of the study area based on industrial AUV data [*Georges and Cauquil*, 2007] showing studied pockmarks (pockmark A to the north and pockmarks C1, C2, and C3 to the south). Deep buried channels (between 80 and 100 ms TWT below seabed) are projected on the bathymetric map (dashed lines). Most pockmarks are located within a NW-SE trending area bounded by two deep-rooted normal faults clearly expressed on the bathymetric map.

the French research vessel "Pourquoi Pas?." The MeBo drill rig enabled recovery of sediments down to approximately 57 mbsf which markedly upgrades the previously acquired data set. Based on newly acquired data, this paper aims at providing the founding elements to answer whether pockmark morphology is related to the stage of evolution and/or distinct modes of pockmark formation. The present research works serve as a companion paper to our previous paper on the "hydrate dissolution as a potential mechanism for pockmark formation in the Niger delta" [*Sultan et al.*, 2010]. In the following and based on key indices, it will be demonstrated that the main process controlling gas hydrate formation and pockmark evolution is dynamic gas inflows and outflows which are controlled by rapid and episodic hydrate growth versus slow hydrate dissolution.

2. Acquired Data

During the Guineco-MeBo expedition a multidisciplinary approach was used, comprising geology, sedimentology, geochemistry and geotechnics, and applying various sampling and measurements tools. Sediment cores were retrieved by means of the MeBo seafloor drill rig, a ship-based Kullenberg-type piston corer (Ifremer Jumbo Calypso corer), a gravity corer, and the pressure-tight Dynamic Autoclave Piston Corer (DAPC). Using MeBo, up to 57 m long sediment cores could be recovered (shown in Figures 2–5). The Ifremer Jumbo Calypso corer and the gravity corer were used to recover shallow sediment samples (Figures 2a and 2b). At selected stations, thermal probes were mounted to the cutting barrel of the gravity corer in order to measure in situ thermal gradients (Figure 2a). The DAPC [*Abegg et al.*, 2008] was used to recover pressurized cores in hydrate-bearing areas of pockmark A (Figure 2a).

The Ifremer Penfeld was used to perform up to 30 m deep piezocone (Figures 2a and 2b) and *P* wave velocity (celerimeter) measurements profiles (Figures 2a and 2b). Finally, the Ifremer piezometer was used to measure

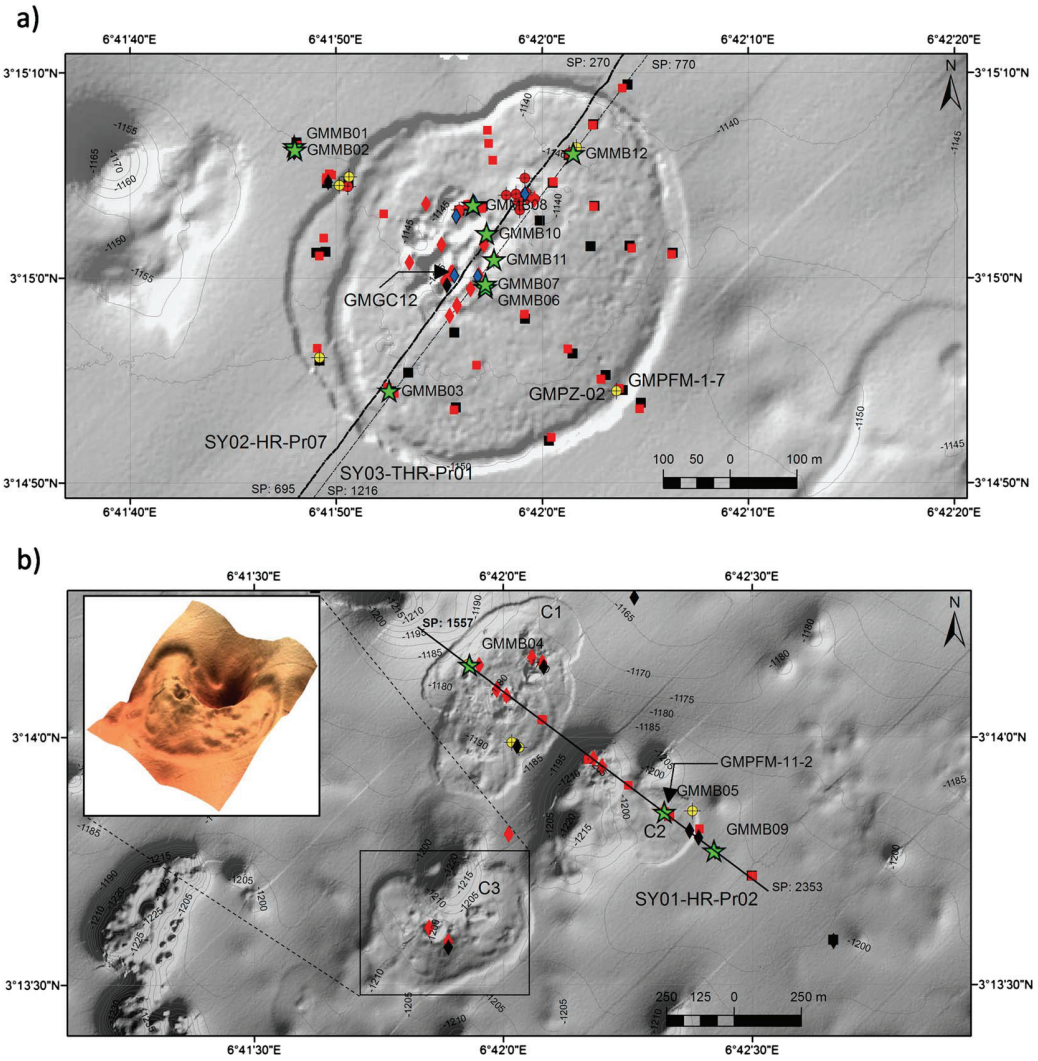

Figure 2. Overview about stations and acquired data. Calypso and gravity cores: blue diamonds; MeBo drills: green stars; Gravity cores with thermal probes: red circle targets; Penfeld piezocone: red squares; Penfeld celerimeter: black squares; Piezometer: yellow circle targets during GM cruise projected on shaded bathymetry maps of (a) pockmark A and (b) pockmarks C1, C2, and C3. Only sites and data used in the present paper are labeled. Locations of SYSIF seismic profiles SY03-THR-PR01, SY02-HR-PR07, and SY01-HR-PR02 and corresponding Shot Point (SP) are also shown. In Figure 2b, a 3-D view of pockmark C3 bathymetry shows the coexistence of two stages of the pockmark going from dome structure to deep depression.

pore pressure and temperature down to 14 mbsf with waiting periods ranging between 6 h and 4 days (Figures 2a and 2b). Data and samples were acquired during the cruise from 15 Calypso cores, 36 gravity cores, 13 gravity cores with temperature measurements, 6 DAPC cores, 12 MeBo deep cores, 52 in situ piezocone measurements, 38 in situ celerimeter measurements, and 10 piezometer deployments.

Measurements of sulfate and chloride concentrations, alkalinity, and pH were carried out on board. Ex situ methane concentrations in pore waters and molecular compositions of hydrate-bound gases were determined. Lithological core descriptions were made on board. An Avaatech X-ray fluorescence core-scanner system was used to perform stepwise (1 cm) analyses of major elements from Al to U on selected core archive halves. In order to identify the key mechanical and physical sediment parameters, an onboard experimental geotechnical program on undisturbed marine sediment samples was undertaken (including the use of the GEOTEK Multi-Sensor Core Logger and shear strength measurements). In order to trace gas hydrate distributions in the sediment, data from continuous infrared thermal core imaging and pore water

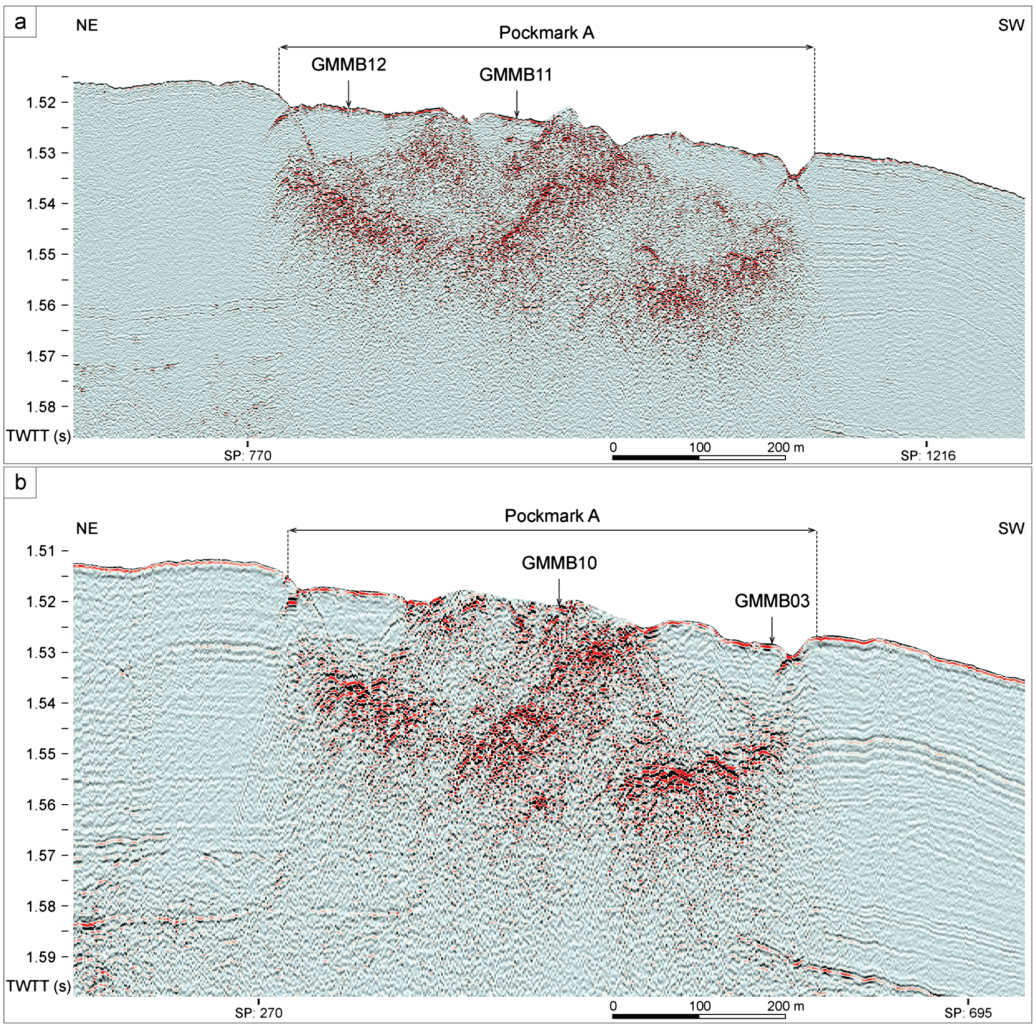

Figure 3. SYSIF seismic profiles (a) SY03-THR-PR01 and (b) SY02-HR-PR07 showing a significant contrast between high-amplitude chaotic facies at the center of pockmark A and low-amplitude subparallel reflectors of surrounding sediments. Four MeBo drill sites are indicated on the seismic lines.

analysis performed before core liner splitting were jointly evaluated with sediment observations. In addition, in situ piezocone geotechnical measurements were used as an indirect indication for the gas hydrate presence. Indeed, gas hydrate is characterized by very high resistance that can be easily detected with the high-corrected cone resistance (qt) recorded during piezocone measurements.

The seismic data used in the present work were acquired during a previous cruise using the Système Sismique Fond (SYSIF) deep towed acquisition system [*Ker et al.*, 2010; *Marsset et al.*, 2010]. SYSIF is a heavy towed apparatus hosting low-frequency acoustic transducers (250–1000 Hz, 650–2000 Hz) and a single channel streamer in order to provide high-resolution (HR) images of the subbottom. The altitude of SYSIF over the seafloor is set to 100 m thus reducing the Fresnel zone, i.e., enhancing the lateral resolution compared to conventional surface towed systems. All those seismic data were not migrated and were already presented in the companion paper [*Sultan et al.*, 2010].

3. Key Mechanisms: Previous Works and New Observations

In the following, the two main processes controlling pockmarks formation and evolution in the area are presented and discussed using background literature, data analysis, and interpretation.

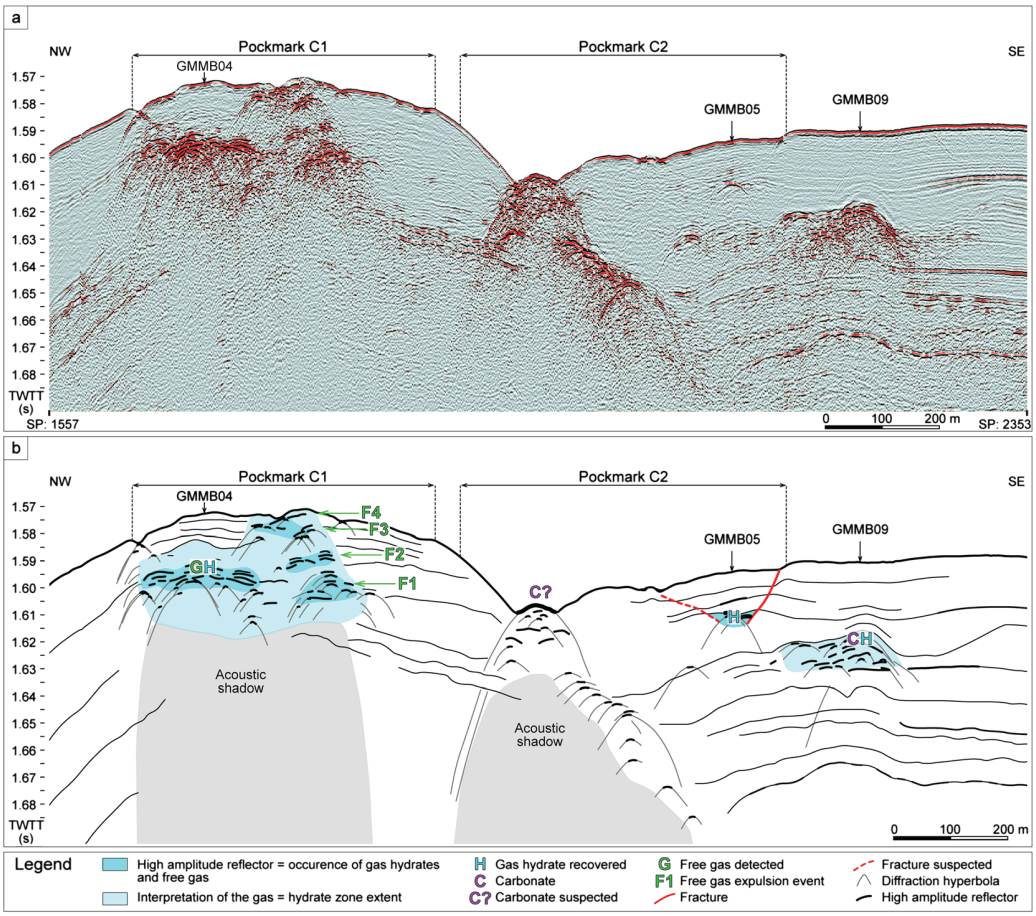

Figure 4. (a) SYSIF SY01-HR-PR02 seismic profile and (b) interpreted profile crossing pockmarks C1 and C2 and indications of MeBo drill sites. The letter G in Figure 4b corresponds to the source of free gas flow generated during MeBo drilling GMMB04. The G fits with a diffraction hyperbola's high-amplitude reflectors preventing a clear detection of the free gas source. On the seismic profile, four reflectors (F1 to F4), which are suspected to result from four natural free gas expulsion events, are indicated. Gas hydrate was recovered from reflector F4 by coring.

3.1. Rapid Hydrate Growth

3.1.1. Coexistence of Free Gas and Gas Hydrate

3.1.1.1. Previous Works and Background

The coexistence of free gas and gas hydrate has been first reported from the Oregon continental margin where ascending saline fluids may lead to a local shift in the gas hydrate stability toward less stable conditions, thereby allowing movement of free gas through the GHSZ [*Trehu et al.*, 2003; *Milkov et al.*, 2004; *Torres et al.*, 2004; *Liu and Flemings*, 2006]. The absence of pore water in sufficient amounts can be an additional cause for the presence of free gas in gas hydrate-bearing sediments [*Lee and Collett*, 2006]. Based on seismic data and in situ *P* wave velocity measurements, free gas and gas hydrate were already suspected to co-occur widespread in the present study area [*Sultan et al.*, 2007].

3.1.1.2. New Acquired Data and Observations

Newly acquired data and mainly coring confirmed the coexistence between free gas and gas hydrate. Highly porous gas hydrate recovered from shallow sediments at the central part of pockmark A (gravity corer GMGC12 in Figure 2a) shows the presence of free gas alveoli isolated in massive gas hydrate (Figure 6a). The pore size of a unit gas alveolus is 2 to 3 mm in diameter. The gas hydrate sample in Figure 2a was recovered from the interval 1 to 2 mbsf.

3.1.1.3. Interpretation

The complete isolation of gas alveoli in the sediment can be explained by rapid injection of gas-rich fluids along fractures into the GHSZ. As a consequence, rapid gas flux results in rapid gas hydrate accumulation

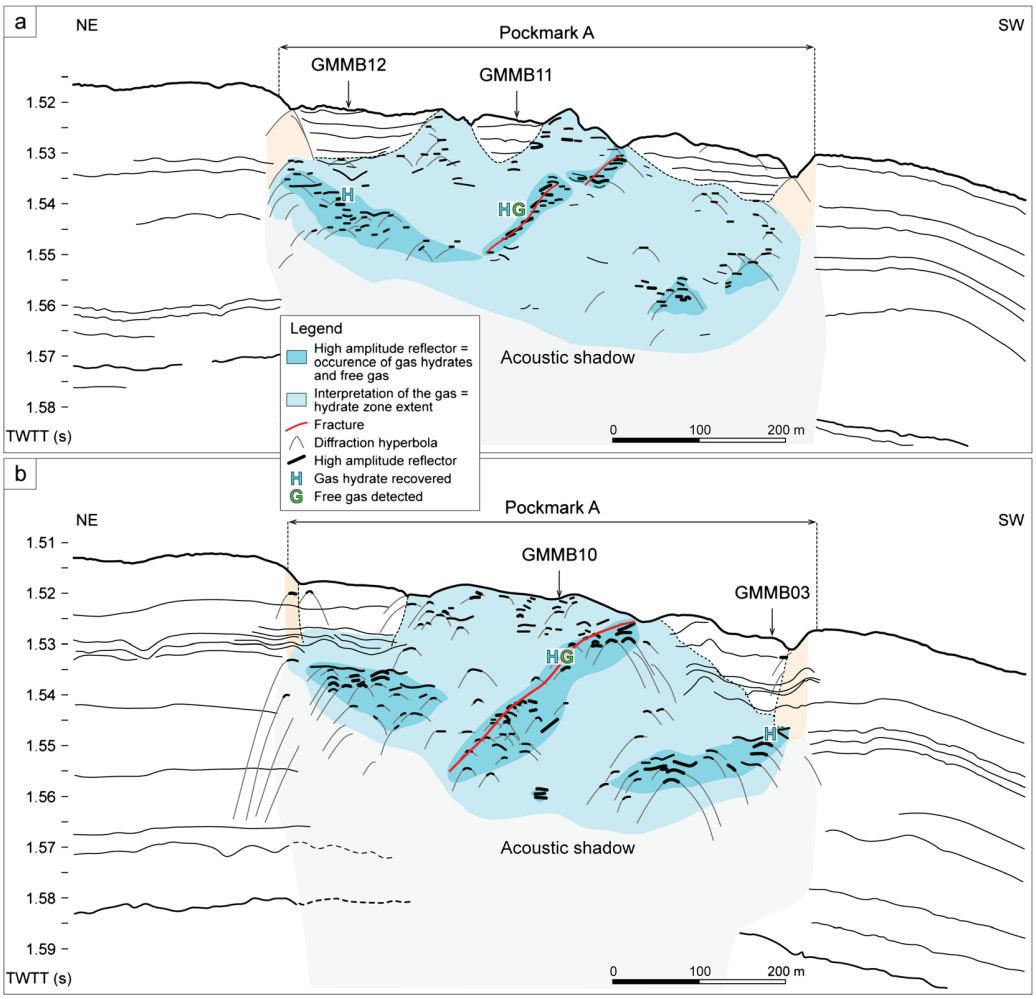

Figure 5. Interpreted SYSIF seismic profiles (a) SY03-THR-PR01 and (b) SY02-HR-PR07 and indications of MeBo drill sites at pockmark A. The letter G corresponds to the sources of free gas flow generated during MeBo drillings after crossing hydrate layers (letter "H"). For GMMB11 and GMMB10, the two Gs fit well with shallow subseabed fractures.

which may isolate free gas zones (i.e., gas-filled pores) from the surrounding pore water. The preservation of those free gas zones can be explained by the very low permeability of gas hydrate for water and gas.

3.1.2. Free Gas in the Water Column Above Pockmark A

3.1.2.1. Previous Works and Background

Gas plumes in the seawater above gas-bearing and gas hydrate-bearing sediments are frequent [e.g., *Paull et al.*, 1995; *Roemer et al.*, 2012]. For instance, *Paull et al.* [1995] reported gas plumes crossing the GHOZ over the Blake Ridge and *Taylor et al.* [2000] suggested that these gas plumes are related to high-pore water salinity. For seep sites in the south-eastern Black Sea, *Pape et al.* [2011] suggested that constant fluid supply from greater depth leads to overpressure in free gas accumulation zones beneath a continuous shallow hydrate layer which may cause hydrate detachment from the seafloor and buoyant rise through the water column.

3.1.2.2. New Acquired Data and Observations

Two hydroacoustic anomalies caused by rising gas bubbles (plumes) of naturally escaping free gas in the central part of pockmark A have been detected during the cruise by the vessel multibeam echosounder (Seabat 7150). The gas plumes disappeared from the records around 500 m above seabed (i.e., 600 mbsl) (Figure 6b). Repeated acoustic water column scanning above the whole study zone (around 40 km^2) during the expedition confirmed (1) continuous natural seepage of free gas from the central part of pockmark A and (2) the absence of other plumes in the area.

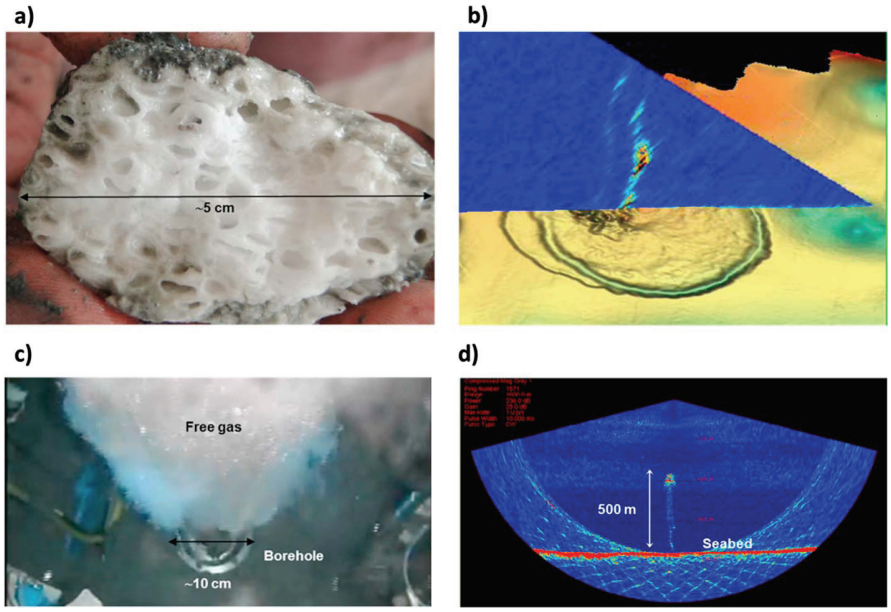

Figure 6. (a) Photograph of a porous hydrate specimen recovered from the central part of pockmark A (GMGC12 in Figure 2a) showing the possible coexistence between gas hydrate and free bubble-forming gas. (b) Two gas plumes sources in the central part of pockmark detected, thanks to the multibeam echosounder (SeaBat 7150). (c) Gas flow from a source at around 18 mbsf (site GMMB04—high amplitude in Figure 4b indicated by "GH") as recorded by the MeBo camera (Marum) during drilling and (d) the detection with the multibeam echosounder of the gas flow generated during drilling (site GMMB04). Gas plumes were dispersed completely 500 m above the seabed (around 600 m below the sea surface).

3.1.2.3. Interpretation

The source of the gas plumes seems to be spatially associated with the shallow fractures shown in the seismic profiles in Figure 5a and is directly linked to the seismic horizon R previously reported (Figure 7). It is noteworthy that the high-amplitude chaotic facies and the numerous diffraction hyperbolas prevent precise identification of fractures. A three-dimensional view of pockmark A sediments, which was constructed from autonomous underwater vehicle (AUV) bathymetric data and industrial 3-D seismic data, illustrates that the seismic reflector R is associated to a horizon forming a gas storage zone (horizon R, Figure 7) at around 0.3 s (TWT) below the seabed (around 232 mbsf for a mean *P* wave velocity of 1550 m/s). Two other pockmarks to the east and the west of pockmark A are supplied by gas from horizon R as well (Figure 7). The vigorous gas flow through the GHOZ into the overlying water column at the central part of pockmark A provides evidence of growth of shallow gas hydrate fueled by gas ascent from horizon R through fractures toward the seafloor rather than slow diffusion.

3.1.3. Free Gas Within the GHOZ

3.1.3.1. New Acquired Data and Observations

The MeBo targets aimed to drill through gas hydrate layers, in particular through shallow subseabed structures (high-amplitude reflectors, suspected fractures) and well expressed seabed depressions (Figure 2). A free gas accumulation was discovered during MeBo drilling GMMB04 at pockmark C1 (Figures 1 and 4). Having penetrated a relatively thin hydrate layer (marked by a very high amplitude chaotic facies on seismic, see Figure 4) at around 18 mbsf by rotary drilling, vigorous flow of free gas suddenly occurred and significant amounts of gas bubbles escaped from the borehole continuously for more than 1 h (Figure 6c). Drilling torque data show that the thin hydrate layer above the free gas layer was characterized by a relatively high stiffness and cameras from the MeBo filmed pieces of hydrate expulsed from the drilling borehole. This gas discharge from the subseafloor structure to the water column was also detected by the vessel multibeam echosounder (SeaBat 7150) (Figure 6d). It was dispersed completely, as for the case of the natural gas plumes, 500 m above the seabed. Drilling operations were aborted during GMMB-04 because of visibility problems (gas hydrate was formed instantaneously on cameras). Other free gas-pocket zones isolated from surrounding gas hydrate-bearing sediments were discovered during MeBo drillings GMMB11 and GMMB10 at pockmark A

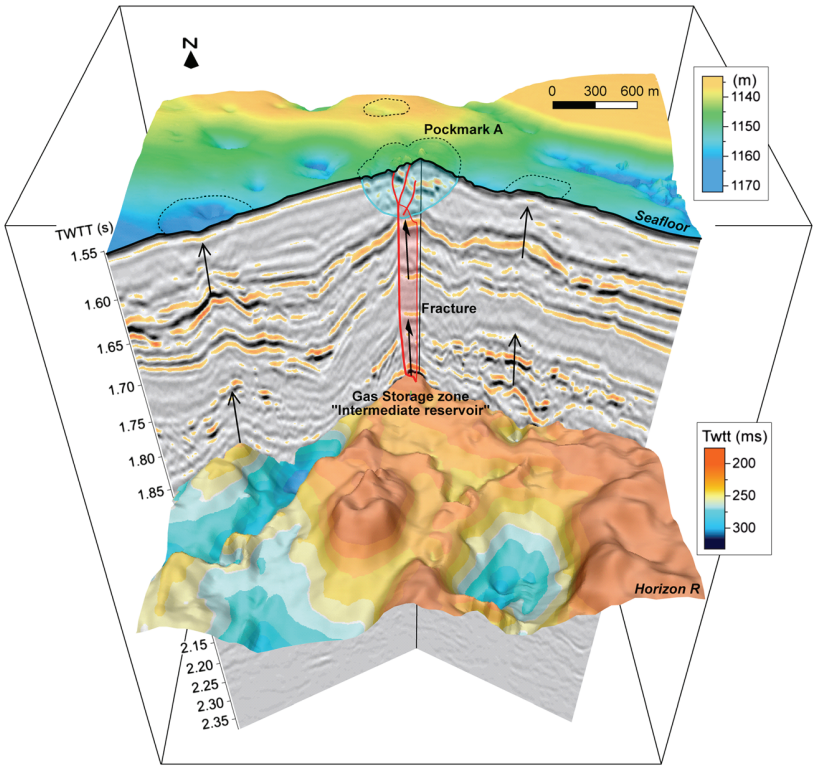

Figure 7. The 3-D cartoon crossing pockmark A and adjacent areas constructed from AUV bathymetric data and industrial 3-D seismic data showing a gas storage zone (Horizon R) at around 0.3 s (TWT) below seabed. Two other pockmarks to the east and the west of pockmark A are also supplied by gas from horizon R as indicated with black arrows but not considered further in the manuscript.

(Figures 1 and 5). The letter "G" below site GMMB11 and GMMB10 represents two other sources of free gas isolated zones (Figure 5) detected, thanks to the MeBo drillings.

An example of the correlation done between the seismic data on one hand and in situ measurements and drilling on the other hand is illustrated in Figure 8. The characterization of a high-amplitude reflector at around 15 ms (two-way travel time) below the seabed on the SYSIF profile SY01-HR-PR02 was possible, thanks to both piezocone measurements and drilling. Indeed, the cone resistance from GMPFM-11-2 shows an early refusal at 11 mbsf corresponding approximately to the top of the high-amplitude reflector (for a mean *P* wave velocity of 1450 m/s). In addition, pore water anomalies of dissolved methane (Figure 8c) and sulfate (Figure 8d) obtained from the porewater of MeBo core GMMB05 fit well with the same high-amplitude reflector. These geochemical anomalies, which are indicators of the presence of gas hydrates, will be discussed in more details later on. The use of a mean *P* wave velocity of 1450 m/s is based on direct in situ *P* wave velocity measurements acquired from the top 30 m of the sediment in the present area [*Sultan et al.*, 2007].

3.1.3.2. Interpretation

For those sites, it is clear that the source of the gas discharges corresponds to the high-amplitude anomalies observed on seismic profiles, which suggest the presence of shallow fractures in the central part of pockmark A. The presence of free gas at such shallow depth was unexpected, since the base of the GHSZ (BGHSZ) for the different sites should be located between 90 m and 120 mbsf considering the measured thermal gradient (approximately 80°C/km) [*Sultan et al.*, 2010]. The probable cause for these isolated gas pockets is rapid gas flux through fractures connected to the intermediate gas reservoir (horizon R in Figure 7).

As exemplified by the coexistence of free gas and gas hydrate at millimeter scale (see Figure 6a), the supply of large amounts of free gas by reopening or creating new fractures followed by gas hydrate formation primarily at the inner surface of such fractures leads to isolation of free gas from the surrounding pore water saturated sediment.

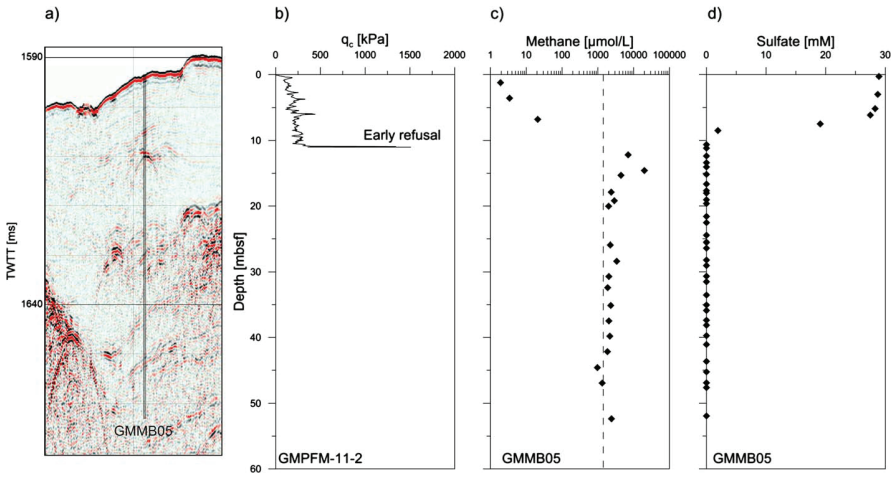

Figure 8. (a) SYSIF SY01-HR-PR02 seismic profile between SP 2000 and 2200 showing the locations of MeBo GMM05 and piezocone GMPFM-11-2. (b) Cone resistance from GMPFM-11-2 as a function of depth shows an early refusal at 11 mbsf corresponding to a high-amplitude reflector in Figure 8a. Pore water anomalies of dissolved (c) methane and (d) sulfate obtained from the pore water of MeBo core GMMB05 fit well also with high-amplitude reflector. The correlation between the seismic data and GMMB05 and GMPFM-11-2 is done for a mean *P* wave velocity of 1450 m/s.

3.1.4. Sediment Temperature and Resistance Anomalies

3.1.4.1. Previous Works and Background

Gas hydrate formation is an exothermic reaction and, thus, characterized by heat emission and a temperature increase in the surrounding sediment. In nature, gas hydrate formation is mainly controlled by molecular diffusion and fluid flow [*Wallmann et al.*, 1997]. In fine-grain sediments where the fluid flow rate is comparably low, gas dispersion is dominated by molecular diffusion [*Haeckel et al.*, 2004]. Thermal diffusivity of fine-grained marine sediments (around 10^{-6} m^2/s) [see e.g., *Waite et al.*, 2009] is several orders of magnitude higher than the molecular diffusivity of methane (10^{-12} m^2/s) [*Bigalke et al.*, 2009]. Therefore, for hydrate formation controlled by gas diffusion, temperature perturbation due to hydrate formation is expected to be negligible and most likely undetectable.

3.1.4.2. New Acquired Data and Observations

Several peak values of the corrected cone resistance (qt) indicate the presence of multiple thin gas hydrate layers at depths between 2.3 and 14.5 mbsf at site GMPFM-1-7 at the southeastern rim of pockmark A (Figures 2a and 8a). At a close-by site (GMPZ-02, Figure 2a), a piezometer was deployed to measure in situ pressure and temperature. Comparison between qt and temperature at equilibrium (Figure 8b) demonstrates that positive temperature anomalies (deviating from the average thermal gradient) correspond to the suspected two uppermost hydrate layers. Additionally, several shallow (between 1 and 2 mbsf) thermal gradient measurements in the central part of pockmark A (Figure 2a) have shown temperature anomalies with the thermal gradient exceeding 150°C/km.

3.1.4.3. Interpretation

These temperature anomalies are a clear evidence of recent hydrate formation and a clear demonstration that gas hydrate at some locations was not formed by diffusion but with a rapid free gas flux through fractures. Temperature anomalies related to upward hot fluid migration are expected to be more continuous with depth than the temperature anomalies in Figure 8b. In other terms, vertical movement of deep hot fluids is expected to cause a progressive temperature increase with depth and not peak temperature anomalies as it is observed in Figure 8.

3.2. Slow Hydrate Dissolution: Evidence From Sulfate and Methane Concentration Profiles Above the GHOZ

3.2.1. Previous Works and Background

The parameters affecting gas hydrate formation include temperature, pore pressure, gas, and pore water composition. Any variance in one of these parameters from equilibrium conditions may result in dissociation and/or dissolution of gas hydrate. Hydrate dissociation is generally caused by thermodynamic instabilities

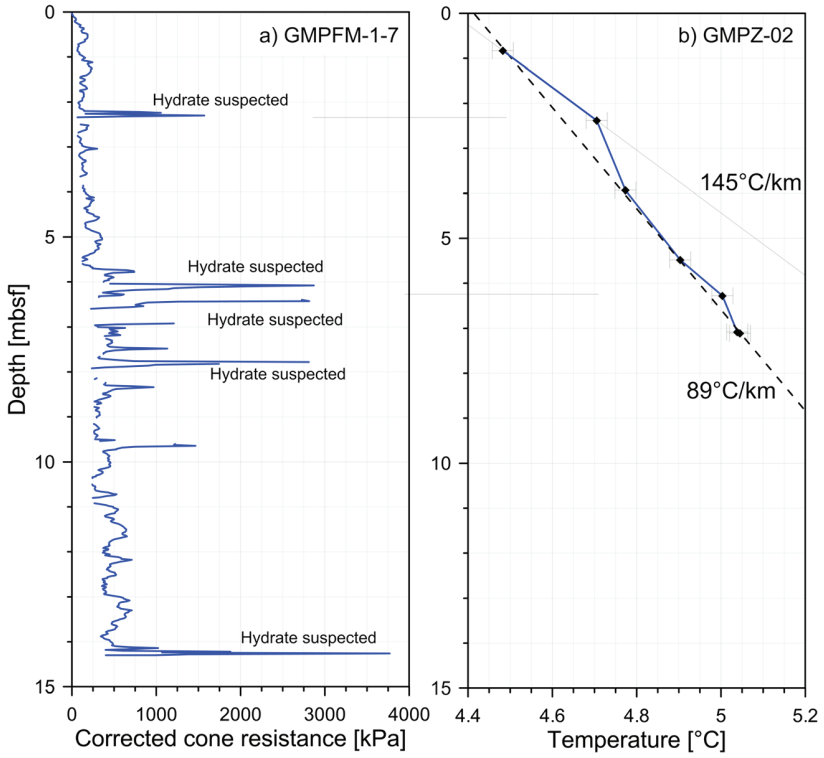

Figure 9. (a) Potential hydrate occurrence zones detected by the use of in situ piezocone measurements (site GMPF-1-7 in Figure 2a) and (b) piezometer measurements (site GMPZ-02 in Figure 2a) acquired within hydrate layers showing a thermal perturbation regime.

with the consequence of rapid release of gas-rich fluids (see for instance *Xu and Germanovich* [2006] and *Kwon et al.* [2008]). Methane hydrate dissolution occurs when hydrate comes in contact with an aqueous phase undersaturated in methane [see e.g., *Lapham et al.*, 2010]. Hydrate-bound methane will be transferred to the aqueous phase to allow new thermodynamic equilibrium conditions to be established [*Rehder et al.*, 2004; *Sultan*, 2007]. Thus, the major cause for hydrate dissolution is a deficit in dissolved methane in the surrounding pore water with dissolved methane concentrations being lower than its solubility. The sulfate-dependent anaerobic oxidation of methane (AOM) at the base of the sulfate zone contributes significantly to lower methane concentrations close to the GHOZ [*Kasten et al.*, 2012; *Iversen and Jorgensen*, 1985; *Borowski et al.*, 1996, 1999; *Hoehler et al.*, 1994]. In summary, the presence of free methane and low sulfate concentrations close to the GHOZs indicates high and rapid gas migration and/or hydrate dissociation, while extremely low methane concentrations (lower than solubility values) and high pore water sulfate concentration point to gas hydrate dissolution.

3.2.2. New Acquired Data and Observations

At drill site GMMB05 at the border of pockmark C2 (for location, see Figures 2 and 4), a high amplitude reflector at around 9.5 mbsf (Figure 4) was penetrated. This reflector was previously considered by *Sultan et al.* [2010] as an indicator for gas hydrate presence at this depth, and a gas hydrate layer has indeed been drilled at the depth of the high amplitude reflector. Infrared (IR) thermal scanning (Figure 9c) confirmed the presence of several gas hydrate layers [*Wei et al.*, 2012]. Figure 9a shows ex situ concentrations of dissolved methane versus depth at site GMMB05. Dissolved methane concentrations below the top of the GHOZ (TGHOZ) range between methane solubility at in situ pressure and temperature conditions and that at atmospheric conditions.

At the same drill site (GMMB05), pore water sulfate concentrations in the uppermost 6 m are characterized by almost constant concentrations of approximately 28 mM (Figure 9b), which is close to normal seawater concentrations. This indicates that insignificant sulfate consumption, e.g., by AOM occurs at this depth interval. Below 6 mbsf the sulfate reduction zone is encountered less than 2 m above the TGHOZ.

3.2.3. Interpretation

Methane concentrations below in situ methane solubility may be explained by gas exsolution during core recovery due to pressure decrease and potential temperature increase. Methane concentrations exceeding onboard methane solubility might be related to potential presence of microsized hydrate particles in the analyzed pore water. Moreover, concentrations of dissolved methane above the TGHOZ are several orders of magnitude lower than the methane solubility at surface conditions.

The sulfate and methane data show matching trends with dissolved methane concentrations above the TGHOZ being much lower than the methane solubility. This steep concentration gradient promotes gas hydrate dissolution from the TGHOZ. Because similar pore water sulfate and methane relations were observed at sites GMMB04 (pockmark C1), GMMB09 (off C2), GMMB03, and GMMB12 (both pockmark A), hydrate dissolution above the TGHOZ might be proposed for sites near the borders of pockmark A and pockmark cluster C as well. Gas plumes detected in the water column above the central part of pockmark A, along with the presence of shallow gas hydrate at sites GMMB10 and GMMB11, nearby prove rapid gas flux and hydrate growth in this region (Figure 6).

4. Discussion: Pockmark Formation and Evolution—The Disequilibrium Between Gas Inflow and Outflow

Previously, it was suggested that pockmark formation and evolution result from a uniform hydrate dissolution process [*Sultan et al.*, 2010]. The newly acquired data confirm that hydrate dissolution occurs in certain parts of the studied pockmarks, and gas hydrate is formed in other parts concurrently. These processes lead to a complex, heterogeneous hydrate distribution characterizing the studied pockmarks. Indeed, concurrent to hydrate dissolution, rapid hydrate growth and in some cases gas venting into the water column occurs in the most recent active parts of the pockmarks (mainly the central part of pockmark A) where gas is directly supplied through the main fracture.

Rapid hydrate growth was confirmed by multiple lines of evidence: (1) positive temperature anomalies in GHOZs (section 3.1.4), (2) free gas trapped in shallow microfractures and cracks near the surface (section 3.1.3) and released into the water column (section 3.1.2), and (3) coexistence of free gas and gas hydrate within the same sediment interval (section 3.1.1). Another possible indication for rapid gas hydrate growth induced by episodic rapid gas ascent is provided by the seismic data which imaged four successive reflectors that may correspond to hydrate/free gas fronts (reflectors F1 to F4 on SY02-HR-Pr02, Figure 4). The interpretation of reflectors F1 to F4 as hydrate/free gas fronts is based on a trial empirical calibration of a comparable seismic reflector below GMMB04 (see Figure 4). Slow hydrate dissolution, in contrast, is evident from methane concentrations being several orders of magnitude lower than the methane solubility at atmospheric temperature and pressure conditions and from the quasi-vertical sulfate profile at less than 2 m above the TGHOZs for several sites (GMMB12 and GMMB03 (both pockmark A), GMMB04 (pockmark C1), GMMB05 (pockmark C2), and GMMB09 (off pockmark C2)).

The newly acquired results also support that the first stage of pockmark formation is fluid flow from greater depth promoting subseabed hydrate accumulation. Hydrate is formed before any type of deformations affects the seafloor. This is visible from drill GMMB09 at the SE rim of pockmark C2, where hydrate and authigenic carbonate concretions were found at around 25 mbsf (SY02-HR-Pr02, Figure 4) without any deformation visible on the seabed bathymetry (Figure 2b).

Another key issue concerns the burial depth of gas hydrate occurrences in the investigated area. The maximum depth of hydrate recovered with MeBo cores was about 40 mbsf, although pore water freshening, indicative for hydrate presence, was observed at one location in deeper intervals as well.

Based on the above summarized observations, it was possible to improve the initial scheme proposed by *Sultan et al.* [2010] to describe formation and evolution of the pockmarks in the present study area. The improved scenario is described below following nine steps (Figure 10):

Step 1. (Figure 11a) Free gas accumulates and fluid pressure increases in intermediate reservoirs equivalent to horizon R in Figure 7. Once the gas pressure exceeds a critical value, free gas migrates upward while reopening annealed fractures or creating new conduits.

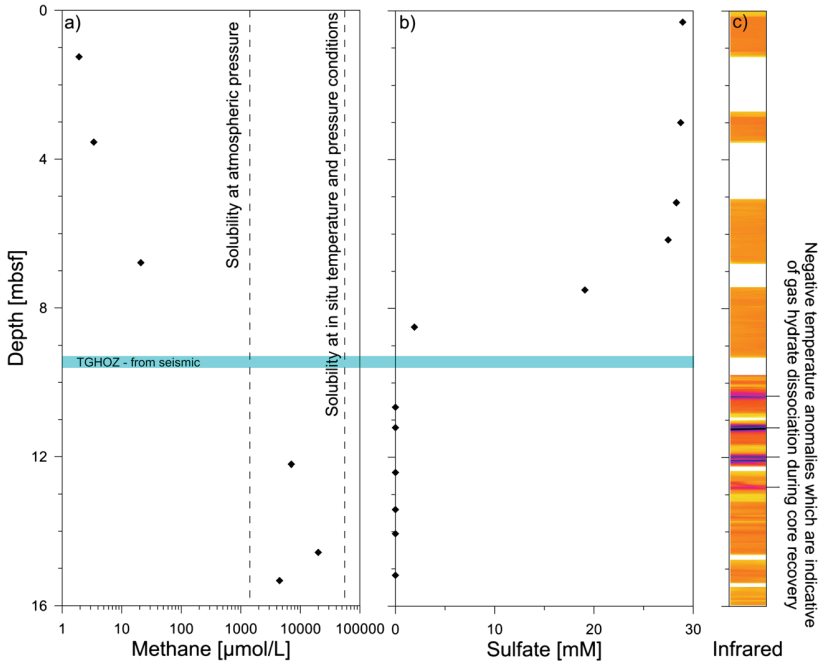

Figure 10. Pore water concentration profiles of dissolved (a) methane and (b) sulfate measured in the uppermost 16 m of MeBo core GMMB05. The shaded horizontal area illustrates the top of the GHOZ (TGHOZ) as identified from seismic data. Both methane solubilities at onboard pressure and temperature conditions as well as at in situ temperature and pressure conditions are added to Figure 10a. The measured concentrations of dissolved methane above the TGHOZ is much lower than both solubilities. The quasi-vertical sulfate profile less than 2 m above the TGHOZ corresponds to the low methane concentration above the GHOZ. (c) The infrared (IR) image shows negative temperature anomalies (purple layers) which are indicative of gas hydrate dissociation during core recovery [*Wei et al.*, 2012].

Step 2. (Figure 11a) Once the ascending free gas passes the local BGHSZ, gas hydrate is formed within the deep cohesive clay. Hydrate formation first occurs at internal surfaces of the fractured zones by creating hydrate plugs. The stiffness of the deep clays seems to be high enough to hamper lateral gas hydrate propagation. At this stage, gas hydrate may isolate free gas from the ambient pore water as it was observed during MeBo drillings. Free gas may continue at this stage to accumulate in hydrate plugs present in the GHSZ.

Step 3. (Figure 11a) The hydrate plugs are breached in case the pressure of free gas exceeds a certain value. Then, the gas can migrate into the upper package of progressively softer sediments, where lateral migration of free gas and creation of lateral fractures can take place. Gas hydrate can therefore grow into lateral direction and fill such fractures. The amount and speed of lateral gas propagation and gas hydrate formation depends mainly on the mechanical properties of the surrounding sediments. Two mechanisms can be considered for these processes (1) shallow soft sedimentary layers are pushed upward during hydrate growth and lateral fractures are created by shearing and (2) free gas pressure accumulation creates initial discontinuities, and—by stress accumulation at the border of these discontinuities—shear fractures (mode II fracture—see for instance *Rao et al.* [2003, Figure 1]) may take place. A detailed mathematical formulation of the second mechanism can be found in *Fialko et al.* [2001] and *Bunger and Detournay* [2005] where an analytical solution for this fracture propagation is obtained for pressurized horizontal circular crack in an elastic half-space.

Step 4. (Figure 11b) Free gas coexists with gas hydrate in the central part of the GHOZ. Free gas ascending from the intermediate reservoir, equivalent to horizon R in Figure 7, causes fluid overpressures and further fracturing of the upper gas hydrate cover. Elongated cap of hydrate, horizontal cracks and lateral shear discontinuities may form. Rapid hydrate growth occurs at this step causing the coexistence of free gas and gas hydrate. These successive fronts of gas hydrate formations are similar to the reflectors indicated in Figure 4 (reflectors F1 to F4).

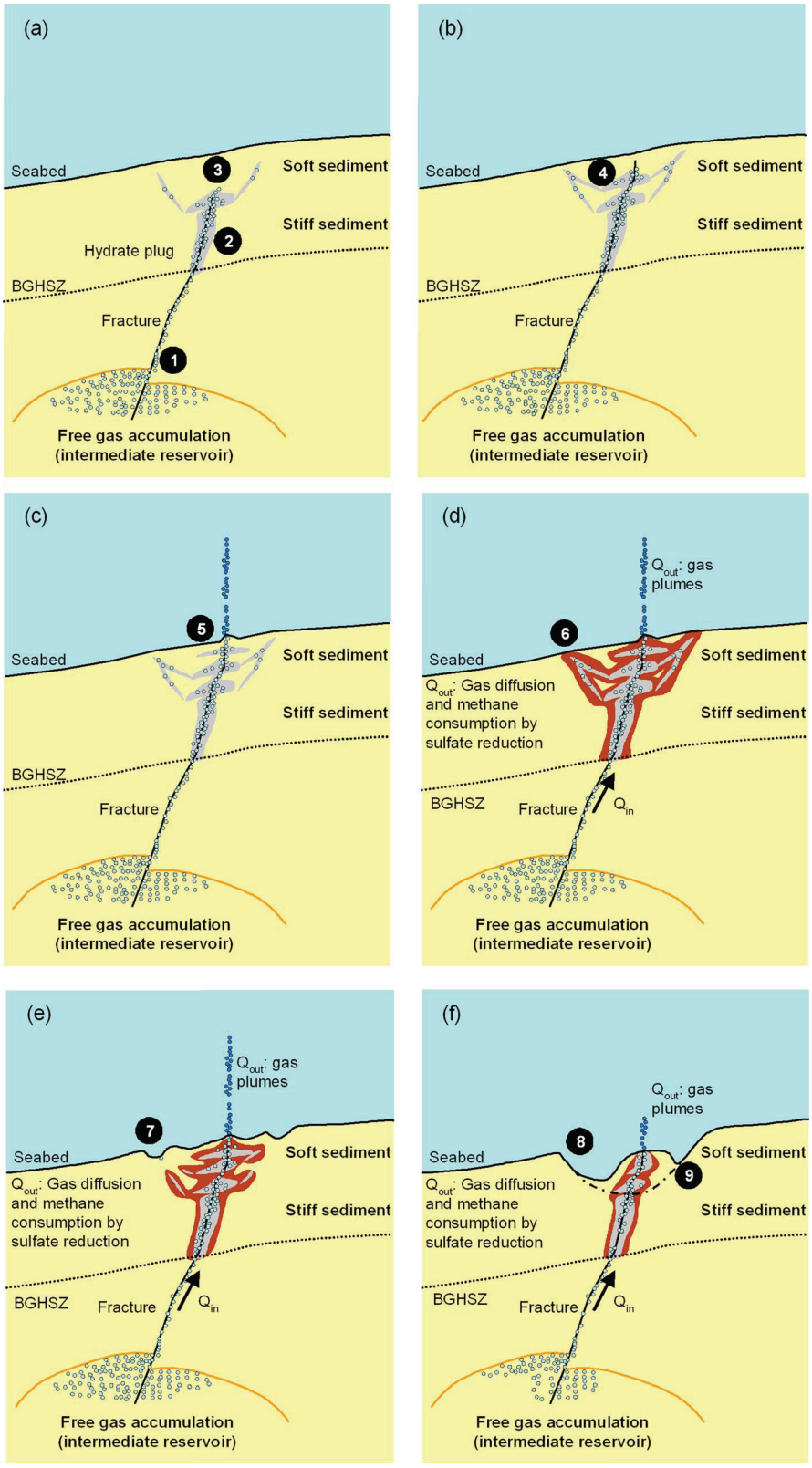

Figure 11. (a to f) Sketch of different steps in pockmark evolution during hydrate formation and dissolution (see text for details and descriptions corresponding to steps 1 to 9). Hydrate dynamics and gas (free and dissolved) inflow (Q_{in}) and outflow (Q_{out}) are the main factors controlling the pockmark formation and evolution.

Step 5. (Figure 11c)Successive elongated hydrate caps/fronts are formed in sediments shallow enough to create fractures reaching the seabed. Those fractures may constitute a direct gas migration pathway from the intermediate reservoirs to the water column. Ascent through such connections may facilitate free gas to escape into the water column as observed for the two gas plumes above pockmark A. At this step, gas fractions ascending from the reservoir are dispersed in the water column and shallow fractures, and deep faults are maintained open by the pressure of upward migrating gas.

Step 6. (Figure 11d) Coincident with rapid hydrate formations in near-vertical fractures, lateral discontinuities, and shear bands, hydrate dissolution occurs at the outer limits of the GHOZ (brown contours in Figures 10d–10f). Indeed, the long-term occurrence of hydrate close to the seafloor must be sustained by gas supply sufficient to maintain boundary layer saturation or even continuous hydrate growth [*Rehder et al.*, 2004]. The huge amount of free gas migrating rapidly almost instantaneously by successive episodes is at the origin of hydrate saturated cracks, shear bands, and fractures. The long-term occurrence of such gas hydrate layers and discontinuities can only be maintained by sufficient supply of gas. Therefore, hydrate formation and dissolution are controlled by the balance between gas inflow (Q_{in}) from the intermediate reservoirs and gas outflow (Q_{out}) including hydrate dissolution at the border of the GHOZ sustained by AOM and gas plumes in the water column. Moreover, rapid formation of gas hydrate slabs and plugs limits significantly lateral gas migration which is required to sustain hydrate stability at the borders of hydrate-bearing zones.

Step 7. (Figure 11e) Due to the obvious differences in gas inflow (Q_{in}) and outflow (Q_{out}) rates and to the low permeability of hydrate-bearing zones for free gas migration, dissolution of gas hydrate and disappearance of hydrate slabs and plugs commences at the border of the GHOZ. As a consequence, a circular collapse structure surrounding the central gas hydrate-rich zone is formed as indicated by the subcircular depressions in the shaded bathymetry in Figure 1.

Step 8. (Figure 11f) Hydrate dissolution is a function of the deficit between Q_{in} and Q_{out} and proceeds from the borders of the GHOZ (brown areas in Figure 10f). The material loss due to hydrate dissolution is accompanied by a deepening of the pockmark rim with a preservation of a dome-like structure in the pockmark center due to the preservation of hydrate adjacent to the free gas conduit. A central dome-like structure is suggested by the seafloor morphology to the south of pockmark C3 (Figure 2b).

Step 9. (Figure 11f) The final stage is caused by interruption of upward gas migrations from the intermediate reservoir. This may lead to complete dissolution of hydrate in near-surface sediments and decay of the central dome-like structure. This may be accompanied by formation of a relatively regular pockmark, for example, pockmark B shown in Figure 1.

The process sequences described above are based on recent observations but remain conceptual. For instance, the time factor controlling the different mechanisms is unknown. In order to verify the scheme presented in Figure 10, a more comprehensive and quantitative overview on short- and long-term processes that shape pockmarks in the present area is necessary with a need to carry out

1. Pore water analyses of dissolved gas and sulfate concentrations in sediments surrounding the GHOZ at selected pockmarks allowing modeling the short-term dynamics of gas hydrate in this area [see for more details *Malinverno et al.* 2008 and *Bhatnagar et al.*, 2007].
2. U/Th dating of authigenic cold seep carbonates which may reveal the dynamic of gas flux over the last few thousand years at selected pockmarks [*Bayon et al.*, 2009; *Feng et al.*, 2010].

5. Conclusion

In the present work, it is shown that rapid gas hydrate growth and slow hydrate dissolution are the main mechanisms affecting seabed pockmarks and subseabed facies architecture observed in the study area. Gas hydrate forms through rapid gas migration, as confirmed by in situ positive temperature anomalies, free gas trapped in shallow microfractures in the GHOZ, and the coexistence between free gas and gas hydrate. At the same time, gas hydrate dissolves relatively slowly due to the methane deficit in the surrounding sediment, where concentrations of dissolved methane are below solubility. The pore water sulfate reduction zone is

limited due to low methane concentrations surrounding gas hydrate (less than 2 m above the GHOZ). Therefore, based on the above observations and on detailed analyses of seabed and subseabed structures, an update of the scenario by *Sultan et al.* [2010] is proposed to describe formation and evolution of the pockmarks in deep water Nigeria.

In conclusion, this work shows that localized gas migration through the center of the GHOZ can coexist with methane deficit at the periphery of the same pockmark. It also provides further evidence about the role of hydrate dissolution for sediment deformations in the GHSZ.

Acknowledgments

The support by officers and crew during Guineco-MeBO cruises is greatly appreciated, as is the dedication of the technical staff during the cruise. Constructive comments by Christian Berndt, Andreia Plaza-Faverola, and the Associate Editor helped improve the manuscript significantly. Additionally, we would like to acknowledge our industrial partner, Total, for providing a part of the used data. Data used in the present paper are covered by a confidentiality agreement between Total, Ifremer, and Marum that restrict access; interested readers can contact the authors for more information.

References

Abegg, F., H. J. Hohnberg, T. Pape, G. Bohrmann, and J. Freitag (2008), Development and application of pressure-core-sampling systems for the investigation of gas- and gas-hydrate-bearing sediments, *Deep Sea Res., Part I*, *55*(11), 1590–1599, doi:10.1016/j.dsr.2008.06.006.

Bayon, G., G. M. Henderson, and M. Bohn (2009), U-Th stratigraphy of a cold seep carbonate crust, *Chem. Geol.*, *260*(1-2), 47–56, doi:10.1016/j.chemgeo.2008.11.020.

Bhatnagar, G., W. G. Chapman, G. R. Dickens, B. Dugan, and G. J. Hirasaki (2007), Generalization of gas hydrate distribution and saturation in marine sediments by scaling of thermodynamic and transport processes, *Am. J. Sci.*, *307*(6), 861–900, doi:10.2475/06.2007.01.

Bigalke, N. K., G. Rehder, and G. Gust (2009), Methane hydrate dissolution rates in undersaturated seawater under controlled hydrodynamic forcing, *Mar. Chem.*, *115*(3-4), 226–234, doi:10.1016/j.marchem.2009.09.002.

Borowski, W. S., C. K. Paull, and W. Ussler (1996), Marine pore-water sulfate profiles indicate in situ methane flux from underlying gas hydrate, *Geology*, *24*(7), 655–658, doi:10.1130/0091-7613(1996)024<0655:mpwspi>2.3.co;2.

Borowski, W. S., C. K. Paull, and W. Ussler (1999), Global and local variations of interstitial sulfate gradients in deep-water, continental margin sediments: Sensitivity to underlying methane and gas hydrates, *Mar. Geol.*, *159*(1-4), 131–154.

Bunger, A. P., and E. Detournay (2005), Asymptotic solution for a penny-shaped near-surface hydraulic fracture, *Eng. Fract. Mech.*, *72*(16), doi:10.1016/j.engfracmech.2005.06.005.

Feng, D., H. H. Roberts, H. Cheng, J. Peckmann, G. Bohrmann, R. L. Edwards, and D. Chen (2010), U/Th dating of cold-seep carbonates: An initial comparison, *Deep Sea Res., Part II*, *57*(21-23), 2055–2060, doi:10.1016/j.dsr2.2010.09.004.

Fialko, Y., Y. Khazan, and M. Simons (2001), Deformation due to a pressurized horizontal circular crack in an elastic half-space, with applications to volcano geodesy, *Geophys. J. Int.*, *146*(1), doi:10.1046/j.1365-246X.2001.00452.x.

Freudenthal, T., G. Wefer, and IEEE (2009), *Shallow Drilling in the Deep Sea: The Sea Floor Drill Rig MEBO, Oceans 2009 - Europe*, vol. 1, 2, pp. 180–183, IEEE, New York.

Georges, R. A., and E. Cauquil (2007), AUV ultrahigh-resolution 3D seismic technique for detailed subsurface investigations, Offshore Technology Conference, Houston, OTC18784.

Haeckel, M., E. Suess, K. Wallmann, and D. Rickert (2004), Rising methane gas bubbles form massive hydrate layers at the seafloor, *Geochim. Cosmochim. Acta*, *68*(21), 4335–4345, doi:10.1016/j.gca.2004.01.018.

Hoehler, T. M., M. J. Alperin, D. B. Albert, and C. S. Martens (1994), Field and laboratory studies of methane oxidation in an anoxic marine sediment: Evidence for a methanogen-sulfate reducer consortium, *Global Biogeochem. Cycles*, *8*, 451–463.

Iversen, N., and B. B. Jorgensen (1985), Anaerobic methane oxidation rates at the sulphate methane transition in marine-sediments from Kattegat and Skagerrak (Denmark), *Limnol. Oceanogr.*, *30*(5), 944–955.

Kasten, S., K. Noethen, C. Hensen, V. Spiess, M. Blumenberg, and R. R. Schneider (2012), Gas hydrate decomposition recorded by authigenic barite at pockmark sites of the northern Congo Fan, *Geo Mar. Lett.*, *32*(5-6), 515–524, doi:10.1007/s00367-012-0288-9.

Ker, S., B. Marsset, S. Garziglia, Y. Le Gonidec, D. Gibert, M. Voisset, and J. Adamy (2010), High-resolution seismic imaging in deep sea from a joint deep-towed/OBH reflection experiment: Application to a Mass Transport Complex offshore Nigeria, *Geophys. J. Int.*, *182*, 1524–1542.

Kwon, T. H., G. C. Cho, and J. C. Santamarina (2008), Gas hydrate dissociation in sediments: Pressure-temperature evolution, *Geochem. Geophys. Geosyst.*, *9*, Q03019, doi:10.1029/2007GC001920.

Lapham, L. L., J. P. Chanton, R. Chapman, and C. S. Martens (2010), Methane under-saturated fluids in deep-sea sediments: Implications for gas hydrate stability and rates of dissolution, *Earth Planet. Sci. Lett.*, *298*, 275–285, doi:10.1016/j.epsl.2010.07.016.

Lee, M. W., and T. S. Collett (2006), Gas hydrate and free gas saturation estimated from velocity logs on Hydrate Ridge, offshore Oregon, U.S.A., in *Proc Ocean Drill Program Sci Results*, vol. 204, edited by A. M. Trehu et al., 1–25, Proc. Ocean Drill Program Sci. Results, College Station, Tex.

Liu, X. L., and P. B. Flemings (2006), Passing gas through the hydrate stability zone at southern Hydrate Ridge, offshore Oregon, *Earth Planet. Sci. Lett.*, *241*(1-2), 211–226, doi:10.1016/j.epsl.2005.10.026.

Malinverno, A., M. Kastner, M. E. Torres, and U. G. Wortmann (2008), Gas hydrate occurrence from pore water chlorinity and downhole logs in a transect across the northern Cascadia margin (Integrated Ocean Drilling Program Expedition 311), *J. Geophys. Res.*, *113*, B08103, doi:10.1029/2008JB005702.

Marsset, T., B. Marsset, S. Ker, Y. Thomas, and Y. Le Gall (2010), High and very high resolution deep-towed seismic system: Performance and examples from deep water geohazard studies, *Deep Sea Res., Part I*, doi:10.1016/j.dsr.2010.01.001.

Milkov, A. V., G. R. Dickens, G. E. Claypool, Y. J. Lee, W. S. Borowski, M. E. Torres, W. Y. Xu, H. Tomaru, A. M. Trehu, and P. Schultheiss (2004), Co-existence of gas hydrate, free gas, and brine within the regional gas hydrate stability zone at Hydrate Ridge (Oregon margin): Evidence from prolonged degassing of a pressurized core, *Earth Planet. Sci. Lett.*, *222*(3-4), 829–843, doi:10.1016/j.epsl.2004.03.028.

Pape, T., A. Bahr, S. A. Klapp, F. Abegg, and G. Bohrmann (2011), High-intensity gas seepage causes rafting of shallow gas hydrates in the southeastern Black Sea, *Earth Planet. Sci. Lett.*, *307*(1-2), doi:10.1016/j.epsl.2011.04.030.

Paull, C. K., W. Ussler, W. S. Borowski, and F. N. Spiess (1995), Methane-rich plumes on the Carolina continental rise – associations with gas hydrates, *Geology*, *23*(1), doi:10.1130/0091-7613(1995)023<0089:mrpotc>2.3.co;2.

Rao, Q. H., Z. Q. Sun, O. Stephansson, C. L. Li, and B. Stillborg (2003), Shear fracture (Mode II) of brittle rock, *Int. J. Rock Mech. Min. Sci.*, *40*(3), doi:10.1016/s1365-1609(03)00003-0.

Rehder, G., S. H. Kirby, W. B. Durham, L. A. Stern, E. T. Peltzer, J. Pinkston, and P. G. Brewer (2004), Dissolution rates of pure methane hydrate and carbon-dioxide hydrate in undersaturated seawater at 1000-m depth, *Geochim. Cosmochim. Acta*, *68*(2), 285–292, doi:10.1016/j.gca.2003.07.001.

Roemer, M., H. Sahling, T. Pape, G. Bohrmann, and V. Spiess (2012), Quantification of gas bubble emissions from submarine hydrocarbon seeps at the Makran continental margin (offshore Pakistan), *J. Geophys. Res.*, *117*, C10015, doi:10.1029/2011JC007424.

Sultan, N. (2007), Comment on "Excess pore pressure resulting from methane hydrate dissociation in marine sediments: A theoretical approach" by Wenyue Xu and Leonid N. Germanovich, *J. Geophys. Res.*, *112*, B02103, doi:10.1029/2006JB004527.

Sultan, N., M. Voisset, T. Marsset, A. M. Vernant, E. Cauquil, J. L. Colliat, and V. Curinier (2007), Detection of free gas and gas hydrate based on 3D seismic data and cone penetration testing: An example from the Nigerian Continental Slope, *Mar. Geol.*, *240*(1-4), 235–255, doi:10.1016/j.margeo.2007.02.012.

Sultan, N., et al. (2010), Hydrate dissolution as a potential mechanism for pockmark formation in the Niger delta, *J. Geophys. Res.*, *115*, B08101, doi:10.1029/2010JB007453.

Taylor, M. H., W. P. Dillon, and I. A. Pecher (2000), Trapping and migration of methane associated with the gas hydrate stability zone at the Blake Ridge Diapir: New insights from seismic data, *Mar. Geol.*, *164*(1-2), doi:10.1016/s0025-3227(99)00128-0.

Torres, M. E., K. Wallmann, A. M. Trehu, G. Bohrmann, W. S. Borowski, and H. Tomaru (2004), Gas hydrate growth, methane transport, and chloride enrichment at the southern summit of Hydrate Ridge, Cascadia margin off Oregon, *Earth Planet. Sci. Lett.*, *226*(1-2), 225–241, doi:10.1016/j.epsl.2004.07.029.

Trehu, A. M., et al. (2003), Proc. ODP, Initial reports, 204, Ocean Drilling Program, College Station, TX. doi:10.2973/odp.proc.ir.204.2003.

Waite, W. F., et al. (2009), Physical properties of hydrate-bearing sediments, *Rev. Geophys.*, *47*, RG4003, doi:10.1029/2008RG000279.

Wallmann, K., P. Linke, E. Suess, G. Bohrmann, H. Sahling, M. Schluter, A. Dahlmann, S. Lammers, J. Greinert, and N. von Mirbach (1997), Quantifying fluid flow, solute mixing, and biogeochemical turnover at cold vents of the eastern Aleutian subduction zone, *Geochim. Cosmochim. Acta*, *61*(24), doi:10.1016/s0016-7037(97)00306-2.

Wei, J. G., G. Bohrmann, N. Sultan, T. Himmler, T. Pape, B. Dennielou, L. Ruffine, S. Garziglia, and the GUINECO-MeBo shipboard scientific party (2012), Distribution of gas hydrates in submarine pockmark deposits of the Nigerian margin inferred from infrared thermal core scanning, Processes and Products, 24-28 September 2012. Hamburg, Germany.

Xu, W. Y., and L. N. Germanovich (2006), Excess pore pressure resulting from methane hydrate dissociation in marine sediments: A theoretical approach, *J. Geophys. Res.*, *111*, B01104, doi:10.1029/2004JB003600.